Universidade do Minho
Escola de Engenharia

Paula Alexandra Cunha Pereira

Glycol Chitosan Nanogels

setembro de 2014

Universidade do Minho
Escola de Engenharia

Paula Alexandra Cunha Pereira

Glycol Chitosan Nanogels

Tese de Doutoramento em Engenharia Biomédica

Trabalho efetuado sob a orientação do
Doutor Francisco Miguel Portela Gama

setembro de 2014

DECLARAÇÃO

Nome: Paula Alexandra Cunha Pereira

Endereço electrónico: paulaacppousada@gmail.com

Título da tese: Glycol Chitosan Nanogels

Orientador: Professor Doutor Francisco Miguel Portela Gama

Ano de conclusão: 2014

Designação do Doutoramento: Engenharia Biomédica

Universidade do Minho, ___/___/_____

Assinatura: _____

Agradecimentos

Com o aproximar da meta final queria deixar o meu reconhecimento a todas as pessoas que tornaram esta longa viagem menos ínvia…

Em primeiro lugar um agradecimento especial ao orientador deste trabalho, Professor Miguel Gama, que para além de conhecimento científico transmitiu-me valores, que fizeram de mim uma melhor profissional. Obrigada por tudo!

Aos meus colegas do FUNCARB e do DEB-UM, sem esquecer os que ja lá não estão, quero deixar um sincero obrigado por todo o bem que me fizeram; que de uma forma ou de outra contribuiram para que a realização deste projecto fosse avante. Em particular quero agradecer à Catarina por me ter aberto as primeiras janelas no mundo da investigação; e em especial à Sílvia Pedrosa, Dina Silva e ao Alexandre Leitão pelas produtivas discussões científicas, companheirismo e essencialmente pela vossa amizade para a vida!

Não poderia deixar de agradecer aos colegas dos laboratórios por onde passei, em especial à Alexandra Correia pela colaboração e horas de trabalho dedicadas às minhas "coisas"! Quero também agradecer à Yasmin Cross que quando eu estava sozinha num laboratório distante me acolheu e me fez sentir em casa!

Aos professores Doutores José Alberto Martins, Paulo Coutinho, Manuel Vilanova, Arwyn Jones, Laurent David e Africa González Fernández; e ainda Cristóvão Lima, Daniela Morgado, Agnès Crepet, Mercedes Peleteiro Olmedo, Jennifer Wymant, Edward Sayers quero agradecer a vossa contribuição neste projecto.

Aos meus familiares quero sobretudo, lamentar a minha ausência quando por vezes o trabalho a isso me obrigava; agradacer-vos a ajuda, dedicação e motivação, força fundamental para que eu tivesse conseguido levar este "barco" a bom porto!

A ti Nuno, por estares sempre a meu lado, permitindo que tudo isto tenha sido possível! À minha pequena princesa quero agradecer-lhe por todos os sorrisos que me destes quando não tinha motivos para tal…também por ela cheguei até aqui.

Obrigada a todos!

Dedico esta tese à minha família,
em especial ao meu marido
e à minha filha…

Abstract

Glycol Chitosan Nanogels

Nanoparticles based on chitosan have been extensively studied for gene, drug and contrast agent delivery. The present work aimed to develop and characterize a glycol chitosan nanogel - also designated macromolecular micelles or hydrogel nanoparticles. The nanogel is obtained by chemically grafting hydrophobic chains on the hydrophilic glycol chitosan backbone, the amphiphilic structure obtained being capable of self-assembly in water, originating quite reproducible nanostructures with few hundred nanometers. The nanogel was decorated with folate conjugated polyethylene glycol, for active targeting purposes, as subsequently confirmed by *in vitro* assays. The positively charged nanogels exhibited colloidal stability up to at least four months. Considering their ability to complex siRNA, nanogels could represent promising vehicles for siRNA delivery. Moreover, their hydrophobic moieties could also carry hydrophobic drugs/imaging agents beyond nucleic acids, according to the theragnosis concept. The safety of the glycol chitosan nanogel as drug delivery system was comprehensively studied, since the biocompatibility of nanogels is still insufficiently reported. No cytotoxicity was detected in cell lines, RAW, 3T3, HMEC and HeLa, although a slight decrease on metabolic activity had been observed. Glycol chitosan nanogel didn't induce cell membrane damage, cell death by apoptosis and/or necrosis, and cell cycling arresting (with exception to G1 arresting in RAW cells). Remarkably, glycol chitosan nanogel was poorly internalized by mouse bone marrow derived macrophages and does not trigger the activation of the complement system. Its blood compatibility was also confirmed through haemolysis and whole blood clotting time assays. The interaction of the nanogel with biological tissues, namely the endocytic mechanisms used by folate functionalized nanogels to entry HeLa cells, and the subsequent intracellular fate were studied using siRNA technology to deplete key proteins on regulation of each tested pathway. The nanogel cellular uptake is folate dependent, as expected since HeLa cells overexpress folate receptors. The internalization occurred mainly through clathrin and caveolin independent mechanisms, specifically by flotillin-1 and Cdc42-dependent endocytosis, as well as through micropinocytosis. Once internalized, after 7 h of incubation, approximately half of the nanogel was visualized in endolysosomal compartments, while the remaining was present in undefined regions of the cytoplasm.

The biodistribution profile of the folate decorated glycol chitosan nanogel was assessed using *in vivo* near infrared fluorescence imaging as tool to track the nanogel over time in a mice model, after intravenous injection. Rapid nanogel whole body distribution was observed at early time points, and it is still detectable in a very wide distribution at least 6 h post-administration. The blood clearance occurred about 6 h post injection, with a blood half-life of approximately 2 h; surprisingly, the linear glycol chitosan seems to undergo a slower blood clearance. No accumulation in the organs was verified, the clearance from the body being observed apparently after a period of about 48h.

In conclusion, the physicochemical features, the ability to complex nucleic acids and certain hydrophobic drugs, cell targeting ability, biocompatibility, internalization and intracellular trafficking, the fairly long blood circulation half-life and suitable body clearance, are pronounced hints of the engineered GC nanogel as a promising drug delivery system.

Resumo

Nanogéis de Glicol Quitosano

Nanopartículas à base de quitosano têm sido largamente estudadas para transportar ácidos nucléicos, fármacos e agentes de contraste. O presente trabalho tem por objectivo desenvolver e caracterizar um nanogel de glicol quitosano - também designado por micelas macromoleculares ou hidrogéis nanoparticulados. O nanogel é obtido através do enxerto químico de cadeias hidrofóbicas na estrutura hidrofílica do glicol quitosano, resultando uma estrutura anfifílica capaz de auto-organizar-se em água, originado nano-estruturas bastantes reprodutivéis com poucas centenas de nanómetros. O nanogel foi decorado com ácido fólico conjugado com polietilenoglicol para efeito de direccionamento controlado, tal como posteriormente confirmado em ensaios *in vitro*. O nanogel de natureza catiónica exibiu estabilidade coloidal pelo menos durante 4 meses. Considerando a sua habilidade para complexar siRNA, os nanogéis podem representar veículos promissores para transporte/entrega de siRNA. Além disso, os domínios hidrofóbicos podem também transportar fármacos hidrofóbicos/agentes de imagem para além de ácidos nucléicos, de acordo com o defendido no conceito de teragnóstico. A fiabilidade do nanogel de glicol quitosano como sistema de entrega de drogas foi estudada exaustivamente, uma vez que a biocompatibilidade dos nanogéis está ainda pouco reportada. Ausência de citotoxicidade foi observada nas linhas celulares RAW, 3T3, HMEC e HeLa, embora se tenha verificado uma ligeira diminuição na actividade metabólica das mesmas. O nanogel de glicol quitosano não danifica a membrana celular, assim como não induz morte celular por apoptose e/ou necrose, nem paragens no ciclo celular (com excepção para as células RAW onde se verifica paragem na fase G1). Surpreendentemente, o nanogel de glicol quitosano foi fracamente internalizado por macrófagos derivados de medula óssea de ratinho, para além de não desencadear a activação do sistema complemento. A sua hemocompatibilidade foi também confirmada através de ensaios de hemólise e de coagulação. A interacção do nanogel com os tecidos biológicos, nomeadamente os mecanismos de endocitose utilizados pelos nanogéis funcionalizados com ácido fólico para entrarem nas células HeLa e subsequente percurso intracelular foram estudados recorrendo à tecnologia de siRNA para silenciar proteínas chave na regulação de cada via analisada. A internalização do nanogel mostrou ser dependente do ácido fólico, tal como esperado uma vez que as células HeLa

sobre-expressam receptores para ácido fólico. A internalização ocorreu principalmente através de mecanismos independentes de clatrina e caveolina, mais especificamente encocitose dependente de flotilina-1 e Cdc42, bem como macropinocitose. Uma vez internalizado, depois de 7 h de incubação, cerca de metade da população do nanogel foi visualizada em compartimentos endolisossomais enquanto que a porção restante se encontra em regiões indefinidas do citoplasma.

O perfil de biodistribuição do nanogel de glicol quitosano decorado com ácido fólico foi avaliado num sistema de imagiologia *in vivo* de fluorescência no infravermelho próximo como ferramenta para monitorizar a distribuição do nanogel após injecção intravenosa ao longo do tempo, num modelo de ratinho. Uma rápida distribuição do nanogel por todo o corpo foi observada logo nos tempos mais precoces, sendo ainda detectável uma ampla distribuição até pelo menos 6 h após a administração. O desaparecimento do nanogel do sangue ocorreu cerca de 6 h após injecção, com um tempo de meia-vida de aproximandamente 2 h; surpreendentemente, o glicol quitosano de estrutura linear mostrou desaparecer mais lentamente do sangue. Não se verificou acumulação nos órgãos, e o desaparecimento do corpo acontece num período de aproximadamente 48h.

Em conclusão, as características físico-químicas, a capacidade de complexar ácidos nucléicos e certamente fármacos hidrofóbicos, direcionamento celular, biocompatibilidade, internalização e percurso intracelular, período de semi-vida no sangue relativamente longo e razoável período de eliminação do corpo, são indícios de que o nanogel produzido poderá ser um sistema promissor de libertação controlada de drogas.

Publications

This thesis is based on the following book chapter and original research articles:

CHAPTER 1: Pereira, P.; Carvalho, V.; Ramos, R.; Gama, F. M., **Chitosan NanoParticles for Biomedical Applications**. Chitosan: Manufacture, Properties and Usage, (ISBN: 978-1-61728-831-9) *Nova Science Publishers*, New York, 2011, 321-364.

CHAPTER 2: Pereira, P.; Morgado, D.; Crepet, A.; David, L.; Gama, F. M., **Glycol chitosan-based nanogel as a potential targetable carrier for siRNA**. *Macromolecular bioscience* 2013, 13, (10), 1369-78.

CHAPTER 3: Pereira, P.; Pedrosa, S. S.; Correia, A.; Lima, C. F.; Olmedo, M.P.; González-Fernández, A.; Vilanova, M.; Gama, F. M., **Biocompatibility of a self-assembled Glycol Chitosan nanogel**. *Toxicology in Vitro (Submitted)*.

CHAPTER 4: Pereira, P.; Pedrosa, S. S.; Wymant, J; Sayers, E.; Correia, A.; Vilanova, M.; Jones, A. T.; Gama, F. M., **siRNA inhibition of endocytic pathways to characterize the cellular uptake mechanisms of folate functionalized glycol chitosan nanogels**. *Biomacromolecules* (*Submitted)*

CHAPTER 5: Pereira, P.; Pedrosa, S. S.; Gama, F. M., *In vivo* imaging of glycol chitosan-based nanogel biodistribution. *(Work still in progress)*

Table of contents

List of Figures

CHAPTER 1

CHAPTER 2

CHAPTER 3

CHAPTER 4

CHAPTER 5

List of Tables

CHAPTER 1

CHAPTER 2

CHAPTER 3

Abbreviations

3T3	Mouse embryonic fibroblast cell line
A549	Human lung adenocarcinoma epithelial cell line
Akt1	V-akt murine thymoma viral oncogene homolog 1
ANEP	Anti-neuroexcitation peptide
ANOVA	Analysis of variance
Arf6	ADP-ribosylation factor 6
ATP	Adenosine triphosphate
Au	Gold
Bcl-2	B-cell lymphoma 2
BMDM	Bone marrow derived macrophages
BMP-2	Bone morphogenetic protein-2
C3	Complement component 3
CAC	Critical aggregation concentration
Caco-2	Human colorectal adenocarcinoma epithelial cell line
Cav-1	Caveolin-1
CCD	Charged coupled device
CD44	Cluster domain 44
Cdc42	Cell division control protein 42
CHC	Clathrin
cIAP-2	Cellular inhibitor of apoptosis 2
CME	Clathrin mediated endocytosis
Cryo-FESEM	Cryo-Field Emission Scanning Electron Microscopy
CS	Chitosan
CT-26	Mouse colon carcinoma cell line
CvME	Caveolin mediated encocytosis
DAPI	4',6-diamidino-2-phenylindole
DIC	Differential interference contrast
DLS	Dynamic light scattering
DMEM	Dulbecco's Modified Eagle Medium
DMSO	Dimethyl sulfoxide
DNA	Deoxyribonucleic acid
dn/dc	Refractive Index Increment
DOX	Doxorubicin
DS	Degree of substitution

EDC	1-Ethyl-3-[3-dimethylaminopropyl]carbodiimide hydrochloride
EDTA	Ethylenediamine tetraacetic acid
EGFP	Enhanced green fluorescent protein
EPR	Enhanced permeability and retention
FBS	Fetal bovine serum
FHL2	FHL2 gene expression
FITC	Fluorescein isothiocyanate
Flot-1	Flotilin-1
GC	Glycol chitosan
GCFA	Glycol chitosan nanogel functionalized with folate-conjugated PEG
GEECs	GPI-enriched early endosomal compartments
GFP	Green fluorescent protein
GPI	Glycosylphosphatidylinositol
GTPases	Hydrolase enzymes to guanosine triphosphate
H1299	Human lung carcinoma cell line
HBs	Hepatitis B virus infection
HEK293	Human embryonic kidney cell line
HeLa	Human cervix adenocarcinoma epithelial cell line
H2B-GFP	human histone-GFP fusion
HEPES	N-2-hydroxyethylpiperazine-N-2-ethane sulfonic acid
HepG2 cells	Human hepatocellular carcinoma cell line
HMEC	Human dermal microvascular endothelial cells
1H NMR	^{1}H Nuclear magnetic resonance analysis
HPMCP	Hydroxypropyl methylcellulose phthalate
HT-29	Human colorectal adenocarcinoma cell line
IFN-γ	Interferon gamma
IgA	Immunoglobulin A
IgG	Immunoglobulin G
IL	Interleukin
IL-1Ra	Interleukin 1 receptor antagonist
IONs	Iron oxide NPs
iSur-pDNA	Survivin shRNA-expressing plasmid
K562 cells	Human bone marrow Chronic myelogenous leukemia
KB	Human HeLa contaminant carcinoma cell line
L929	Mouse fibroblast cell line
LCCM	L929 cell conditioned medium
LDH	Lactate dehydrogenase

Leu-Enk	Leucine-enkephalin
LoVo	Human colorectal adenocarcinoma cell line
MALLS	Multi-angle laser light scattering
Map4k4	Human colorectal adenocarcinoma cell line
MFI	Mean Fluorescence Intensity
MHDA	Mercapto hexadecanoic acid
miR-34a	microRNA-34
Mn	Number Molecular Weight
MPS	Mononuclear Phagocyte System
mRNA	messenger RNA
MTT	3-(4,5-dimethylthiazol-2-yl)-2,5-diphenyl tetrazolium bromide
Mw	Molecular Weight
Mz	z-average Molecular Weight
NADH	Nicotinamide adenine dinucleotide
NCTC 3749	mature murine macrophage-like cell line
NHS	N-hydroxysulfosuccinimide
NIR	Near infrared
N/P	stoichiometry of CS's nitrogen and DNA's phosphate
NR	Nile Red
Opti-MEM	Reduced Serum Media
p53	tumor suppressor protein
Pak-1	p21-activated kinase 1
PBS	Phosphate buffered saline
PBST	PBS Tween 20 (0.025%, v/v)
PEG	Polyethylene glycol
PEG2000	O-methyl-O'-succinylpolyethyene glycol 2000
PEG3000	O-(2-Aminoethyl)-O'-(2-carboxyethyl)polyethylene glycol 3000 hydrochloride
pEGFP-C1	Vector for fusing EGFP to the N-terminus of a partner protein
PI	Propidium iodide
pKa	Acid dissociation constant
PLA	Poly(lactic acid)
PLGA	Poly(D,L-lactide-co-glycolide)
PTX	Paclitaxel
Rac1	Ras-related C3 botulinum toxin substrate 1
RAW	Mouse leukaemic monocyte macrophage cell line
RBCs	Red blood cells

RGD	Arginylglycylaspartic acid
RhoA	Ras homolog gene family, member A
RISC	RNA-induced silencing complex
RNAi	RNA-interference
RPMI-1640	Roswell Park Memorial Institute 1640 Medium
SCC7	Squamous cell carcinoma
SD	Standard deviation
SDS-PAGE	Sodium dodecyl sulfate polyacrylamide gel electrophoresis
SEC	Size exclusion chromatography
shRNA	short hairpin RNA
siRNA	small interfering RNA
SKOV3	Human ovary adenocarcinoma cell line
SRB	sulforhodamine B
TMC	N-trimethyl Chitosan
TNF-α	Tumor necrosis factor alpha
TPP	Tripolyphosphate
TSP	3-(trimethylsilyl)propionic-2,2,3,3-d4 acid
UV	Ultraviolet
VP1	Viral protein 1
VA10	Human bronchial epithelial cell line
w/o	Water-in-oil
ZO-1	Tight junction protein
γ-PGA	gamma-polyglutamic acid

Aims and thesis outline

The use of nanoparticles in Nanomedicine is revolutionizing the clinical practice, regarding both diagnosis and therapy. Due to their multifunctional nature, large surface area, structural diversity, and long circulation time in blood, NPs have emerged as attractive vehicle for biomedical applications. Among polymeric drug delivery systems, chitosan based nanoparticles have emerged as a promising vehicle, mainly for gene delivery, due to their exclusive properties, noteworthy for being a natural cationic polymer, biocompatible, biodegradable and mucoadhesive.

The major motivation of the present work has been the development of a chitosan based nanogel, so called for its hydrogel-like character and nanometric size, aiming a drug delivery application. Glycol chitosan was chosen as chitosan derivative due to its improved solubility at physiological pH.

Chapter 1 covers the recent developments on chitosan nanoparticles, namely methodologies, and essentially their applicability in biomedical field – protein/peptide, gene and low molecular weight drugs delivery.

Chapter 2 describes the synthesis of a self-assembled glycol chitosan nanogel, through chemical grafting of hydrophobic chains onto the hydrophilic chitosan backbone. Folate decorated nanogel - obtained using polyethylene glycol as a linker - showed ability to target HeLa cells. Preliminary assay of the potential of the glycol chitosan nanogels to complex siRNA was carried out using a gel retardation assay. The characterization of the physical-chemical features of the nanogel is presented.

Chapter 3 provides a comprehensive study regarding to nanogel biocompatibility, namely its effect on cell viability (metabolic activity and cell membrane integrity) and cell death (apoptosis or necrosis); cell cycle arresting; complement activation; monocuclear phagocytic system (macrophages) evasion; haemolysis index and also whole blood clotting time.

Chapter 4 assesses the internalization mechanism(s) used by folate functionalized glycol chitosan nanogel, as well as its intracellular fate in HeLa cells through siRNA

inhibition of key proteins involved on the regulation of different endocytic pathways. The main pathways responsible for the cell internalization are identified.

Chapter 5, evaluate the whole body distribution profile, and blood circulation half-life of the nanogel comparatively with linear glycol chitosan, using a non-invasive *in vivo* near infrared imaging system.

Finally, chapter 6 comprises a summary of the main conclusions and future perspectives.

1. Chitosan-based nanoparticles for biomedical applications

Adapted and updated from:

Pereira, P. (2010). Chitosan nanoparticles for biomedical applications. *Biotechnology in Agriculture, Industry and Medicine*, Nova Science Publishers, New York.

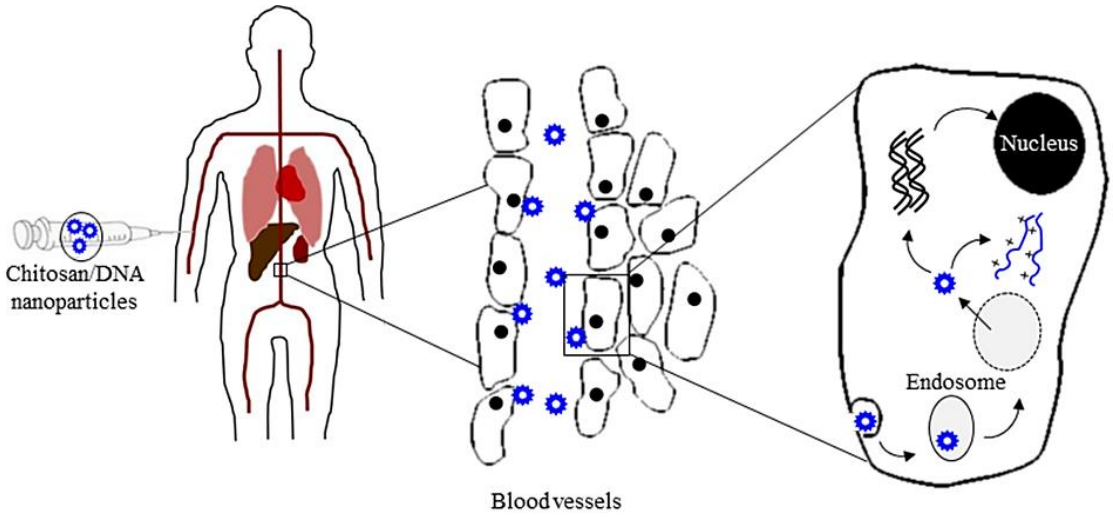

Chitosan is a rather abundant material with exquisite properties, which may be processed into a variety of materials including nanoparticulate systems, hydrogels, fibers, membranes, among others. The production of chitosan-based nanoparticles, also known as macromolecular micelles or nanogels, has been successfully achieved using different techniques. This chapter covers in detail the properties and applications of chitosan nanoparticles in the biomedical field, namely as a drug delivery vehicle for biopharmaceuticals. The main achievements and recent developments will be thoroughly addressed.

1.1. Introduction

Chitosan (CS) (poly[β-(1-4)-2-amino-2-deoxy-D-glucopyranose]) is a natural, non-toxic and biodegradable linear polysaccharide, composed by β-(1-4)-linked N-glucosamine and N-acetyl-glucosamine residues linked through glycosidic bonds [1]. CS is obtained upon partial deacetylation of chitin – the second most abundant polysaccharide in nature, next to cellulose. It is a structural element in the exoskeleton of crustaceans, insects, mushrooms envelopes, green algae cell walls, and yeasts. Nevertheless, being insoluble in water and chemically inert, applications of chitin are limited. In turn, having hydroxyl and amine reactive groups, CS is susceptible to structural modifications [2, 3].

CS is insoluble in water and organic solvents, but soluble in dilute aqueous acidic solutions (pH < 6.5), due to the protonation of the glucosamine residues into the soluble form $R\text{-}NH_3^{+4}$. However several water soluble CS derivatives, such as glycol chitosan (GC), trimethyl chitosan (TMC), carboxymethyl CS, quarternized CS, sulfated CS, which remain soluble at physiological pH, have emerged in biomedical field [5-9]. Commercially available CS has an average molecular weight (Mw) ranging from 3800 to 2 000 000 Daltons (Da) and a deacetylation degree - the proportion of glucosamine residues - of 66 to 100% [10]. Both, Mw and degree of deacetylation are determinant on various properties including solubility, biodegradability, toxicity, antimicrobial activity, transfection efficiency, etc [11]. The reactivity and polycationic character allow the production of a variety of formulations with different properties, ranging from hydrogels, rods and fibers to microparticles/nanoparticles (NPs) and membranes [12]. Chitosan and its derivatives may be sterilized by irradiation. Altogether, these properties make of medical grade CS a versatile material with extensive application in the biomedical and biotechnological fields [13]. Table 1 summarizes relevant biomedical applications.

Different types of CS-based nanoparticles have been conceived for applications in different fields of biomedical sciences, specifically in drug and gene delivery, cell imaging and biosensors. Its cationic character conferred by primary amino groups is responsible for a set of unique and attractive properties, namely drug loading and controlled release, enhanced cellular uptake, mucoadhesiveness, permeation and transfection enhancing, pH responsive behavior [14-16].

Table 1. Range of biomedical applications of CS-based materials.

Biomedical application	**Remarks**	**Ref.**
Artificial skin and wound healing	Structural similarity with glycosaminoglycans makes CS and its derivatives eligible for skin replacement; they support blood coagulation, prevent abnormal fibroblastic reactivity, and act as a bactericide and wound-healing accelerators.	3, 17-21
Orthopedic/ periodontal field	CS coating and calcium-based compounds with CS used as bone substitutes.	22-25
Tissue engineering	Porous biodegradable matrixes for cell seeding, proliferation and/or differentiation.	26-29
Ophthalmology	CS possesses the characteristics required for making contact lens: optical clarity, mechanical stability, satisfactory optical correction, gas permeability and wettability; ability to prolong ophthalmic drug retention.	30-33
Blood anticoagulants	Sulfated derivatives act as blood-thinner and lipoprotein lipase-releasing agents	34, 35
Hypocholesterolemic and hypolipidemic effects	CS reduces the plasma and liver triacylglycerol and total cholesterol owing to its binding capacity.	36, 37
Immune activity	CS Oligosaccharides induced innate immune responses by up-regulating IL-1, TNF-α and IFN-γ.	37
Homeostasis	CS interacts with the erythrocytes, linking them together to establish a cellular clot or hemostatic plug. CS hemostatic effect also extends to platelet aggregation.	38
Antimicrobial applications	Antibacterial, antifungal and antiparasitic activity	39-43
Drug delivery systems	CS has unique characteristics for drug delivery platforms, including its active primary amino groups for chemical modification, simple and mild preparation methods, and capacity to associate macromolecules/nucleic acids and facilitate their transport across mucosae.	44-46

1.2. Development of CS-based nanoparticles

CS NPs are widely studied as drug delivery systems. These carriers offer many advantages, providing targeted delivery of drugs, improving the bioavailability and stability of the therapeutic agents against chemical/enzymatic degradation [47]. The NPs may hold the cargo attached to the matrix, dissolved, encapsulated or entrapped [48].

Different methods have been used to prepare CS particulate systems, namely, ionotropic/ionic gelation, covalent cross-linking, emulsion cross-linking, coacervation/precipitation, emulsion droplet coalescence, reverse micelles, polymerization, and self-assembly [49-55]. The selection of one of these methods depends upon the specificities and requirements associated to each application, namely the physicochemical properties and thermal-chemical stability of the active agent, the envisaged release kinetic profile, biodistribution, cellular uptake efficiency and intracellular fate of the NPs, etc.

1.2.1. Ionotropic/ionic gelation

The complexation between oppositely charged macromolecules (polyelectrolyte complexes) has gathered considerable interest on CS NPs preparation, because the process is very simple and mild. So, CS NPs have been produced by autoaggregation of chitosan or its derivatives and macromolecules of opposite charge, through electrostatic interactions. The most commonly used ionic crosslinking agent is sodium tripolyphosphate (TPP),a non-toxic multivalent polyanion [56-59]. When an acidic solution of CS is added dropwise, under constant stirring, to the polyanionic TPP solution, the interaction between oppositely charged species, allows the ionic gelation to occur, giving rise to spherical particles (Figure 1). The particles size and surface charge can be modified by varying the ratio of CS and stabilizer. The efficiency of the method is dependent upon the deacetylation of CS, since the gelation process occurs through the interaction of the protonated amino groups of CS. One of the major drawbacks of this technique is the poor stability and mechanical properties of the NPs, thus limiting their usage in drug delivery.

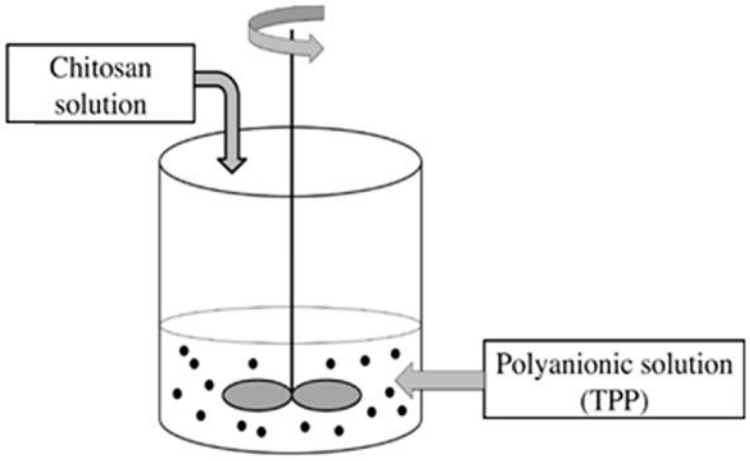

Figure 1. Preparation of CS NPs by the ionotropic gelation method.

Furthermore, the separation and redispersion processes are difficult to achieve. However, as ionic crosslinking can be performed at room temperature and in absence of organic solvent, this method has been largely used to produce CS-drug or gene complexes. The negatively charged DNA can also form polyelectrolyte complexes with cationic CS, through ionic gelation, as demonstrated by Mansouri *et al.* [60]. The CS properties, namely the Mw, degree of deacetylation and concentration used, have a significant impact on the properties of those NPs and on its performance as drug carriers [61-63].

1.2.2. Covalent cross-linking

CS NPs can also been produced though covalent bonds between CS backbone and a functional crosslinking agent. Among usually used coupling agents are glutaraldehyde, genipin, glyoxal, dextran sulfate, oxidized cyclodextrins, ethylene glycoldiglyceryl ether, epichlorohydrin, polyethylene glycol (PEG) dicarboxylic, etc. [64-67]. Ohya *et al.*[68] described the use of this method to produce CS NPs containing 5-fluorouracil with glutaraldehyde as cross-linking agent. This approach is often used to treat NPs already obtained by other strategies, in order to improve their properties. For instance, stable CS-thioglycolic acid NPs were obtained through ionic and covalent cross-linking [69]. Covalently crosslinked NPs showed improved stability in simulated body fluids and adhesion capacity to intestinal mucosal as compared to unmodified ionically cross-linked chitosan.

1.2.3. Emulsion crosslinking

This technique is based on the reaction between the primary amines and a multifunctional crosslinking agent bearing aldehyde groups. In this process, a CS solution in acetic acid is emulsified in liquid paraffin (w/o emulsion). The aqueous droplets are stabilized using a suitable surfactant. The emulsion is then reticulated with an appropriate crosslinking agent such as glutaraldehyde, to stabilize the polysaccharide droplets (Figure 2). The amount of crosslinking agent varies according to the crosslinking density required. The nanospheres are then washed and dried [70-72]. The incorporation of drugs is achieved by dispersion in the CS solution, in the beginning of the process, becoming entrapped during the crosslinking reaction. The entrapment efficiency may be improved by performing multiple emulsions [73]. Major drawbacks of this method are associated with the use of organic solvents and crosslinking agents, that may adversely affect the stability of proteins [74]. The complete removal of the unreacted - often toxic - crosslinker is difficult to achieve. Moreover, glutaraldehyde crosslinked NPs present negative effects on cell viability.

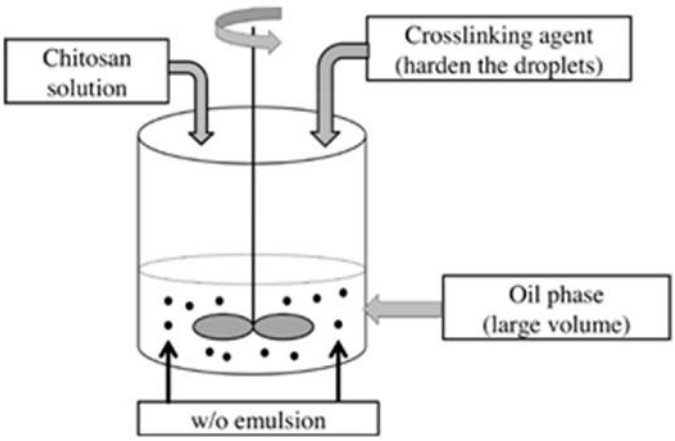

Figure 2. Emulsion crosslinking methodology for the preparation of CS NPs.

1.2.4. Coacervation/Precipitation

This method takes advantage of the physicochemical properties of CS. There are several approaches to achieve NPs precipitation/coacervation, all relying on CS solubility. Specifically, one of them relates to CS insolubility in alkaline pH. CS is dissolved in acidic solution and coacervates/precipitates in contact with an alkaline solution. Spraying the CS solution into sodium hydroxide, NaOH-methanol or ethanediamine alkaline solutions, using compressed air, originates coacervated droplets, forming the NPs [75]. Separation and purification of the particles is finally achieved by centrifugation, followed by successive washing steps with hot and cold water. The size of the NPs can be controlled changing the diameter of the compressed air nozzle. Another methodology is based on desolvation, where a flocculant (usually sodium sulfate) is added to a water CS solution under mild agitation and continuous sonication for 30 min. Progressive elimination of solvation water surrounding chitosan occurs as a consequence of the higher affinity of water for the salt. This process leads to the polymer insolubilisation and its consequent precipitation due to hydrogen bonds between molecules [76].

Yet anoother type is based on diffusion of emulsified solvent. The water phase containing CS and a stabilizer (e.g. poloxamer and lecithin) is dispersed in the organic phase (e.g. methylene chloride an acetone) containing the hydrophobic drug, under stirring. After emulsion homogenization, methylchloride is removed under reduced pressure at room temperature, leading to acetone diffusion to the aqueous phase, leading to decreasing on CS solubility allowing NPs formation upon polymer precipitation [76].

The drawbacks of this approach are the large NPs produced and the use of organic solvent [77].

1.2.5. Emulsion-Droplet Coalescence Method

This technique was developed by Tokumitsu *et al.* [54]. In this methodology, precipitation is induced by allowing CS droplets to combine with NaOH droplets. This method involves both emulsion crosslinking and precipitation. A stable emulsion containing the aqueous CS solution along with the drug in liquid paraffin oil is produced. A second emulsion, containing a NaOH solution, is produced in a similar way. When both emulsions are mixed under high-speed stir, droplets of each emulsion collide at random, coalesce, and finally precipitate as small size particles. NPs are obtained within the emulsion-droplets. The method is schematically shown in Figure 3. The particle size varies inversely with the CS degree of deacetylation [54].

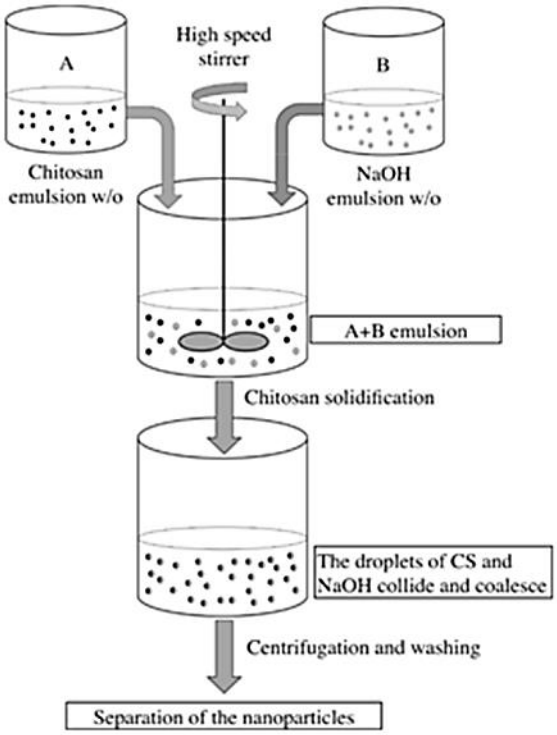

Figure 3.Production of CS NPs using the emulsion-droplet coalescence technique.

1.2.6. Reverse Micelles Method

Reverse micelles are thermodynamically stable liquid mixtures of water, oil and surfactant. Macroscopically, the emulsion is homogeneous and isotropic, structured on a

microscopic scale, with the aqueous and oil microdomains separated by surfactant-rich films. The aqueous core of the reverse micellar droplets can be used as a nanoreactor to prepare NPs. Since the size of the obtained reverse micellar droplets usually lies between 1 and 10 nm [76], the preparation of drug-loaded NPs will produce extremely fine particles with a narrow size distribution. In this technique, the reverse micelles are formed by dissolving a surfactant into an organic solvent, giving rise to a water-in-oil micellar system (Figure 4). The aqueous phase containing the CS and the drug are added to this emulsion with constant vortexing and the NPs forms in the core of the reverse micelles. An additional amount of water may be added to produce larger sized NPs. The maximum amount of drug that can be dissolved in reverse micelles has to be determined for each case, by gradually increasing the amount of drug, until the clear microemulsion is transformed into a translucent solution. To this transparent solution, a cross-linking agent is added with constant overnight stirring. The organic solvent is then evaporated. The material is redispersed in water with sonication and the surfactant is salted out. The mixture is finally centrifuged and the supernatant solution, which contains the drug-loaded NPs, is dialyzed and lyophilized to dry powder [77].

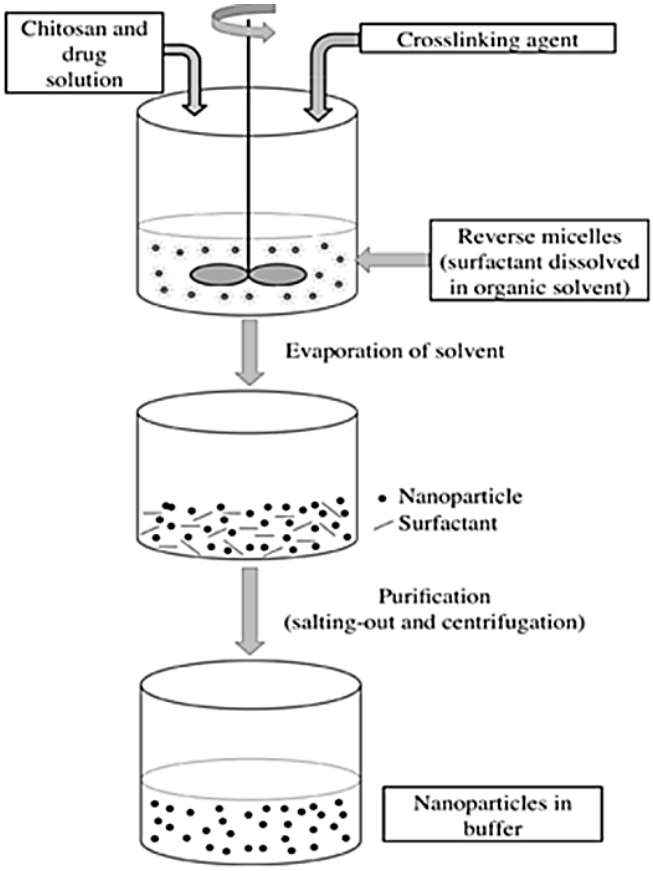

Figure 4. Reverse micelles method of preparation of CS NPs.

1.2.7. Radical polymerization

In this technique, the NPs are obtained upon template polymerization of acrylic monomers next to the chitosan backbone. CS is firstly dissolved in an acrylic monomer solution under magnetic stirring. Due to the ionic interaction, the negatively charged acrylic monomers align along the chitosan molecules. After complete dissolution of CS, the acrylic monomers polymerization is started by adding an initiator (e.g. $K_2S_2O_8$) under stirring at 70ºC. The complete polymerization leads to the appearance of an opalescent solution, indicating the NPs formation. The NPs solution is then filtered and dialysed to remove the residual monomers and initiator. The obtained NPs are positively charged, uniformly spherical and present a consistent size distribution (50 to 400 nm) [49, 78].

1.2.8. Self-assembly

The self-assembly process, defined as the autonomous organization of components into structurally well-defined aggregates, is characterized by numerous beneficial attributes; it is cost-effective, versatile and facile. The process occurs towards the system's thermodynamic minima, resulting in stable and robust structures. These characteristics simplify the nanogel development, allowing the scale-up [79].

Molecular self-assembly is characterized by diffusion followed by specific association of molecules through non-covalent interactions, including electrostatic, hydrogen bonds and/or hydrophobic associations. Individually, such interactions are weak, but dominate the structural and conformational behavior of the assembly due to the large number of interactions involved. While oppositely charged polysaccharides associate readily as a result of electrostatic attractions, interactions among neutral polysaccharides tend to be weaker, or nonexistent, a modification with chemical entities able to trigger assembly being necessary [80]. Hydrophobically modified CS is an interesting strategy, consisting on chemical linkage of hydrophobic compounds on hydrophilic backbone, to induce the formation of NPs via hydrophobic interactions [55, 81-83]. Upon contact with an aqueous environment, hydrophobically modified CS spontaneously form self-aggregated NPs, via intra- or intermolecular associations between the hydrophobic moieties, primarily to minimize the interfacial free energy.

1.3. Biomedical applications

The biomedical application for CS nanogels is particularly relevant concerning the development of delivery systems for biopharmaceuticals, although many papers describe also its use as carriers for low molecular weight drugs. The recent progresses in these biomedical applications are reviewed in this section.

1.3.1. Protein/peptide delivery

Therapeutic proteins are becoming available for the treatment of a wide range of diseases, such as cancer, autoimmune diseases, infections, and metabolic disorders. A main problem limiting the efficiency of protein therapeutics is the reduced stability and short circulation half-lives after parenteral administration (i.e. intravenous, intramuscular, or subcutaneous) [84]. As a result of the invasive nature, injectable formulations are frequently faced with patient discomfort and noncompliance. In the case of proteins, susceptibility to proteolysis and colloidal instability are additional difficulties. Consequently, a high drug concentration or a high dosing frequency becomes necessary, which may lead to adverse side effects [85-88]. Thus, drug delivery systems are urgently needed for the enhancement of the protein/peptide solubility and bioavailability, allowing a controlled and sustained release instead of burst release, avoiding undesirable side-effects, improving biodistribution and enabling the targeting of the diseased tissue *in vivo* [89]. Aiming at achieving an effective protein/peptide delivery, carriers such as liposomes and micro- and NPs have been developed [90-93]. Among them, nanometer-sized polymeric hydrogels have attracted growing interest. CS NPs have been tested as carriers for proteins, peptides and oligosaccharides [94-96].

Usually, proteins and vaccines are delivered via parenteral routes, due to their low bioavailability and/or poor immunogenicity when administered via non-parenteral routes. In recent years, substantial progresses have been made on the use of non-invasive routes, such as mucosal (oral, nasal, pulmonary and colon) and transdermal, for the delivery of proteins and vaccines, yielding better patient compliance [97, 98].

1.3.1.1. Oral delivery

The oral protein delivery should fulfill the following prerequisites: pH-sensitive behavior, protecting the drug at the stomach pH and releasing it at the intestine; targeted

release, i.e., close to the absorption surface to avoid intestinal proteases; selective and reversible opening of the tight junctions; controlled and sustained released, to achieve the physiological drug concentration in blood; biocompatibility [95, 99, 100]. It has been reported that CS gathers all these criteria. Being a mucoadhesive polymer, it is able to enhance absorption in the intestinal lumen, transient opening of the tight junctions in the mucosal membrane, enabling good protein transport [101-103]. The mucoadhesive properties are attributed to an interaction between the positively charged CS and the negatively charged sialic and sulphonic acids of the mucus, which provides a prolonged contact time with the mucosal surface, thereby promoting absorption [104, 105]. It has also been suggested that interactions of the CS positively charged amino groups with the negatively charged cell surfaces and tight junctions, induce a redistribution of F-actin and tight junction's protein ZO-1, which triggers the increased paracellular permeability.

Nevertheless, at neutral pH CS is not soluble in aqueous solution, which can be a barrier for its application as a potential oral insulin delivery system. This poor solubility can be improved by derivatization of the amine group or adding the hydrophilic ethylene glycol group on C-2 position, yielding GC and rendering the polymer soluble [95].

Lin *et al.* [106] reported the production, by ionic gelation, of NPs composed of CS and poly-γ-glutamic acid (γ-PGA) for insulin delivery. In the gastrointestinal tract, the pH varies from acidic in the stomach to slightly alkaline in the small intestine. The fasting pH of the stomach is about 2.5 to 3.7, but in the presence of food, it drops to about 1.0 to 2.0, due to hydrochloric acid secreted by parietal cells. The proximal part of the small intestine (duodenum) has a pH value of about 6.0–6.6 due to neutralization of the acid by bicarbonates secreted by the duodenal mucosa and pancreas. The jejunum and ileum are the middle portion and terminal part of the small intestine, respectively, and their pH values are about 7.4. Therefore, characterization of NPs at distinct pH values, simulating the environments of the gastrointentinal tract, was investigated. The stability and functionality of NPs were studied *in vitro*, using Caco-2 cell monolayers, and *in vivo*, in a rat model. The pKa values of CS and γ-PGA are 6.5 and 2.9, respectively. In the range of pH 2.5–6.6, CS and γ-PGA are ionized and can form polyelectrolyte complexes, which results in a spherical shaped structure. Outside of this pH range, the NPs become unstable and subsequently broken apart. This is because, at pH 1.2, γ-PGA is not charged. Therefore, the little electrostatic interaction between the positively

charged CS and the neutral γ-PGA causes the instability of NPs. Similarly, at pH 7.4, CS is neutral and thus NPs collapse. The authors observed that the CS NPs could transiently and reversibly open the tight junctions between Caco-2 cells, thus enhancing the paracellular permeability. However, the CS NPs at pH 7.4 appear to be less effective in opening tight junctions than at pH 6.6, due to the less positively charged CS. The pH sensitivity and functionality of the CS NPs were confirmed in an animal study. At the duodenum (pH 6.0–6.6), while adhering and infiltrating into the mucus layer, the orally administered NPs may be degraded due to the presence of digestive enzymes in the intestinal fluids. Additionally, the pH environment may be changed (becoming neutral) while the NPs were infiltrating into the mucosa layer and approaching the intestinal epithelial cells. This may further lead to the collapse of NPs due to the change in the exposed pH environment. The dissociated CS from the degraded/collapsed NPs is then able to interact and modulate the function of ZO-1 proteins between epithelial cells. ZO-1 proteins are thought to link the occludin and actin cytoskeleton, playing important roles in the rearrangement of cell–cell contacts. Oral intake of NPs/insulin demonstrated a sustained decrease of the blood glucose level over a long period of time, at least 10 h. In a further development of this work, Sonaje *et al.* [107] prepared self-assembled NPs, by mixing γ-PGA with CS in the presence of $MgSO_4$ and TPP. The introduction of $MgSO_4$ in the preparation of CS NPs improved the stability in a broader pH range. The intestinal paracellular transport of insulin was investigated using Caco-2 cell monolayers. Additionally, the efficacy of NPs for oral delivery and intestinal absorption of insulin was investigated, in a diabetic rat model. Similarly to previous studies, the *In vitro* results showed that the mucoadhesive properties of CS NPs are affected by the pH and additionally, the transport of insulin across Caco-2 cell monolayers is pH-dependent: with increasing pH, the amount of insulin transported decreased significantly, due to the lower positive surface charge of the NPs, hence lower mucoadhesive and absorption enhancement ability. In addition, oral administration of insulin-loaded NPs demonstrated a significant hypoglycemic action for at least 10 hours, in diabetic rats. Based on the work of Lin *et al.* [106] and Sonaje *et al.* [107], a mechanism for the paracellular delivery of insulin through the gastrointestinal tract using CS NPs was proposed (Figure 5).

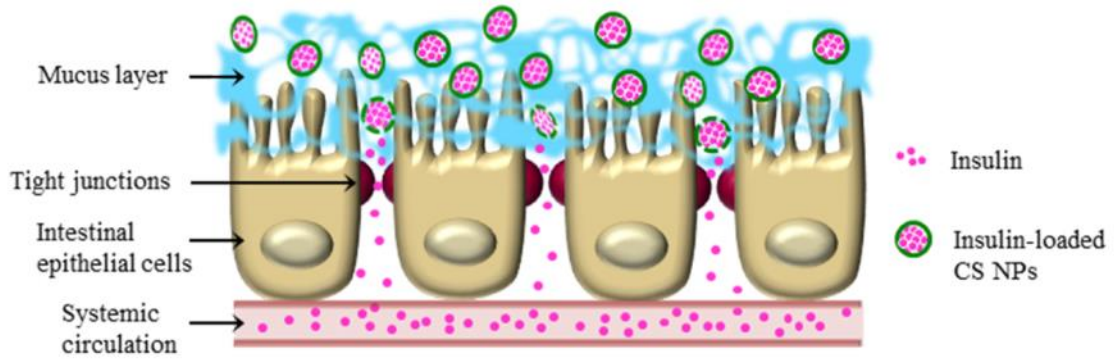

Figure 5. Schematic illustration of the hypothetic mechanism of the paracellular transport of insulin released from CS NPs via oral administration. NPs adhere and infiltrate into the mucus layer of intestinal epithelium. The infiltrated NPs disintegrate due the near neutral pH and release the loaded insulin; simultaneously, the CS opens the tight junctions allowing the insulin permeation through the paracellular pathway.

Despite some encouraging results, the poor solubility at physiological pH is a limitation for a more effective use of CS based NPs. Indeed, it has been shown that only protonated – soluble – CS can trigger the opening of the tight junctions, facilitating the paracellular transport of hydrophilic compounds [108]. The pH of the intestinal lumen is higher than the CS pKa (6.5), limiting its efficiency as an absorption enhancer and suitability for protein delivery in neutral and physiological environments. Notwithstanding, recent *in vitro* and *in vivo* studies have been published showing the potential of CS/insulin self-assembled NPs (complexes obtained by electrostatic interaction) as important vehicles for delivering insulin via oral route [109].

Introducing a permanent positive charge, such as with TMC, is a way of increasing physiological aqueous solubility of the polymer, thereby enabling effective permeation enhancement on mucosal surfaces [100, 102, 110]. In an attempt to combine the mucoadhesion and the permeation enhancing effects of TMC and thiolated polymers, Yin *et al.* [111] synthetized a TMC-cysteine conjugate. Thiolated polymers have been developed as a category of mucoadhesive polymers with reactive thiol groups immobilized on the polymeric structure. They can tightly and long lasting adhere to the intestinal mucus layer, through covalent bonding with mucin glycoproteins, via thiol-disulfide exchange reactions, hence providing a steep drug concentration gradient at the absorption sites and exerting an additional permeation enhancing effect. But, as thiolated CS is also insoluble at physiological pH, which restricts its application, a TMC-cysteine/insulin NPs were prepared through self-assembly driven by the electrostatic interaction between oppositely charged TMC-cysteine and insulin. The authors [111] confirmed that, when reaching the small intestine, the positively charged

NPs are directed to the mucus layer, through electrostatic interaction with the negatively charged sialic acid residues on mucin glycoproteins. Meanwhile, the free thiol groups on TMC-cysteine are oxidized at neutral pH and disulfide bonds form between TMC-cystein and cysteine-rich mucin, contributing to the notably higher amount of NPs immobilized in the mucus layer. So, mucoadhesion and permeation enhancing effects are significantly higher due to the presence of cysteine conjugates. Besides being biocompatible, TMC-cysteine NPs showed improved hypoglycemic effect following both oral and ileal administration in normal rats, as compared with TMC NPs.

Other strategies to overcome the CS solubility drawback have been developed. Qian *et al.* [112] produced hydrophilic CS NPs by free radical polymerization of methyl methacrylate, N-dimethylaminoethyl methacrylate hydrochloride, or N-trimethylaminoathyl methacrylate chloride, which show a higher solubility in a broader pH range. These graft copolymer NPs enhanced the absorption and improved the bioavailability of insulin via gastrointestinal tract of normal rats.

Acid-stable CS NPs formulated by ionic cross-linking with hydroxypropyl methylcellulose phthalate (HPMCP), a pH-sensitive polymer, were also used for the oral delivery of insulin [113]. The pKa of the free carboxylic groups of HPMCP is approximately 5.2, which becomes negatively charged at higher pH values and represents the driving force for the electrostatic interaction with CS. This formulation was able to protect insulin against pepsin degradation and showed improved mucosal adhesion when compared to CS/TPP formulation. These results could be attributed to the ability of HPMCP to protect CS NPs from dissociation in the stomach owing to its pH stability. Therefore, higher percentage of intact particles could reach the small intestine and interact with the intestinal membrane. These improvements –higher resistance against acid degradation and higher fraction of the intact NPs that could reach and adhere to the site of absorption in the small intestine - were certainly responsible for a higher and prolonged hypoglycemic effect observed with CS/HPMCP NPs. By virtue of the mucoadhesive and permeation enhancing properties of CS, CS/HPMCP NPs could promote the absorption of the released insulin via the paracellular pathway, as well as by transcytosis of the encapsulated protein through the intestinal enterocytes and Peyer's patches.

CS/cyclodextrin NPs in addition to being used for insulin delivery [114], their potential for peptide glutathione oral delivery have already been studied by Trapani *et al.* [115]. CS or CS/ cyclodextrin based NPs were prepared according to a modified ionic gelation

method. The release properties of the gluthatione, located in the NPs core based on cyclodextrin, could be modulated by selecting an appropriate cyclodextrin type. Transport studies performed in the frog intestine model confirmed that both CS and CS/cyclodextrin NPs could induce permeabilization of the intestinal epithelia. However, CS/sulphobutyl ether-β-cyclodextrin NPs were able to provide significant enhancement in GSH transport in all segments of the duodenum, whereas CS NPs effect was restricted to the first segment of the duodenum.

Lalatsa *et al.* [116, 117] have been explored the use of quaternary ammonium palmitoyl GC NPs for peptides brain delivery following orally administration. Analyzed the oral biodistribution of radiolabeled NPs, the oral biodistribution of the model peptide leucine-enkephalin and coherent anti-Stokes Raman scattering microscopy tissue images after an oral dose of deuterated NPs concluded that although only 10-15% of orally administered NPs were absorbed from the gastrointestinal tract, about 2–3% of the oral NPs dose is detected in the blood 30 min after dosing. They also verified that only peptide loaded polymeric particles with a polymer Mw greater than 6 kDa were able to taken up by enterocytes and peptide delivery to the brain after oral administration. Thus amphiphilic GC NPs facilitate oral peptide absorption by protecting it from gastrointestinal degradation, adhering to the mucus increasing residence time, transport across the enterocytes and to the systemic circulation, where NPs stabilized peptide during transport to the brain.

1.3.1.2. Nasal delivery

The nasal mucosa is an attractive route for the delivery of vaccines because it has a relatively large absorptive surface and low proteolytic activity [118-124]. Importantly, nasally administered vaccines can induce both local and systemic immune responses. However, most proteins are not well absorbed from the nasal cavity when administered as simple solutions. The major factors limiting the absorption of nasally administered proteins are the poor ability to cross the nasal epithelia, and the mucociliary clearance, which rapidly removes protein solutions from the absorption site [118, 119, 125]. Mucoadhesive, hydrophilic NPs have received much attention to overcome these obstacles and deliver protein antigens via the nasal route, because they strongly attach the mucosa increasing mucin viscosity [118, 121, 125, 126]. By these means, mucoadhesive NPs in particular CS-based delivery nanocarriers are able to decrease the nasal

mucociliary clearance rate and thus increase the residence time of the formulation in the nasal cavity [127, 128].

Amidi and colleagues [129] prepared and characterized protein loaded TMC NPs as a nasal delivery system, by ionic crosslinking a TMC solution (with or without ovalbumin, the model protein studied) with TPP. It was observed that TMC NPs have a high loading efficiency (fraction of protein loaded) and capacity (amount of protein loaded per NPs dry weight) up to 50% (w/w). The integrity of the entrapped ovalbumin was preserved and release studies showed that more than 70% of the protein remained associated with the NPs for at least 3h of incubation in PBS (pH 7.4), at 37ºC. Regarding biocompatibility, the NPs were non-cytotoxic, whereas a partially reversible cilio-inhibiting effect on the chicken trachea was observed. *In vivo* uptake studies indicated the transport of the protein across the nasal mucosa. Other authors tested CS NPs as a nasal delivery system for insulin. Zhang *et al.* [130] used PEG-grafted CS NPs to improve the systemic absorption of insulin, following nasal administration. The NPs were prepared by ionotropic gelation using TPP ions as the crosslinking agent. *In vitro* release studies showed an initial burst, followed by a slow release of insulin. Intranasal administration of the NPs in rabbits enhanced the absorption of insulin to a greater extent than the free protein. The nasal delivery of insulin using CS-acetyl-L-cysteine NPs was proposed by Wang *et al.* [131], showing that intranasal administration of these NPs in rats enhanced the protein absorption by the nasal mucosa

Immunization studies were performed using the Hepatitis B virus surface antigen loaded on TMC NPs, administrated by intranasal delivery as described by Subbiah *et al.* [123]. Cumulative release of the antigen was achieved *In vitro* over prolonged period of 43 days. The *in vivo* immunological study performed in mice model showed adjuvant efficiency of NPs and improved stability of the antigen [122-124, 129]. The great interest in mucosal vaccine delivery arises from the fact that mucosal surfaces represent the major site of entry for many pathogens. Hence, mucosal vaccine strategies have emerged as a viable and attractive alternative to parenteral immunization. Advantages associated with mucosal vaccination are numerous: easy and low cost of administration, patient compliance, avoidance of the hepatic first pass metabolism and ability to induce mucosal as well as systemic immunity. Furthermore, the immune response generated at one mucosal site is able to induce a strong immune response at distal mucosal surfaces [132]. Westerink *et al.* [133] examined the effect of mucosal administration of tetanus toxoid in the presence of a non-ionic copolymer, Pluronic® F127 with CS or

lysophosphatidylcholine, on the systemic and mucosal immune response. The results suggest that the two components of Pluronic/CS appear to exert an additive or synergistic effect on the immune response. Intranasal administration with recombinant influenza hemagglutinin antigen or inactivated virus loaded poly γ-PGA/CS NPs was performed by Moon *et al.* [134] Intranasal immunization with this mixture triggered high anti-hemagglutinin immunoglobulin A (IgA) response in lung and IgG in serum, as well as hemagglutinin-neutralizing antibodies, besides producing an influenza virus-specific cell mediated immune response. Actually, intranasal administration of this formulation was able to show a complete protection against challenge with lethal doses of the highly pathogenic influenza A H5N1 virus. Moreover, PC NPs showed to be equivalent to potent mucosal adjuvant, cholera toxin.

1.3.1.3. Pulmonary delivery

Pulmonary drug delivery for both local and systemic treatments has many advantages over other delivery routes. The lungs have a large surface area (43 to 102 m^2) [135]. In addition, mucociliary clearance is slower at the alveoli of the lungs than in the airways. Furthermore, the epithelium is thinner and more permeable, making possible the systemic absorption of peptides and proteins. Indeed, a number of high Mw drugs were demonstrated to be absorbed successfully through the lungs [135-137]. The successful delivery of the inhaled particles depends mostly on their size and density, and hence, on the aerodynamic diameter. To deposit protein formulations efficiently into the lungs, they preferably have aerodynamic diameters ranging from 1 – 5 μm [97, 138]. Independently of the method used to produce the aerosol, before reaching the deep lung, inhaled particles must overcome certain obstacles and lung defense mechanisms, essentially the effect of the branched airways structure and the mucus layer, which protects the epithelium in the tracheobronchial region. Particles targeted to the deep lung should be small enough to pass through the mouth, throat and conducting airways; however, if too small, they may fail to deposit, being breathed out again. Even with a right aerodynamic diameter, a certain number of particles will be transported away from the lung by mucociliary clearance [138, 139]. Once in the deep lung, particles will have to face at least two other defense mechanisms: the alveolar macrophages, and the enzymatic activity. The alveolar surface is covered by a thin layer of fluid with suspended macrophages, which play an important role in the lung defense. With the

capacity of moving freely in the surface, they are able to engulf "foreign" substances from the airway surface, eliminating potentially damaging agents [139]. There is no consensus concerning the ideal size range to avoid or delay phagocytosis; however, it has been reported that the phagocytic activity is maximum for particles of 1–2 μm, decreasing for both smaller and larger particles out of this range [140]. Concerning the second defense mechanism (enzymatic activity), it is known that the lung presents a lower enzymatic activity when compared to other mucosal surfaces, such as the gastric.inc.

CS and its derivatives have been extensively studied as an attractive system for transmucosal drug delivery, e.g. pulmonary administration. The transport of insulin loaded on CS NPs to the deep lung, where it is absorbed into systemic circulation, was evaluated *in vivo* by Al-Qadi *et al.* [141]The insulin-loaded CS NPs, prepared by ionotropic gelation, were co-spray dried with mannitol resulting in a dry powder with suitable aerodynamic properties for deposition in deep lungs. Plasmatic glucose levels after intratracheal administration to rats showed that the microencapsulated insulin-loaded CS NPs induced a more pronounced and prolonged hypoglycemic effect when compared to the controls.

Benediktsdóttir *et al.* [102] using the VA10 cell line, which resembles the native bronchial epithelia, found that TMC did not cause any alterations in the tight junction protein claudin-4 or in F-actin architecture. However, F-actin disbandment or redistribution plays a role in the permeation enhancing properties of CS. Actually they found that a reversibly decrease of the transepithelial electrical resistance, was responsible for the enhanced permeation caused by TMC.

1.3.1.4. Colon delivery

Colon targeted drug delivery is useful in improving the absorption of peptide drugs via the gastrointestinal tract. Site specific drug delivery to the colon is of special interest for drugs instable in the upper part of the gastrointestinal tract, because of the peptidase activity in the small intestine. The colon is thought to have lower enzymatic activity than other regions of the gastrointestinal, hence a greater absorption efficiency in this region would be expected, as long as the proteins/peptides are released locally [142]. Due to negligible activity of brush-border membrane and much less activity of peptidases

and pancreatic enzymes, the colon has been considered suitable for the delivery of peptides and proteins.

Bayat *et al.* [143] developed a nanoparticulate system using two new quarternized derivatives of CS, triethyl CS and dimethylethyl CS, for insulin colon delivery. Insulin/(CS, triethyl CS and dimethylethyl CS) NPs were prepared by the polyelectrolyte complexation method. The three kinds of NPs showed a positive charge that could facilitate insulin uptake, allowing a low bursting effect and a steady release of insulin *In vitro*. Triethyl CS and dimethylethyl CS NPs had smaller particle size, higher insulin loading capacity, improved transport and absorption of insulin in gastrointestinal tract and higher blood glucose lowering effect after injection into ascending colon, as compared with CS NPs.

Numerous studies highlight the importance of CS NPs for protein, peptide and oligosaccharide delivery, as summarized in table 2.

1.3.2. Gene delivery

Gene therapy is an emerging field in medical and pharmaceutical sciences, a very promising one due its potential for the treatment of a wide range of diseases, both inborn and acquired, by replacing defective genes, substituting missing ones, or silencing unwanted gene expression. However, naked therapeutic genes are rapidly degraded by nucleases, showing poor and non-specific cellular uptake and also low transfection efficiency [144]. Hence, the development of safe and efficient gene carriers is primordial for the success of gene therapy. Gene delivery systems include viral vectors, cationic liposomes and polycationic complexes. In spite of high transfection efficiency, the immune and oncogenic responses associated to viral vectors limit their therapeutic applications *in vivo*. To overcome these limitations, non-viral delivery systems (cationic liposomes and cationic polymers) have been proposed as a safer alternative. Besides being functional groups with targeting ability. On the other hand, there is some controversy around its transfection efficiency; some reports suggest this is relatively low, compromising potential clinical easily synthesized in large-scale, these nanoparticulate systems are targetable, have low immune response and high DNA packaging capacity[145]. Non-viral systems, based on cationic polymers bearing amine groups in their backbone, are now extensively used as gene carriers; they form stable complexes with DNA, keeping it safe from nuclease degradation, and readily interact

with cells membrane. Among non-viral vectors, CS and its derivatives are good delivery systems for DNA, antisense oligodeoxynucleotides and siRNA. CS gathers a number of desirable characteristics that explain its use in more than 80% of NPs designed for genes and interfering components: cationic charge, biodegradability, biocompatibility, low toxicity, mucoadhesivness and application, while others reinforce its transfection ability [146]. Several studies have been carried out to elucidate the influence of the CS-based formulation parameters on the gene expression [144]. In this section, we review the state of the art of DNA and siRNA CS-based delivery systems.

Table 2. Representative examples of the use CS NPs for proteins, peptides, and oligosaccharide delivery.

Route of administration	Method of preparation	Remarks	Ref.
Therapeutic agent / Associated disease: Insulin / Diabetes Mellitus			
Oral	pH-responsive NP system composed of CS and γ-PGA	CS NPs can adhere and infiltrate the mucus layer. The NPs release insulin that moves across the opened paracellular pathway into the systemic circulation. CS NPs showed superiority over the injectable insulin.	147
	Functional NPs were prepared by mixing cationic CS with anionic γ-PGA-Diethylene triamine pentaacetic acid conjugate.	Diethylene triamine pentaacetic acid was used exploiting its ability to disrupt intestinal tight junctions and inhibit intestinal proteases. pH responsive behavior was achieved due to γ-PGA. NPs could promote the insulin absorption throughout the entire small intestine and produced a prolonged reduction in blood glucose levels.	148
	CS and γ-PGA NPs were prepared by an ionic-gelation method	Enteric-coated capsule loaded with freeze-dried CS NPs remain intact upon oral administration in acidic environment of stomach, but dissolved rapidly in the proximal segment of the small intestine, releasing the NPs. Thus enhanced intestinal insulin absorption was achieved, providing a prolonged reduction in blood glucose levels.	149
Pulmonary	Low Mw CS NPs prepared by solvent evaporation method.	*In vivo* administration of CS NPs containing insulin showed hypoglycemic activity.	150
Therapeutic agent/Associated disease: Calcitonin / Osteoporosis			
Oral	CS–PEG nanocapsules obtained by the solvent displacement technique.	*In vivo* studies showed that CS–PEG nanocapsules enhance and prolong the intestinal absorption of salmon calcitonin.	151
Pulmonary	Surface-modified poly(D,L-lactide-co-glycolide) (PLGA) NPs with CS prepared by the emulsion solvent diffusion method.	CS-modified PLGA NPs loaded with calcitonin reduced blood calcium levels to 80% of the initial concentration and prolonged the pharmacological action to 24 h.	152
	NPs based GC coupled with thioglycolic acid were obtained by ionic gelation with TPP.	Enhanced mucoadhesion to lung tissue of the GC– thioglycolic acid NPs as compared to non-thiolated NPs. Calcitonin-loaded GC and GC– thioglycolic acid NPs resulted in a pronounced hypocalcemic effect for at least 12 and 24 h.	153
Therapeutic agent / Effect: Heparin / Anticoagulant and anti-astmathic			
Oral	NPs prepared by ionic gelation method with heparin.	No significant anticoagulant activity was detected after oral administration of the free heparin solution in a rat model, while administration of NPs was effective in the delivery of heparin into the blood stream	154
Pulmonary	CS and GC NPs prepared by ionotropic gelation, containing the surfactant Lipoid S100.	Low Mw heparin loaded GC NPs prepared at neutral pH was efficiently delivered to blood stream following pulmonary aerosolization.	155

(Table 2. continued)

Therapeutic agent / Effect: Cyclosporin-A / Immunosuppressant and extraocular disorders			
Ocular	Cyclosporin-A-loaded CS NPs obtained using the spray-drying technique.	*In vivo* studies performed in sheep model showed that cyclosporin-A was found in aqueous and vitreous humour samples over 72 h, assuming prolonged release of active agent from positively charged CS formulations, attributed to enhanced residence time at the corneal and conjunctival surfaces.	156
Therapeutic agent/Associated disease: Prolidase / Prolidase deficiency			
Parenteral	CS NPs prepared by combining ionotropic gelation, with TPP, and ultrasonication treatment.	*Ex vivo* experiments performed by incubating different amounts of prolidase loaded CS NPs with skin human fibroblasts from prolidase deficient patients for scheduled times.	157
	CS NPs loaded with PEGylated prolidase,obtained by combining ionotropic gelation and ultrasonication treatment.	The *ex vivo* evaluation of prolidase activity on PD fibroblasts indicated a good level of prolidase activity replacement up to 10 days.	158
Therapeutic agent / Effect: RGD / Anti-carcinogenic			
Intratumoral	Hydrophobically modified GC NPs containing a cyclic RGD peptide prepared by a solvent evaporation method.	Intratumoral administration of RGD- hydrophobically modified GC significantly decreased tumor growth and microvessel density compared to native RGD peptide injected either intravenously or intratumorally.	159
Therapeutic agent / Purpose: Tetanus toxoid / Tetanus vaccination			
Nasal	PEG-coated poly(lactic acid) (PLA) NPs, CS-coated PLGA NPs, and CS NPs prepared by ionotropic gelation with TPP.	The coating of PLGA NPs with the mucoadhesive polymer CS improved the stability of the particles in the presence of lysozyme. Moreover, these particles were very efficient in improving the local and systemic immune responses to tetanus toxoid.	160
Therapeutic agent / Associated disease: Anti-neuroexcitation peptide (ANEP) / Neuroexcitation associated diseases			
Intravenous	ANEP-loaded TMC NPs prepared by ionic crosslinking of TMC with TPP.	The results showed that the targetability of ANEP to brain was significantly increased by TMC NPs. Absorptive-mediated transcytosis was believed to be the main pathway for the brain-targeting of ANEP-TMC/NPs.	161
Therapeutic agent /Effect: Leucine-enkephalin (Leu-Enk) / neurotransmitter or neuromodulator			
Nasal	TMC NPs were prepared by ionic gelation method	Permeability of Leu-Enk released from NPs was 35 fold improved from the nasal mucosa as compared to Leu-Enk solution. Enhanced brain uptake of Leu-Enk, when administered by TMC NPs resulted into significant improvement in the antinociceptive effect of Leu-Enk.	94
Therapeutic agent / Effect: Bone morphogenetic protein-2 (BMP-2) / pro-osteogenic and pro-angiogenic			
Local rabbit radius defect	Complex coacervation method was adapted to formulate 2-N,6-O-sulfated CS based NPs	A gelatin based implant with BMP-2 loaded NP showed an initial burst release of 15% (24 h) and a gradual release for 21 days to 77.8%. Peripheral and new vessels formation were significantly increased by the BMP-2/NP treatment, along with the bridged defects so early as 2 weeks, in healed defects at 8 weeks and the reunion of bone marrow cavity at 12 weeks.	162

1.3.2.1. CS features influencing transfection

Many reports highlight the potential of CS as an efficient polymeric gene carrier. At acidic pH, below the pKa, the primary amines in the CS backbone are positively charged and interact with negatively charged DNA leading to the spontaneous formation of nanosized complexes. Under neutral or alkaline conditions, CS is only slightly charged, thus the CS and DNA binding is stabilized mainly by hydrogen bonding and hydrophobic interactions [163]. DNA can be carried entrapped into the NPs by hydrophobic [164] or ionic interactions [165]. Numerous factors influence the stability and transfection efficiency of CS-based systems, including Mw, degree of deacetylation, stoichiometry of CS's nitrogen and DNA's phosphate (N/P ratio), pH, serum and additives, which will be discussed below.

The CS Mw has a major influence on the size of the NPs, the CS/DNA complex stability [166], the unpacking of DNA after endocytosis and thus, overall, on the transfection efficiency [167]. Huang *et al.* [168] reported that CS with low Mw (< 20 kDa) only poorly retains the DNA upon dilution, consequentially being less capable of protecting it from degradation by DNase and serum components, resulting in low transfection efficiencies. Also Xu *et al.* [169] found that long chain length TMCs, in comparison to short chain length, mediated higher gene transfection. According to this authors, polycation-DNA polyplex stability, addition of polycation free chains in solution (unbound from polyplex), cellular uptake pathway, and intracellular trafficking were the key factors that determined higher transfection efficiency, more than polycation-DNA polyplex binding affinity, particle size in water, zeta-potential, serum, cytotoxicity, and cellular uptake efficiency. On the other hand, Köpping-Höggard *et al.* [170] developed highly effective gene delivery systems using CS oligomers (1.2 to 10 kDa). The easier dissociation of the polyplexes was reflected in a greater gene expression, when compared to the more stable high-molecular-weight ultrapure CS-DNA polyplexes. Consequently, a balance between polyplex stability and polyplex unpacking must be achieved: the optimal CS Mw that allow extracellular DNA protection (favored by high Mw) versus efficient intracellular DNA release (favored by low Mw), in order to optimize the levels of transfection [144, 171].

Higher degree of deacetylation results in increased positive charge, hence greater DNA binding capacity and cellular uptake [144, 171]. According to Köpping-Höggard *et al.* [172], only CS with high charge density form stable complexes with pDNA. Similarly,

Huang *et al.* [168] observed that CS with low Mw or degree of deacetylation (46 kDa and 61%, respectively) did not retain DNA efficiently and showed poor cellular uptake. Also, Kiang *et al.* [173] concluded that the DNA binding efficacy decrease for degree of deacetylation < 70%, resulting in low luciferase expression, due to the particle destabilization caused by the bulky acetyl groups in the polymer chains. Lavertu *et al.* [174] reported as well high levels of luciferase expression, equivalent to those obtained with positive controls (Lipofectamine TM and FuGENE 6), using CS formulations with degree of deacetylation >80% and low Mw (10kDa), at pH 6.5.

The surface charge of the polyplexes depends on the N/P ratio, which influences the particles ability to interact with the negatively charged cell membrane [175]. Ishii *et al.* [176] reported that the transfection efficiency increases for charge ratios of 3 and 5, decreasing for further higher values. Another study, developed by Kim *et al.* [177] using galactosylated CS/DNA, showed that complete shielding of DNA occurs at charge ratio of 5, with no significant improvement in the range 5–20. Galactosylated CS/DNA complexes with charge ratio above 5 (slightly positive zeta potential) were suitable for effective gene transfer. The most enhanced stability was obtained at charge ratio 10, due to the prevention of self-aggregation.

It has been suggested that strong interactions between CS and DNA results in highly stable particles, thereby preventing dissociation within the cell and leading to the absence of DNA translation. Attempting to reduce the CS-DNA interaction, Douglas *et al.* [178] associated an anionic biopolymer (alginate, 12–80 kDa) with low Mw CS (10 kDa and 90% of degree of deacetylation). The presence of alginate in the complexes improved the yield of cell transfection. With the same aim, Duceppe *et al.* [167] used NPs made of ultra low Mw CS (<10 kDa)/Hyaluronic acid, as a novel potential carrier for gene delivery. Addition of hyaluronic acid to the NP formulation improved transfection rate from 0,7 to 25%. Peng and colleagues [179] demonstrated that mixtures of CS, DNA and γ-PGA in aqueous media lead to the formation of "compounded NPs", containing domains of CS/DNA and CS/γ-PGA. With this internal structure, the compounded NPs might disintegrate into a number of even smaller sub-particles, after cellular internalization, improving the dissociation capacity of CS and DNA. Consequently, an improved transfection was obtained. Liao *et al.* [180] also added γ-PGA to CS/DNA complexes, achieving higher cellular uptake (via a γ-PGA-specific receptor-mediated

pathway) and expedite intracellular unpacking due to electrostatic repulsion. So, enhanced gene expression was found when compared with their CS/DNA counterparts.

The transfection efficiency of the CS complexes is dependent on the pH of the culture medium. A pH slightly below 7 is optimal to achieve a good balance between DNA association and dissociation [144]. However, the polyplex stability under different pH is also important [181]. At pH 5.5, unmodified CS was most efficient in the DNA condensation. Conversely, when the pH was adjusted to 7.4, in the presence of high ionic strength, the condensation was strongly compromised, due to the reduction of both the degree of ionization and solubility. As reported by Kadyala *et al.* [182], the higher rate of transport of CS-based NP in Caco-2 cell layers occur at pH 5.5, because increasing the pH decreases the transport efficiency by 3 and 10-folds, for pH 6.4 and 7.4 respectively, owing to the NPs aggregation. It is therefore essential the use of CS derivatives with a broad range of pH solubility. The condensation of DNA with TMC (50kDa) and TMC grafted with PEG is less sensitive to pH and, at neutral pH, to the ionic strength.

A mandatory requirement for the *in vivo* therapeutic application of gene delivery systems is the stability in serum. According to Ishii *et al.* [183] the presence of 10–20% serum enhances transfection, higher concentrations of serum yielding poorer results. Probably, the optimal serum concentration is determined by the overall effect on cells.

1.3.2.2. Biological barriers in cell transfection

The body defense barriers at the humoral and cellular level have evolved to efficiently prevent intrusion of exogenous entities. Thus, the transfer of foreign genetic material to cells is most challenging, implying a safe and efficient method to deliver therapeutic genes to target cells. The gene carriers must meet a number of physical-chemical requirements; namely, the nanocarrier should have the following properties: stability in biological fluids, access to the target cells and cellular uptake, endosomal escape ability, appropriate intracellular trafficking, unpacking of the polyplexes and nuclear transport (Figure 6) [184, 185].

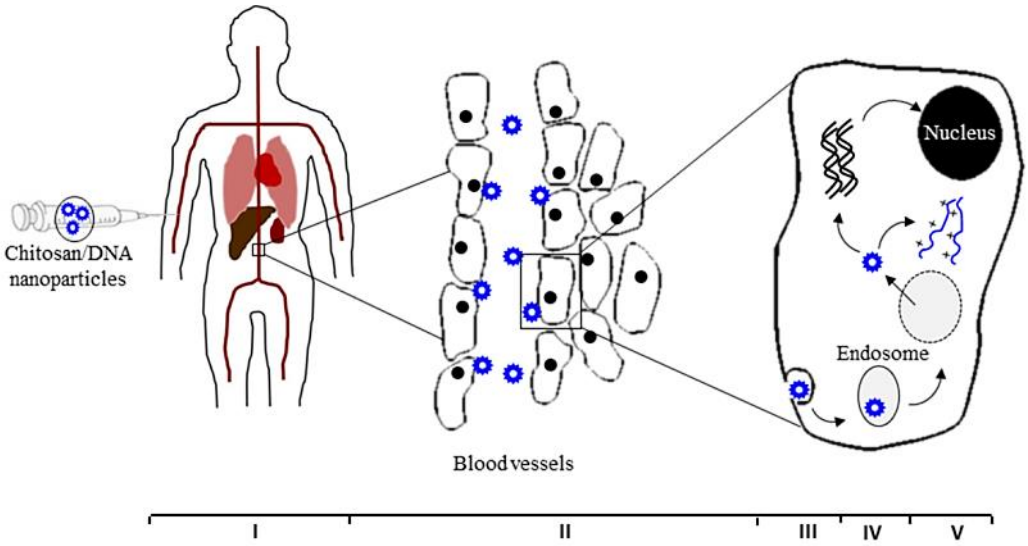

Figure 6. Biological barriers for gene delivery follow intravenous administration. Firstly, the polymeric complex should (I) be stable in the systemic circulation for a fairly long period of time, (II) able to access to the target cells and be internalized, (III) escape the endosomes to avoid degradation, (IV) reach the perinuclear space and allow unpacking of the DNA complexes and finally (V) translocation to the nucleus.

The cationic surfaces increase the solubility of the complexes in aqueous medium and facilitate its interaction with cells. However, when systemically administered, they readily interact with serum components, such as negatively charged serum albumin and opsonins, originating the aggregation of particles in the blood stream through reduction of the zeta potential, thereby decreasing the ionic repulsion between particles. Opsonization results in the rapid clearance by cells of the mononuclear phagocytic system, specially macrophages in the liver (the Kupffer cells), spleen and bone marrow. In order to minimize the interactions with serum proteins, augmenting DNA survival in the bloodstream for the period of time necessary to reach the target tissue, hydrophilic polymers can be conjugated with CS (Figure 6, step I) [186]. PEGlyation of CS increases the systemic circulation time after intravenous administration, possibly by sterically avoiding the non-specific interactions between the serum-driven components and polyplexes [187]. Jiang *et al.* [188] synthesized a galactosylated PEG-CS-Polyethylenimine (PEI) as a potential hepatocyte-targeting gene carrier. After intravenous injection, PEI/DNA complexes rapidly accumulated in the lungs, whereas galactosylated PEG-CS-PEI/DNA complexes accumulated in the lungs, heart and liver, indicating that complexes had increased circulation time *in vivo* due to the hydrophilic group. Park and colleagues [189] introduced another hydrophilic group, poly(vinyl pyrrolidone), into

galactosylated CS to prevent aggregation of the complexes and the interaction with plasma proteins..

The polyplexes should reach the target cells without loss of integrity (Figure 6, step II). The positively charged particles readily attach to the cell surface via ionic interactions, thereby facilitating internalization by different endocytic mechanisms [190]. The cellular uptake of the polymeric polyplexes mostly occurs via non-specific adsorptive endocytosis. However, to improve cellular uptake efficiency and specificity, CS can be decorated with specific ligands (Table 3), which specifically recognize and bind receptors of the target cells (receptor-mediated endocytosis), improving the transfection efficiency [186].

The introduction of the hydrophobic units in the CS-based complexes is also expected to increase transfection efficiency by modulating the complex interactions with cells, such as adsorption on cell surfaces and subsequent endocytosis, alleviate serum inhibition, confer protection from enzymatic degradation, and facilitate intracellular pDNA association [184, 186]. In addition, hydrophobic units in the polymeric carriers may assist in the dissociation of polymer/DNA complexes, facilitating the release of DNA which otherwise would be strongly bound through ionic interactions. Lee *et al.* [191] described the potential of thiolated CS for enhanced gene transfer. Indeed, the thiolated CS/pDNA nanocomplexes exhibited a gradual increase in mucin adsorption, probably due to the formation of covalent bonds between thiolated CS and cysteine-rich subdomains of mucin. *In vitro* and *in vivo* studies confirmed that thiolation of CS increases the transfection efficiency and sustained gene expression. The introduction of a trimethyltriazole group in CS, at the C-6 position, improved the DNA binding ability, serum stability and significant increasing of cellular uptake, as compared to unmodified CS [192]. This effect was assigned to the ability of the trimethylammonium groups to open the tight junctions, leading to increased paracellular permeability and consequently higher transfection efficiency.

Table 3. Representative examples of the CS and CS derivatives/ DNA complexes modified with cell specific ligands to improve the specificity to target cells, and consequently the transfection efficiency.

CS NPs formulations	Targeting ligands	Target cells	Remarks	Ref.
Folate-TMC	Folate	Cancer cells (KB and SKOV3) - folate receptor over-expressing	Folate conjugation increased the cellular uptake of the complex in KB cells and SKOV3 cells via folate receptor. The intracellular trafficking of the folate-TMC/pDNA was faster than TMC/pDNA due to the use of different trafficking pathways.	193
KNOB-CS	KNOB protein	Kidney cells (HEK293) Cancer cells (HeLa)	KNOB conjugated NPs improved gene expression level in HeLa and HEK293 cells by 130 and 7-folds, respectively.	194
Transferrin-High Mw CS	Transferrin	Cancer cells (Caco-2)	CS NPs decorated with transferrin enhanced the transport of NPs trough cell layers by 3- to 5-fold and led to higher stability of the NPs at higher pH.	182
Oleoyl-carboxymethy-CS/hyaluronic acid	Hyaluronic acid	Cancer cells (Caco-2)	Oleoyl-carboxymethy-CS/hyaluronic acid /DNA NPs internalization by Caco-2 cells was mediated by hyaluronan receptor - CD44.	195
Mannosylated CS-graft-PEI	Mannose	Antigen presenting cells	The transfection efficiency of mannosylated CS-graft-PEI /DNA complexes into macrophage cell line, which has mannose receptors, was higher than CS-graft-PEI as well as PEI.	196
Galactosylated PEG-CS-graft-PEI	Galactose	Hepatocytes	Galactosylated PEG-CS-graft-PEI /DNA complexes transfected liver cells more effectively than PEI. Galactosylated-CS is reported as hepatocyte-targeting gene carrier due to specific ligand–receptor interactions between galactose-moieties and asialoglycoprotein receptors.	188
Transactivator of transcription peptide and luteinizing hormone-releasing hormone conjugated with low Mw CS	Luteinizing hormone-releasing hormone	Breast, ovarian, prostate and hepatic cancer cells	Hepatoma and normal liver cells, transfected with transactivator of transcription peptide-luteinizing hormone releasing hormone-CS/DNA NPs carrying pGL3-control pDNA encoding for luciferase, showed luciferase activity in hepatoma cells 110 times higher than that in normal liver cells, supporting the superior selectivity of NPs for hepatoma cells over normal liver cells.	197

Once taken up by cells, via either adsorptive or receptor-mediated endocytosis, polyplexes are localized within the endosomal compartments, where pH rapidly drops to about 5 by the action of membrane bound ATP-driven proton pumps. The endosomes mature to lysosomes, where the arrested polyplexes disassemble due to the low pH and the released DNA may degrade. Therefore, the escape of polyplexes from the endosome is a critical step in the process (Figure 6, step III). Partially protonated polymers retain a substantial buffering capacity, which can lead to the protection of DNA from degradation. Since protons are diverted, the acidification of endosome is prevented; the continued action of the proton pump leads to the retention of chloride ions and therefore osmotic swelling occurs leading to subsequent endosome disruption – the proton sponge swelling effect [176]. It is generally accepted that the buffering capacity of CS (pKa=6.5) is weak compared with PEI (pKa=8,7). Hence, CS have been frequently conjugated with PEI to take advantage of this effect [198]. The combination of PEI with CS/DNA complex dramatically increased the luciferase expression in various cell lines, and the synergistic effect was proved to be induced by proton sponge effect of PEI [199]. However, CS-graft-PEI/DNA complexes frequently display higher transfection efficiency than PEI/DNA [200]. Köpping-Höggard *et al.* [172] studied in detail the effect of the addition of PEI to CS in the transfection efficiency. In this study, in contrast to PEI, ultrapure CS displayed no buffering capacity at the acid endosomal pH-interval of 4.5–5.5, and thus the authors suggested the enzymatic degradation as a more likely mechanism for the endosomal escape of ultrapure CS polyplexes. Indeed, the enzymatic degradation products (oligo- and monosaccharides) may increase the osmolarity, followed by water influx, subsequent swelling and rupture of the vesicular membranes. It was stated that, whatever the mechanism, the efficiency of the PEI and ultrapure CS polyplexes depend on the rates at which the two polymers escape the endo/lysosomal compartment.

Interestingly, Richard *et al.* [201] found that CS has a higher buffering capacity (on a molar basis) than PEI in the endolysosomal pH range, in opposite what is generally accepted. However the formation of CS-DNA complexes reduces CS buffering capacity due to negative electrostatic environment of nucleic acids, which facilitates CS ionization. So, the data suggest that CS have a similar capacity as PEI to mediate endosomal escape through the proton sponge effect, perhaps in a way that depends on the presence of excess CS.

Even so, several modifications of CS have been attempted to improve the ability of the complex CS/DNA escape from endosomes. Imidazole-containing polymers have also been reported to act as a proton sponge, consequently enhancing the release of the complex into the cytoplasm following endocytosis. Kim *et al.* [202] used water soluble CS conjugated with urocanic acid bearing an imidazole ring. The transfection efficiency was enhanced by grafting CS with urocanic acid, an effect that increases with the urocanic acid contents. Hu *et al.* [203] grafted hydrophobic moieties, stearic acid, with CS oligosaccharide. Transfection using the CS oligosaccharide–stearic acid/DNA complexes reached an efficiency of 15%, slightly below the figures obtained with LipofectamineTM (about 20%). The high transfection of these complexes – as compared with CS oligosaccharide/DNA - is believed to rely on the chain of stearic acid, which may favor the escape of CS oligosaccharide–stearic acid/DNA complex from endosome, owing to endosomal membrane instability. When the CS oligosaccharide–stearic acid was used as a transfection carrier of pEGFP-C1, the fluorescence intensity increased gradually with the post-transfection time (until 76 h), and during this period cellular growth was observed. Conversely, a sharp increase on the transfection was detected with LipofectamineTM/DNA in 24h post-transfection, though after this period the DNA expression decreased rapidly, possibly due to the cytotoxicity of the formulation. The continuous, yet with relatively low efficiency, transfection of CS oligosaccharide–stearic acid may be related to the slow rate of release of DNA. The pH sensitivity of the poly(propyl acrylic acid) can also be used to enhance the release of endocytosed drugs into the cytoplasmic compartment, because it exhibits maximal membrane disruption ability at pH 6. By incorporating this polymer in a CS gene carrier, Kiang *et al.* [204] confirmed the enhancement of the pDNA release from the endosomal compartment and improved gene expression.

After escaping from endosome, the complex should be able to unpack quickly, allowing the DNA to move towards the perinuclear space, where nuclear translocation of DNA takes place (Figure 6, step IV). While highly stable polyplexes may provide robust protection of DNA from extra- and intra-cellular nuclease attack, maximum transfection efficiency may not be achieved due to restriction in transcription. In contrast, polyplexes with lower stability may go through rapid uncoupling, causing premature degradation of plasmid DNA in the cytosol. Therefore, maximum transfection efficiency may be achieved using a polymer with intermediate stability. The unpacking can be carried out within the endosome [205] or cytoplasm [206]. In the following

step, the DNA or complex should move to the perinuclear space. To better understand the intracellular trafficking of pDNA/lactosylated-CS complexes, Hashimoto *et al.* [206] examined the effect of the endocytosis inhibitors on the transfection efficiency. Bafilomycin A1, a proton pump inhibitor, greatly depressed the luciferase activity of both pDNA/CS and pDNA/lactosylated-CS complexes. Monensin, an inhibitor of endosomal acidification, significantly decreased the gene expression of the pDNA/CS and pDNA/lactosylated-CS complexes. Nocodazole, which blocks transport from the early to late endosomes, resulted in the accumulation of cargo in the endosome compartment and improved transfection efficiency of the pDNA/CS complex, by about 2-3-fold. In contrast, in the case of pDNA/lactosylated-CS complexes, the transfection efficiency was decreased by nocodazole to 60% for HepG2 cells. Thus, the entrapment of pDNA/lactosylated-CS complexes in early endosome resulted in the obstruction of the release from the endosome. Although the transport of pDNA complexes to the late endosome/lysosome would raise the risk of DNA hydrolysis, the pDNA/lactosylated-CS complex showed high transfection efficiency, taking advantage of the release in perinuclear region.

Efficient nuclear localization of DNA is considered the final destination of gene delivery, since eukaryotic transcription is an essential intermediate step to convert genetic information into protein and is performed in the nucleus (Figure 6, step V). However, the mechanism of nuclear translocation of DNA from CS/DNA complexes is not fully understood [187]. Parelkar *et al.* [207] believes that the success of non-viral transfection using polymers involves an efficient nuclear uptake of nucleic acid cargo. They observed that incorporating PKKKRKV heptapeptide pendent groups as nuclear localization signals on a polymer backbone, resulted in superior protein expression levels than those achieved with JetPEI and Lipofectamine 2000, commercial transfection reagents.

1.3.2.3. DNA therapy

Gene therapy is the treatment of human disorders by the introduction DNA into specific target cells of a patient, where production of the encoded protein will occur. Recent advances in gene delivery emphasize the application of CS-based NPs as gene carriers in cancer, rheumatoid arthritis, atherosclerosis, allergic asthma, tuberculosis, hemophilia A, hepatitis B, coxsackievirus B3 and respiratory syncytial virus infections, among others as shown in table 4 .

Table 4. Representative examples of the use CS/DNA NPs in gene therapy.

Disease	Therapeutic agent	Administration	Remarks	Ref.
Colon adeno-carcinoma	IL-12 gene	Intratumoral	Mannosylated CS/pmIL-12 complexes administered in BALB/c mice bearing CT-26 tumor cells resulted in high expression levels of IL-12 and IFN-γ, suggesting that tumor growth was retarded due to the higher production of both cytokines. The IL-12 down-regulated angiogenesis and together with IFN-γ promotes apoptosis and cell cycle arrest.	208
Rheumatoid arthritis	IL-1 Ra gene	Intravenous	The human IL-1Ra remained in the serum of rats for 10 days and reverted the alterations in bone turnover (bone resorption versus formation) observed in arthritic animals.	209
Atherosclerosis	pCR-X8-HBc-cholesteryl ester transfer protein (pCETP)	Intranasal	Significant serum anti-CETP IgG were detected and lasted for 21 weeks. The aortic lesions in the rabbits with NPs were lower than those treated with saline control. CS/pCETP NPs could significantly attenuate the progression of atherosclerosis.	210
Asthma	IFN-γ pDNA	Intranasal	CS/IFN-γ pDNA NPs led to the normalization of airway inflammation and hyperresponsiveness, and return to normal lung morphology from the hyper-inflammatory condition induced by Ovalbumin sensitization.	211
Tuberculosis	pDNA T-cell epitopes from Mycobacterium tuberculosis	Pulmonary	CS/DNA was able to induce the maturation of dendritic cells. pDNA incorporated in CS NPs induced increased levels of IFN-γ secretion compared to pDNA in solution.	212
Hemofilia A	Factor VIII pDNA	Oral	DNA polyplexes were detected in gastrointestinal tissues as well as in liver, spleen and additional systemic tissues in the hemophilia A mice. Functional Factor VIII protein was found in plasma reaching a level of 2-4% FVIII at day 22 after delivery.	213
Hepatitis B virus infection (HBs)	pRc/CMV-HBs	Nasal	pRc/CMV-HBs loaded CS NPs resulted in serum anti-hepatitis B virus surface antigen and IgA titers in the mucosal secretions. CS NPs were able to induce humoral and cellular immune responses.	214
Coxsackievirus B3 infection	pcDNA3-VP1 (encoding VP1, major structural protein of CVB3)	Intranasal	Mice immunized with CS/pcDNA3-VP1 produced higher levels of IgG and IgA. CS/DNA vaccine induced CVB3-specific systemic immunity (humoral and cellular) and protected mice from lethal CVB3 challenge.	215
Respiratory syncytial virus infection	pDNA encoding a cytotoxic T-lymphocytes epitope	Intranasal	Immunization with pDNA conjugated with CS induced *in vivo* peptide- and virus-specific cytotoxic T-lymphocyte responses. In CS/DNA immunized mice a significant reduction in virus loaded in the lungs was observed.	216

1.3.2.4. siRNA delivery

RNA-interference (RNAi) mediates knockdown of harmful or unwanted genes. In the RNAi process, double-stranded small interfering RNA (siRNA) with 21–23 nucleotides, endogenously produced or exogenously introduced, associates with a nucleic acid-protein complex called RNA-induced silencing complex (RISC). One of the strands is used to target a specific sequence in a particular messenger RNA (mRNA), leading to its degradation. Hence, the synthesis of the protein encoded by that mRNA molecule is prevented [45, 217]. The successful application of siRNA is largely dependent on the development of the delivery vehicle, due to its rapid degradation and poor cellular uptake i*n vitro* and *in vivo* [218]. So, an ideal carrier for siRNA should be able to bind and condense siRNA, provide protection against degradation, specifically direct the siRNA to target cells, facilitate its intracellular uptake and escape from the endosome/lysosome into cytosol, and finally promote efficient gene silencing [45]. Recently, Katas and Alper [219] were the first to explore the use of CS as polymeric carrier for siRNA delivery. In comparison to usual DNA-based gene delivery, the extra vulnerability of RNA to enzymatic degradation represent additional hurdles to CS-mediated gene transfer, and make it even more challenging than conventional pDNA delivery.

As the structure and size of siRNA are quite different from those of pDNA, the influence of the N/P ratio, serum and CS Mw, is also different; however, the effect of degree of deacetylation and pH is similar. Therefore, all parameters must be optimized specifically for the CS/siRNA complexes.

NPs stability is required for extracellular siRNA protection, but disassembly is needed to allow RNA-mediated gene silencing through interaction with the intracellular RISC. An appropriate balance between protection and release of siRNA needs to be achieved, using a CS with the convenient Mw [45]. Liu and colleagues [220] verified that CS with high Mw and degree of deacetylation result in the formation of discrete and stable NPs, 200 nm in size. CS/siRNA formulations prepared with low Mw CS (~10 kDa) showed almost no knockdown, whereas highest gene silencing efficiency (80%) was achieved using CS/siRNA NPs at N:P 150, with high Mw CS (114 and 170 kDa) and degree of deacetylation of 84% [170]. The influence of N/P ratio, here defined as the ratio of CS amino groups (N) to RNA phosphate groups (P), in the size of NPs was described by Howard *et al.*, [221] using a CS with Mw of 114 kDa. The NPs

hydrodynamic radius increased along with decreasing the N/P ratio. This suggests siRNA bridges the CS chains, higher concentrations leading to greater CS incorporation and possible interparticle aggregation. Liu *et al.* [220] investigated the influence of N/P ratio on the gene knockdown efficiency using CS/siRNA NPs (CS with 170 kDa and degree of deacetylation of 84%) in H1299 human lung carcinoma cells. It was found that the level of EGFP knockdown increased at higher N/P ratios (50 and 150), in comparison to low N/P (2 and 10) formulations; the NPs formed at N/P 150 showed the greatest level (80%) of EGFP knockdown. This result was explained by the increased NPs stability at high N:P. Indeed, removal of excess polycations prior to transfection resulted in virtually no cellular knockdown, suggesting a possible role of a CS excess in the cellular permeation. Inside cells, the siRNA must be resistant to digestion by nucleases. Katas and Alper [219] studied the effect of serum in the free siRNA and CS–siRNA NPs stability and protection from nuclease degradation. After incubation with 5% FBS, free siRNA was intact only up to 30 min, being fully degraded after 48 h; on the other hand, siRNA in CS/TPP NPs started to degrade after 24 h incubation and full degradation was only observed after 72 h incubation. Interestingly, the siRNA recovered from CS–siRNA NPs was intact up to 7 h and fully degraded after 48 h incubation in 50% serum, while complete degradation of free siRNA was observed from the very first moments of incubation. Indeed, CS–siRNA NPs significantly protected siRNA from nuclease activity.

In order to improve the efficiency of RNA transfer using CS, several attempts on the vector improvement have been made over the past years.

Katas and Alpar [219] synthesized CS NPs by ionic gelation using CS salts (CS hydrochloride and glutamate) and sodium TPP. Compared with standard CS, these NPs showed efficient siRNA transfer, which may be related to the higher RNA binding capacity and loading efficiency. Later, another group conjugated CS with thiamine pyrophosphate, a thiamine derivative [222]. The CS-thiamine diphosphate-mediated siRNA silencing of endogenous EGFP gene occurred at best with 70–73% efficiency. This efficiency was associated with the increased nucleic acid binding ability and improved water solubility of the vector, due to the addition of extra amine groups from thiamine diphosphate and to the salt formation between the phosphate group of thiamine diphosphate and the amine group of CS. Lee *et al.* [223] synthesized CS NPs, by coacervation, to encapsulate siRNA in the presence of polyguluronate, a block of guluronic acid residues present in the alginate backbone. Its ability to form stable NPs

with CS was hypothesized, given its low Mw and ionic interactions with cations. CS-polyguluronate/siRNA NPs were the most efficient formulation to deliver siRNA into HEK 293FT and HeLa cells, as compared with NPs without polyguluronate or with alginate replacing polyguluronate. Ji and colleagues [224] developed CS/FHL2 siRNA NPs with a hydrodynamic radius of about 148 nm, which FHL2 gene expression knockdown in human colorectal cancer LoVo cells was about 67%, very similar to the 69% reduction gene expression when siRNA was transfected with LipofectamineTM. PLGA nanospheres with CS surface-modified were prepared by Tahara *et al.* [225] for siRNA delivery. CS-PLGA nanospheres exhibited much higher encapsulation efficiency and were more effectively taken up by the cells than unmodified PLGA NPs, possibly due to electrostatic interactions with cell membrane. The gene silencing efficiency of CS-PLGA nanospheres was higher and more prolonged. A new approach based on incorporation of siRNA/polyelectrolyte complexes, of CS oligosaccharides conjugated with deoxycholic acids, into biodegradable PLGA NPs in order to stabilize the siRNA into a hydrophobic matrix was performed by Lee *et al.* [226]. As expected an excellent structural stability was achieved and efficient cellular uptake, followed by significant gene silencing. The influence of PLGA encapsulation was remarkable for cells incubated for longer periods of time. In these conditions the sharp decline on GFP expression, indicate that the biological active siRNA was slowly released from complexes in PLGA NPs.

1.3.2.5. Gene silencing *in vivo*

Only a few studies report the use of CS/siRNA for *in vivo* therapy. Some works described ahead in this review show the success of CS/siRNA NPs as a promising approach for the inhibition of gene expression *In vitro* and *in vivo*, and its therapeutic potential for the treatment of infections, allergic and inflammatory chronic diseases and cancer Table 5).

Table 5. Knockdown of gene expression using CS NPs as gene delivery system.

Disease	Therapeutic agent	Administrati	Remarks	Ref.
Respiratory syncytial virus infection	Respiratory syncytial virus-NS1gene siRNA	Intranasal	Treatment of rats with respiratory syncytial virus-NS1gene siRNA prior to virus exposure reduced virus titers in the lung and prevented the inflammation and airway hyperresponsiveness associated with the infection and development of asthma.	[227]
Asthma	Imiquimod and natriuretic peptide receptor A siRNA	Transdermal	Imiquimod cream containing natriuretic peptide receptor A siRNA/CS NPs showed significantly reduced airway hyperresponsiveness, eosinophilia, lung histopathology and pro-inflammatory cytokines IL-4 and IL-5 in lung homogenates compared to controls.	[228]
Rheumatoid arthritis	anti-TNF-α Dicer-substrate siRNA	Intraperitoneal	CS NPs containing siRNA mediated TNF-α knockdown in primary peritoneal macrophages. Histological analysis of joints revealed minimal cartilage destruction and inflammatory cell infiltration in anti-TNF-α-treated mice.	[229]
Lung cancer	onco-protein Akt1 siRNA	Nasal	CS-graft-PEI carrier efficiently delivered onco-protein Akt1 siRNA and silenced onco-protein Akt1.	[230]
Cervical cancer	siRNA (siBcl-2)	Subcutaneous	*In vivo* studies showed that siRNA could be effectively delivered through NPs. Significant decrease in the tumor volume was observed after CS containing siRNA treatment. Blocking the expression of anti-apoptotic Bcl-2 can enhance the sensitivity of cancerous cells to anti-cancer drugs and the apoptosis rate.	[231]
hepatocellular carcinoma	short hairpin RNA (shRNA) directed against vascular endothelial growth factor	Intravenous and intratumoral	Low Mw CS/vascular endothelial growth factor shRNA complexes significantly inhibited its expression in hepatocellular carcinoma cells and liver tumor tissues. CS obviously enhanced and prolonged the deposition of shRNA at the tumor site. Intratumoral or intravenous injection of the complexes showed higher effectiveness on suppression of tumor angiogenesis and tumor growth compared with naked shRNA.	[232]
Ulcerative colitis	siRNA (si Map4k4)	Oral	Cellular uptake of galactosylated-TMC-cysteine/TPP NPs in activated macrophages was significantly enhanced owing to galactose receptor. siMap4k4 loaded NPs effectively inhibited TNF-α production. Oral dosage of siMap4k4 loaded NPs successfully protected mice from dextran sulfate sodium-induced Ulcerative colitis at a relatively low therapeutic dose by attenuating colonic TNF-α production.	[233]

1.3.3. Delivery of low molecular weight drugs

Currently, the research on NPs based drug delivery systems focus on the selection of nanoparticulate carriers for suitable drug release profiles and also on its surface decoration, aiming at improving the targeting ability and *in vivo* biodistribution [234]. These are crucial goals, since drugs often fail to get favorable clinical outcomes, due to instability, reduced bioavailability and undesirable side effects. Furthermore, drugs need to be protected from degradation in the biological environment. The bioactivity is often limited by the inability to cross biological barriers and to reach the target site, particularly when intracellular or intranuclear sites of action must be reached [157]. In addition, significant amounts of the administrated drug may distribute over the healthy tissues or organs, often leading to severe side effects. Among other drug delivery strategies, a great deal of attention has been directed to CS NPs as promising systems able to improve drug bioavailability, modify pharmacokinetics and/or encapsulated drug protection [235]. In fact, as already mentioned CS NPs improve transmucosal permeability, enhancing transport through the transcellular and paracellular pathway, due to the good bio- and mucoadhesive properties, and induction of structural reorganization of tight junction, respectively [236, 237]. CS derivatives have been designed to improve the properties of native CS. Chemical modifications of CS originate amphiphilicity, an important characteristic for the formation of self-assembled NPs, potentially suited for drug delivery applications. The hydrophobic cores of the NPs may act as reservoirs for a variety of bioactive substances [238]. CS-based NPs as delivery systems of low molecular weight drugs have attracted attention for cancer and organ-specific therapy.

1.3.3.1. Cancer-targeted drug delivery

Most anticancer agents do not specifically target cancer cells, but also normal tissues, leading to adverse effects following systemic administration. In addition, anticancer drugs are often poorly soluble in water; thus, organic solvents or detergents are necessary for clinical applications, resulting in undesirable side effects such as venous irritation and respiratory distress. Therefore, in an attempt to circumvent these limitations, research efforts have been concentrated on the development of new nanoparticulate drug delivery systems able to encapsulate a large quantity of drugs. Targeted drug delivery using long-circulating particulate drug carriers, such as

polymeric NPs of controlled size, has high potential to improve the cancer therapy, providing a selective effect owing to the concentration of drugs at the tumor site, through enhanced permeability and retention (EPR) effect and allowing lower distribution in healthy tissues [239, 240] (Figure 7).

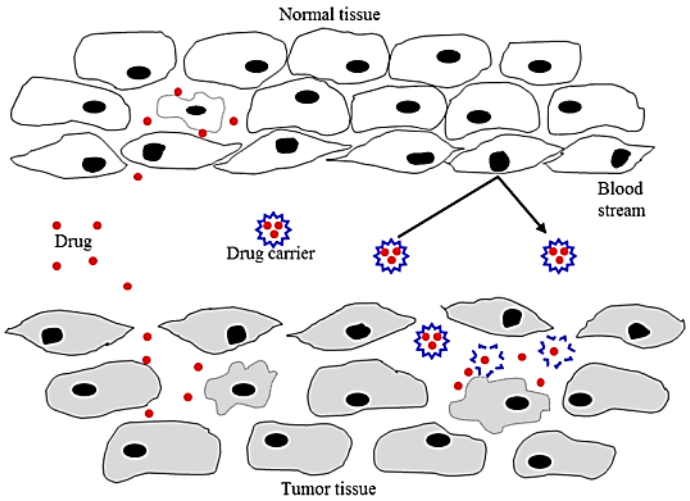

Figure 7. Schematic representation of anatomical differences between normal and tumor tissues. The defective tumor vasculature with disorganized endothelium allows passive targeting of NPs carrier due EPR effect.

The use of polymeric NPs has been recognized as an effective strategy for passive tumor targeting, because its prolonged circulation time allows the accumulation and extravasation into the tumor tissue. The NPs may diffuse through the anatomical and pathophysiological abnormalities of the tumor vasculature, due to the EPR effect [241]. So, NPs ranging from 10 to 200 nm can easily penetrate the leaky vessel wall around tumor and then retain in tumor region at high concentration and for long time due to the insufficient venous and lymphatic clearance. Beyond the nature of tumor vasculature, the size and surface of nanoparticulate carriers play a crucial role in this process. Particles ranging 10-200 nm in diameter and hydrophilic surfaces tend to exhibit improved EPR effect, due to the increased residence time with higher concentration in the blood stream, which can only be possible escaping renal clearance and mononuclear phagocyte system (MPS) during circulation following distribution into organs [240].

Due to the complexity of tumor tissue signaling network, the conventional chemotherapy hitting single target in tumor cells are therefore largely limited. Hence, the combination of chemotherapy and gene therapy provides a promising modality to

improve the therapeutic effect through simultaneous modulation of multiple signaling pathways in tumor cells [242, 243]. CS self-assembled nanogels represent a promising co-delivery system, due to their amphiphilic and cationic nature: the hydrophobic core allow solubilization of hydrophobic antitumor drug, while the cationic hydrophilic shell in aqueous solution could complex with anionic gene. Yu *et al.* [244] synthesized amphiphilic NPs, linoleic acid and poly (β-malic acid) double grafted CS, functionalized with folate for co-delivery of paclitaxel (PTX) (chemotherapeutic drug) and survivin shRNA-expressing plasmid (iSur-pDNA) (therapeutic gene that can suppress the expression of oncogene survivin). The effective cellular uptake, nuclear accumulation of pDNA, *In vitro* gene silencing efficiency, and cell growth inhibition were attributed to folate modification and higher substitution degree of linoleic acid. The suppressed protein adsorption was achieved by poly (β-malic acid) grafting. Co-delivery of PTX and iSur-pDNA exhibited enhanced antitumor efficacy and prolonged survival period in tumor-bearing mice as compared with single delivery of drug or iSur-pDNA. Deng and colleagues [245] explored the potential of co-delivering tumor suppressive miRNAs and chemotherapeutic agents. miR-34a, a potent endogenous tumor suppressive molecule in breast cancer, was co-loaded with doxorubicin (DOX) into hyaluronic acid-CS NPs and simultaneously delivered into breast cancer cells, synergistically improving the drug therapeutic effect. *In vivo* experiments showed that miR-34a enhanced the anti-tumor effects of DOX, by suppressing the expression of non-pump resistance and anti-apoptosis proto-oncogene Bcl-2. Moreover, intracellular replacement of miR-34a inhibited breast cancer cell migration, via targeting Notch-1 signaling.

Drug encapsulation on CS-based NPs can be achieved physically by hydrophobic interactions [246, 247], by covalent binding to the polymer via a biodegradable spacer [248, 249] or even using chemical cross-linkers [250, 251]. CS NPs have been investigated as carriers for diverse small molecular drugs, in recent years, as referred in table 6.

Table 6. Recent studies using CS-based NPs for the delivery of low Mw drugs.

Drug	CS NPs formulations	Remarks	Ref.
Camptothecin	Hydrophobically (5β-cholanic acid) modified GC	The camptothecin-hydrophobically modified GC NPs intravenous injected exhibited significant antitumor effect and high tumor targeting ability towards human breast cancer xenografts, owing to prolonged blood circulation time and high accumulation in tumors.	252
	Poly(N-isopropylacrylamide)/CS	Poly(N-isopropylacrylamide)/CS NPs were sensitive to pH, which can be advantageous to target tumor cells. The camptothecin loaded NPs drastically enhanced the cytotoxicity at pH 6.8	253
DOX	DOX conjugated CS via acid-cleavable hydrazone bond	CS-hydrazone-DOX NPs presented no burst release at neutral pH, excellent cellular uptake and remarkable drug accumulation in tumor cells. Inside the cells DOX was quickly released from the NPs, due to the decrease of pH from pH 7.4 to pH 6.0 or 5.0.	254
	PEG-conjugated CS oligosaccharide-arachidic acid	NPs size stability in serum over 72 h. The uptake rate of DOX loaded NPs by K562 cells was higher than from the solution. *In vivo* clearance rate of DOX from PEG-CS-arachidic acid NPs group was slower than other groups, subsequently prolonging the circulation period.	255
	CS/O-carboxymethyl CS/TPP	Ex vivo intestinal adhesion and permeation indicated that NPs was able to enhance absorption of DOX throughout the entire small intestine. Oral administration of DOX/NPs effectively delivered DOX into blood, giving an absolute bioavailability of 42%.	256
PTX	Linoleic acid and poly(β-malic acid) grafted CS	The PTX/NPs was more effective in tumor suppression than free PTX, because the hydrophilic poly(β-malic acid) on the surface of NPs decreased the uptake by the mononuclear phagocytic system.	257
	Hydrotropic oligomers conjugated GC	PTX/NPs presented rapid cellular uptake and lower *In vitro* cytotoxicity compared to Cremophor EL/ethanol formulation of PTX. Higher PTX/NPs accumulation in tumor tissue was observed in tumor-bearing mice. Furthermore, PTX/NPs showed improved therapeutic efficacy, as compared to Abraxane®.	82
Cisplatin	Hydrophobically modified GC	Cisplatin loaded NPs were successfully accumulated by tumor tissues in tumor-bearing mice, due to the prolonged circulation and EPR effect.	258
Curcumin	CS/TPP	CS NPs prevented degradation of curcumin in mouse plasma in comparison to free curcumin. Oral delivery of CS NPs/curcumin to healthy mice showed that they can cross the mucosal barrier intact and one hour after feeding they were detected in the blood. Oral administration of curcumin bound to CS NPs cured mice from Plasmodium yoelii infection.	259
Mitomycin C	poly-ε-caprolactone coated with CS	CS- poly-ε-caprolactone NPs were selectively incorporated by bladder cancer cell line and Mitomycin C loaded NPs exhibited higher toxicity than free drug.	260
5-fluorouracil	CS-polyaspartic acid	The Bcl-2 gene family (regulatory factor group in apoptosis) was regulated by CS-polyaspartic acid /5-fluorouracil and 5-fluorouracil. Its effect was more evident to CS-polyaspartic acid/5-fluorouracil NPs, with enhancing the inhibition and inducing apoptosis of the gastric carcinoma.	261

Table 6. (Continued).

Rivastigmine	CS/TPP	An enhanced brain uptake of CS/ rivastigmine NPs was clearly observed following nose to brain delivery. Direct nose to brain transport bypassing the blood–brain barrier proving the superiority of CS/rivastigmine NPs over rivastigmine solution intravenously.	262
Norcantharidin	Galactosylated CS	Norcantharidin/Galactosylated CS NPs displayed tumor inhibition in mice	263
Protophorphyrin IX	Hydrophobically modified GC	The released protophorphyrin IX from NPs became highly phototoxic upon visible irradiation and in SCC7 tumor-bearing mice exhibited enhanced tumor specificity and increased therapeutic efficacy compared to free drug.	264
All-trans retinoic acid	Methoxy PEG-grafted CS	*In vitro* results suggested that tumor cell migration was most effectively inhibited by the polyion complex micelles than all-trans retinoic acid free.	265
Docetaxel	Hydrophobically modified GC	Docetaxel/NPs presented deformability, passing through the smaller pore size, owing their highly flexible features, prolonged circulation time, tumor targeting ability and higher antitumor efficacy.	266
Bortezomib	CS coated superparamagnetic iron oxide NPs	Pro-apoptotic PUMA and NOXA genes were upregulated, while anti-apoptotic BCL-2, SURVIVIN and cIAP-2 genes were downregulated at Bortezomib loaded NPs treated cells. Immunocytochemical analyses assessed an increase in p53 tumor suppressor protein levels at treated cells.	267
Curcumin / 5-fluorouracil	Thiolated CS	Combination of these NPs formulations showed enhanced anticancer activity on colon cancer cells *in vitro* and improved the bioavailability of the drugs *in vivo*.	268
Methotrexate	Methoxy PEG conjugated CS	*In vivo* optical imaging in mice showed that methotrexate was released from particles and targeted the tumor tissue, showing significant prolonged retention and specific selectivity.	269
Rifampicin	Mannose-conjugated CS	Extent accumulation of mannose-CS NPs in macrophage rich organs, particularly in liver and spleen, were significantly higher compared to free drug. Ex vivo uptake of mannose-CS NPs was 2.31 times higher compared to unconjugated CS NPs. So, mannose-CS NPs represent efficient, viable, safe, and cheaper targeted delivery system of rifampicin for the treatment of visceral leishmaniasis.	270
Oridonin	Galactosylated CS	Pharmacokinetic study showed that oridonin loaded galactosylated CS and non-functionalized NPs could prolong the drug plasma levels compared with free drug solution. However, the distribution of oridonin loaded galactosylated CS liver was higher than that of oridonin/non-functionalized NPs and free drug.	271
Gemcitabine	CS/PEG-anisamide	The results indicated targeting delivery provided by the high affinity of anisamide to sigma receptors found in a variety of tumors (namely non-small cell lung carcinoma), less organ toxicity and higher antitumor activity i*n vitro* as well as *in vivo*.	

The surface decoration of CS NPs with PEG has attracted attention since it increases the physical stability of NPs, prolonging the circulation time in blood by avoiding the removal by the mononuclear phagocytic system and decreasing the positive charge of the particle surface. Hu *et al.* [272] verified that the PEGylation of stearic acid-grafted CS oligosaccharide micelles reduce significantly the cellular uptake by macrophages, not affecting the internalization by normal and tumor liver cells. A similar effect was observed by Qu *et al.* [273] using PTX loaded CS micelles based on CS conjugated with hydrophobic moieties of octyl and hydrophilic moieties of sulfate and PEG monomethyl groups.

However, the accumulation of drugs in the tumor tissue is not always a guarantee of a successful therapy if the drug misses the target site within the tumor cell, such as the cell membrane, cytosol, or nucleus. Park *et al.* [274] synthesized self-assembled NPs made of N-acetyl histidine-conjugated GC, a promising system for intracytoplasmic delivery of PTX. Cellular uptake of N-acetyl histidine-GC NPs occurred by adsorptive endocytosis initiated by nonspecific interactions between NPs and cell membranes. Then, the NPs were exocytosed or localized in endosomes. In the slightly acidic environment of the endosomes, the drug-loaded NPs were disassembled due to breakdown of the hydrophilic/hydrophobic balance by the protonation of the imidazole group of N-acetyl histidine-GC, providing a drug release into the cytosol. Therein, PTX was effective in inducing arrest of cell growth. You *et al.* [275] developed another strategy for PTX delivery. Micelles made of stearic acid and CS hold multiple hydrophobic "minor cores" near the surface, which improved the micelles internalization into cancer cells and accumulation of the drug in the cytoplasm. For antitumor drugs acting on the nucleus, effective internalization and nucleus accumulation is mandatory. Although nuclear import of many nuclear proteins is based on the presence of a peptidic nuclear localization signals, other non-peptidic nuclear localization signals exist, namely sugar molecules. You *et al.* [276] observed that the CS-graft-stearic acid micelles loaded DOX presented an enhanced nuclear location comparing to free DOX, possibly due to the import of the micelles loaded drug occurring via a sugar-dependent manner.

Cancer cells often over-express specific antigens or receptors on the cell surface that can be used for active targeting. Chemical modification of the drug carrier using targeting moieties can precisely direct NPs to receptors on the tumor tissue [238]. For successful active targeting, the specific receptors should be expressed exclusively on the cancer cells. The targeting moieties most used are galactose, transferrin, folic and

hyaluronic acids. Glycotargeting takes advantage of a highly specific interaction between the carbohydrate ligands conjugated on macromolecules and the endogenous lectins present on the targeted cells. Because of their high density on the surface of hepatoma cells in the liver cancers, the asialoglycoprotein receptors are a particularly attractive site for glycotargeting. Among the glycoconjugated macromolecules, galactosylated CS was found to be a suitable material for liver-targeting drug/gene delivery [277]. Mi *et al.* [277] confirmed that the galactosylated CS NPs had higher specific interaction with hepatoma cells than CS NPs, via the ligand-receptor (asialoglycoprotein)-mediated recognition, leading to a high affinity to HepG2 cells. The transferrin is also over-expressed in tumor tissues, hence it can be used as a ligand for tumor targeting. Transferrin was covalently bound to the Dox-loaded palmitoylated GC vesicles by Dufes *et al.* [278]. The transferrin decorated vesicles were taken up faster (after 1–2 h) and DOX reached the nucleus after 60–90 min, leading to higher cytotoxicity than palmitoylated GC/DOX *In vitro*, although this good *In vitro* performance did not translate into a therapeutic advantage *in vivo*. All vesicles reduced the tumor size on day 2, but were, overall, less active than the free drug. Folate receptors are also frequently over-expressed in human epithelial cancerous cells. Therefore, folate-conjugated drugs or carriers can be rapidly internalized into cancer cells via receptor-mediated endocytosis. Folate-conjugated stearic acid grafted CS NPs, produced by You *et al.* [279], were rapidly took up by HeLa cells (over-expressed folate receptors) as compared to A549 cells (deficient folate receptors cell line). PTX was encapsulated into these micelles; the lethal half dose of taxol (a clinical formulation containing PTX) on A549 and HeLa cells is 7.0 and 11.0 μg ml^{-1}, respectively while for PTX-loaded micelles these values were reduced to 0.32 μg ml^{-1} and 0.268 μg ml^{-1}. These results were attributed to the increased intracellular delivery of the drug. Most malignant solid tumors and their surrounding stromal tissue contain elevated levels of hyaluronic acid, which can provide a matrix that facilitates invasion [280]. Hyaluronic acid receptors, such CD44, are also over-expressed in tumor cells; indeed, cells with metastatic potential often show enhanced binding and internalization of hyaluronic acid. Jain and Jain [280] explored the utilization of hyaluronic acid grafted CS NPs for the effective delivery of 5-fluorouracil to colon tumors. Hyaluronic acid-CS NPs showed significantly higher uptake by cancer cells, about 7.9 fold as compared to uncoupled NPs, which clearly indicate that the uptake of hyaluronic acid coupled NPs occurred via CD44 receptors of HT-29 cancer cells.

1.3.3.2. Organ specific drug delivery

NPs constitute a versatile drug delivery system, with the ability to overcome physiological barriers, guiding drugs to specific cells or intracellular compartments, either by passive or receptor-mediated targeting mechanisms. The NPs can be targeted to organs such as the eye, brain, liver, spleen, lung and lymph; because of their very small size, they can pass through the narrowest capillaries [281].

1.3.3.2.1. Ocular delivery

Efforts in ocular drug delivery have been made to improve the bioavailability and to prolong the residence time of drugs applied topically onto the eye [282]. Campus *et al.* [283] concluded that CS-coated poly-ε-caprolactone nanocapsules enhanced the penetration of an encapsulated dye through the cornea, probably due to the extended adhesion of nanocapsules at the superficial layers of the epithelium. *In vivo* studies showed that the amounts of fluorescent CS in cornea and conjunctiva were significantly higher for fluorescent CS NPs than for a control fluorescent CS solution, these amounts being fairly constant for up to 24 h [284]. Badawi *et al.* [285] observed that, following topical instillation of a CS nanocarrier loaded with indomethacin to rabbits, it was possible to achieve therapeutic concentration in the cornea and fairly high level in the inner ocular structure. These concentrations were significantly higher than those obtained following instillation of an indomethacin solution. The drug delivered from nanocarriers in the cornea was sufficiently high to adequately suppress inflammatory process. More recently, Jian *et al.* [286] used a mucoadhesive nanoparticulate carrier system based on CS to improve the betaxolol hydrochloride ocular delivery; these are necessary because many effective anti-glaucoma drugs are associated with rapid and extensive precorneal loss, resultant from drainage and high tear fluid turnover. *In vivo* pharmacodynamic studies carried out in dexamethasone induced glaucoma model in rabbits showed that NPs were effective in decreasing the intraocular pressure, as compared to commercial formulations. Ocular delivery of amphotericin B, incorporated into the hydrophobic core of poly(lactic acid)-grafted-CS self-aggregated NPs, was also successfully achieved by Zhou *et al.* [287]. The minimal inhibitory concentration of the amphotericin B loaded NPs exhibited antifungal activity similar to that of the free drug against *Candida albicans*. Prolonged residence time at the ocular surface and NPs penetration into the cornea was suggested in the *in vivo* ocular pharmacokinetic studies. Similar studies

carried out by Bhatta *et al.* [288] presented lecithin/CS NPs as useful approach aiming to prolong ocular residence time, own to mucin adhesion and consequently lower ocular clearance, thus allowing reduced dosage frequency of natamycin.

1.3.3.2.2. Liver-Target Drug Delivery

The diammonium glycyrrhizinate is used for the treatment of chronic hepatitis. Yang *et al.* [289] produced lactose-conjugated PEG-grafted-CS to promote liver-targeted delivery of this drug, because lactose can be recognized by asialoglycoprotein receptor on the cell surface of liver. Indeed, the lactose-PEG-graft-CS NPs delivered into the liver glycyrrhizinate more effectively than the PEG-graft-CS micelles. Although reported as a therapeutic agent, the presence of abundant receptors on hepatocyte membranes to glycyrrhizin have led to its extensive use for the surface decoration of the CS NPs, a novel hepatocyte-targeted delivery system [290-295]. Bu *et al.* [296] developed an active liver targeted delivery system to trans-resveratrol based on CS NPs modified either by biotin or by biotin and avidin. Trans-resveratrol loaded NPs (both formulations) showed significantly higher anticancer activity compared to trans-resveratrol solution.

1.3.3.2.3. Brain-Target Drug Delivery

The Alzheimer disease is a chronic neurodegenerative disorder accompanied by the gradual and progressive loss of functional and psychomotor abilities. The female sex hormone, 17β-estradiol, is involved in the regulation of brain development. Long-term oestrogen replacement has proved to be beneficial in the prevention and treatment of Alzheimer's disease [297]. Considering the therapeutic potential of estradiol, Wang *et al.* [297] studied the levels of estradiol in blood and the cerebrospinal fluid in rats following intranasal administration of estradiol-loaded CS NPs. The estradiol was directly transported from the nasal cavity into the cerebrospinal fluid, in rats; the CS NPs are thus able to significantly improve the estradiol transport to central nervous system. Later, the same group synthesized TMC surface-modified PLGA NPs [298]. As a cationic ligand, TMC can facilitate the active transport of NPs via absorptive-mediated transcytosis across the cerebral endothelium and so TMC-modified NPs could be used as a drug carrier for brain delivery, overcoming the blood–brain barrier. PLGA–NP and TMC/PLGA–NP loaded 6-coumarin, as a probe, were injected into the caudal vein of

mice; higher accumulation of TMC/PLGA NPs in the cortex and third ventricle was observed, as compared to PLGA NPs, demonstrating that the TMC/PLGA NPs pass through the endothelial cells of the blood–brain barrier, reaching the brain parenchyma. This effect was confirmed by the behavior tests in Alzheimer disease transgenic mice, in which the neuroprotective effects of TMC/PLGA NPs loaded with coenzyme Q10 were superior to the PLGA NPs and solution, and markedly improved the spatial memory. Shadab *et al* [299] explored the potential of CS NPs as a non-invasive nose to brain delivery system of bromocriptine for the treatment of Parkinson's disease. A low dose of haloperidol was able to induce oxidative stress and behavioural deficits that resemble Parkinson disease, namely catalepsy and akinesia. Animals treated with bromocriptine in solution and most evident to bromocriptine loaded CS NPs showed a reversal in catalepsy and akinesia behaviour when compared to haloperidol treated mice. Biodistribution of bromocriptine formulations follow intravenous and intranasal administration achieved by gamma scintigraphy imaging are suggestive of direct nose to brain transport bypassing the blood–brain barrier.

1.3.3.2.4. Lung-Target Drug Delivery

In general, NPs delivery to the lungs is an attractive concept because retention of the particles in the lungs, accompanied with a prolonged drug release, can be achieved using large porous NPs matrices. On the other hand, it has been shown that NPs uptake by alveolar macrophages can be reduced using particles smaller than 260 nm. Both effects combined might improve local pulmonary drug therapy [300]. Asthma is a chronic inflammatory disease of the airway characterized by the infiltration of eosinophils, epithelial hyperplasia leading to hypersecretion of mucus and the presence of airway hyperresponsiveness to a variety of stimuli. Theophylline was used for the treatment of asthma but side effects limit its application. Thus, Lee *et al.* [301] hypothesized that the absorption of theophylline through bronchial mucosa could be enhanced by administration with thiolated CS NPs, because of their greater mucoadhesiveness and permeability properties. In an allergic asthma mouse model, intranasal delivery of theophylline complexed with thiolated CS NPs augmented the anti-inflammatory effects of the drug compared to theophylline administered alone, or loaded into unmodified CS NPs.

1.3.3.3. Theragnosis

The concept "theragnosis" recently arose, combining diagnostic and therapy as a single platform, emerging from progresses on molecular imaging and nanomedicine. Advances in nanomedicine contribute to theragnosis with targeted drug delivery systems, reducing the systemic[55]. For accurate diagnosis, a variety of imaging tools may be used, such as fluorescence optical imaging, magnetic resonance imaging, positron-emission tomography, and computed tomography [302]. Hence, combining advanced imagiology technologies with targeted drug delivery is expected to achieve early diagnosis and personalized medicine, NPs playing a key role in this approach [303]. Theragnostic NPs comprise diagnostic and therapeutic functions in one integrated system, enabling diagnosis through noninvasive imaging agents, therapy, and monitorization of therapeutic response in simultaneous [304].

Self-assembled glycol CS NPs have shown to be efficient as theragnosis systems because they could simultaneously deliver different imaging agents and therapeutics (chemodrugs, nucleotides, peptides and photodynamic chemicals) [55]. The therapeutic agents could be simply encapsulated into NPs through hydrophobic or electrostatic interactions. Sun and colleagues verified that the stability of gold(Au) NPs increased owing to GC coating layer on the surface [305]. Tomographic images of tumor were successfully obtained in the tumor-xenografted animal model when the GC-Au NPs were used as a computed tomography contrast agent. The targetability of Au NPs was due to GC properties, because GC-AuNPs were accumulated in the tumor, while heparin-coated NPs were observed in the liver and spleen.

The effectiveness of the oleyl-CS as a stabilizer of iron oxide NPs (IONs) was assessed by Lee *et al.* [306]. EPR effect was responsible by higher tumor accumulation of iron oxide NPs/oleyl-CS NP observed by near infrared fluorescence optical and magnetic resonance imaging.

1.4. Conclusions

The application of CS nanoparticulate systems in drug delivery has great potential. Exciting concepts and sophisticated formulations have been produced using CS and its derivatives. However, several issues must be addressed such that these possibilities can be fully exploited and reach clinical application. A wider choice of pure, medical grade CS and its derivatives is needed. A better control over the stability of the NPs is

necessary, in particular at physiological pH. In many cases, *in vitro* results are not reproduced *in vivo*, hence more knowledge on the fate of the CS NPs *in vivo* is mandatory. The interaction of NPs with serum proteins (in the blood), the biodistribution and intracellular trafficking must be more comprehensively characterized, as well as toxicological issues.

Acknowledgments

Paula Pereira, Vera Carvalho and Reinaldo Ramos were supported respectively by the grant SFRH/BD/64977/2009, SFRH/BD/27359/2006, SFRH/BD/27404 / 2006, from Fundação para a Ciência e Tecnologia (FCT), Portugal. This review was also supported by FCT through the project PTDC/BIO/67160/2006.

1.5. References

1. Kas, H. S., Chitosan: properties, preparations and application to microparticulate systems. *J Microencapsul* **1997,** 14, (6), 689-711.
2. Muzzarelli, R. A. A., *Chitin / by Riccardo A. A. Muzzarelli*. Pergamon Press: Oxford ; New York :, 1977.
3. Croisier, F.; Jérôme, C., Chitosan-based biomaterials for tissue engineering. *European Polymer Journal* **2013,** 49, (4), 780-792.
4. Chandy, T.; Sharma, C. P., Chitosan--as a biomaterial. *Biomater Artif Cells Artif Organs* **1990,** 18, (1), 1-24.
5. He, C.; Yin, L.; Tang, C.; Yin, C., Trimethyl chitosan-cysteine nanoparticles for systemic delivery of TNF-alpha siRNA via oral and intraperitoneal routes. *Pharm Res* **2013,** 30, (10), 2596-606.
6. Lee, S. J.; Huh, M. S.; Lee, S. Y.; Min, S.; Lee, S.; Koo, H.; Chu, J.-U.; Lee, K. E.; Jeon, H.; Choi, Y.; Choi, K.; Byun, Y.; Jeong, S. Y.; Park, K.; Kim, K.; Kwon, I. C., Tumor-Homing Poly-siRNA/Glycol Chitosan Self-Cross-Linked Nanoparticles for Systemic siRNA Delivery in Cancer Treatment. *Angewandte Chemie International Edition* **2012,** 51, (29), 7203-7207.
7. Teng, Z.; Luo, Y.; Wang, Q., Carboxymethyl chitosan–soy protein complex nanoparticles for the encapsulation and controlled release of vitamin D3. *Food Chemistry* **2013,** 141, (1), 524-532.
8. Tian, Q.; Wang, X. H.; Wang, W.; Zhang, C. N.; Wang, P.; Yuan, Z., Self-assembly and liver targeting of sulfated chitosan nanoparticles functionalized with glycyrrhetinic acid. *Nanomedicine* **2012,** 8, (6), 870-9.
9. Uccello-Barretta, G.; Balzano, F.; Aiello, F.; Senatore, A.; Fabiano, A.; Zambito, Y., Mucoadhesivity and release properties of quaternary ammonium-chitosan conjugates and their nanoparticulate supramolecular aggregates: an NMR investigation. *Int J Pharm* **2014,** 461, (1-2), 489-94.
10. Sinha, V. R.; Singla, A. K.; Wadhawan, S.; Kaushik, R.; Kumria, R.; Bansal, K.; Dhawan, S., Chitosan microspheres as a potential carrier for drugs. *Int J Pharm* **2004,** 274, (1-2), 1-33.
11. Larsson, M.; Huang, W.-C.; Hsiao, M.-H.; Wang, Y.-J.; Nydén, M.; Chiou, S.-H.; Liu, D.-M., Biomedical applications and colloidal properties of amphiphilically modified chitosan hybrids. *Progress in Polymer Science* **2013,** 38, (9), 1307-1328.
12. Denkbas, E. B.; Ottenbrite, R. M., Perspectives on: Chitosan drug delivery systems based on their geometries. *Journal of Bioactive and Compatible Polymers* **2006,** 21, (4), 351-368.
13. Muzzarelli, R. A. A.; Muzzarelli, C., Chitosan chemistry: Relevance to the biomedical sciences. *Polysaccharides 1: Structure, Characterization and Use* **2005,** 186, 151-209.
14. Bernkop-Schnurch, A.; Dunnhaupt, S., Chitosan-based drug delivery systems. *Eur J Pharm Biopharm* **2012,** 81, (3), 463-9.

15. Unsoy, G.; Khodadust, R.; Yalcin, S.; Mutlu, P.; Gunduz, U., Synthesis of Doxorubicin loaded magnetic chitosan nanoparticles for pH responsive targeted drug delivery. *Eur J Pharm Sci* **2014,** 62C, 243-250.

16. Chuah, L. H.; Roberts, C. J.; Billa, N.; Abdullah, S.; Rosli, R., Cellular uptake and anticancer effects of mucoadhesive curcumin-containing chitosan nanoparticles. *Colloids Surf B Biointerfaces* **2014,** 116, 228-36.

17. Chen, X. G.; Wang, Z.; Liu, W. S.; Park, H. J., The effect of carboxymethyl-chitosan on proliferation and collagen secretion of normal and keloid skin fibroblasts. *Biomaterials* **2002,** 23, (23), 4609-4614.

18. Mi, F. L.; Wu, Y. B.; Shyu, S. S.; Schoung, J. Y.; Huang, Y. B.; Tsai, Y. H.; Hao, J. Y., Control of wound infections using a bilayer chitosan wound dressing with sustainable antibiotic delivery. *Journal of Biomedical Materials Research* **2002,** 59, (3), 438-449.

19. Mi, F. L.; Shyu, S. S.; Wu, Y. B.; Lee, S. T.; Shyong, J. Y.; Huang, R. N., Fabrication and characterization of a sponge-like asymmetric chitosan membrane as a wound dressing. *Biomaterials* **2001,** 22, (2), 165-173.

20. Dai, T.; Tanaka, M.; Huang, Y. Y.; Hamblin, M. R., Chitosan preparations for wounds and burns: antimicrobial and wound-healing effects. *Expert review of anti-infective therapy* **2011,** 9, (7), 857-79.

21. Bonferoni, M. C.; Sandri, G.; Dellera, E.; Rossi, S.; Ferrari, F.; Mori, M.; Caramella, C., Ionic polymeric micelles based on chitosan and fatty acids and intended for wound healing. Comparison of linoleic and oleic acid. *Eur J Pharm Biopharm* **2014,** 87, (1), 101-6.

22. Bumgardner, J. D.; Wiser, R.; Gerard, P. D.; Bergin, P.; Chestnutt, B.; Marin, M.; Ramsey, V.; Elder, S. H.; Gilbert, J. A., Chitosan: potential use as a bioactive coating for orthopaedic and craniofacial/dental implants. *J Biomater Sci Polym Ed* **2003,** 14, (5), 423-38.

23. Nikpour, M. R.; Rabiee, S. M.; Jahanshahi, M., Synthesis and characterization of hydroxyapatite/chitosan nanocomposite materials for medical engineering applications. *Composites Part B: Engineering* **2012,** 43, (4), 1881-1886.

24. Yokoyama, A.; Yamamoto, S.; Kawasaki, T.; Kohgo, T.; Nakasu, M., Development of calcium phosphate cement using chitosan and citric acid for bone substitute materials. *Biomaterials* **2002,** 23, (4), 1091-1101.

25. Zhang, Y.; Zhang, M. Q., Three-dimensional macroporous calcium phosphate bioceramics with nested chitosan sponges for load-bearing bone implants. *Journal of Biomedical Materials Research* **2002,** 61, (1), 1-8.

26. Levengood, S. K. L.; Zhang, M., Chitosan-based scaffolds for bone tissue engineering. *Journal of Materials Chemistry B* **2014,** 2, (21), 3161-3184.

27. Martins, A. M.; Eng, G.; Caridade, S. G.; Mano, J. F.; Reis, R. L.; Vunjak-Novakovic, G., Electrically Conductive Chitosan/Carbon Scaffolds for Cardiac Tissue Engineering. *Biomacromolecules* **2014,** 15, (2), 635-643.

28. Raftery, R.; O'Brien, F. J.; Cryan, S. A., Chitosan for gene delivery and orthopedic tissue engineering applications. *Molecules (Basel, Switzerland)* **2013,** 18, (5), 5611-47.

29. Ragetly, G. R.; Slavik, G. J.; Cunningham, B. T.; Schaeffer, D. J.; Griffon, D. J., Cartilage tissue engineering on fibrous chitosan scaffolds produced by a replica molding technique. *J Biomed Mater Res A* **2010,** 93, (1), 46-55.

30. Ravi Kumar, M. N. V., A review of chitin and chitosan applications. *Reactive and Functional Polymers* **2000,** 46, (1), 1-27.

31. Fulgencio Gde, O.; Viana, F. A.; Ribeiro, R. R.; Yoshida, M. I.; Faraco, A. G.; Cunha-Junior Ada, S., New mucoadhesive chitosan film for ophthalmic drug delivery of timolol maleate: in vivo evaluation. *Journal of ocular pharmacology and therapeutics : the official journal of the Association for Ocular Pharmacology and Therapeutics* **2012,** 28, (4), 350-8.

32. Yang, L. Q.; Lan, Y. Q.; Guo, H.; Cheng, L. Z.; Fan, J. Z.; Cai, X.; Zhang, L. M.; Chen, R. F.; Zhou, H. S., Ophthalmic drug-loaded N,O-carboxymethyl chitosan hydrogels: synthesis, *In vitro* and in vivo evaluation. *Acta pharmacologica Sinica* **2010,** 31, (12), 1625-34.

33. Ameeduzzafar; Ali, J.; Bhatnagar, A.; Kumar, N.; Ali, A., Chitosan nanoparticles amplify the ocular hypotensive effect of cateolol in rabbits. *Int J Biol Macromol* **2014,** 65, 479-91.

34. Vikhoreva, G.; Bannikova, G.; Stolbushkina, P.; Panov, A.; Drozd, N.; Makarov, V.; Varlamov, V.; Gal'braikh, L., Preparation and anticoagulant activity of a low-molecular-weight sulfated chitosan. *Carbohydrate Polymers* **2005,** 62, (4), 327-332.

35. Hirano, S., Chitin and chitosan as novel biotechnological materials. *Polymer International* **1999,** 48, (8), 732-734.

36. Liu, J.; Zhang, J.; Xia, W., Hypocholesterolaemic effects of different chitosan samples *In vitro* and in vivo. *Food Chemistry* **2008,** 107, (1), 419-425.

37. Zhang, J.; Xia, W.; Liu, P.; Cheng, Q.; Tahi, T.; Gu, W.; Li, B., Chitosan Modification and Pharmaceutical/Biomedical Applications. *Marine Drugs* **2010,** 8, (7), 1962-1987.

38. El-Mekawy, A.; Hegab, H. M.; El-Baz, A.; Hudson, S. M., Fabrication and Characterization of Fungal Chitosan-SAP Membranes for Hemostatic Application. *Current Biochemical Engineering* **2014,** 1, 75-82.

39. Gaafar, M. R.; Mady, R. F.; Diab, R. G.; Shalaby, T. I., Chitosan and silver nanoparticles: Promising anti-toxoplasma agents. *Experimental Parasitology* **2014,** 143, (0), 30-38.

40. Jeon, S. J.; Oh, M.; Yeo, W.-S.; Galvão, K. N.; Jeong, K. C., Underlying Mechanism of Antimicrobial Activity of Chitosan Microparticles and Implications for the Treatment of Infectious Diseases. *PLoS ONE* **2014,** 9, (3), e92723.

41. Kong, M.; Chen, X. G.; Xing, K.; Park, H. J., Antimicrobial properties of chitosan and mode of action: a state of the art review. *International journal of food microbiology* **2010,** 144, (1), 51-63.

42. Mohamed, R. R.; Sabaa, M. W., Synthesis and characterization of antimicrobial crosslinked carboxymethyl chitosan nanoparticles loaded with silver. *Int J Biol Macromol* **2014,** 69C, 95-99.

43. Tan, H.; Ma, R.; Lin, C.; Liu, Z.; Tang, T., Quaternized chitosan as an antimicrobial agent: antimicrobial activity, mechanism of action and biomedical applications in orthopedics. *International journal of molecular sciences* **2013,** 14, (1), 1854-69.

44. Garcia-Fuentes, M.; Alonso, M. J., Chitosan-based drug nanocarriers: where do we stand? *Journal of controlled release : official journal of the Controlled Release Society* **2012,** 161, (2), 496-504.

45. Ragelle, H.; Vandermeulen, G.; Preat, V., Chitosan-based siRNA delivery systems. *J Control Release* **2013,** 172, (1), 207-18.

46. Sayari, E.; Dinarvand, M.; Amini, M.; Azhdarzadeh, M.; Mollarazi, E.; Ghasemi, Z.; Atyabi, F., MUC1 aptamer conjugated to chitosan nanoparticles, an efficient targeted carrier designed for anticancer SN38 delivery. *Int J Pharm* **2014**.

47. Panyam, J.; Labhasetwar, V., Biodegradable nanoparticles for drug and gene delivery to cells and tissue. *Advanced Drug Delivery Reviews* **2003,** 55, (3), 329-347.

48. Nagarwal, R. C.; Kant, S.; Singh, P. N.; Maiti, P.; Pandit, J. K., Polymeric nanoparticulate system: A potential approach for ocular drug delivery. *Journal of Controlled Release* **2009,** 136, (1), 2-13.

49. Hu, Y.; Jiang, X. Q.; Ding, Y.; Ge, H. X.; Yuan, Y. Y.; Yang, C. Z., Synthesis and characterization of chitosan-poly(acrylic acid) nanoparticles. *Biomaterials* **2002,** 23, (15), 3193-3201.

50. Mitra, S.; Gaur, U.; Ghosh, P. C.; Maitra, A. N., Tumour targeted delivery of encapsulated dextran–doxorubicin conjugate using chitosan nanoparticles as carrier. *Journal of Controlled Release* **2001,** 74, (1–3), 317-323.

51. Nipun , B. V.; Kannan, S., Enhanced delivery of baicalein using cinnamaldehyde cross-linked chitosan nanoparticle inducing apoptosis. *Int J Biol Macromol* **2012,** 51, (5), 1103-8.

52. Rampino, A.; Borgogna, M.; Blasi, P.; Bellich, B.; Cesàro, A., Chitosan nanoparticles: Preparation, size evolution and stability. *International Journal of Pharmaceutics* **2013,** 455, (1–2), 219-228.

53. Tavares, I. S.; Caroni, A. L.; Dantas Neto, A. A.; Pereira, M. R.; Fonseca, J. L., Surface charging and dimensions of chitosan coacervated nanoparticles. *Colloids Surf B Biointerfaces* **2012,** 90, 254-8.

54. Tokumitsu, H.; Ichikawa, H.; Fukumori, Y., Chitosan-gadopentetic acid complex nanoparticles for gadolinium neutron-capture therapy of cancer: preparation by novel emulsion-droplet coalescence technique and characterization. *Pharm Res* **1999,** 16, (12), 1830-5.

55. Yhee, J. Y.; Son, S.; Kim, S. H.; Park, K.; Choi, K.; Kwon, I. C., Self-assembled glycol chitosan nanoparticles for disease-specific theranostics. *J Control Release* **2014**.

56. Bodmeier, R.; Chen, H. G.; Paeratakul, O., A novel approach to the oral delivery of micro- or nanoparticles. *Pharm Res* **1989,** 6, (5), 413-7.

57. Calvo, P.; Remunan-Lopez, C.; Vila-Jato, J. L.; Alonso, M. J., Chitosan and chitosan/ethylene oxide-propylene oxide block copolymer nanoparticles as novel carriers for proteins and vaccines. *Pharm Res* **1997,** 14, (10), 1431-6.

58. Fernandez-Urrusuno, R.; Calvo, P.; Remunan-Lopez, C.; Vila-Jato, J. L.; Alonso, M. J., Enhancement of nasal absorption of insulin using chitosan nanoparticles. *Pharm Res* **1999,** 16, (10), 1576-81.

59. Liu, C.; Tan, Y.; Liu, C.; Chen, X.; Yu, L., Preparations, characterizations and applications of chitosan-based nanoparticles. *Journal of Ocean University of China (English Edition)* **2007,** 6, (3), 237-243.

60. Mansouri, S.; Cuie, Y.; Winnik, F.; Shi, Q.; Lavigne, P.; Benderdour, M.; Beaumont, E.; Fernandes, J. C., Characterization of folate-chitosan-DNA nanoparticles for gene therapy. *Biomaterials* **2006,** 27, (9), 2060-5.

61. Chen, F.; Zhang, Z. R.; Huang, Y., Evaluation and modification of N-trimethyl chitosan chloride nanoparticles as protein carriers. *Int J Pharm* **2007,** 336, (1), 166-73.

62. Gan, Q.; Wang, T., Chitosan nanoparticle as protein delivery carrier--systematic examination of fabrication conditions for efficient loading and release. *Colloids Surf B Biointerfaces* **2007,** 59, (1), 24-34.

63. Xu, Y.; Du, Y., Effect of molecular structure of chitosan on protein delivery properties of chitosan nanoparticles. *Int J Pharm* **2003,** 250, (1), 215-26.

64. Anitha, A.; Rejinold, N. S.; Bumgardner, J. D.; Nair, S. V.; Jayakumar, R., Approaches for Functional Modification or Cross-Linking of Chitosan. In *Chitosan-Based Systems for Biopharmaceuticals*, John Wiley & Sons, Ltd: 2012; pp 107-124.

65. Lin, Y. H.; Tsai, S. C.; Lai, C. H.; Lee, C. H.; He, Z. S.; Tseng, G. C., Genipin-cross-linked fucose-chitosan/heparin nanoparticles for the eradication of Helicobacter pylori. *Biomaterials* **2013,** 34, (18), 4466-79.

66. Bodnar, M.; Hartmann, J. F.; Borbely, J., Synthesis and Study of Cross-Linked Chitosan-N-Poly(ethylene glycol) Nanoparticles. *Biomacromolecules* **2006,** 7, (11), 3030-3036.

67. Pujana, M. A.; Pérez-Álvarez, L.; Cesteros Iturbe, L. C.; Katime, I., "Water dispersible pH-responsive chitosan nanogels modified with biocompatible crosslinking-agents". *Polymer* **2012,** 53, (15), 3107-3116.

68. Ohya, Y.; Shiratani, M.; Kobayashi, H.; Ouchi, T., Release Behavior of 5-Fluorouracil from Chitosan-Gel Nanospheres Immobilizing 5-Fluorouracil Coated with Polysaccharides and Their Cell Specific Cytotoxicity. *Journal of Macromolecular Science, Part A* **1994,** 31, (5), 629-642.

69. Barthelmes, J.; Dunnhaupt, S.; Hombach, J.; Bernkop-Schnurch, A., Thiomer nanoparticles: stabilization via covalent cross-linking. *Drug delivery* **2011,** 18, (8), 613-9.

70. Thanoo, B. C.; Sunny, M. C.; Jayakrishnan, A., Cross-Linked Chitosan Microspheres - Preparation and Evaluation as a Matrix for the Controlled Release of Pharmaceuticals. *Journal of Pharmacy and Pharmacology* **1992,** 44, (4), 283-286.

71. Akbuga, J.; Durmaz, G., Preparation and Evaluation of Cross-Linked Chitosan Microspheres Containing Furosemide. *International Journal of Pharmaceutics* **1994,** 111, (3), 217-222.

72. Jameela, S. R.; Jayakrishnan, A., Glutaraldehyde Cross-Linked Chitosan Microspheres as a Long-Acting Biodegradable Drug-Delivery Vehicle - Studies on the in-Vitro Release of Mitoxantrone and in-Vivo Degradation of Microspheres in Rat Muscle. *Biomaterials* **1995,** 16, (10), 769-775.

73. Pavanetto, F.; Perugini, P.; Conti, B.; Modena, T.; Genta, I., Evaluation of process parameters involved in chitosan microsphere preparation by the o/w/o multiple emulsion method. *Journal of Microencapsulation* **1996,** 13, (6), 679-688.

74. Hennink, W. E.; van Nostrum, C. F., Novel crosslinking methods to design hydrogels. *Advanced Drug Delivery Reviews* **2002,** 54, (1), 13-36.

75. Nishimura, K.; Nishimura, S.; Seo, H.; Nishi, N.; Tokura, S.; Azuma, I., Macrophage activation with multi-porous beads prepared from partially deacetylated chitin. *J Biomed Mater Res* **1986,** 20, (9), 1359-72.

76. Maitra, A., Determination of size parameters of water-Aerosol OT-oil reverse micelles from their nuclear magnetic resonance data. *The Journal of Physical Chemistry* **1984,** 88, (21), 5122-5125.

77. Agnihotri, S. A.; Mallikarjuna, N. N.; Aminabhavi, T. M., Recent advances on chitosan-based micro- and nanoparticles in drug delivery. *J Control Release* **2004,** 100, (1), 5-28.

78. de Moura, M. R.; Aouada, F. A.; Mattoso, L. H. C., Preparation of chitosan nanoparticles using methacrylic acid. *Journal of Colloid and Interface Science* **2008,** 321, (2), 477-483.

79. Shi, J.; Xiao, Z.; Kamaly, N.; Farokhzad, O. C., Self-Assembled Targeted Nanoparticles: Evolution of Technologies and Bench to Bedside Translation. *Accounts of Chemical Research* **2011,** 44, (10), 1123-1134.

80. Gonçalves, C.; Pereira, P.; Gama, M., Self-Assembled Hydrogel Nanoparticles for Drug Delivery Applications. *Materials* **2010,** 3.

81. Quinones, J. P.; Gothelf, K. V.; Kjems, J.; Yang, C.; Caballero, A. M.; Schmidt, C.; Covas, C. P., Self-assembled nanoparticles of modified-chitosan conjugates for the sustained release of DL-alpha-tocopherol. *Carbohydr Polym* **2013,** 92, (1), 856-64.

82. Koo, H.; Min, K. H.; Lee, S. C.; Park, J. H.; Park, K.; Jeong, S. Y.; Choi, K.; Kwon, I. C.; Kim, K., Enhanced drug-loading and therapeutic efficacy of hydrotropic oligomer-conjugated glycol chitosan nanoparticles for tumor-targeted paclitaxel delivery. *J Control Release* **2013,** 172, (3), 823-31.

83. Quinones, J. P.; Gothelf, K. V.; Kjems, J.; Caballero, A. M.; Schmidt, C.; Covas, C. P., N,O6-partially acetylated chitosan nanoparticles hydrophobically-modified for controlled release of steroids and vitamin E. *Carbohydr Polym* **2013,** 91, (1), 143-51.

84. Dimitrov, D. S., Therapeutic proteins. *Methods in molecular biology (Clifton, N.J.)* **2012,** 899, 1-26.

85. Haag, R.; Kratz, F., Polymer therapeutics: concepts and applications. *Angew Chem Int Ed Engl* **2006,** 45, (8), 1198-215.

86. Schellekens, H., Bioequivalence and the immunogenicity of biopharmaceuticals. *Nat Rev Drug Discov* **2002,** 1, (6), 457-62.

87. Nair, L. S.; Laurencin, C. T., Polymers as biomaterials for tissue engineering and controlled drug delivery. *Adv Biochem Eng Biotechnol* **2006,** 102, 47-90.

88. Schellekens, H., Immunogenicity of therapeutic proteins: clinical implications and future prospects. *Clin Ther* **2002,** 24, (11), 1720-40; discussion 1719.

89. Tan, M. L.; Choong, P. F. M.; Dass, C. R., Recent developments in liposomes, microparticles and nanoparticles for protein and peptide drug delivery. *Peptides* **2010,** 31, (1), 184-193.

90. Branco, M. C.; Schneider, J. P., Self-assembling materials for therapeutic delivery. *Acta Biomater* **2009,** 5, (3), 817-31.

91. Kim, S.; Kim, J. H.; Jeon, O.; Kwon, I. C.; Park, K., Engineered polymers for advanced drug delivery. *Eur J Pharm Biopharm* **2009,** 71, (3), 420-30.

92. Pisal, D. S.; Kosloski, M. P.; Balu-Iyer, S. V., Delivery of therapeutic proteins. *Journal of Pharmaceutical Sciences* **2010,** 99, (6), 2557-2575.

93. Yun, Y.; Cho, Y. W.; Park, K., Nanoparticles for oral delivery: Targeted nanoparticles with peptidic ligands for oral protein delivery. *Advanced Drug Delivery Reviews* **2013,** 65, (6), 822-832.

94. Kumar, M.; Pandey, R. S.; Patra, K. C.; Jain, S. K.; Soni, M. L.; Dangi, J. S.; Madan, J., Evaluation of neuropeptide loaded trimethyl chitosan nanoparticles for nose to brain delivery. *Int J Biol Macromol* **2013,** 61, 189-95.

95. Mukhopadhyay, P.; Mishra, R.; Rana, D.; Kundu, P. P., Strategies for effective oral insulin delivery with modified chitosan nanoparticles: A review. *Progress in Polymer Science* **2012,** 37, (11), 1457-1475.

96. Piras, A. M.; Maisetta, G.; Sandreschi, S.; Esin, S.; Gazzarri, M.; Batoni, G.; Chiellini, F., Preparation, physical–chemical and biological characterization of chitosan nanoparticles loaded with lysozyme. *International Journal of Biological Macromolecules* **2014,** 67, (0), 124-131.

97. Amidi, M.; Mastrobattista, E.; Jiskoot, W.; Hennink, W. E., Chitosan-based delivery systems for protein therapeutics and antigens. *Advanced Drug Delivery Reviews* **2010,** 62, (1), 59-82.

98. Jitendra; Sharma, P. K.; Bansal, S.; Banik, A., Noninvasive routes of proteins and peptides drug delivery. *Indian journal of pharmaceutical sciences* **2011,** 73, (4), 367-75.

99. Lin, Y. H.; Sonaje, K.; Lin, K. M.; Juang, J. H.; Mi, F. L.; Yang, H. W.; Sung, H. W., Multi-ion-crosslinked nanoparticles with pH-responsive characteristics for oral delivery of protein drugs. *J Control Release* **2008,** 132, (2), 141-9.

100. Mi, F. L.; Wu, Y. Y.; Lin, Y. H.; Sonaje, K.; Ho, Y. C.; Chen, C. T.; Juang, J. H.; Sung, H. W., Oral delivery of peptide drugs using nanoparticles self-assembled by poly(gamma-glutamic acid) and a chitosan derivative functionalized by trimethylation. *Bioconjug Chem* **2008,** 19, (6), 1248-55.

101. Rosenthal, R.; Günzel, D.; Finger, C.; Krug, S. M.; Richter, J. F.; Schulzke, J.-D.; Fromm, M.; Amasheh, S., The effect of chitosan on transcellular and paracellular mechanisms in the intestinal epithelial barrier. *Biomaterials* **2012,** 33, (9), 2791-2800.

102. Benediktsdóttir, B. E.; Gudjónsson, T.; Baldursson, Ó.; Másson, M., N-alkylation of highly quaternized chitosan derivatives affects the paracellular permeation enhancement in bronchial epithelia *In vitro*. *European Journal of Pharmaceutics and Biopharmaceutics* **2014,** 86, (1), 55-63.

103. Siew, A.; Le, H.; Thiovolet, M.; Gellert, P.; Schatzlein, A.; Uchegbu, I., Enhanced Oral Absorption of Hydrophobic and Hydrophilic Drugs Using Quaternary Ammonium Palmitoyl Glycol Chitosan Nanoparticles. *Molecular Pharmaceutics* **2011,** 9, (1), 14-28.

104. Thanou, M.; Verhoef, J. C.; Junginger, H. E., Oral drug absorption enhancement by chitosan and its derivatives. *Adv Drug Deliv Rev* **2001,** 52, (2), 117-26.

105. Bravo-Osuna, I.; Vauthier, C.; Farabollini, A.; Palmieri, G. F.; Ponchel, G., Mucoadhesion mechanism of chitosan and thiolated chitosan-poly(isobutyl cyanoacrylate) core-shell nanoparticles. *Biomaterials* **2007,** 28, (13), 2233-43.

106. Lin, Y., Chen, CT., Liang, HF., Kulkarni, A. R., Lee, PW., Chen, CH., Sung, HW, Novel nanoparticles for oral insulin delivery via the paracellular pathway. *Nanotechnology* **2007,** 18, 105102-105113.

107. Sonaje, K.; Lin, Y.-H.; Juang, J.-H.; Wey, S.-P.; Chen, C.-T.; H-W., S., In vivo evaluation of safety and efficacy of self-assembled nanoparticles for oral insulin delivery. *Biomaterials* **2009,** 30, 2329-2339.

108. Kotze, A. F.; Luessen, H. L.; de Leeuw, B. J.; de Boer, A. G.; Verhoef, J. C.; Junginger, H. E., Comparison of the effect of different chitosan salts and N-trimethyl chitosan chloride on the permeability of intestinal epithelial cells (Caco-2). *J Control Release* **1998,** 51, (1), 35-46.

109. Mukhopadhyay, P.; Sarkar, K.; Chakraborty, M.; Bhattacharya, S.; Mishra, R.; Kundu, P. P., Oral insulin delivery by self-assembled chitosan nanoparticles: *In vitro* and in vivo studies in diabetic animal model. *Materials Science and Engineering: C* **2013,** 33, (1), 376-382.

110. Jintapattanakit, A.; Junyaprasert, V. B.; Mao, S.; Sitterberg, J.; Bakowsky, U.; Kissel, T., Peroral delivery of insulin using chitosan derivatives: a comparative study of polyelectrolyte nanocomplexes and nanoparticles. *Int J Pharm* **2007,** 342, (1-2), 240-9.

111. Yin, L.; Ding, J.; He, C.; Cui, L.; Tang, C.; Yin, C., Drug permeability and mucoadhesion properties of thiolated trimethyl chitosan nanoparticles in oral insulin delivery. *Biomaterials* **2009,** 30, (29), 5691-700.

112. Qian, F.; Cui, F.; Ding, J.; Tang, C.; Yin, C., Chitosan graft copolymer nanoparticles for oral protein drug delivery: preparation and characterization. *Biomacromolecules* **2006,** 7, (10), 2722-7.

113. Makhlof, A.; Tozuka, Y.; Takeuchi, H., Design and evaluation of novel pH-sensitive chitosan nanoparticles for oral insulin delivery. *European Journal of Pharmaceutical Sciences* **2011,** 42, (5), 445-451.

114. Zhang, N.; Li, J.; Jiang, W.; Ren, C.; Li, J.; Xin, J.; Li, K., Effective protection and controlled release of insulin by cationic β-cyclodextrin polymers from alginate/chitosan nanoparticles. *International Journal of Pharmaceutics* **2010,** 393, (1–2), 213-219.

115. Trapani, A.; Lopedota, A.; Franco, M.; Cioffi, N.; Ieva, E.; Garcia-Fuentes, M.; Alonso, M. J., A comparative study of chitosan and chitosan/cyclodextrin nanoparticles as potential carriers for the oral delivery of small peptides. *European Journal of Pharmaceutics and Biopharmaceutics* **2010,** 75, (1), 26-32.

116. Lalatsa, A.; Schatzlein, A. G.; Uchegbu, I. F., Strategies To Deliver Peptide Drugs to the Brain. *Molecular Pharmaceutics* **2014,** 11, (4), 1081-1093.

117. Lalatsa, A.; Garrett, N. L.; Ferrarelli, T.; Moger, J.; Schätzlein, A. G.; Uchegbu, I. F., Delivery of Peptides to the Blood and Brain after Oral Uptake of Quaternary Ammonium Palmitoyl Glycol Chitosan Nanoparticles. *Molecular Pharmaceutics* **2012,** 9, (6), 1764-1774.

118. Soane, R. J.; Hinchcliffe, M.; Davis, S. S.; Illum, L., Clearance characteristics of chitosan based formulations in the sheep nasal cavity. *Int J Pharm* **2001,** 217, (1-2), 183-91.

119. Soane, R. J.; Frier, M.; Perkins, A. C.; Jones, N. S.; Davis, S. S.; Illum, L., Evaluation of the clearance characteristics of bioadhesive systems in humans. *Int J Pharm* **1999,** 178, (1), 55-65.

120. Davis, S. S., Nasal vaccines. *Adv Drug Deliv Rev* **2001,** 51, (1-3), 21-42.

121. Illum, L.; Jabbal-Gill, I.; Hinchcliffe, M.; Fisher, A. N.; Davis, S. S., Chitosan as a novel nasal delivery system for vaccines. *Adv Drug Deliv Rev* **2001,** 51, (1-3), 81-96.

122. Liu, Q.; Zheng, X.; Zhang, C.; Shao, X.; Zhang, X.; Zhang, Q.; Jiang, X., Antigen-conjugated N-trimethylaminoethylmethacrylate Chitosan Nanoparticles Induce Strong Immune Responses After Nasal Administration. *Pharm Res* **2014**.

123. Subbiah, R.; Ramalingam, P.; Ramasundaram, S.; Kim, D. Y.; Park, K.; Ramasamy, M. K.; Choi, K. J., N,N,N-Trimethyl chitosan nanoparticles for controlled intranasal delivery of HBV surface antigen. *Carbohydrate Polymers* **2012,** 89, (4), 1289-1297.

124. Verheul, R. J.; Hagenaars, N.; van Es, T.; van Gaal, E. V. B.; de Jong, P. H. J. L. F.; Bruijns, S.; Mastrobattista, E.; Slütter, B.; Que, I.; Heldens, J. G. M.; van den Bosch, H.; Glansbeek, H. L.; Hennink, W. E.; Jiskoot, W., A step-by-step approach to study the influence of N-acetylation on the adjuvanticity of N,N,N-trimethyl chitosan (TMC) in an intranasal nanoparticulate influenza virus vaccine. *European Journal of Pharmaceutical Sciences* **2012,** 45, (4), 467-474.

125. Illum, L., Nasal drug delivery--possibilities, problems and solutions. *J Control Release* **2003,** 87, (1-3), 187-98.

126. Illum, L.; Farraj, N. F.; Davis, S. S., Chitosan as a novel nasal delivery system for peptide drugs. *Pharm Res* **1994,** 11, (8), 1186-9.

127. Vicente, S.; Peleteiro, M.; Díaz-Freitas, B.; Sanchez, A.; González-Fernández, Á.; Alonso, M. J., Co-delivery of viral proteins and a TLR7 agonist from polysaccharide nanocapsules: A needle-free vaccination strategy. *Journal of Controlled Release* **2013,** 172, (3), 773-781.

128. Casettari, L.; Illum, L., Chitosan in nasal delivery systems for therapeutic drugs. *J Control Release* **2014**.

129. Amidi, M.; Romeijn, S. G.; Borchard, G.; Junginger, H. E.; Hennink, W. E.; Jiskoot, W., Preparation and characterization of protein-loaded N-trimethyl chitosan nanoparticles as nasal delivery system. *J Control Release* **2006,** 111, (1-2), 107-16.

130. Zhang, X.; Zhang, H.; Wu, Z.; Wang, Z.; Niu, H.; Li, C., Nasal absorption enhancement of insulin using PEG-grafted chitosan nanoparticles. *Eur J Pharm Biopharm* **2008,** 68, (3), 526-34.

131. Wang, X.; Zheng, C.; Wu, Z.; Teng, D.; Zhang, X.; Wang, Z.; Li, C., Chitosan-NAC Nanoparticles as a Vehicle for Nasal Absorption Enhancement of Insulin. *J Biomed Mater Res Part B: Appl Biomater B* **2009,** 88, 150-161.

132. Csaba, N.; Garcia-Fuentes, M.; Alonso, M. J., Nanoparticles for nasal vaccination. *Adv Drug Deliv Rev* **2009,** 61, (2), 140-57.

133. Westerink, M. A.; Smithson, S. L.; Srivastava, N.; Blonder, J.; Coeshott, C.; Rosenthal, G. J., ProJuvant (Pluronic F127/chitosan) enhances the immune response to intranasally administered tetanus toxoid. *Vaccine* **2001,** 20, (5-6), 711-23.

134. Moon, H. J.; Lee, J. S.; Talactac, M. R.; Chowdhury, M. Y.; Kim, J. H.; Park, M. E.; Choi, Y. K.; Sung, M. H.; Kim, C. J., Mucosal immunization with recombinant influenza hemagglutinin protein and poly gamma-glutamate/chitosan nanoparticles induces protection against highly pathogenic influenza A virus. *Veterinary microbiology* **2012,** 160, (3-4), 277-89.

135. Kohler, D., Aerosols for systemic treatment. *Lung* **1990,** 168 Suppl, 677-84.

136. Yamamoto, A., [Improvement of transmucosal absorption of biologically active peptide drugs]. *Yakugaku Zasshi* **2001,** 121, (12), 929-48.

137. Garcia-Contreras, L.; Morcol, T.; Bell, S. J.; Hickey, A. J., Evaluation of novel particles as pulmonary delivery systems for insulin in rats. *AAPS PharmSci* **2003,** 5, (2), E9.

138. Paranjpe, M.; Muller-Goymann, C. C., Nanoparticle-mediated pulmonary drug delivery: a review. *International journal of molecular sciences* **2014,** 15, (4), 5852-73.

139. Courrier, H. M.; Butz, N.; Vandamme, T. F., Pulmonary drug delivery systems: recent developments and prospects. *Crit Rev Ther Drug Carrier Syst* **2002,** 19, (4-5), 425-98.

140. Ahsan, F.; Rivas, I. P.; Khan, M. A.; Torres Suarez, A. I., Targeting to macrophages: role of physicochemical properties of particulate carriers--liposomes and microspheres--on the phagocytosis by macrophages. *J Control Release* **2002,** 79, (1-3), 29-40.

141. Al-Qadi, S.; Grenha, A.; Carrión-Recio, D.; Seijo, B.; Remuñán-López, C., Microencapsulated chitosan nanoparticles for pulmonary protein delivery: In vivo evaluation of insulin-loaded formulations. *Journal of Controlled Release* **2012,** 157, (3), 383-390.

142. Asghar, L. F.; Chandran, S., Multiparticulate formulation approach to colon specific drug delivery: current perspectives. *J Pharm Pharm Sci* **2006,** 9, (3), 327-38.

143. Bayat, A.; Dorkoosh, F. A.; Dehpour, A. R.; Moezi, L.; Larijani, B.; Junginger, H. E.; Rafiee-Tehrani, M., Nanoparticles of quaternized chitosan derivatives as a carrier for colon delivery of insulin: ex vivo and in vivo studies. *Int J Pharm* **2008,** 356, (1-2), 259-66.

144. Mao, S.; Sun, W.; Kissel, T., Chitosan-based formulations for delivery of DNA and siRNA. *Adv Drug Deliv Rev* **2009**.

145. Jayakumar, R.; Chennazhi, K. P.; Muzzarelli, R. A. A.; Tamura, H.; Nair, S. V.; Selvamurugan, N., Chitosan conjugated DNA nanoparticles in gene therapy. *Carbohydrate Polymers* **2010,** 79, (1), 1-8.

146. Vauthier, C.; Zandanel, C.; Ramon, A. L., Chitosan-based nanoparticles for in vivo delivery of interfering agents including siRNA. *Current Opinion in Colloid & Interface Science* **2013,** 18, (5), 406-418.

147. Sung, H.-W.; Sonaje, K.; Liao, Z.-X.; Hsu, L.-W.; Chuang, E.-Y., pH-Responsive Nanoparticles Shelled with Chitosan for Oral Delivery of Insulin: From Mechanism to Therapeutic Applications. *Accounts of Chemical Research* **2012,** 45, (4), 619-629.

148. Su, F.-Y.; Lin, K.-J.; Sonaje, K.; Wey, S.-P.; Yen, T.-C.; Ho, Y.-C.; Panda, N.; Chuang, E.-Y.; Maiti, B.; Sung, H.-W., Protease inhibition and absorption enhancement by functional nanoparticles for effective oral insulin delivery. *Biomaterials* **2012,** 33, (9), 2801-2811.

149. Sonaje, K.; Chen, Y.-J.; Chen, H.-L.; Wey, S.-P.; Juang, J.-H.; Nguyen, H.-N.; Hsu, C.-W.; Lin, K.-J.; Sung, H.-W., Enteric-coated capsules filled with freeze-dried chitosan/poly(γ-glutamic acid) nanoparticles for oral insulin delivery. *Biomaterials* **2010,** 31, (12), 3384-3394.

150. Huang, X.; Du, Y.-Z.; Yuan, H.; Hu, F.-Q., Preparation and pharmacodynamics of low-molecular-weight chitosan nanoparticles containing insulin. *Carbohydrate Polymers* **2009,** 76.

151. Prego, C.; Torres, D.; Fernandez-Megia, E.; Novoa-Carballal, R.; Quinoa, E.; Alonso, M. J., Chitosan-PEG nanocapsules as new carriers for oral peptide delivery. Effect of chitosan pegylation degree. *J Control Release* **2006,** 111, (3), 299-308.

152. Yamamoto, H.; Kuno, Y.; Sugimoto, S.; Takeuchi, H.; Kawashima, Y., Surface-modified PLGA nanosphere with chitosan improved pulmonary delivery of calcitonin by mucoadhesion and opening of the intercellular tight junctions. *J Control Release* **2005,** 102, (2), 373-81.

153. Makhlof, A.; Werle, M.; Tozuka, Y.; Takeuchi, H., Nanoparticles of glycol chitosan and its thiolated derivative significantly improved the pulmonary delivery of calcitonin. *International Journal of Pharmaceutics* **2010,** 397, (1–2), 92-95.

154. Chen, M. C.; Wong, H. S.; Lin, K. J.; Chen, H. L.; Wey, S. P.; Sonaje, K.; Lin, Y. H.; Chu, C. Y.; Sung, H. W., The characteristics, biodistribution and bioavailability of a chitosan-based nanoparticulate system for the oral delivery of heparin. *Biomaterials* **2009,** 30, (34), 6629-37.

155. Trapani, A.; Di Gioia, S.; Ditaranto, N.; Cioffi, N.; Goycoolea, F. M.; Carbone, A.; Garcia-Fuentes, M.; Conese, M.; Alonso, M. J., Systemic heparin delivery by the pulmonary route using chitosan and glycol chitosan nanoparticles. *Int J Pharm* **2013,** 447, (1-2), 115-23.

156. Başaran, E.; Yenilmez, E.; Berkman, M. S.; Büyükköroğlu, G.; Yazan, Y., Chitosan nanoparticles for ocular delivery of cyclosporine A. *Journal of Microencapsulation* **2014,** 31, (1), 49-57.

157. Colonna, C.; Conti, B.; Perugini, P.; Pavanetto, F.; Modena, T.; Dorati, R.; Iadarola, P.; Genta, I., Ex vivo evaluation of prolidase loaded chitosan nanoparticles for the enzyme replacement therapy. *Eur J Pharm Biopharm* **2008,** 70, (1), 58-65.

158. Colonna, C.; Conti, B.; Perugini, P.; Pavanetto, F.; Modena, T.; Dorati, R.; Iadarola, P.; Genta, I., Site-directed PEGylation as successful approach to improve the enzyme replacement in the case of prolidase. *Int J Pharm* **2008,** 358, (1-2), 230-7.

159. Kim, J. H.; Kim, Y. S.; Park, K.; Kang, E.; Lee, S.; Nam, H. Y.; Kim, K.; Park, J. H.; Chi, D. Y.; Park, R. W.; Kim, I. S.; Choi, K.; Chan Kwon, I., Self-assembled glycol chitosan nanoparticles for the sustained and prolonged delivery of antiangiogenic small peptide drugs in cancer therapy. *Biomaterials* **2008,** 29, (12), 1920-30.

160. Vila, A.; Sanchez, A.; Tobio, M.; Calvo, P.; Alonso, M. J., Design of biodegradable particles for protein delivery. *J Control Release* **2002,** 78, (1-3), 15-24.

161. Wang, S.; Jiang, T.; Ma, M.; Hu, Y.; Zhang, J., Preparation and evaluation of anti-neuroexcitation peptide (ANEP) loaded N-trimethyl chitosan chloride nanoparticles for brain-targeting. *Int J Pharm* **2009**.

162. Cao, L.; Wang, J.; Hou, J.; Xing, W.; Liu, C., Vascularization and bone regeneration in a critical sized defect using 2-N,6-O-sulfated chitosan nanoparticles incorporating BMP-2. *Biomaterials* **2014,** 35, (2), 684-98.

163. Messai, I.; Lamalle, D.; Munier, S.; Verrier, B.; Ataman-Onal, Y.; Delair, T., Poly(D,L-lactic acid) and chitosan complexes: interactions with plasmid DNA. *Colloids and Surfaces a-Physicochemical and Engineering Aspects* **2005,** 255, (1-3), 65-72.

164. Yoo, H. S.; Lee, J. E.; Chung, H.; Kwon, I. C.; Jeong, S. Y., Self-assembled nanoparticles containing hydrophobically modified glycol chitosan for gene delivery. *J Control Release* **2005,** 103, (1), 235-43.

165. Dai, H.; Jiang, X.; Tan, G. C.; Chen, Y.; Torbenson, M.; Leong, K. W.; Mao, H. Q., Chitosan-DNA nanoparticles delivered by intrabiliary infusion enhance liver-targeted gene delivery. *Int J Nanomedicine* **2006,** 1, (4), 507-22.

166. Strand, S. P.; Lelu, S.; Reitan, N. K.; de Lange Davies, C.; Artursson, P.; Varum, K. M., Molecular design of chitosan gene delivery systems with an optimized balance between polyplex stability and polyplex unpacking. *Biomaterials* **2010,** 31, (5), 975-87.

167. Duceppe, N.; Tabrizian, M., Factors influencing the transfection efficiency of ultra low molecular weight chitosan/hyaluronic acid nanoparticles. *Biomaterials* **2009,** 30, (13), 2625-31.

168. Huang, M.; Fong, C. W.; Khor, E.; Lim, L. Y., Transfection efficiency of chitosan vectors: effect of polymer molecular weight and degree of deacetylation. *J Control Release* **2005,** 106, (3), 391-406.

169. Xu, T.; Wang, S.; Shao, Z., Insight into Polycation Chain Length Affecting Transfection Efficiency by O-Methyl-Free N,N,N-Trimethyl Chitosans as Gene Carriers. *Pharmaceutical Research* **2014,** 31, (4), 895-907.

170. Koping-Hoggard, M.; Varum, K. M.; Issa, M.; Danielsen, S.; Christensen, B. E.; Stokke, B. T.; Artursson, P., Improved chitosan-mediated gene delivery based on easily dissociated chitosan polyplexes of highly defined chitosan oligomers. *Gene Ther* **2004,** 11, (19), 1441-52.

171. Saranya, N.; Moorthi, A.; Saravanan, S.; Devi, M. P.; Selvamurugan, N., Chitosan and its derivatives for gene delivery. *Int J Biol Macromol* **2011,** 48, (2), 234-8.

172. Koping-Hoggard, M.; Tubulekas, I.; Guan, H.; Edwards, K.; Nilsson, M.; Varum, K. M.; Artursson, P., Chitosan as a nonviral gene delivery system. Structure-property relationships and characteristics compared with polyethylenimine *In vitro* and after lung administration in vivo. *Gene Ther* **2001,** 8, (14), 1108-21.

173. Kiang, T.; Wen, J.; Lim, H. W.; Leong, K. W., The effect of the degree of chitosan deacetylation on the efficiency of gene transfection. *Biomaterials* **2004,** 25, (22), 5293-301.

174. Lavertu, M.; Methot, S.; Tran-Khanh, N.; Buschmann, M. D., High efficiency gene transfer using chitosan/DNA nanoparticles with specific combinations of molecular weight and degree of deacetylation. *Biomaterials* **2006,** 27, (27), 4815-24.

175. Nafee, N.; Taetz, S.; Schneider, M.; Schaefer, U. F.; Lehr, C. M., Chitosan-coated PLGA nanoparticles for DNA/RNA delivery: effect of the formulation parameters on complexation and transfection of antisense oligonucleotides. *Nanomedicine* **2007,** 3, (3), 173-83.

176. Ishii, T.; Okahata, Y.; Sato, T., Mechanism of cell transfection with plasmid/chitosan complexes. *Biochim Biophys Acta* **2001,** 1514, (1), 51-64.

177. Kim, T. H.; Park, I. K.; Nah, J. W.; Choi, Y. J.; Cho, C. S., Galactosylated chitosan/DNA nanoparticles prepared using water-soluble chitosan as a gene carrier. *Biomaterials* **2004,** 25, (17), 3783-92.

178. Douglas, K. L.; Piccirillo, C. A.; Tabrizian, M., Effects of alginate inclusion on the vector properties of chitosan-based nanoparticles. *J Control Release* **2006,** 115, (3), 354-61.

179. Peng, S. F.; Yang, M. J.; Su, C. J.; Chen, H. L.; Lee, P. W.; Wei, M. C.; Sung, H. W., Effects of incorporation of poly(gamma-glutamic acid) in chitosan/DNA complex nanoparticles on cellular uptake and transfection efficiency. *Biomaterials* **2009,** 30, (9), 1797-808.

180. Liao, Z.-X.; Peng, S.-F.; Chiu, Y.-L.; Hsiao, C.-W.; Liu, H.-Y.; Lim, W.-H.; Lu, H.-M.; Sung, H.-W., Enhancement of efficiency of chitosan-based complexes for

gene transfection with poly(γ-glutamic acid) by augmenting their cellular uptake and intracellular unpackage. *Journal of Controlled Release* **2014**, (0).

181. Germershaus, O.; Mao, S.; Sitterberg, J.; Bakowsky, U.; Kissel, T., Gene delivery using chitosan, trimethyl chitosan or polyethylenglycol-graft-trimethyl chitosan block copolymers: establishment of structure-activity relationships *In vitro*. *J Control Release* **2008,** 125, (2), 145-54.

182. Kadiyala, I.; Loo, Y.; Roy, K.; Rice, J.; Leong, K. W., Transport of chitosan-DNA nanoparticles in human intestinal M-cell model versus normal intestinal enterocytes. *Eur J Pharm Sci* **2009**.

183. Sato, T.; Ishii, T.; Okahata, Y., *In vitro* gene delivery mediated by chitosan. Effect of pH, serum, and molecular mass of chitosan on the transfection efficiency. *Biomaterials* **2001,** 22, (15), 2075-2080.

184. Wang, B.; He, C.; Tang, C.; Yin, C., Effects of hydrophobic and hydrophilic modifications on gene delivery of amphiphilic chitosan based nanocarriers. *Biomaterials* **2011,** 32, (20), 4630-8.

185. Scholz, C.; Wagner, E., Therapeutic plasmid DNA versus siRNA delivery: Common and different tasks for synthetic carriers. *Journal of Controlled Release* **2012,** 161, (2), 554-565.

186. Kim, T. H.; Jiang, H. L.; Jere, D.; Park, I. K.; Cho, M. H.; Nah, J. W.; Choi, Y. J.; Akaike, T.; Cho, C. S., Chemical modification of chitosan as a gene carrier *In vitro* and in vivo. *Progress in Polymer Science* **2007,** 32, (7), 726-753.

187. Jeong, J. H.; Kim, S. W.; Park, T. G., Molecular design of functional polymers for gene therapy. *Progress in Polymer Science* **2007,** 32, (11), 1239-1274.

188. Jiang, H. L.; Kwon, J. T.; Kim, E. M.; Kim, Y. K.; Arote, R.; Jere, D.; Jeong, H. J.; Jang, M. K.; Nah, J. W.; Xu, C. X.; Park, I. K.; Cho, M. H.; Cho, C. S., Galactosylated poly(ethylene glycol)-chitosan-graft-polyethylenimine as a gene carrier for hepatocyte-targeting. *J Control Release* **2008,** 131, (2), 150-7.

189. Park, I. K.; Ihm, J. E.; Park, Y. H.; Choi, Y. J.; Kim, S. I.; Kim, W. J.; Akaike, T.; Cho, C. S., Galactosylated chitosan (GC)-graft-poly(vinyl pyrrolidone) (PVP) as hepatocyte-targeting DNA carrier. Preparation and physicochemical characterization of GC-graft-PVP/DNA complex (1). *J Control Release* **2003,** 86, (2-3), 349-59.

190. Dang, J. M.; Leong, K. W., Natural polymers for gene delivery and tissue engineering. *Adv Drug Deliv Rev* **2006,** 58, (4), 487-99.

191. Lee, D.; Zhang, W.; Shirley, S. A.; Kong, X.; Hellermann, G. R.; Lockey, R. F.; Mohapatra, S. S., Thiolated chitosan/DNA nanocomplexes exhibit enhanced and sustained gene delivery. *Pharm Res* **2007,** 24, (1), 157-67.

192. Gao, Y.; Zhang, Z.; Chen, L.; Gu, W.; Li, Y., Synthesis of 6-N,N,N-trimethyltriazole chitosan via "click chemistry" and evaluation for gene delivery. *Biomacromolecules* **2009,** 10, (8), 2175-82.

193. Zheng, Y.; Cai, Z.; Song, X.; Yu, B.; Bi, Y.; Chen, Q.; Zhao, D.; Xu, J.; Hou, S., Receptor mediated gene delivery by folate conjugated N-trimethyl chitosan *In vitro*. *Int J Pharm* **2009,** 382, (1-2), 262-9.

194. Mao, H. Q.; Roy, K.; Troung-Le, V. L.; Janes, K. A.; Lin, K. Y.; Wang, Y.; August, J. T.; Leong, K. W., Chitosan-DNA nanoparticles as gene carriers: synthesis, characterization and transfection efficiency. *J Control Release* **2001,** 70, (3), 399-421.

195. Liu, Y.; Kong, M.; Cheng, X. J.; Wang, Q. Q.; Jiang, L. M.; Chen, X. G., Self-assembled nanoparticles based on amphiphilic chitosan derivative and hyaluronic acid for gene delivery. *Carbohydr Polym* **2013,** 94, (1), 309-16.

196. Jiang, H. L.; Kim, Y. K.; Arote, R.; Jere, D.; Quan, J. S.; Yu, J. H.; Choi, Y. J.; Nah, J. W.; Cho, M. H.; Cho, C. S., Mannosylated chitosan-graft-polyethylenimine as a gene carrier for Raw 264.7 cell targeting. *Int J Pharm* **2009,** 375, (1-2), 133-9.

197. Liu, L.; Dong, X.; Zhu, D.; Song, L.; Zhang, H.; Leng, X. G., TAT-LHRH conjugated low molecular weight chitosan as a gene carrier specific for hepatocellular carcinoma cells. *Int J Nanomedicine* **2014,** 9, 2879-89.

198. Xu, Z. G.; Wan, X. P.; Zhang, W.; Wang, Z.; Peng, R.; Tao, F.; Cai, L.; Li, Y.; Jiang, Q.; Gao, R., Synthesis of biodegradable polycationic methoxy poly(ethylene glycol)-polyethylenimine-chitosan and its potential as gene carrier. *Carbohydrate Polymers* **2009,** 78, (1), 46-53.

199. Kim, T. H.; Kim, S. I.; Akaike, T.; Cho, C. S., Synergistic effect of poly(ethylenimine) on the transfection efficiency of galactosylated chitosan/DNA complexes. *J Control Release* **2005,** 105, (3), 354-66.

200. Jiang, H. L.; Kim, Y. K.; Arote, R.; Nah, J. W.; Cho, M. H.; Choi, Y. J.; Akaike, T.; Cho, C. S., Chitosan-graft-polyethylenimine as a gene carrier. *J Control Release* **2007,** 117, (2), 273-80.

201. Richard, I.; Thibault, M.; De Crescenzo, G.; Buschmann, M. D.; Lavertu, M., Ionization behavior of chitosan and chitosan-DNA polyplexes indicate that chitosan has a similar capability to induce a proton-sponge effect as PEI. *Biomacromolecules* **2013,** 14, (6), 1732-40.

202. Kim, T. H.; Ihm, J. E.; Choi, Y. J.; Nah, J. W.; Cho, C. S., Efficient gene delivery by urocanic acid-modified chitosan. *J Control Release* **2003,** 93, (3), 389-402.

203. Hu, F. Q.; Zhao, M. D.; Yuan, H.; You, J.; Du, Y. Z.; Zeng, S., A novel chitosan oligosaccharide-stearic acid micelles for gene delivery: properties and *In vitro* transfection studies. *Int J Pharm* **2006,** 315, (1-2), 158-66.

204. Kiang, T.; Bright, C.; Cheung, C. Y.; Stayton, P. S.; Hoffman, A. S.; Leong, K. W., Formulation of chitosan-DNA nanoparticles with poly(propyl acrylic acid) enhances gene expression. *J Biomater Sci Polym Ed* **2004,** 15, (11), 1405-21.

205. Lee, J. I.; Ha, K. S.; Yoo, H. S., Quantum-dot-assisted fluorescence resonance energy transfer approach for intracellular trafficking of chitosan/DNA complex. *Acta Biomater* **2008,** 4, (4), 791-8.

206. Hashimoto, M.; Morimoto, M.; Saimoto, H.; Shigemasa, Y.; Sato, T., Lactosylated chitosan for DNA delivery into hepatocytes: the effect of lactosylation on the physicochemical properties and intracellular trafficking of pDNA/chitosan complexes. *Bioconjug Chem* **2006,** 17, (2), 309-16.

207. Parelkar, S. S.; Letteri, R.; Chan-Seng, D.; Zolochevska, O.; Ellis, J.; Figueiredo, M.; Emrick, T., Polymer–Peptide Delivery Platforms: Effect of Oligopeptide

Orientation on Polymer-Based DNA Delivery. *Biomacromolecules* **2014,** 15, (4), 1328-1336.

208. Kim, T. H.; Jin, H.; Kim, H. W.; Cho, M. H.; Cho, C. S., Mannosylated chitosan nanoparticle-based cytokine gene therapy suppressed cancer growth in BALB/c mice bearing CT-26 carcinoma cells. *Mol Cancer Ther* **2006,** 5, (7), 1723-32.
209. Fernandes, J. C.; Wang, H.; Jreyssaty, C.; Benderdour, M.; Lavigne, P.; Qiu, X.; Winnik, F. M.; Zhang, X.; Dai, K.; Shi, Q., Bone-protective effects of nonviral gene therapy with folate-chitosan DNA nanoparticle containing interleukin-1 receptor antagonist gene in rats with adjuvant-induced arthritis. *Mol Ther* **2008,** 16, (7), 1243-51.
210. Yuan, X.; Yang, X.; Cai, D.; Mao, D.; Wu, J.; Zong, L.; Liu, J., Intranasal immunization with chitosan/pCETP nanoparticles inhibits atherosclerosis in a rabbit model of atherosclerosis. *Vaccine* **2008,** 26, (29-30), 3727-34.
211. Kumar, M.; Kong, X.; Behera, A. K.; Hellermann, G. R.; Lockey, R. F.; Mohapatra, S. S., Chitosan IFN-gamma-pDNA Nanoparticle (CIN) Therapy for Allergic Asthma. *Genet Vaccines Ther* **2003,** 1, (1), 3.
212. Bivas-Benita, M.; van Meijgaarden, K. E.; Franken, K. L.; Junginger, H. E.; Borchard, G.; Ottenhoff, T. H.; Geluk, A., Pulmonary delivery of chitosan-DNA nanoparticles enhances the immunogenicity of a DNA vaccine encoding HLA-A*0201-restricted T-cell epitopes of Mycobacterium tuberculosis. *Vaccine* **2004,** 22, (13-14), 1609-15.
213. Bowman, K.; Sarkar, R.; Raut, S.; Leong, K. W., Gene transfer to hemophilia A mice via oral delivery of FVIII-chitosan nanoparticles. *J Control Release* **2008,** 132, (3), 252-9.
214. Khatri, K.; Goyal, A. K.; Gupta, P. N.; Mishra, N.; Vyas, S. P., Plasmid DNA loaded chitosan nanoparticles for nasal mucosal immunization against hepatitis B. *Int J Pharm* **2008,** 354, (1-2), 235-41.
215. Xu, W.; Shen, Y.; Jiang, Z.; Wang, Y.; Chu, Y.; Xiong, S., Intranasal delivery of chitosan-DNA vaccine generates mucosal SIgA and anti-CVB3 protection. *Vaccine* **2004,** 22, (27-28), 3603-12.
216. Iqbal, M.; Lin, W.; Jabbal-Gill, I.; Davis, S. S.; Steward, M. W.; Illum, L., Nasal delivery of chitosan-DNA plasmid expressing epitopes of respiratory syncytial virus (RSV) induces protective CTL responses in BALB/c mice. *Vaccine* **2003,** 21, (13-14), 1478-85.
217. Howard, K. A., Delivery of RNA interference therapeutics using polycation-based nanoparticles. *Adv Drug Deliv Rev* **2009,** 61, (9), 710-20.
218. Lai, W. F.; Lin, M. C., Nucleic acid delivery with chitosan and its derivatives. *J Control Release* **2009,** 134, (3), 158-68.
219. Katas, H.; Alpar, H. O., Development and characterisation of chitosan nanoparticles for siRNA delivery. *J Control Release* **2006,** 115, (2), 216-25.
220. Liu, X.; Howard, K. A.; Dong, M.; Andersen, M. O.; Rahbek, U. L.; Johnsen, M. G.; Hansen, O. C.; Besenbacher, F.; Kjems, J., The influence of polymeric properties on chitosan/siRNA nanoparticle formulation and gene silencing. *Biomaterials* **2007,** 28, (6), 1280-8.

221. Howard, K. A.; Rahbek, U. L.; Liu, X.; Damgaard, C. K.; Glud, S. Z.; Andersen, M. O.; Hovgaard, M. B.; Schmitz, A.; Nyengaard, J. R.; Besenbacher, F.; Kjems, J., RNA interference *In vitro* and in vivo using a novel chitosan/siRNA nanoparticle system. *Mol Ther* **2006,** 14, (4), 476-84.

222. Rojanarata, T.; Opanasopit, P.; Techaarpornkul, S.; Ngawhirunpat, T.; Ruktanonchai, U., Chitosan-thiamine pyrophosphate as a novel carrier for siRNA delivery. *Pharm Res* **2008,** 25, (12), 2807-14.

223. Lee, D. W.; Yun, K. S.; Ban, H. S.; Choe, W.; Lee, S. K.; Lee, K. Y., Preparation and characterization of chitosan/polyguluronate nanoparticles for siRNA delivery. *J Control Release* **2009,** 139, (2), 146-52.

224. Ji, A. M.; Su, D.; Che, O.; Li, W. S.; Sun, L.; Zhang, Z. Y.; Yang, B.; Xu, F., Functional gene silencing mediated by chitosan/siRNA nanocomplexes. *Nanotechnology* **2009,** 20, (40), 405103.

225. Tahara, K.; Yamamoto, H.; Hirashima, N.; Kawashima, Y., Chitosan-modified poly(d,l-lactide-co-glycolide) nanospheres for improving siRNA delivery and gene-silencing effects. *Eur J Pharm Biopharm* **2009**.

226. Lee, J. Y.; Lee, S. H.; Oh, M. H.; Kim, J. S.; Park, T. G.; Nam, Y. S., Prolonged gene silencing by siRNA/chitosan-g-deoxycholic acid polyplexes loaded within biodegradable polymer nanoparticles. *J Control Release* **2012,** 162, (2), 407-13.

227. Kong, X.; Zhang, W.; Lockey, R. F.; Auais, A.; Piedimonte, G.; Mohapatra, S. S., Respiratory syncytial virus infection in Fischer 344 rats is attenuated by short interfering RNA against the RSV-NS1 gene. *Genet Vaccines Ther* **2007,** 5, 4.

228. Wang, X.; Xu, W.; Mohapatra, S.; Kong, X.; Li, X.; Lockey, R. F.; Mohapatra, S. S., Prevention of airway inflammation with topical cream containing imiquimod and small interfering RNA for natriuretic peptide receptor. *Genet Vaccines Ther* **2008,** 6, 7.

229. Howard, K. A.; Paludan, S. R.; Behlke, M. A.; Besenbacher, F.; Deleuran, B.; Kjems, J., Chitosan/siRNA nanoparticle-mediated TNF-alpha knockdown in peritoneal macrophages for anti-inflammatory treatment in a murine arthritis model. *Mol Ther* **2009,** 17, (1), 162-8.

230. Jere, D.; Jiang, H. L.; Kim, Y. K.; Arote, R.; Choi, Y. J.; Yun, C. H.; Cho, M. H.; Cho, C. S., Chitosan-graft-polyethylenimine for Akt1 siRNA delivery to lung cancer cells. *Int J Pharm* **2009,** 378, (1-2), 194-200.

231. Jagani, H.; Rao, J. V.; Palanimuthu, V. R.; Hariharapura, R. C.; Gang, S., A nanoformulation of siRNA and its role in cancer therapy: *In vitro* and in vivo evaluation. *Cellular & molecular biology letters* **2013,** 18, (1), 120-36.

232. Huang, Z.; Dong, L.; Chen, J.; Gao, F.; Zhang, Z.; Chen, J.; Zhang, J., Low-molecular weight chitosan/vascular endothelial growth factor short hairpin RNA for the treatment of hepatocellular carcinoma. *Life Sciences* **2012,** 91, (23–24), 1207-1215.

233. Zhang, J.; Tang, C.; Yin, C., Galactosylated trimethyl chitosan-cysteine nanoparticles loaded with Map4k4 siRNA for targeting activated macrophages. *Biomaterials* **2013,** 34, (14), 3667-77.

234. Liu, Z. H.; Jiao, Y. P.; Wang, Y. F.; Zhou, C. R.; Zhang, Z. Y., Polysaccharides-based nanoparticles as drug delivery systems. *Advanced Drug Delivery Reviews* **2008,** 60, (15), 1650-1662.

235. Agnihotri, S. A.; Mallikarjuna, N. N.; Aminabhavi, T. M., Recent advances on chitosan-based micro- and nanoparticles in drug delivery. *Journal of Controlled Release* **2004,** 100, (1), 5-28.

236. Hafner, A.; Lovric, J.; Voinovich, D.; Filipovic-Grcic, J., Melatonin-loaded lecithin/chitosan nanoparticles: physicochemical characterisation and permeability through Caco-2 cell monolayers. *Int J Pharm* **2009,** 381, (2), 205-13.

237. Chen, M.-C.; Mi, F.-L.; Liao, Z.-X.; Hsiao, C.-W.; Sonaje, K.; Chung, M.-F.; Hsu, L.-W.; Sung, H.-W., Recent advances in chitosan-based nanoparticles for oral delivery of macromolecules. *Advanced Drug Delivery Reviews* **2013,** 65, (6), 865-879.

238. Park, J. H.; Saravanakumar, G.; Kim, K.; Kwon, I. C., Targeted delivery of low molecular drugs using chitosan and its derivatives. *Adv Drug Deliv Rev* **2009**.

239. Bisht, S.; Maitra, A., Dextran-doxorubicin/chitosan nanoparticles for solid tumor therapy. *Wiley Interdiscip Rev Nanomed Nanobiotechnol* **2009,** 1, (4), 415-25.

240. Jee, J.-P.; Na, J. H.; Lee, S.; Kim, S. H.; Choi, K.; Yeo, Y.; Kwon, I. C., Cancer targeting strategies in nanomedicine: Design and application of chitosan nanoparticles. *Current Opinion in Solid State and Materials Science* **2012,** 16, (6), 333-342.

241. Kim, K.; Kim, J. H.; Kim, S.; Choi, K.; Kwon, I. C., Self-Assembled Nanoparticles of Bile Acid Modified Glycol Chitosans and Their Applications for Cancer Therapy. *Macromolecular Research* **2005,** 13, (3), 167-175.

242. Wei, W.; Lv, P. P.; Chen, X. M.; Yue, Z. G.; Fu, Q.; Liu, S. Y.; Yue, H.; Ma, G. H., Codelivery of mTERT siRNA and paclitaxel by chitosan-based nanoparticles promoted synergistic tumor suppression. *Biomaterials* **2013,** 34, (15), 3912-23.

243. Zhu, Q. L.; Zhou, Y.; Guan, M.; Zhou, X. F.; Yang, S. D.; Liu, Y.; Chen, W. L.; Zhang, C. G.; Yuan, Z. Q.; Liu, C.; Zhu, A. J.; Zhang, X. N., Low-density lipoprotein-coupled N-succinyl chitosan nanoparticles co-delivering siRNA and doxorubicin for hepatocyte-targeted therapy. *Biomaterials* **2014,** 35, (22), 5965-76.

244. Yu, B.; Tang, C.; Yin, C., Enhanced antitumor efficacy of folate modified amphiphilic nanoparticles through co-delivery of chemotherapeutic drugs and genes. *Biomaterials* **2014,** 35, (24), 6369-78.

245. Deng, X.; Cao, M.; Zhang, J.; Hu, K.; Yin, Z.; Zhou, Z.; Xiao, X.; Yang, Y.; Sheng, W.; Wu, Y.; Zeng, Y., Hyaluronic acid-chitosan nanoparticles for co-delivery of MiR-34a and doxorubicin in therapy against triple negative breast cancer. *Biomaterials* **2014,** 35, (14), 4333-44.

246. Kim, J. H.; Kim, Y. S.; Kim, S.; Park, J. H.; Kim, K.; Choi, K.; Chung, H.; Jeong, S. Y.; Park, R. W.; Kim, I. S.; Kwon, I. C., Hydrophobically modified glycol chitosan nanoparticles as carriers for paclitaxel. *J Control Release* **2006,** 111, (1-2), 228-34.

247. Liu, K. H.; Chen, B. R.; Chen, S. Y.; Liu, D. M., Self-assembly behavior and doxorubicin-loading capacity of acylated carboxymethyl chitosans. *J Phys Chem B* **2009,** 113, (35), 11800-7.

248. Lee, E.; Lee, J.; Lee, I. H.; Yu, M.; Kim, H.; Chae, S. Y.; Jon, S., Conjugated chitosan as a novel platform for oral delivery of paclitaxel. *J Med Chem* **2008,** 51, (20), 6442-9.

249. Son, Y. J.; Jang, J. S.; Cho, Y. W.; Chung, H.; Park, R. W.; Kwon, I. C.; Kim, I. S.; Park, J. Y.; Seo, S. B.; Park, C. R.; Jeong, S. Y., Biodistribution and anti-tumor efficacy of doxorubicin loaded glycol-chitosan nanoaggregates by EPR effect. *J Control Release* **2003,** 91, (1-2), 135-45.

250. Hu, F. Q.; Ren, G. F.; Yuan, H.; Du, Y. Z.; Zeng, S., Shell cross-linked stearic acid grafted chitosan oligosaccharide self-aggregated micelles for controlled release of paclitaxel. *Colloids Surf B Biointerfaces* **2006,** 50, (2), 97-103.

251. Hu, F. Q.; Wu, X. L.; Du, Y. Z.; You, J.; Yuan, H., Cellular uptake and cytotoxicity of shell crosslinked stearic acid-grafted chitosan oligosaccharide micelles encapsulating doxorubicin. *Eur J Pharm Biopharm* **2008,** 69, (1), 117-25.

252. Min, K. H.; Park, K.; Kim, Y. S.; Bae, S. M.; Lee, S.; Jo, H. G.; Park, R. W.; Kim, I. S.; Jeong, S. Y.; Kim, K.; Kwon, I. C., Hydrophobically modified glycol chitosan nanoparticles-encapsulated camptothecin enhance the drug stability and tumor targeting in cancer therapy. *J Control Release* **2008,** 127, (3), 208-18.

253. Fan, L.; Wu, H.; Zhang, H.; Li, F.; Yang, T. H.; Gu, C. H.; Yang, Q., Novel super pH-sensitive nanoparticles responsive to tumor extracellular pH. *Carbohydrate Polymers* **2008,** 73.

254. Chen, C.; Zhou, J. L.; Han, X.; Song, F.; Wang, X. L.; Wang, Y. Z., A prodrug strategy based on chitosan for efficient intracellular anticancer drug delivery. *Nanotechnology* **2014,** 25, (25), 255101.

255. Termsarasab, U.; Yoon, I. S.; Park, J. H.; Moon, H. T.; Cho, H. J.; Kim, D. D., Polyethylene glycol-modified arachidyl chitosan-based nanoparticles for prolonged blood circulation of doxorubicin. *Int J Pharm* **2014,** 464, (1-2), 127-34.

256. Feng, C.; Wang, Z.; Jiang, C.; Kong, M.; Zhou, X.; Li, Y.; Cheng, X.; Chen, X., Chitosan/o-carboxymethyl chitosan nanoparticles for efficient and safe oral anticancer drug delivery: *In vitro* and in vivo evaluation. *International Journal of Pharmaceutics* **2013,** 457, (1), 158-167.

257. Zhao, Z.; He, M.; Yin, L.; Bao, J.; Shi, L.; Wang, B.; Tang, C.; Yin, C., Biodegradable Nanoparticles Based on Linoleic Acid and Poly(beta-malic acid) Double Grafted Chitosan Derivatives as Carriers of Anticancer Drugs. *Biomacromolecules* **2009**.

258. Kim, J. H.; Kim, Y. S.; Park, K.; Lee, S.; Nam, H. Y.; Min, K. H.; Jo, H. G.; Park, J. H.; Choi, K.; Jeong, S. Y.; Park, R. W.; Kim, I. S.; Kim, K.; Kwon, I. C., Antitumor efficacy of cisplatin-loaded glycol chitosan nanoparticles in tumor-bearing mice. *J Control Release* **2008,** 127, (1), 41-9.

259. Akhtar, F.; Rizvi, M. M.; Kar, S. K., Oral delivery of curcumin bound to chitosan nanoparticles cured Plasmodium yoelii infected mice. *Biotechnology advances* **2012,** 30, (1), 310-20.

260. Bilensoy, E.; Sarisozen, C.; Esendagli, G.; Dogan, A. L.; Aktas, Y.; Sen, M.; Mungan, N. A., Intravesical cationic nanoparticles of chitosan and polycaprolactone for the delivery of Mitomycin C to bladder tumors. *Int J Pharm* **2009,** 371, (1-2), 170-6.

261. Zhang, D. Y.; Shen, X. Z.; Wang, J. Y.; Dong, L.; Zheng, Y. L.; Wu, L. L., Preparation of chitosan-polyaspartic acid-5-fluorouracil nanoparticles and its anti-carcinoma effect on tumor growth in nude mice. *World J Gastroenterol* **2008,** 14, (22), 3554-62.

262. Fazil, M.; Md, S.; Haque, S.; Kumar, M.; Baboota, S.; Sahni, J. K.; Ali, J., Development and evaluation of rivastigmine loaded chitosan nanoparticles for brain targeting. *Eur J Pharm Sci* **2012,** 47, (1), 6-15.

263. Wang, Q.; Zhang, L.; Hu, W.; Hu, Z. H.; Bei, Y. Y.; Xu, J. Y.; Wang, W. J.; Zhang, X. N.; Zhang, Q., Norcantharidin-associated galactosylated chitosan nanoparticles for hepatocyte-targeted delivery. *Nanomedicine* **2009**.

264. Lee, S. J.; Park, K.; Oh, Y. K.; Kwon, S. H.; Her, S.; Kim, I. S.; Choi, K.; Kim, H.; Lee, S. G.; Kim, K.; Kwon, I. C., Tumor specificity and therapeutic efficacy of photosensitizer-encapsulated glycol chitosan-based nanoparticles in tumor-bearing mice. *Biomaterials* **2009,** 30, (15), 2929-39.

265. Jeong, Y. I.; Kim, S. H.; Jung, T. Y.; Kim, I. Y.; Kang, S. S.; Jin, Y. H.; Ryu, H. H.; Sun, H. S.; Jin, S.; Kim, K. K.; Ahn, K. Y.; Jung, S., Polyion complex micelles composed of all-trans retinoic acid and poly (ethylene glycol)-grafted-chitosan. *J Pharm Sci* **2006,** 95, (11), 2348-60.

266. Hwang, H. Y.; Kim, I. S.; Kwon, I. C.; Kim, Y. H., Tumor targetability and antitumor effect of docetaxel-loaded hydrophobically modified glycol chitosan nanoparticles. *J Control Release* **2008,** 128, (1), 23-31.

267. Unsoy, G.; Yalcin, S.; Khodadust, R.; Mutlu, P.; Onguru, O.; Gunduz, U., Chitosan magnetic nanoparticles for pH responsive Bortezomib release in cancer therapy. *Biomedicine & pharmacotherapy = Biomedecine & pharmacotherapie* **2014**.

268. Anitha, A.; Deepa, N.; Chennazhi, K. P.; Lakshmanan, V. K.; Jayakumar, R., Combinatorial anticancer effects of curcumin and 5-fluorouracil loaded thiolated chitosan nanoparticles towards colon cancer treatment. *Biochim Biophys Acta* **2014,** 1840, (9), 2730-2743.

269. Chen, J.; Huang, L.; Lai, H.; Lu, C.; Fang, M.; Zhang, Q.; Luo, X., Methotrexate-Loaded PEGylated Chitosan Nanoparticles: Synthesis, Characterization, and *In vitro* and in Vivo Antitumoral Activity. *Mol Pharm* **2014,** 11, (7), 2213-23.

270. Chaubey, P.; Mishra, B., Mannose-conjugated chitosan nanoparticles loaded with rifampicin for the treatment of visceral leishmaniasis. *Carbohydr Polym* **2014,** 101, 1101-8.

271. Zheng, D.; Duan, C.; Zhang, D.; Jia, L.; Liu, G.; Liu, Y.; Wang, F.; Li, C.; Guo, H.; Zhang, Q., Galactosylated chitosan nanoparticles for hepatocyte-targeted delivery of oridonin. *Int J Pharm* **2012,** 436, (1-2), 379-86.

272. Hu, F. Q.; Meng, P.; Dai, Y. Q.; Du, Y. Z.; You, J.; Wei, X. H.; Yuan, H., PEGylated chitosan-based polymer micelle as an intracellular delivery carrier for anti-tumor targeting therapy. *European journal of pharmaceutics and biopharmaceutics : official journal of Arbeitsgemeinschaft fur Pharmazeutische Verfahrenstechnik e.V* **2008,** 70, (3), 749-57.

273. Qu, G.; Yao, Z.; Zhang, C.; Wu, X.; Ping, Q., PEG conjugated N-octyl-O-sulfate chitosan micelles for delivery of paclitaxel: *In vitro* characterization and in vivo evaluation. *Eur J Pharm Sci* **2009,** 37, (2), 98-105.

274. Park, J. S.; Han, T. H.; Lee, K. Y.; Han, S. S.; Hwang, J. J.; Moon, D. H.; Kim, S. Y.; Cho, Y. W., N-acetyl histidine-conjugated glycol chitosan self-assembled nanoparticles for intracytoplasmic delivery of drugs: endocytosis, exocytosis and drug release. *J Control Release* **2006,** 115, (1), 37-45.

275. You, J.; Hu, F. Q.; Du, Y. Z.; Yuan, H., Polymeric micelles with glycolipid-like structure and multiple hydrophobic domains for mediating molecular target delivery of paclitaxel. *Biomacromolecules* **2007,** 8, (8), 2450-6.

276. You, J.; Hu, F. Q.; Du, Y. Z.; Yuan, H., Improved cytotoxicity of doxorubicin by enhancing its nuclear delivery mediated via nanosized micelles. *Nanotechnology* **2008,** 19.

277. Mi, F. L.; Wu, Y. Y.; Chiu, Y. L.; Chen, M. C.; Sung, H. W.; Yu, S. H.; Shyu, S. S.; Huang, M. F., Synthesis of a novel glycoconjugated chitosan and preparation of its derived nanoparticles for targeting HepG2 cells. *Biomacromolecules* **2007,** 8, (3), 892-8.

278. Dufes, C.; Muller, J. M.; Couet, W.; Olivier, J. C.; Uchegbu, I. F.; Schatzlein, A. G., Anticancer drug delivery with transferrin targeted polymeric chitosan vesicles. *Pharmaceutical research* **2004,** 21, (1), 101-7.

279. You, J.; Li, X.; de Cui, F.; Du, Y. Z.; Yuan, H.; Hu, F. Q., Folate-conjugated polymer micelles for active targeting to cancer cells: preparation, *In vitro* evaluation of targeting ability and cytotoxicity. *Nanotechnology* **2008,** 19, (4), -.

280. Jain, A.; Jain, S. K., *In vitro* and cell uptake studies for targeting of ligand anchored nanoparticles for colon tumors. *Eur J Pharm Sci* **2008,** 35, (5), 404-16.

281. Nagarwal, R. C.; Kant, S.; Singh, P. N.; Maiti, P.; Pandit, J. K., Polymeric nanoparticulate system: a potential approach for ocular drug delivery. *J Control Release* **2009,** 136, (1), 2-13.

282. de la Fuente, M.; Ravina, M.; Paolicelli, P.; Sanchez, A.; Seijo, B.; Alonso, M. J., Chitosan-based Nanostructures: A Delivery Platform for Ocular Therapeutics. *Adv Drug Deliv Rev* **2010,** 62, (1), 100-117.

283. De Campos, A. M.; Sanchez, A.; Gref, R.; Calvo, P.; Alonso, M. J., The effect of a PEG versus a chitosan coating on the interaction of drug colloidal carriers with the ocular mucosa. *Eur J Pharm Sci* **2003,** 20, (1), 73-81.

284. de Campos, A. M.; Diebold, Y.; Carvalho, E. L.; Sanchez, A.; Alonso, M. J., Chitosan nanoparticles as new ocular drug delivery systems: *In vitro* stability, in vivo fate, and cellular toxicity. *Pharm Res* **2004,** 21, (5), 803-10.

285. Badawi, A. A.; El-Laithy, H. M.; El Qidra, R. K.; El Mofty, H.; El dally, M., Chitosan based nanocarriers for indomethacin ocular delivery. *Arch Pharm Res* **2008,** 31, (8), 1040-9.

286. Jain, K.; Kumar, R. S.; Sood, S.; Dhyanandhan, G., Betaxolol hydrochloride loaded chitosan nanoparticles for ocular delivery and their anti-glaucoma efficacy. *Current drug delivery* **2013,** 10, (5), 493-9.

287. Zhou, W.; Wang, Y.; Jian, J.; Song, S., Self-aggregated nanoparticles based on amphiphilic poly(lactic acid)-grafted-chitosan copolymer for ocular delivery of amphotericin B. *Int J Nanomedicine* **2013,** 8, 3715-28.

288. Bhatta, R. S.; Chandasana, H.; Chhonker, Y. S.; Rathi, C.; Kumar, D.; Mitra, K.; Shukla, P. K., Mucoadhesive nanoparticles for prolonged ocular delivery of natamycin: *In vitro* and pharmacokinetics studies. *International Journal of Pharmaceutics* **2012,** 432, (1–2), 105-112.

289. Yang, K. W.; Li, X. R.; Yang, Z. L.; Li, P. Z.; Wang, F.; Liu, Y., Novel polyion complex micelles for liver-targeted delivery of diammonium glycyrrhizinate: *In vitro* and in vivo characterization. *J Biomed Mater Res A* **2009,** 88, (1), 140-8.

290. Lin, A.; Liu, Y.; Huang, Y.; Sun, J.; Wu, Z.; Zhang, X.; Ping, Q., Glycyrrhizin surface-modified chitosan nanoparticles for hepatocyte-targeted delivery. *Int J Pharm* **2008,** 359, (1-2), 247-53.

291. Lin, A.; Chen, J.; Liu, Y.; Deng, S.; Wu, Z.; Huang, Y.; Ping, Q., Preparation and evaluation of N-caproyl chitosan nanoparticles surface modified with glycyrrhizin for hepatocyte targeting. *Drug Dev Ind Pharm* **2009**.

292. Tian, Q.; Zhang, C.-N.; Wang, X.-H.; Wang, W.; Huang, W.; Cha, R.-T.; Wang, C.-H.; Yuan, Z.; Liu, M.; Wan, H.-Y.; Tang, H., Glycyrrhetinic acid-modified chitosan/poly(ethylene glycol) nanoparticles for liver-targeted delivery. *Biomaterials* **2010,** 31, (17), 4748-4756.

293. Tian, Q.; Wang, X.-H.; Wang, W.; Zhang, C.-N.; Wang, P.; Yuan, Z., Self-assembly and liver targeting of sulfated chitosan nanoparticles functionalized with glycyrrhetinic acid. *Nanomedicine: Nanotechnology, Biology and Medicine* **2012,** 8, (6), 870-879.

294. Mishra, D.; Jain, N.; Rajoriya, V.; Jain, A. K., Glycyrrhizin conjugated chitosan nanoparticles for hepatocyte-targeted delivery of lamivudine. *Journal of Pharmacy and Pharmacology* **2014,** 66, (8), 1082-1093.

295. Shi, L.; Tang, C.; Yin, C., Glycyrrhizin-modified O-carboxymethyl chitosan nanoparticles as drug vehicles targeting hepatocellular carcinoma. *Biomaterials* **2012,** 33, (30), 7594-7604.

296. Bu, L.; Gan, L.-C.; Guo, X.-Q.; Chen, F.-Z.; Song, Q.; Qi, Z.; Gou, X.-J.; Hou, S.-X.; Yao, Q., Trans-resveratrol loaded chitosan nanoparticles modified with biotin and avidin to target hepatic carcinoma. *International Journal of Pharmaceutics* **2013,** 452, (1–2), 355-362.

297. Wang, X.; Chi, N.; Tang, X., Preparation of estradiol chitosan nanoparticles for improving nasal absorption and brain targeting. *Eur J Pharm Biopharm* **2008,** 70, (3), 735-40.

298. Wang, Z. H.; Wang, Z. Y.; Sun, C. S.; Wang, C. Y.; Jiang, T. Y.; Wang, S. L., Trimethylated chitosan-conjugated PLGA nanoparticles for the delivery of drugs to the brain. *Biomaterials* 31, (5), 908-15.

299. Md, S.; Khan, R. A.; Mustafa, G.; Chuttani, K.; Baboota, S.; Sahni, J. K.; Ali, J., Bromocriptine loaded chitosan nanoparticles intended for direct nose to brain delivery: Pharmacodynamic, Pharmacokinetic and Scintigraphy study in mice model. *European Journal of Pharmaceutical Sciences* **2013,** 48, (3), 393-405.

300. Azarmi, S.; Roa, W. H.; Lobenberg, R., Targeted delivery of nanoparticles for the treatment of lung diseases. *Adv Drug Deliv Rev* **2008,** 60, (8), 863-75.

301. Lee, D. W.; Shirley, S. A.; Lockey, R. F.; Mohapatra, S. S., Thiolated chitosan nanoparticles enhance anti-inflammatory effects of intranasally delivered theophylline. *Respir Res* **2006,** 7, 112.

302. Key, J.; Cooper, C.; Kim, A. Y.; Dhawan, D.; Knapp, D. W.; Kim, K.; Park, J. H.; Choi, K.; Kwon, I. C.; Park, K.; Leary, J. F., In vivo NIRF and MR dual-modality imaging using glycol chitosan nanoparticles. *J Control Release* **2012,** 163, (2), 249-55.

303. Koo, H.; Huh, M. S.; Sun, I.-C.; Yuk, S. H.; Choi, K.; Kim, K.; Kwon, I. C., In Vivo Targeted Delivery of Nanoparticles for Theranosis. *Accounts of Chemical Research* **2011,** 44, (10), 1018-1028.

304. Ryu, J. H.; Koo, H.; Sun, I.-C.; Yuk, S. H.; Choi, K.; Kim, K.; Kwon, I. C., Tumor-targeting multi-functional nanoparticles for theragnosis: New paradigm for cancer therapy. *Advanced Drug Delivery Reviews* **2012,** 64, (13), 1447-1458.

305. Sun, I. C.; Na, J. H.; Jeong, S. Y.; Kim, D. E.; Kwon, I. C.; Choi, K.; Ahn, C. H.; Kim, K., Biocompatible glycol chitosan-coated gold nanoparticles for tumor-targeting CT imaging. *Pharm Res* **2014,** 31, (6), 1418-25.

306. Lee, C.-M.; Jang, D.; Kim, J.; Cheong, S.-J.; Kim, E.-M.; Jeong, M.-H.; Kim, S.-H.; Kim, D. W.; Lim, S. T.; Sohn, M.-H.; Jeong, Y. Y.; Jeong, H.-J., Oleyl-Chitosan Nanoparticles Based on a Dual Probe for Optical/MR Imaging in Vivo. *Bioconjugate Chemistry* **2011,** 22, (2), 186-192.

2. Glycol chitosan based nanogel as a potential targetable carrier for siRNA

Adapted from: Macromol Biosci. 2013 Oct; 13(10):1369-78

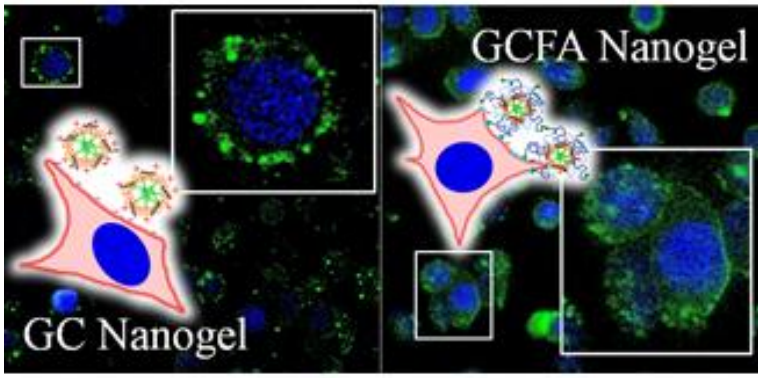

A self-assembled GC nanogel was synthesized by chemically grafting hydrophobic chains onto the polysaccharide, which was comprehensively characterized. The obtained macromolecular micelle was decorated with folate-conjugated PEG (GCFA). An average size distribution of 250nm and 200nm was observed, respectively for the GC and GCFA nanogels. Differential cell localization was observed incubating the materials with HeLa cells. While the GC nanogel was detected on the cell surface, GCFA was localized in the cytoplasm. The cell viability was not compromised by the nanogels. Interestingly, GC nanogel was poorly internalized by bone marrow derived macrophages (BMDM), and GCFA was not phagocytosed. Given its ability to complex siRNA, the targetable GC nanogel could be a promising vehicle for siRNA delivery.

2.1. Introduction

Gene therapy is an emerging field in medical and pharmaceutical sciences. However, naked therapeutic genes are rapidly degraded by nucleases, showing poor and non-specific cellular uptake and low transfection efficiency [1]. Therefore the development of safe and efficient gene carrier is primordial for the success of gene therapy. Systems based on CS macromolecular micelles, also called as nanogel, are now extensively used in drug delivery; they form stable complexes with nucleic acids, protect them from nuclease degradation, interact readily with cellular membrane and shows pH buffering capacity, that is critical for endosomal escape and subsequent gene silencing efficiency, although commonly accepted as less efficiently than PEI [2].

CS, a main component of the exoskeleton of insects, crustaceans, and cell walls of fungi, is obtained by chitin extensive deacetylation. This linear polysaccharide is composed of glucosamine and N-acetylglucosamine units linked through glycosidic bonds [3]. It gathers a number of desirable characteristics such as: cationic charge, biodegradability, biocompatibility, low toxicity, muco-adhesiveness and reactive sites for chemical modifications [2, 4]. However, its poor solubility at physiological and basic pH (pKa values range from 6.2 to 7), has limited its effective utilization [5]. Among water-soluble CS derivatives, GC has emerged as novel gene carrier due to its solubility at physiological pH provided by ethylene oxide units, besides its proved biocompatibility *in vivo* [6, 7]. Its positive charge under slightly acidic conditions allows the electrostatic interaction between GC and negatively charged siRNA. The siRNA loading depends among other parameters of the N/P ratio, defined as the molar ratio of chitosan amino groups to nucleic acid phosphate groups. Higher N/P ratios have been required to complex efficiently siRNA and achieve greatest level of silencing [4]. Under neutral or alkaline conditions the binding is stabilized essentially by hydrogen bonding and hydrophobic interactions [8]. Successful transfection efficiency is also related to a specific cellular uptake. In this study, folate was selected as model targeting molecule because folate receptors are overexpressed in a wide range of tumours and rarely found in normal cells [9]. Folate was conjugated to GC using a PEG linker. Since Chan *et al.* [10] verified that the folate grafting slightly decrease the solubility we add an extra amount of PEG to overcome this issue. PEGlyation - in addition to improve the solubility - also reduces the opsonin adsorption and subsequent scavenging by the mononuclear phagocyte system, enhancing the longevity of nanogel in blood [11].

The aim of present study was to develop GC based nanogel through chemical grafting of hydrophobic chains on hydrophilic backbone, resulting in an amphiphilic polymer capable of self-assembling in aqueous environment. Targeting ability was assessed using folate as ligand. The ability of GC nanogel complex siRNA was evaluated to explore their potential as siRNA delivery system. Cell viability and the response of macrophages to nanogel were also investigated. The results showed that GC nanogel would be a promising carrier for targeted gene delivery.

2.2. Experimental

2.2.1. Materials

Culture medium reagents were purchased from Biochrom. GC (G7753), mercapto hexadecanoic acid (MHDA), folate, N-hydroxysulfosuccinimide (NHS), 1-Ethyl-3-[3-dimethylaminopropyl]carbodiimide hydrochloride (EDC), O-methyl-O'-succinylpolyethyene glycol 2000 (PEG2000), O-(2-Aminoethyl)-O'-(2-carboxyethyl)polyethylene glycol 3000 hydrochloride (PEG3000) were acquired from Sigma-Aldrich. 5/6-carboxyfluorescein succinimidyl ester was purchased from Thermo Scientific.

2.2.2. GC analysis

2.2.2.1. ^{1}H Nuclear magnetic resonance analysis (^{1}H NMR)

The ^{1}H RMN spectra was obtained using a Varian Unity Plus 300 spectrometer operating at 299.94 MHz and 70ºC. The GC solution sample was prepared at 10mg/mL in 2% DCl/D_2O. 0.05 wt. % 3-(trimethylsilyl)propionic-2,2,3,3-d4 acid (TSP) was used as a quantification reference for all chemical shifts.

2.2.2.2. Refractive Index Increment (dn/dc)

d*n*/d*c* was evaluated with a differential refractometer operating at λ= 658 nm (Optilab rEX). Six solutions (a parent solution and five dilutions) were analyzed to determine each value of d*n*/d*c*.

2.2.2.3. Gel permeation chromatography

Size exclusion chromatography (SEC) coupled online with a multi-angle laser light scattering (MALLS) detector. SEC was performed by means of an IsoChrom LC pump

(Spectra Physics) connected to TSK gel 2500 PW and TSK gel 6000PW columns. A Optilab rEX differential refractometer and a multi-angle laser-light scattering detector, operating at 690 nm (Wyatt Dawn EOS) and 18 angles, were connected online. A 0.15 M ammonium acetate/0.2 M acetic acid buffer (pH=4.5) was used as the eluent. The flow rate was 0.5 ml/min. The polymer solutions were prepared by dissolving 1mg of polymer in 1ml of buffer solution, then filtered on a 0.45 µm pore size membrane (Millipore) before the injection of 50 µl of solution.

2.2.3. Self-assembled nanogel synthesis

2.2.3.1. Preparation of GC nanogel

GC nanogel was prepared by chemical conjugation of MHDA to GC, through carbodiimide chemistry, as depicted in Figure 1 A [12, 13]. In detail, GC (200mg) was dissolved in 24mL of distilled water at 50ºC for 2h, under magnetic stirring. Then the GC solution was diluted in methanol 1:3 (v/v) (water/methanol). After homogenization, MHDA was added according to the desirable degree of substitution (DS) and left dissolving for 3h. EDC and NHS were then mixed (both in 1.5-fold molar excess with regard to MHDA) to activate MHDA. The reaction was performed for 24h at 50ºC under magnetic stirring. The reaction product was extensively dialysed (Mw cutoff 10-12 kDa) against distilled water, followed by freeze-drying. The lyophilized GC nanogel, a blank fluffy product, was stored at room temperature.

2.2.3.2. Functionalization of GC nanogel with folate (GCFA nanogel)

The functionalization of nanogel with folate occurs in two steps. In the first one folate is conjugated to PEG3000 (FA-PEG3000), as described by Zheng et al.; then, in the second step, FA-PEG3000, PEG2000 and MHDA are grafted on the GC polymer [14]. In brief, folate was activated by reacting with EDC and NHS (using 10 and 1.2-fold molar excess, respectively) in anhydrous DMSO, for 3 h. Then, 2-mercaptoethanol (10-fold molar excess to EDC) was added to quench the unreacted EDC. The reactive folate solution was joined dropwising to PEG3000 dissolved in anhydrous DMSO, under stirring. The reaction was conducted for 18 h, at room temperature, in the dark. The resulting mixture was dialysed (Mw cutoff 1 kDa) first against DMSO, to remove unbounded folate and then with distilled water. The dialyzed product was freeze-dried. The second step consists in the same reaction as described above for the GC nanogel synthesis; however, in this case, in addition to MHDA also FA-PEG3000 and PEG2000

were added to the reaction mixture, as shown on Figure 1 B. The lyophilized GCFA nanogel had a yellowish tonality; it was stored at room temperature, protected from light.

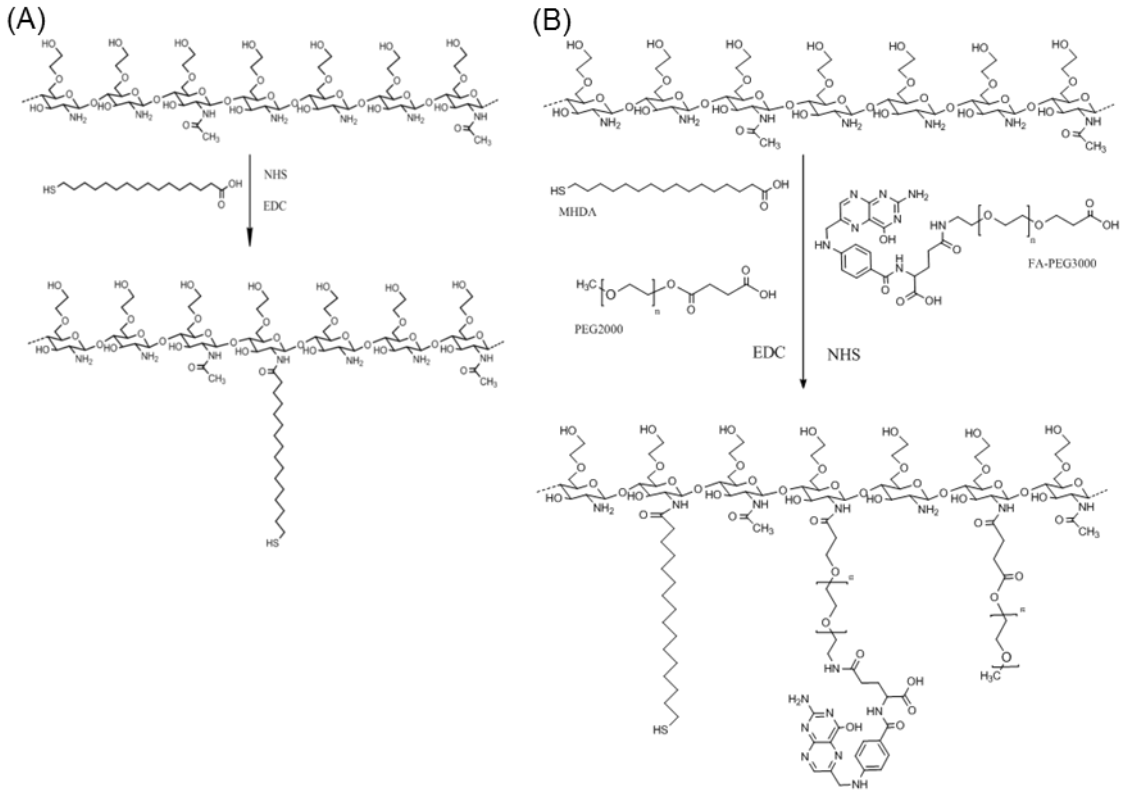

Figure 1. Representation of (A) GC and (B) GCFA nanogels synthesis.

2.2.3.3. Nanogel self-assembling

The lyophilized samples were dispersed in distilled water under magnetic stirring at 50 ºC. After 48 h, the nanogel solution was filtered using a membrane with a pore size of 0.45 µm and stored at 4 ºC.

2.2.4. Nanogel characterization

2.2.4.1. ^{1}H Nuclear magnetic resonance analysis (^{1}H NMR)

The MHDA substitution degree was quantified by preparing a nanogel dispersion with a concentration of 7mg/mL in 2% (v/v) DCl/D_2O followed by the acquisition of ^{1}H RMN spectra on a Varian Unity Plus 300 spectrometer operating at 299.94 MHz at 70ºC.

2.2.4.2. Dynamic light scattering (DLS)

The size distribution, mean hydrodynamic diameter and surface charge of the nanogels were evaluated using a Malvern Zetasizer NANO ZS (Malvern Instruments Limited, U.K.). The nanogel dispersions (1 mg/mL in distilled water, prepared as described above) were analysed at 25 °C in a polystyrene cell using a detector angle of 173°.

2.2.4.3. Cryo-Field Emission Scanning Electron Microscopy (Cryo-FESEM)

The GC nanogel (1 mg/mL in distilled water) was frozen at -200 ºC with liquid nitrogen and transferred to the cryo stage (Gatan, Alto 2500, U.K.) of the electronic microscope (SEM/EDS: FESEM JEOL JSM6301F/Oxford Inca Energy 350). Each sample was fractured with a knife, and sublimated for 10 min at -95 ºC to remove an ice layer, allowing nanogels being exposed. At -140 ºC, the samples were sputter coated with gold and palladium using an accelerating voltage of 10 kV. The samples observation was done at – 140 ºC and 15 kV.

2.2.4.4. Fluorescence spectroscopy

The critical aggregation concentration (CAC) of GC and GCFA nanogels were determined measuring the fluorescence intensity of a hydrophobic probe Nile Red (NR) loaded onto the core of the nanogel. Lyophilized nanogel was dispersed in water at 1mg/mL, as above mentioned. Then, nanogel suspension was diluted to a range of concentrations from 1 to 0.001 mg/mL in 1ml of final volume. Then, 5 µL of a NR solution with a concentration of $4x10^{-5}$ M in ethanol was added to each tube, yielding a NR final concentration of $2x10^{-7}$ M and 0.5 % of ethanol. The nanogel solutions containing NR were left over night in a turning wheel to keep the solution agitated, at room temperature. The solutions were then analysed using a Spex Fluorolog 3 spectrofluorimeter, with excitation at 550 nm and recording the emission in the range from 560 to 760 nm.

2.2.5. Cell culture

HeLa cell line

HeLa cells were maintained at 37 ºC in a humidified air containing 5% CO_2 in RPMI-1640 supplemented with 10% heat-inactivated fetal bovine serum (FBS), 100 IU/mL penicillin and 0.1 mg/mL streptomycin.

Mouse leukaemic monocyte macrophage (RAW) cell line

RAW cell line was maintained in DMEM supplemented with 10% FBS and 100 IU/mL penicillin and 0.1 mg/mL streptomycin. The cells were incubated at 37 ºC in a humidified air containing 5% CO_2.

Murine Bone Marrow-Derived Macrophages (BMDM)

Macrophages were collected from femoral and tibial mouse bone marrow. Mouse long bones were extracted from the mousse under aseptic conditions and flushed with RPMI-1640. The resulting cell suspension was centrifuged at 500 g during 10 min. The cell pellet was resuspended in RPMI-1640 supplemented with 10 mM HEPES, 10% heat-inactivated FBS, 60 µg/mL penicillin/streptavidin, 0.005 mM β-mercaptoethanol (RPMI complete medium) and 10% L929 Cell Conditioned Medium (LCCM). To remove adherent bone marrow cells, the cell suspension was incubated overnight at 37 ºC and 5% CO_2 atmosphere in a Petri dish. The non-adherent cells were collected, centrifuged at 500 g (10 min) and seeded in 24 well plates at 5 x 10^5 cells per well in RPMI complete medium containing 10% of LCCM and incubated at 37 ºC in a 5% CO_2 atmosphere. Four days after seeding 10% of LCCM was re-added to the cultures. The culture medium was replaced with fresh RPMI complete medium containing 10% LCCM on day 7. After 10 days in culture, cells were completely differentiated into macrophages [15, 16].

2.2.6. *In vitro* cell cytotoxicity studies

*C*ells were seeded in 96 well plates at a density of 2500 per well for HeLa and 5000 for RAW cell lines, and left adhering in 0.2 ml of culture medium overnight. The medium was replaced by nanogel dispersions in culture medium containing 25% of water v/v. After 24, 48 and 72 h the cellular viability was determined using the MTT (3-(4,5-dimethylthiazol-2-yl)-2,5-diphenyl tetrazolium bromide) [17] quantitative colorimetric assay. The tetrazolium salt is reduced by metabolically active cells using mitochondrial succinate dehydrogenase enzymes. The resulting dark blue formazan crystals can be solubilized in Dimethyl sulfoxide and quantified spectrophotometrically at 570 nm, subtracting the background optical density (690 nm). The test was performed in triplicate.

2.2.7. Cellular uptake

2.2.7.1. Preparation of NHS-Fluorescein nanogel

The production of GC and GCFA nanogels labelled with NHS-Fluorescein was achieved by grafting the fluorophore agent through an amide linkage, as described ahead. The NHS-Fluorescein was dissolved in DMSO, at a concentration of 1%. The molar ratio of NHS-Fluorescein carboxylic groups to the GC and GCFA nanogels free amine groups was 0.25. The dye was added to a stirred nanogel suspension at a concentration of 1 mg/mL in PBS. The reaction was allowed to occur overnight at room temperature, in the dark. The reaction mixture was thoroughly dialysed (MW cutoff 10-12 kDa) against distilled water to remove free NHS-fluorescein. As to verify the absence of free dye, the final solution of nanogel-Fluorescein was purified by centrifugation through a 10 kDa Mw cutoff filter.

2.2.7.2. Confocal laser scanning microscopy

HeLa cells and BMDM were seeded at a density of 5 x 10^5 cells per well in a 24 well plate (with a coverslip in each well), and left adhering overnight. The cells were incubated with 0.2 mg/mL of each nanogel-Fluorescein suspension in culture medium containing 25% of water v/v. After 6 h, the coverslips were washed twice with PBS at room temperature and the cells were fixed with paraformaldehyde 2% for 25 min. After washing the cells twice with PBS twice, 4',6-diamidino-2-phenylindole (DAPI, 120 ng/mL) was used to stain the nucleus for 3 min at room temperature. After washing the preparations were observed in a confocal laser scanning microscope Leica SP2 AOBS SE (Leica Mycrosystems, Germany).

2.2.8. siRNA-nanogel interaction

The siRNA binding ability of the nanogel was tested by gel retardation assay. Suspensions of the nanogel in buffer solution at pH 4.5 were mixed with siRNA (1 µg) under three different molar ratios of amine to phosphate groups, and gently vortexed. The formulations nanogel/siRNA were incubated for 30min at room temperature prior to loading into a 4% agarose gel electrophoresis to allow the formation of the nanogel/siRNA complexes. The electrophoresis was carried out at 100V for 30min in Tris-acetate-EDTA buffer [40 mM Tris-HCl, 1% (v/v) acetic acid, 1 mM EDTA]. SYBR Safe was used to visualize siRNA using a UV transilluminator at 365 nm.

2.2.9. Statistical analysis

Data were expressed as mean ± stand deviation. All statistics to cell viability results were performed applying two-way ANOVA tests through Prism software (GraphPad software version 5.00, USA). Differences were considered significant when $P<0.05$.

2.3. Results and discussion

2.3.1. GC characterization

The GC used for nanogel synthesis was purchased from Sigma Aldrich. A comprehensive characterization of this material is not available in the product data sheet and the characterization found in the literature is not consistent [18-22]. Therefore, the degree of deacetylation and the molecular weights of the polymer were analysed by ^{1}H NMR spectroscopy and size exclusion chromatography.

Figure 2 shows the ^{1}H NMR spectrum of GC dissolved in 2% (v/v) DCl/D_2O, obtained at 70 ºC. The characterization of GC by ^{1}H NMR spectroscopy has been extensively used, since it allows the straightforward assignment of the GC proton peaks [22] and thereby the determination of the degree of deacetylation [23]. The ^{1}H NMR measurements at 70 ºC cause the shift of the solvent proton peak from 4.8 ppm to 4.3, allowing the H-1 peak to become visible. A GC degree of deacetylation of ~88% was calculated according to the approach described by Lavertu and colleagues [23], using the integral intensity of the proton H1 of deacetylated monomer (H1-D) and the three protons of methyl group (-CH_3). The degree of deacetylation was also determined according to Hirai *et al.* [24] equation and a similar value was achieved.

The SEC-MALLS GC mass determination, namely the number, weight and Z-average molecular weight (Mn, Mw and Mz, respectively) and polydispersity index (Mw/Mn) are described in Table 1.

Table 1. SEC-MALLS characterization of GC using a value of dn/dc=0.153 mL/g.

Mn (g/mol)	Mw (g/mol)	Mz (g/mol)	Mw/Mn
67 000 ± 5%	100 000 ± 3%	167 000 ± 13%	1.509 ± 6%

The values of Mn (67 kDa) and Mw (100 kDa) obtained are not in agreement with those reported by Knight et al. 178 kDa and 237 kDa, respectively, although GC from Sigma was used also in that case [22]. Also using the same source, Park *et al.* [21] reported a

Mw of 250 kDa. Also regarding the GC degree of acetylation some inconsistency is noted comparing the values obtained in this work with those reported in the literature: Dufes *et al.* obtained a value of 33% and Park *et al.* 17.3% [19, 21]. It is not clear whether the different samples described in the literature correspond to different batches of glycol chitosan or whether the different properties reported arise from technical issues. Nevertheless, the properties of GC used for the development of biomedical materials must be well characterized in order to make possible a proper comparison of data obtained in different labs.

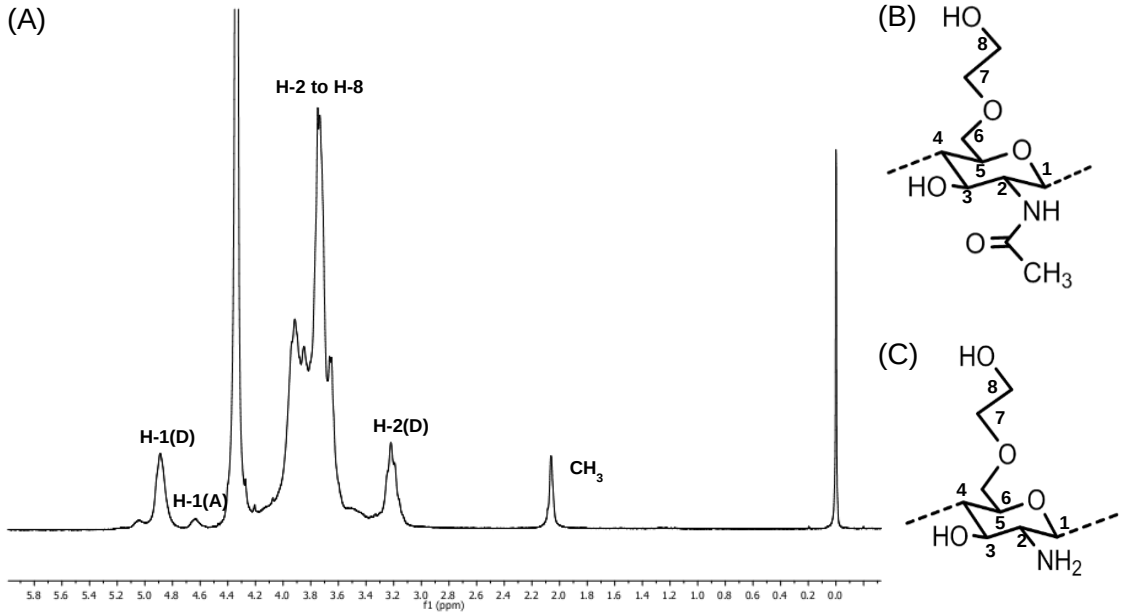

Figure 2. 300 MHz ^{1}H NMR spectrum of GC in 2% (v/v) DCl/D_2O at 70ºC (A) and schematic representation of GC monomer acetylated (B) and deacetylated (C).

2.3.2. Synthesis and physicochemical characterization of nanogels

The covalent attachment of hydrophobic chains on the hydrophilic GC backbone results in the generation of amphiphilic material which self-assembles in water. The decoration of the nanogel with FA-PEG3000 and PEG2000 was also mediated by a crosslinking reaction. The presence of MHDA, PEG and folate on the polysaccharide were confirmed by ^{1}H NMR spectroscopy. The MHDA DS was calculated from de following equation:

$$DS_{MHDA} = \frac{12\ a}{26\ b} \times 100$$

where (a) represents the integral of MHDA $-CH_2-$ protons signal detected between 1.2 and 1.6ppm (which does not include the $-CH_2-$ protons signals next to the carbonyl and

thiol groups) and (b) the integral of GC proton peaks observed from 3 to 4.2 ppm, (Figure 3 A). The DS obtained was about 9%, *i.e.* 9 out of 100 sugar residues are substituted with the alkane chain. Given the theoretical DS, 15%, the reaction efficiency is about 60%. The yield reaction was reproducible for all batches.

The successful conjugation of FA-PEG3000 and PEG2000 on GC was confirmed by the presence of characteristic peaks between 6 and 9 ppm assigned to aromatic protons of folic acid and at ~3.7 ppm (-CH_2CH_2O-) for PEG protons (Figure 3 B) [14]. Nonetheless it has not been possible to determine the corresponding DS due to overlapping of the proton signal derived from PEG and sugar residues. Since these molecules are grafted through a similar reaction used for MHDA, it may be speculated that the reaction yield might have been similar. Based on this assumption, the FA-PEG3000 and PEG2000 DS would correspond to 6% and 12%, respectively. PEG was used to improve the folate water-solubility, also performing as a spacer and enabling an efficient binding to the folate receptor [14, 25].

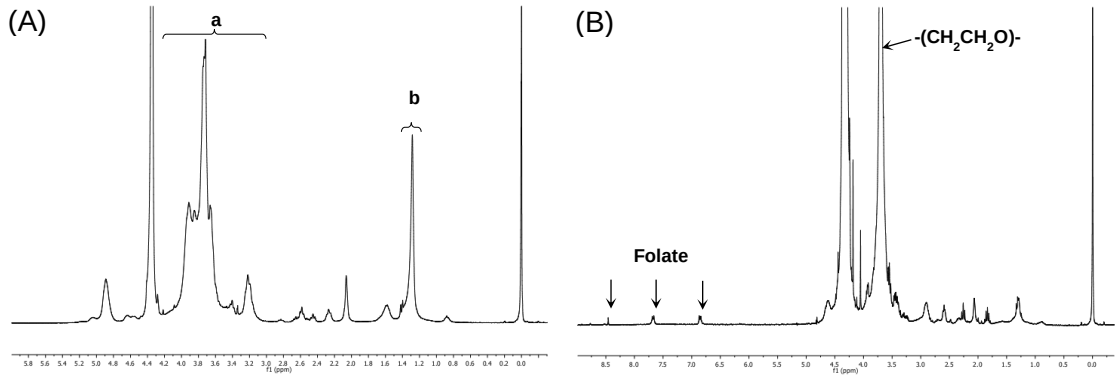

Figure 3. ^{1}H NMR spectra of (A) GC nanogel and (B) GCFA in 2 % (v/v) DCl/D_2O at 70ºC.

Self-assembled nanogels give rise to a unimodal particle size distributions, between 100 to 400 nm for the GC nanogel (Figure 4 A), with an average size of 250nm, and between 60 to 500 nm for GCFA (Figure 4 C) with 200nm as mean diameter. The functionalized nanogel population was slightly more polydisperse than GC nanogel, with polydispersity indexes of 0.4 and 0.3, respectively. The surface charge of the nanogels in aqueous solution was positive (potential zeta of about 25-30 mV) due to presence of protonated amine groups. As expected, the GCFA nanogel surface charge was less positive, because fewer free amine groups are available. The nanogel morphology under cryo-FESEM was spherical as shown in Figure 4 B, and the size distribution observed confirm the results obtained by dynamic light scattering. Cryo-

FESEM allows the observation of the nanogel close to its natural liquid state, preserving the three dimensional structure [26]. The stability of the nanogels in aqueous solution was studied over time by dynamic light scattering. As observed in Figure 4 D, both nanogels are stable for at least 4 months, which represents a high colloidal stability.

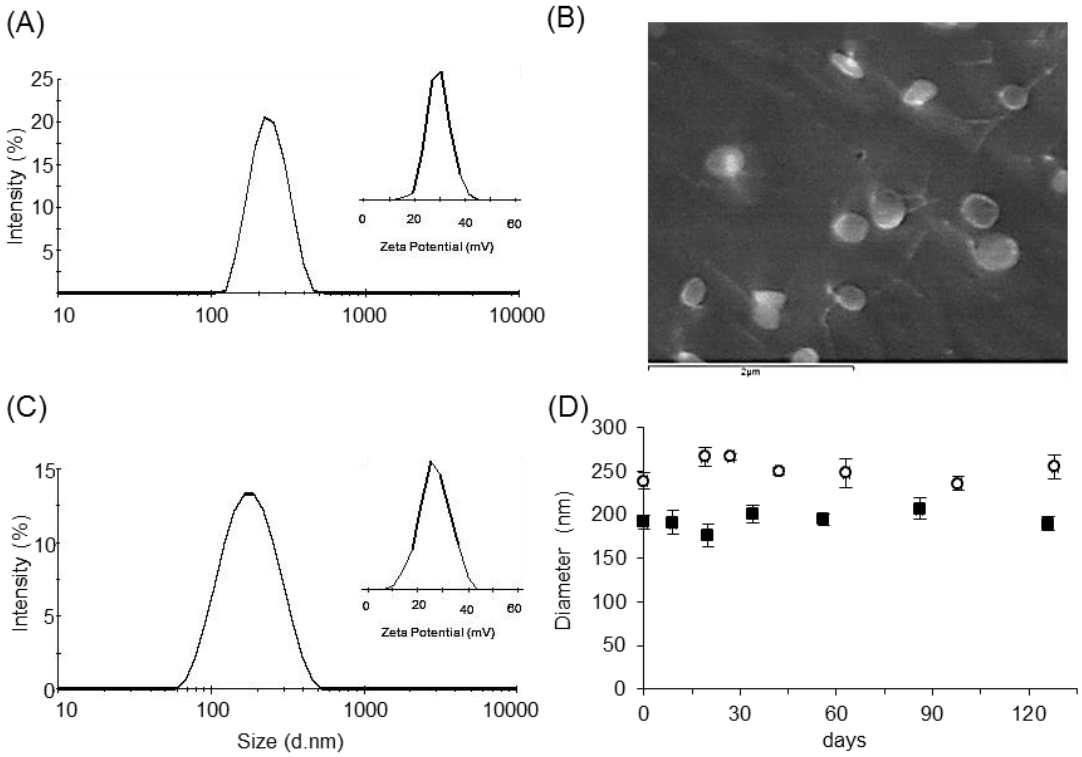

Figure 4. (A) Size distribution by intensity, zeta potential and (B) Cryo-FESEM micrograph of GC nanogel (scale bar: 2µm); (C) size distribution by intensity and zeta potential of GCFA nanogel; (D) colloidal stability of nanogels evaluated by average hydrodynamic diameter of GC (O) and GCFA (■) nanogels overtime. Both nanogel samples were prepared in distilled water and stored at 4 ºC. The measurements were performed at 25 ºC.

Self-aggregation behaviour of GC and GCFA nanogels was studied using NR as a hydrophobic fluorescent probe, whose absorbance and emission maxima shift to higher wavelengths with increasing polarity of the probe environment [27, 28]. The fluorescence emission spectra of NR as function of the nanogel concentration are shown in Figures 5 A and B, respectively. At low concentrations, in aqueous solution, the emission is close to the background intensity. However, the intensity increases abruptly above a certain nanogel concentration, indicating the formation of hydrophobic regions able to dissolve the NR probe. Associated to the increased fluorescence intensity a shift of the emission maxima towards lower wavelengths was observed with rising of the nanogel concentration, due to the lower polarity surrounding the probe hydrophobic cores of the

nanogels [29]. This transitional concentration is commonly named CAC, the minimal concentration required for the amphiphilic polyssacharide conjugates (Figure 5 D) to self-assemble forming a nanogel. The CAC value of the GC nanogel was 0.1 mg/mL (Figure 5 C). Values in the same order of magnitude have been reported by [30] for fluorescent chitosan NPs (0.06 mg/mL) and by [31] (0.123 mg/mL) for cholesterol modified GC. The modification of the nanogel with PEG, besides conferring increased solubility, also enhances the softness of GC main chain, which facilitates polymer aggregation [32]. Consequently the CAC achieved for the GCFA nanogel was significantly reduced to 0.0075 mg/mL.

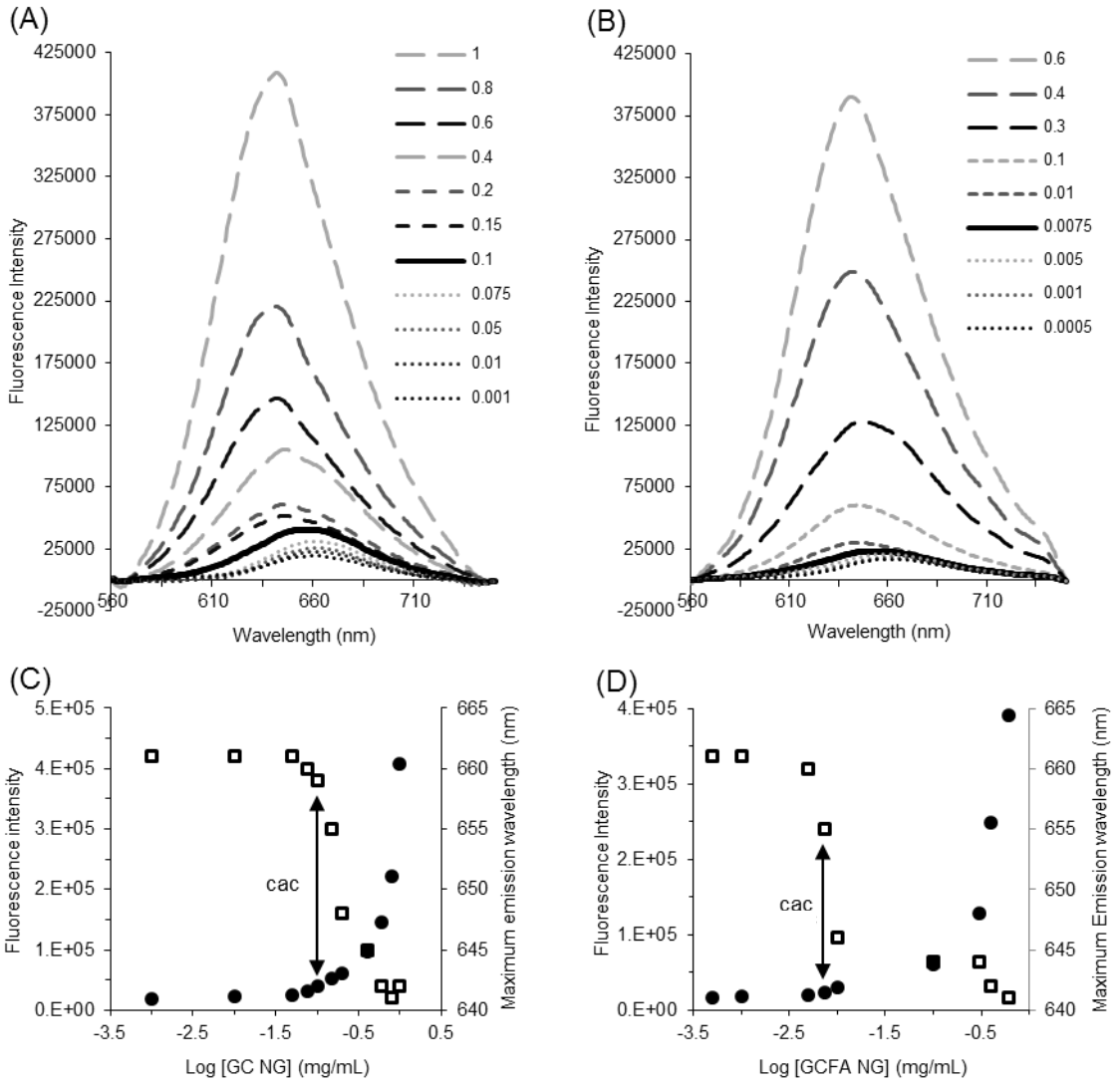

Figure 5. Emission spectra of NR ($2x10^{-7}$ M) as function of (A) GC and (B) GCFA nanogel concentration in mg/mL (λex= 550 nm); Plot of fluorescence intensity (●) and maximum emission wavelength (□) of NR versus (C) GC or (D) GCFA nanogel concentration.

2.3.3. Cell viability

Chitosan and its derivatives are not significantly toxic [33], GC being one of the less toxic derivatives [34]. Further GC modifications could improve or decrease the final cytotoxicity. The effect of the nanogel on cell viability and cell growth was gauged using RAW and HeLa cell lines in a MTT assay. As shown on Figure 6 A the proliferation of HeLa cells was significantly affected in the presence of the nanogels. However, cell growth was still observed. Indeed, the treated cells were able to grow, although with a lower rate than observed for the controls. RAW cell line (Figure 6 B) exhibited an even slower growth rate, but the cell number never decreased below the initial value, suggesting that cell viability is not compromised.

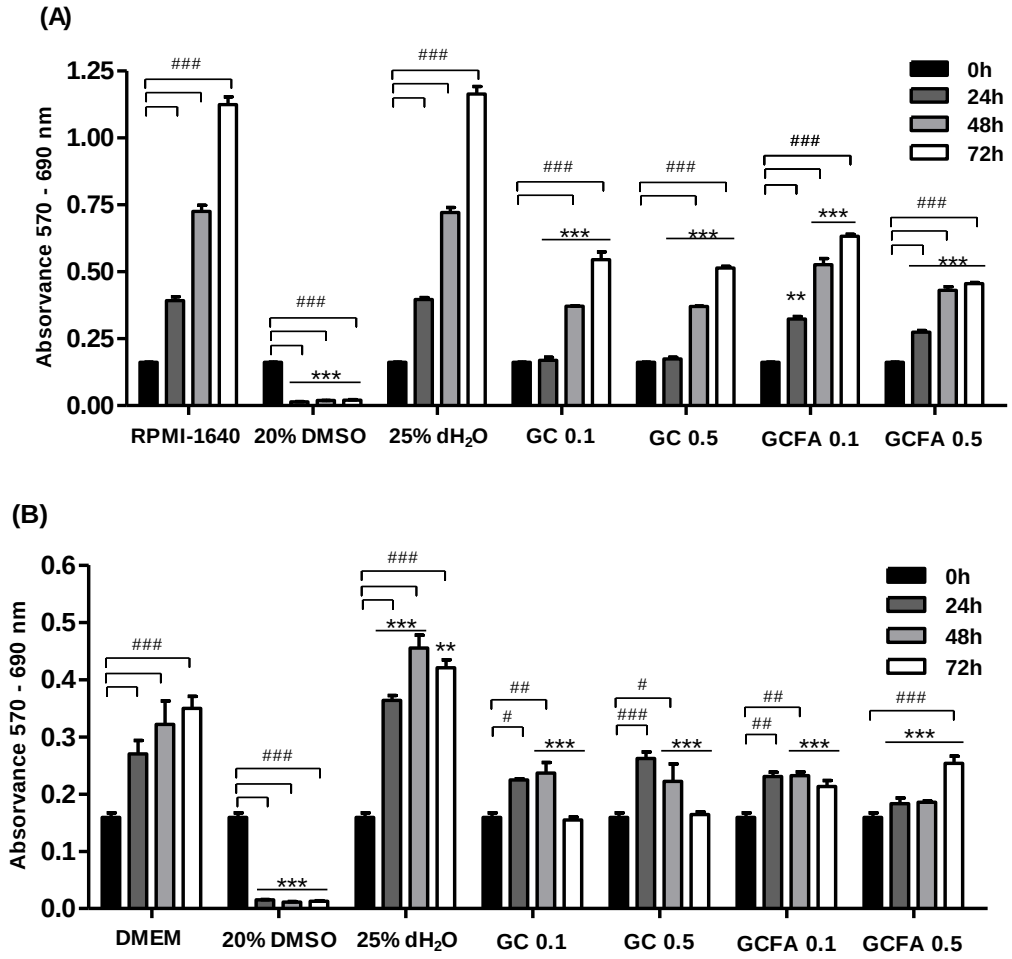

Figure 6. Effect of GC and GCFA nanogels (0.1 and 0.5 mg/mL) on viability of (A) HeLa and (B) RAW cells, measured by MTT assay. Cell culture medium was used as negative control (RPMI-1640 to HeLa cells and DMEM to RAW cell line) and 20% of DMSO as positive control. 25% dH_2O condition was also studied because each nanogel sample in culture medium containing 25% of water v/v. Statistical differences between negative control group (cell culture medium) and remaining samples at each time of incubation are represented as (*) and (#) means the statistical differences between 0h incubation time and remaining incubation times for each condition. Significance degree (one, two or three symbols) was chosen according to P values ($P<0.05$, $P<0.01$ and $P<0.0001$, respectively).

Overall, the presence of folate didn´t affect the cell viability, in agreement with the observation by Qu *et al.* [35], who reported that folate moieties didn´t influence cell cytotoxicity.

2.3.4. Cellular uptake

2.3.4.1. *In vitro* targeting ability

Folate receptors are extensively expressed in several kinds of tumour, including cervical cancer [36]. Hence, HeLa cells were used to assess the targeting ability conferred by the folate moiety grafted on the nanogel surface Figure 7. Cells treated with the nanogels labelled with a fluorescent probe were observed by confocal microscopy. Cells incubated with nanogel without ligand exhibited a fluorescent signal punctuated on the cell surface and minimal fluorescence on the cytoplasm, as shown in the amplified insert image. Probably, in the absence of targeting ligand and due to the slightly positive surface charge, the nanogel accumulates at the surface of the cellular membrane. In contrast nanogel bearing folate provided significant internalization, which suggests that the enhancement of GCFA nanogel uptake was due to folate receptor mediated endocytosis.

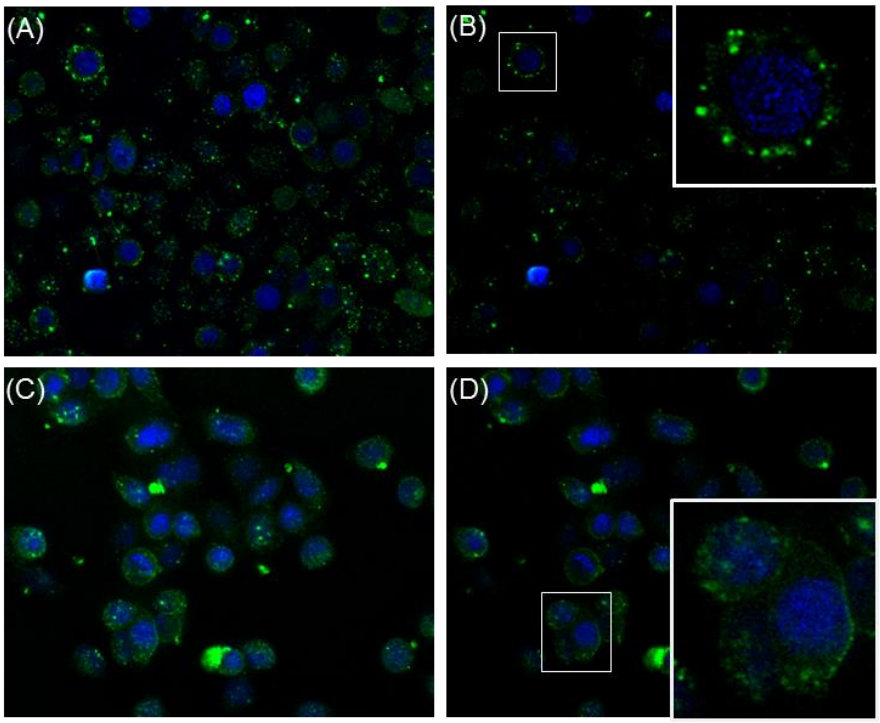

Figure 7. Internalization of nanogels labelled with NHS-Fluorescein by HeLa cells with and without folate. (A, B) Distribution pattern of non-functionalized nanogel and (C, D) Nanogel with folate, after sixth hours of incubation. Images on the left correspond to the sum of all captured plans, while images on the right side refer just to the fourth plan, corresponding to an internal section of the cells, such that the observed green fluorescence should correspond to material inside the cells, not surface adsorbed.

2.3.4.2. BMDM cellular uptake

The interaction with the mononuclear phagocyte system is crucial when a carrier is conceived for systemic application. In order to investigate whether the nanogels are phagocytosed by macrophages, fluorescent nanogels were incubated with BMDM. Figure 8 (A, B and C) illustrate the cellular uptake of FITC labelled dextrin nanogel (used as a positive control of macrophages uptake, as shown by Gonçalves et al.), NHS-Fluorescein labelled GC and GCFA nanogels, respectively [37]. Interestingly, the GC nanogel was poorly internalized by BMDM as compared with dextrin nanogels. Sarmento et al. [38] also reported that chitosan coated solid lipid NPs were neglectfully internalized within RAW 264.7 cells, as compared with uncoated solid lipid NPs. As verified by Parveen and Sahoo the PEG content chosen (~10%) was determinant on decreasing of macrophage cellular uptake [11]. Indubitably this is a promising result since GC nanogel may thus evade blood clearance and keep on circulation enough time to find the target site. GCFA nanogel was also not internalized by BMDM, hinting that this vehicle is a promising vector for drug and gene delivery. The effectiveness of GCFA nanogel in escaping macrophage uptake is probably due to PEG, which avoids opsonisation and consequently increase the circulation time on bloodstream [11, 39].

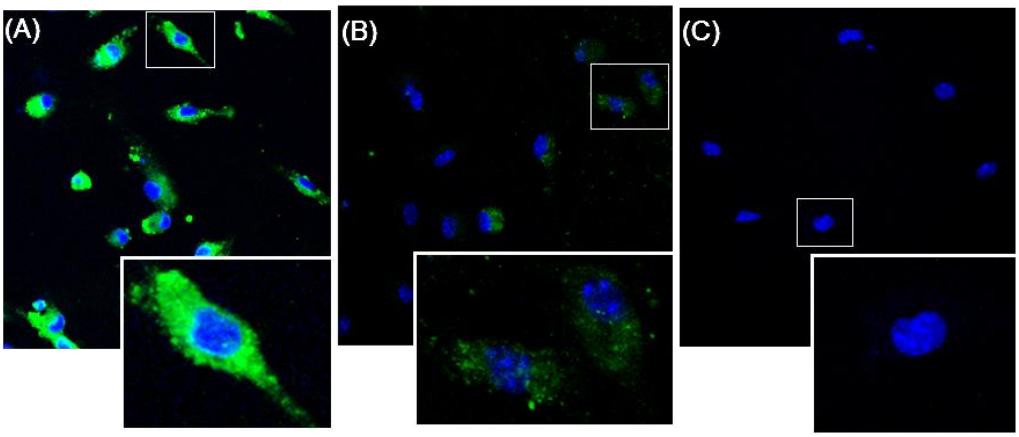

Figure 8. Confocal microscopic images of BMDM treated with fluorescent labelled (A) dextrin nanogel, (B) GC and (C) GCFA nanogels for 6h.

2.3.5. siRNA-nanogel interaction

The GC nanogel complexes siRNA through electrostatic interactions. As GC possesses amino groups with a pKa close to 6.5, below this pH the amino groups are protonated [40, 41]. Accordingly, in order to induce a stronger interaction between negatively charged phosphate groups from siRNA and positively charged amino groups

from GC, we used a nanogel solution in 0.2 M sodium acetate buffer pH 4.5. A gel retardation assay was used to evaluate the nanogel-siRNA interaction. Figure 9 shows the gel retardation results obtained for different N/P ratios. The use of a N/P molar ratio of 10 resulted in a delayed migration of the siRNA, as compared to naked siRNA. However, the electrophoretic mobility of siRNA was retarded more effectively with increasing N/P ratio and complete retardation of siRNA migration on agarose matrix was observed for the higher N/P ratio. The retention of siRNA in the loading well suggests that at this molar ratio a tight and stable interaction between nanogel and siRNA occurs.

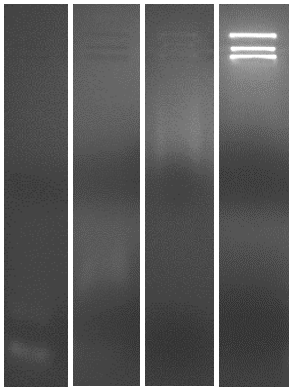

Figure 9. Gel retardation assay of GC nanogel/siRNA complex. Lane 1 is a 21bp siRNA unknown sequence; lanes 2-4 are GC/siRNA formulation with N/P molar ratio of 10, 50 and 100, respectively.

2.4. Conclusions

A self-assembled nanogel made of amphiphilic GC was successfully developed. Decoration with folate moiety conferred the nanogel the ability to improve the interaction with folate-receptor expressing cells, supporting its internalization through receptor mediated endocytosis. The nanogels were not cytotoxic for tested cell lines, although growth inhibition was observed to some extent. GC nanogels showed to be attractive for systemic administration due to their ability to escape from macrophages and consequently elongate lifetime in circulation until achieve the target site. GC nanogel proved to be a promising gene carrier, but besides complex siRNA efficiently, could also load low molecular weight hydrophobic drugs in the hydrophobic core.

Acknowledgments

Paula Pereira thanks FCT the PhD grant ref SFRH / BD / 64977 / 2009.

2.5. References

1. Mao, S.; Sun, W.; Kissel, T., Chitosan-based formulations for delivery of DNA and siRNA. Advanced drug delivery reviews 2010, 62, (1), 12-27.
2. Garcia-Fuentes, M.; Alonso, M. J., Chitosan-based drug nanocarriers: where do we stand? J Control Release 2012, 161, (2), 496-504.
3. Holzerny, P.; Ajdini, B.; Heusermann, W.; Bruno, K.; Schuleit, M.; Meinel, L.; Keller, M., Biophysical properties of chitosan/siRNA polyplexes: profiling the polymer/siRNA interactions and bioactivity. Journal of controlled release : official journal of the Controlled Release Society 2012, 157, (2), 297-304.
4. Riva, R.; Ragelle, H.; des Rieux, A.; Duhem, N.; Jérôme, C.; Préat, V., Chitosan and Chitosan Derivatives in Drug Delivery and Tissue Engineering Chitosan for Biomaterials II. In Jayakumar, R.; Prabaharan, M.; Muzzarelli, R. A. A., Eds. Springer Berlin / Heidelberg: 2011; Vol. 244, pp 19-44.
5. Wong, T. W., Chitosan and its use in design of insulin delivery system. Recent patents on drug delivery & formulation 2009, 3, (1), 8-25.
6. Na, J. H.; Koo, H.; Lee, S.; Min, K. H.; Park, K.; Yoo, H.; Lee, S. H.; Park, J. H.; Kwon, I. C.; Jeong, S. Y.; Kim, K., Real-time and non-invasive optical imaging of tumor-targeting glycol chitosan nanoparticles in various tumor models. Biomaterials 2011, 32, (22), 5252-61.
7. Huh, M. S.; Lee, S. Y.; Park, S.; Lee, S.; Chung, H.; Choi, Y.; Oh, Y. K.; Park, J. H.; Jeong, S. Y.; Choi, K.; Kim, K.; Kwon, I. C., Tumor-homing glycol chitosan/polyethylenimine nanoparticles for the systemic delivery of siRNA in tumor-bearing mice. Journal of controlled release : official journal of the Controlled Release Society 2010, 144, (2), 134-43.
8. Xu, S.; Dong, M.; Liu, X.; Howard, K. A.; Kjems, J.; Besenbacher, F., Direct force measurements between siRNA and chitosan molecules using force spectroscopy. Biophysical journal 2007, 93, (3), 952-9.
9. You, J.; Li, X.; de Cui, F.; Du, Y. Z.; Yuan, H.; Hu, F. Q., Folate-conjugated polymer micelles for active targeting to cancer cells: preparation, *In vitro* evaluation of targeting ability and cytotoxicity. Nanotechnology 2008, 19, (4), 045102.
10. Chan, P.; Kurisawa, M.; Chung, J. E.; Yang, Y. Y., Synthesis and characterization of chitosan-g-poly(ethylene glycol)-folate as a non-viral carrier for tumor-targeted gene delivery. Biomaterials 2007, 28, (3), 540-9.
11. Parveen, S.; Sahoo, S. K., Long circulating chitosan/PEG blended PLGA nanoparticle for tumor drug delivery. European journal of pharmacology 2011, 670, (2-3), 372-83.
12. Kwon, S.; Park, J. H.; Chung, H.; Kwon, I. C.; Jeong, S. Y.; Kim, I.-S., Physicochemical Characteristics of Self-Assembled Nanoparticles Based on Glycol Chitosan Bearing 5β-Cholanic Acid. Langmuir 2003, 19, (24), 10188-10193.
13. Kim, J.-H.; Kim, Y.-S.; Kim, S.; Park, J. H.; Kim, K.; Choi, K.; Chung, H.; Jeong, S. Y.; Park, R.-W.; Kim, I.-S.; Kwon, I. C., Hydrophobically modified glycol chitosan nanoparticles as carriers for paclitaxel. Journal of Controlled Release 2006, 111, (1–2), 228-234.

14. Zheng, Y.; Song, X.; Darby, M.; Liang, Y.; He, L.; Cai, Z.; Chen, Q.; Bi, Y.; Yang, X.; Xu, J.; Li, Y.; Sun, Y.; Lee, R. J.; Hou, S., Preparation and characterization of folate-poly(ethylene glycol)-grafted-trimethylchitosan for intracellular transport of protein through folate receptor-mediated endocytosis. Journal of biotechnology 2010, 145, (1), 47-53.

15. Carvalho, V.; Castanheira, P.; Madureira, P.; Ferreira, S. A.; Costa, C.; Teixeira, J. P.; Faro, C.; Vilanova, M.; Gama, M., Self-assembled dextrin nanogel as protein carrier: controlled release and biological activity of IL-10. Biotechnology and bioengineering 2011, 108, (8), 1977-86.

16. Cerca, F.; Andrade, F.; Franca, A.; Andrade, E. B.; Ribeiro, A.; Almeida, A. A.; Cerca, N.; Pier, G.; Azeredo, J.; Vilanova, M., Staphylococcus epidermidis biofilms with higher proportions of dormant bacteria induce a lower activation of murine macrophages. Journal of medical microbiology 2011, 60, (Pt 12), 1717-24.

17. Mosmann, T., Rapid colorimetric assay for cellular growth and survival: application to proliferation and cytotoxicity assays. Journal of immunological methods 1983, 65, (1-2), 55-63.

18. Uchegbu, I. F.; SchÄTzlein, A. G.; Tetley, L.; Gray, A. I.; Sludden, J.; Siddique, S.; Mosha, E., Polymeric Chitosan-based Vesicles for Drug Delivery. Journal of Pharmacy and Pharmacology 1998, 50, (5), 453-458.

19. Dufes, C.; Muller, J. M.; Couet, W.; Olivier, J. C.; Uchegbu, I. F.; Schatzlein, A. G., Anticancer drug delivery with transferrin targeted polymeric chitosan vesicles. Pharm Res 2004, 21, (1), 101-7.

20. Cho, Y. W.; Park, S. A.; Han, T. H.; Son, D. H.; Park, J. S.; Oh, S. J.; Moon, D. H.; Cho, K. J.; Ahn, C. H.; Byun, Y.; Kim, I. S.; Kwon, I. C.; Kim, S. Y., In vivo tumor targeting and radionuclide imaging with self-assembled nanoparticles: mechanisms, key factors, and their implications. Biomaterials 2007, 28, (6), 1236-47.

21. Park, K.; Kim, J.-H.; Nam, Y. S.; Lee, S.; Nam, H. Y.; Kim, K.; Park, J. H.; Kim, I.-S.; Choi, K.; Kim, S. Y.; Kwon, I. C., Effect of polymer molecular weight on the tumor targeting characteristics of self-assembled glycol chitosan nanoparticles. Journal of Controlled Release 2007, 122, (3), 305-314.

22. Knight, D. K.; Shapka, S. N.; Amsden, B. G., Structure, depolymerization, and cytocompatibility evaluation of glycol chitosan. Journal of biomedical materials research. Part A 2007, 83, (3), 787-98.

23. Lavertu, M.; Xia, Z.; Serreqi, A. N.; Berrada, M.; Rodrigues, A.; Wang, D.; Buschmann, M. D.; Gupta, A., A validated 1H NMR method for the determination of the degree of deacetylation of chitosan. Journal of pharmaceutical and biomedical analysis 2003, 32, (6), 1149-58.

24. Hirai, A.; Odani, H.; Nakajima, A., Determination of degree of deacetylation of chitosan by ¹H NMR spectroscopy. Polymer Bulletin 1991, 26, (1), 87-94.

25. Tan, Y.-l.; Liu, C.-G., Preparation and characterization of self-assemblied nanoparticles based on folic acid modified carboxymethyl chitosan. J Mater Sci: Mater Med 2011, 22, (5), 1213-1220.

26. Krauel, K.; Girvan, L.; Hook, S.; Rades, T., Characterisation of colloidal drug delivery systems from the naked eye to Cryo-FESEM. Micron 2007, 38, (8), 796-803.

27. Nizri, G.; Magdassi, S., Solubilization of hydrophobic molecules in nanoparticles formed by polymer-surfactant interactions. Journal of colloid and interface science 2005, 291, (1), 169-74.

28. Krishna, M. M. G., Excited-State Kinetics of the Hydrophobic Probe Nile Red in Membranes and Micelles. The Journal of Physical Chemistry A 1999, 103 (19), 3589-3595.

29. Coutinho, P. J. G.; Castanheira, E. M. S.; Rei, M. C.; Oliveira, M. E. C. D. R., Nile Red and DCM Fluorescence Anisotropy Sudies in C12E7/DPPC Mixed Systems. The Journal of Physical Chemistry B 2002, 106, 12841-12846.

30. Cui, W.; Lu, X.; Cui, K.; Wu, J.; Wei, Y.; Lu, Q., Fluorescent Nanoparticles of Chitosan Complex for Real-Time Monitoring Drug Release. Langmuir 2011, 27, (13), 8384-8390.

31. Sahu, A.; Bora, U.; Kasoju, N.; Goswami, P., Synthesis of novel biodegradable and self-assembling methoxy poly(ethylene glycol)-palmitate nanocarrier for curcumin delivery to cancer cells. Acta biomaterialia 2008, 4, (6), 1752-61.

32. Yang, X.; Zhang, Q.; Wang, Y.; Chen, H.; Zhang, H.; Gao, F.; Liu, L., Self-aggregated nanoparticles from methoxy poly(ethylene glycol)-modified chitosan: synthesis; characterization; aggregation and methotrexate release *In vitro*. Colloids and surfaces. B, Biointerfaces 2008, 61, (2), 125-31.

33. Kean, T.; Thanou, M., Biodegradation, biodistribution and toxicity of chitosan. Advanced drug delivery reviews 2010, 62, (1), 3-11.

34. Carreño-Gómez, B.; Duncan, R., Evaluation of the biological properties of soluble chitosan and chitosan microspheres. International Journal of Pharmaceutics 1997, 148, (2), 231-240.

35. Qu, D.; Lin, H.; Zhang, N.; Xue, J.; Zhang, C., *In vitro* evaluation on novel modified chitosan for targeted antitumor drug delivery. Carbohydrate Polymers 2012, (0).

36. Morris, V. B.; Sharma, C. P., Folate mediated *In vitro* targeting of depolymerised trimethylated chitosan having arginine functionality. Journal of colloid and interface science 2010, 348, (2), 360-8.

37. Goncalves, C.; Torrado, E.; Martins, T.; Pereira, P.; Pedrosa, J.; Gama, M., Dextrin nanoparticles: studies on the interaction with murine macrophages and blood clearance. Colloids and surfaces. B, Biointerfaces 2010, 75, (2), 483-9.

38. Sarmento, B.; Mazzaglia, D.; Bonferoni, M. C.; Neto, A. P.; do Céu Monteiro, M.; Seabra, V., Effect of chitosan coating in overcoming the phagocytosis of insulin loaded solid lipid nanoparticles by mononuclear phagocyte system. Carbohydrate Polymers 2011, 84, (3), 919-925.

39. Hu, F. Q.; Meng, P.; Dai, Y. Q.; Du, Y. Z.; You, J.; Wei, X. H.; Yuan, H., PEGylated chitosan-based polymer micelle as an intracellular delivery carrier for anti-tumor targeting therapy. Eur J Pharm Biopharm 2008, 70, (3), 749-57.

40. Bajaj, G.; Van Alstine, W. G.; Yeo, Y., Zwitterionic chitosan derivative, a new biocompatible pharmaceutical excipient, prevents endotoxin-mediated cytokine release. PloS one 2012, 7, (1), e30899.

41. Malmo, J.; Sorgard, H.; Varum, K. M.; Strand, S. P., siRNA delivery with chitosan nanoparticles: Molecular properties favoring efficient gene silencing. Journal of controlled release : official journal of the Controlled Release Society 2012, 158, (2), 261-8.

3. Biocompatibility of a self-assembled Glycol Chitosan nanogel

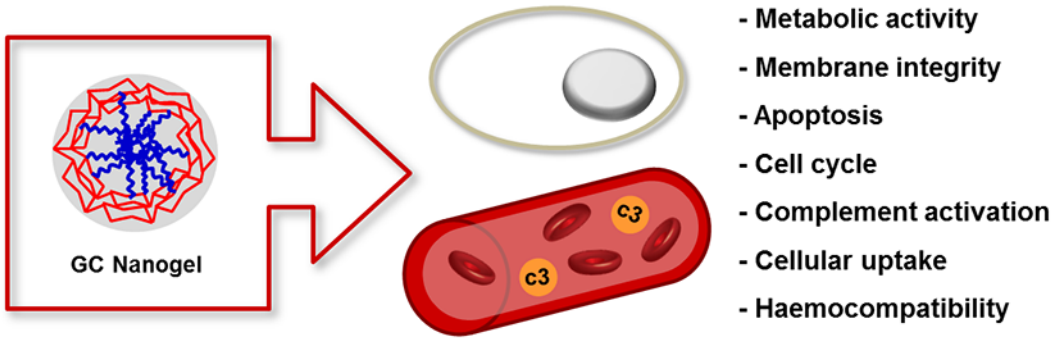

The research of chitosan-based nanogel for biomedical applications has grown exponentially in the last years; however, its biocompatibility is still insufficiently reported. Hence, the present work provides a thorough study of the biocompatibility of a GC nanogel. The obtained results showed that GC nanogel induced slight decrease on metabolic activity of RAW, 3T3 and HMEC cell cultures, although no effect on cell membrane integrity was verified. The nanogel does not promote cell death by apoptosis and/or necrosis, exception made for the HMEC cell line challenged with the higher GC nanogel concentration. Cell cycle arrest on G1 phase was observed only in the case of RAW cells. Remarkably, the nanogel is poorly internalized by bone marrow derived macrophages and does not trigger the activation of the complement system. GC nanogel blood compatibility was confirmed through haemolysis and whole blood clotting time assays. Overall, the results demonstrated the safety of the use of the GC nanogel as drug delivery system.

3.1. Introduction

NPs have been largely researched as drug nanocarriers, yet their interaction with cells and extracellular environment is still poorly explored. The evaluation of the potential effects of drug delivery devices on the biological systems is indeed a crucial requirement in the development of nanomedicines: cytotoxicity, haematocompatibility (haemolysis and complement activation), inflammatory response; biodegradability and potential cytotoxicity of the degradation products, cellular uptake and intracellular fate, *in vivo* biodistribution studies, all assist in allowing a better definition of the biological properties of the novel polymers and their polymeric NPs [1-3]. The so called "biocompatibility" is largely dependent on the physical and chemical properties of the NPs (size, shape and surface characteristics), as well as on the used raw material [1, 4].

The use of polymeric NPs based on chitosan has been extensively reported in biomedical applications, due to its interesting characteristics. Non-toxicity, biocompatibility, biodegradability, antibacterial activity, mucoadhesiveness and permeation enhancing properties are among the features that have been reported, the cationic character being responsible for some of them [5, 6]. Although often claimed as biocompatible, more comprehensive studies are required for a proper understanding of the biological effects of this polymer and of its nanoformulations.

As reported previously, a polymeric nanoparticle made of GC, here designated GC nanogel, has been synthesized in our lab by chemical grafting hydrophobic chains on the GC backbone, yielding an amphiphilic polymer capable of self-assembling in aqueous environment [7]. The present work focuses on the detailed evaluation of the biocompatibility of this nanogel. For this purpose, *In vitro* cell toxicity of the GC nanogel was evaluated using the 3-(4,5-dimethylthiazol-2-yl)-2,5-diphenyltetrazolium bromide (MTT) and lactate dehydrogenase (LDH) release assays to gauge the nanogel cytotoxicity. Induction of apoptosis and/or cell cycle arresting was tested through flow cytometry. The complement activation was semi-quantified by western blot, analysing the degradation of the C3 factor. Interaction with murine macrophages was observed through confocal microscopy. Finally, the nanogel haemocompatibility was evaluated through haemolysis and whole blood clotting time assays.

3.2. Experimental

3.2.1. Materials

GC (G7753), mercapto hexadecanoic acid (MHDA), N-hydroxysulfosuccinimide (NHS) and 1-Ethyl-3-[3-dimethylaminopropyl]carbodiimide hydrochloride (EDC), 3-(4,5-dimethylthiazol-2-yl)-2,5-diphenyl tetrazolium bromide (MTT), NADH, pyruvate, haemoglobin from bovine blood and Drabkin's reagent were acquired from Sigma-Aldrich. 5/6-Carboxyfluorescein succinimidyl ester was purchased from Thermo Scientific. Cell Culture reagents and culture medium were purchased from Biochrom.

3.2.2. Nanogel self-assembling

GC nanogel was synthesized and characterized as previously reported [7]. Briefly, GC nanogel was prepared by conjugation of the mercapto hexadecanoic acid (MHDA) to GC, through a carbodiimide reaction. Nanogel dispersions used in the different experiments were obtained after dispersing the lyophilized reaction product in distilled water, under magnetic stirring at 50ºC for 48h, and passed through a cellulose acetate syringe filter (pore size 0.45 µm).

3.2.3. Cell cultures

3T3 fibroblasts and mouse leukaemic monocyte macrophage (RAW 264.7) cell lines were maintained in DMEM supplemented with 10% bovine calf serum or fetal bovine serum (FBS), respectively, 100 IU/mL penicillin and 0.1mg/mL streptomycin. Human microvascular endothelial cells (HMEC) were grown in RPMI-1640 supplemented with 10% FBS, Epidermal Growth Factor (EGF, 10 ng/mL), Hydrocortisone (1 µg/mL), 100 IU/mL penicillin and 0.1 mg/mL streptomycin. All cell lines were cultured as a monolayer in a humidified atmosphere containing 5% CO_2 at 37 ºC.

Murine Bone Marrow-Derived Macrophages were collected from femoral and tibial mouse bone marrow using a previously published protocol [8, 9]. Briefly, mouse long bones were extracted from the mousse under aseptic conditions and flushed with RPMI-1640. The resulting cell suspension was centrifuged at 500 g during 10 min. The cell pellet was resuspended in RPMI-1640 supplemented with 10mM HEPES, 10% heat-inactivated FBS, 60 µg/mL penicillin/streptavidin, 0.005mM β-mercaptoethanol (RPMI complete medium) and 10% LCCM. To remove adherent bone marrow cells, the cell suspension was incubated overnight at 37 ºC and 5% CO_2 atmosphere in a Petri dish.

The non-adherent cells were collected, centrifuged at 500g (10min) and seeded in 24 well plates at 5 x 10^5 cells per well in RPMI complete medium containing 10% of LCCM and incubated at 37 ºC in a 5% CO_2 atmosphere. Four days after seeding 10% of LCCM was re-added to the cultures. The culture medium was replaced with fresh RPMI complete medium containing 10% LCCM on day 7. After 10 days in culture, cells were completely differentiated into macrophages.

3.2.4. *In vitro* cell toxicity

3.2.4.1. MTT assay

The cytotoxicity of GC nanogel was evaluated by using the quantitative colorimetric MTT assay. Cells were seeded onto 24-well cell culture plates at a density of 1×10^4 cells per well for 3T3 and RAW and of 2×10^4 for HMEC, and left adhering in 0.5mL of culture medium overnight. Afterward, the cells were incubated with nanogel dispersions at 0.1 and 0.5 mg/mL in fresh culture medium containing 25% of distilled water (v/v). Cells cultivated in medium with or without 25% of distilled water (v/v) (without nanogel) were used as controls. After 24, 48 and 72 h the metabolic activity was measured adding MTT (3-(4,5-dimethylthiazol-2-yl)-2,5-diphenyl tetrazolium bromide). The tetrazolium salt is reduced by metabolically active cells using mitochondrial succinate dehydrogenase enzymes [10]. The MTT solution (0.5 mg/mL in PBS) was carefully removed from each well and the resulting dark blue formazan crystals were solubilized in dimethyl sulfoxide and quantified spectrophotometrically at 570 nm. The experiments were performed in triplicate and the metabolic activity results were shown as percentage of the values obtained at 0h time point.

3.2.4.2. LDH release assay

Cytotoxicity can also be assessed by the degree of membrane damage. The LDH release assay measures the membrane integrity as function of the amount of cytoplasmic LDH leaked into the culture medium. The conversion of NADH and pyruvate into NAD^+ and lactate catalysed by LDH is the basis of the method [2]. Cells were seeded in 12-well plate at a density of the $2x10^5$ cells per well for 3T3 and HMEC and $1x10^5$ for RAW and allowed to settle overnight in 0.5 mL of culture medium. The cells were treated with nanogel dispersions with a concentration of 0.1 and 0.5 mg/mL, in fresh culture medium containing 25% of distilled water (v/v). Untreated cells, exposed to 20% DMSO (v/v) or 25% distilled water (v/v) in culture media were used as controls.

At the 24 and 48h time points the culture medium from each well was collected and centrifuged at 13000 rpm for 1min and the cell free supernatant was collected and stored on ice for further extracellular LDH measurement. The respective cells were scraped with the aid of a Tris solution 15 mM and lysed through sonication. Supernatants of centrifuged samples were used to quantify the intracellular LDH. Samples of extracellular (40 µL) or intracellular (10 µL) LDH were plated into a new microplate and 250 µL of the NADH solution 0.31 mM in phosphate buffer 0.05 M, pH7.4 added to each well. Finally, 10 µL of a 8.96 mM piruvate solution in phosphate buffer (substrate solution) was added and immediately afterwards the variation of the absorbance at 340 nm was read in a microplate spectrophotometer, as to determine the rate of NADH consumption (slope of the line). LDH leakage was expressed as the ratio between extracellular and total LDH, corresponding the inverse value to the cell membrane integrity. Untreated cells were used as a reference for the estimation of the maximum membrane integrity. Each experiment was performed in triplicate.

3.2.5. Apoptosis assay

The FITC Annexin V Apoptosis Detection Kit was used to determine apoptotic cell membrane changes in 3T3, HMEC and RAW cell lines. Cells ($2x10^5$/well) were seeded in a 12-well plate and left adhering overnight. The cells were then incubated with nanogel dispersions at 0.1 and 0.5 mg/mL in fresh culture medium containing 25% of distilled water (v/v). A negative control assay was carried out without nanogel (the dilution with 25% of distilled water had no effect on the assay outcome), while H_2O_2 was used as positive control for apoptosis using different incubation times and concentrations according to the cell line (0.5 mM for 6 h – RAW; 0.2 mM for 24 h – HMEC and 5 mM for 3 h - 3T3) [11, 12]. After 24 h the cells were treated with 250 uL trypsin/EDTA 0.25%/0.02% in PBS for 2 min at 37 ºC. The cell suspension was transferred to flow cytometry sample tubes (Beckman Coulter) and washed twice with cold PBS. Double staining with FITC-Annexin V/PI was performed as recommended by the supplier (BD Pharmigen) with minor modifications. In detail, each sample was incubated with 40 µL of the work solution (1.8 µL of the Annexin V and PI diluted in 36.4 µL of the annexin V binding buffer) for 15min at room temperature, in the dark. Finally, 200 µL of annexin V binding buffer was added to the samples that were then analysed by flow cytometry using a Coulter Epics XL Flow Cytometer (Beckman Coulter Inc., Miami, FL, USA)

3.2.6. Cell cycle analysis

To evaluate the effect of GC nanogel on cell cycle, 3T3 and RAW cells were seeded at a density of 5×10^4 cells per well, while HMEC cells were cultured at $1x10^5$, in 6-well plates, in 2 mL of the respective culture medium. In the following day, medium was replaced by GC nanogel dispersions with concentrations of 0.1 and 0.5 mg/mL, in 2 mL of fresh culture medium containing 25% of distilled water (v/v). An additional condition without nanogel was carried out as a negative control (the dilution with 25% of distilled water had no effect on the assay). After 24 h, cells were harvested and processed for flow cytometry analysis. In summary, the collected cells and the respective culture medium were centrifuged and washed with PBS. The cell suspension was kept on ice for 15 min. Ice cold absolute ethanol was used to fix the cells during 15min on ice. After washing with PBS to remove residual ethanol, the cells were treated with RNase A (20 µg/mL) during 15 min at 37 ºC. PI staining solution was added at least 15 min before sample analysis on the flow cytometer. Cell cycle progression of at least 20,000 single cells per sample was analyzed by flow cytometry using a Coulter Epics XL Flow Cytometer (Beckman Coulter Inc., Miami, FL, USA) and analysed by using the FlowJo Analysis Software (Tree Star, Inc., Ashland, OR, USA).

3.2.7. Complement activation

Complement cascade was studied as reported previously [13] and based on the NCL (Nanotechnology Characterization Laboratory) protocol for qualitative determination of total complement activation by Western blot analysis. Briefly, a pool of human plasma from healthy donors was incubated with 1mg/mL of GC nanogel in the presence of veronal buffer. Equal volumes (50uL) of plasma, buffer and sample were mixed and incubated at 37 °C for 60 minutes. Cobra venom factor from Quidel Corporation (San Diego, CA, USA), and PBS were used as positive and negative controls, respectively. Proteins were resolved by 10% SDS-PAGE, and then transferred to a membrane (Immun-Blot PVDF Membrane, Biorad, Hercules, USA) using the transblot semidry BioRad transfer equipment (Trans blot SD, BioRad, Hercules, USA). The membranes were incubated for 90 min with a mouse monoclonal antibody against human C3 diluted 1:1000 (Abcam, Cambridge, UK), washed and incubation with secondary polyclonal goat anti-mouse IgG antibodies conjugated with alkaline phosphatase diluted 1:2000 (Dako, Glostrup, Denmark). The membrane was finally revealed with 5-Bromo-

4-Chloro-3-Indolyl Phosphate (BCIP) (Sigma). For further analysis, membranes were scanned with ChemiDoc™XRS+ System (Bio-Rad; Hercules, CA). The percentage of the lower band was then quantified with Image Lab™ Software 3.0.

3.2.8. Confocal laser scanning microscopy

GC nanogels were labelled with NHS-Fluorescein, through an amide linkage, in order to study their cellular uptake by murine macrophages. In detail, the NHS-Fluorescein was dissolved in DMSO, at a concentration of 1%. The molar ratio of NHS-Fluorescein carboxylic groups to the GC nanogel free amine groups was 0.25. The dye was added to a stirred nanogel suspension at a concentration of 1 mg/mL in PBS. The reaction was allowed to occur overnight at room temperature, in the dark. The reaction mixture was thoroughly dialysed (M w cutoff 10-12 kDa) against distilled water to remove free NHS-fluorescein. As to verify the absence of free dye, the final solution of NHS-fliorescein labelled nanogel was purified by centrifugation through a 10kDa MW cutoff filter.

Murine macrophages were seeded at a density of 5 x 10^5 cells per well in a 24 well plate (with a coverslip in each well), and left adhering overnight. The cells were incubated with 0.2 mg/mL of each NHS-Fluorescein labelled nanogel suspension in culture medium containing 25% of water v/v. After 6 h, the coverslips were washed twice with PBS at room temperature and the cells were fixed with paraformaldehyde 2% for 25min. After washing the cells twice with PBS twice, 4',6-diamidino-2-phenylindole (DAPI, 120ng/mL) was used to stain the nucleus for 3 min at room temperature. After washing the preparations were observed in a confocal laser scanning microscope Leica SP2 AOBS SE (Leica Mycrosystems, Germany).

3.2.9. Haemocompatibility studies

The whole blood was collected from three independent healthy donors using citrated blood collection tubes.

3.2.9.1. Haemolysis Index

The haemolysis assay was performed in agreement to the procedure described by the *American Society for Testing Materials (ASTM F756-00, 2000)*, with slight modifications. Briefly, 0.5 mL of diluted blood at 10 mg/mL was added to 3.5 mL of

the nanogel solution in PBS at 0.5 mg/mL and 0.1 mg/mL and incubated at 37 ºC for 3 h. The tubes were gently inverted at each 30 min to homogenize the mixture. Ultrapure water and phosphate-buffered saline (PBS) were used as positive and negative control, respectively. Then, the suspension was centrifuged at 750 g for 15 min. 0.5 mL of the resulted supernatant was joined to a 0.5 mL Drabkin's reagent and left 15 min at room temperature. Finally, the absorbance was read at 540 nm. The haemoglobin concentration of the freshly derived human blood was calculated using a calibration curve previously prepared with haemoglobin from bovine blood.

3.2.9.2. Whole blood clotting time

Whole blood kinetic clotting times of nanogel samples was performed as described by A.F. Leitão *et al.* (2013) [14]. Previously, the clotting was induced by addiction of 10% 0.1 M $CaCl_2$ to whole blood. The nanogel samples at 0.1 and 0.5 mg/mL, glass microspheres (positive control) and 25% v/v of PBS (negative control) in a 24-well polystyrene microtitter plate were incubated for 0, 5, 10, 20 and 30 min at room temperature with 150 µL of activated whole blood. At the end of each time point, 3 mL of distilled water was added to the well and incubated for 5 min, in order to lyse the red blood cells (RBCs) (and consequent haemoglobin release) that were not entrapped in the thrombus. 200 µL of the supernatant was transferred to a 96-well polystyrene microtitter plate to measure the concentration of the released heamoglobin by spectrophotometric analysis at 540 nm. All the samples were studied in triplicate.

3.2.10. Statistical analysis

The results were expressed as mean ± SD of 3 independent experiments (n=3). Statistical significances were performed applying t-test or two-way ANOVA tests through Prism software (GraphPad software version 5.00, USA). Significance of the results is indicated according to P values with one, two and three of the used symbols (*, +, #) corresponding to $P<0.05$, $P<0.005$ and $P<0.0001$, respectively).

3.3. Results

3.3.1. Cytotoxicity studies

3.3.1.1. Metabolic activity

The cytotoxicity of the GC nanogel was assessed by MTT assay using a set of cell lines; slightly different results were obtained with each one (Figure 1). The control with culture medium diluted with 25% of water presents a lower cell growth as compared to the straight medium, an effect probably due to the dilution of the nutrients. It must be remarked that in none of the tested nanogel concentrations the mitochondrial activity was lower than the one observed at time zero, indicating that the GC nanogel did not induce cell death.

On the other hand, all tested cell lines showed a lower metabolic activity in the presence of the nanogel when compared with the diluted medium control. A nanogel dose dependent effect on decreasing of cell proliferation rate was exhibited by HMEC (at 48 and 72 h incubation time), while no such correlation was observed for 3T3 an RAW cells. The HMEC and RAW cell lines were clearly more susceptible to nanogel treatment, mainly for later incubation times.

3.3.2. Cell membrane integrity

The potential cytotoxicity of the GC nanogel was also evaluated by measuring the cell membrane integrity through LDH leakage quantification. As shown in Figure 2, the GC nanogel in concentrations of 0.1 and 0.5 mg/mL did not affect the cell membrane integrity, since a significant LDH release to the culture medium was observed only in the positive control (20% of DMSO).

3.3.3. Apoptosis assay

Annexin V FITC/propidium iodide dual staining was used to investigate the influence of GC nanogel on cell death induction. This assay is based on the observation, in early stages of apoptosis, of the phosphatidylserine translocation to the external surface of the plasma membrane. Annexin V was used as a sensitive probe since it is a calcium-dependent phospholipid binding protein, with high affinity to phosphotidylserine. Cells in later stages of apoptosis (Annexin V^+ / PI^+) or necrosis (Annexin V^- / PI^+) were identified through detection of PI binding to nuclear DNA allowed by loss of cell membrane integrity [15, 16]. Viable and early apoptotic cells were

recognized through Annexin V^- / PI^- and Annexin V^+ / PI^- staining pattern, respectively. As shown in figure 3, the percentage of apoptotic and late-apoptotic cells incubated with the nanogel was not significantly different from the negative control, exception made for the HMEC cell line, which displays a slight increase in the Annexin positive cells. A dose dependent effect on apoptosis induction was indeed observed in this case.

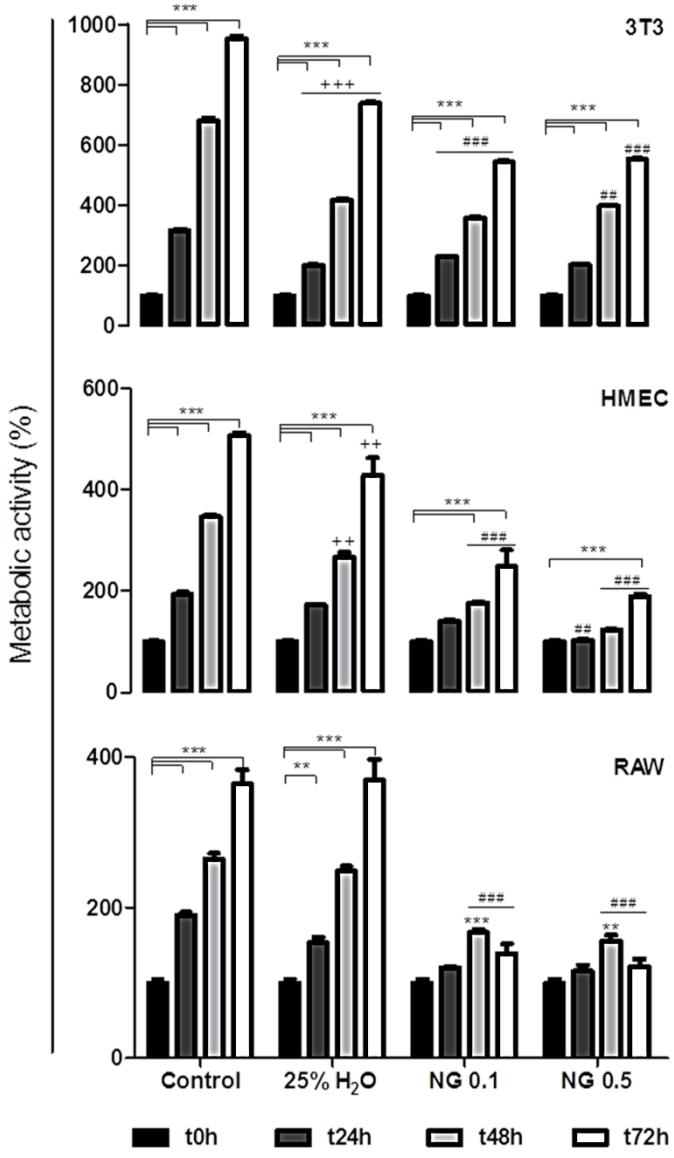

Figure 1. Effect of GC nanogel at 0.1 and 0.5 mg/mL after at 24, 48 and 72 h of incubation with 3T3 fibroblasts, HMEC and RAW cell lines, assessed by MTT assay and expressed taking as reference the initial value. Statistical differences are determined through a 2-way ANOVA and represented by (+) for the differences between cell culture medium (Control) and 25% of water content (v/v) into the well; whereas the differences between 25% H_2O and both concentrations of nanogel (NG 0.1 and NG 0.5) are shown as (#); finally, concerning cell growth over the time, comparing 0h incubation time with remaining incubation times for each condition, the statistical differences are presented as (*).

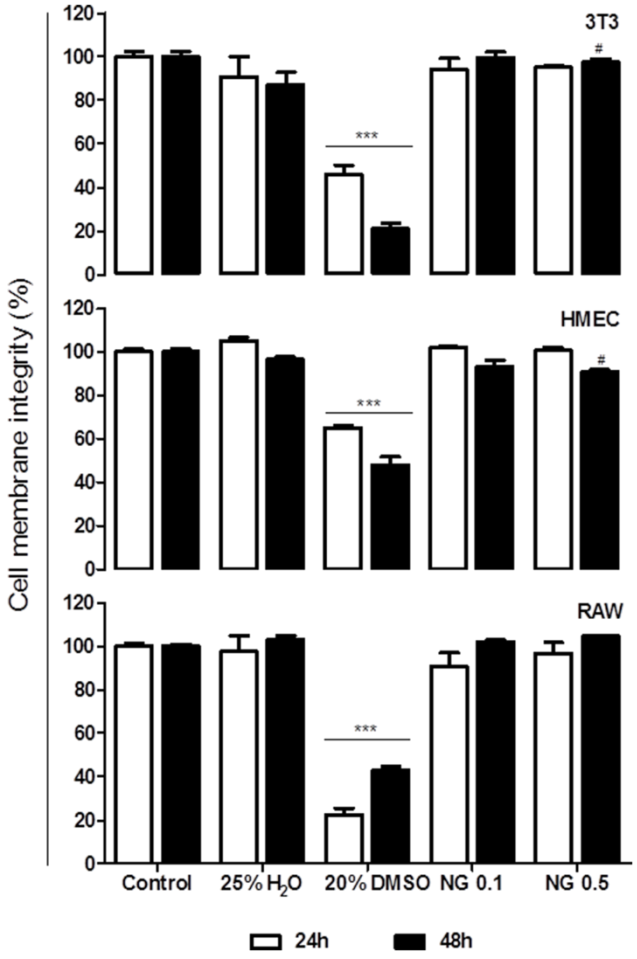

Figure 2. Effect of GC nanogel at 0.1 and 0.5 mg/mL after 24 and 48 h of incubation with 3T3 fibroblasts, HMEC and RAW cells on the amount of LDH released to culture *medium*. Cell culture medium and 20% of DMSO were used as negative and positive control, respectively. Statistical differences were found by a t-test in each time of incubation between negative control and 25%H_2O or 20% DMSO are shown as (*); while differences between 25% H_2O and nanogel samples (NG 0.1 and NG 0.5) are represented as (#).

3.3.4. Effect of the nanogel on cell cycle arrest

Cell cycle analysis was performed to ascertain whether cell growth inhibition observed in the MTT assay was correlated with cell cycle arrest, since no effect on cell death by apoptosis/necrosis was verified. The distribution of cell cycle phases of 3T3, HMEC and RAW cells treated with nanogel at 0.1 and 0.5 mg/mL for 24 h is shown on figure 4A. As could be observed no effect on HMEC and 3T3 cell cycle progression was verified, except for the 3T3 population incubated with the higher nanogel concentration, where a slight decrease of the G2 phase was observed. However, in RAW cells, a highly significant dose dependent cell cycle arresting was verified on G1

phase. This increase of G1 population is correlated with a reduction of the S and G2 phases, as may be observed on the cell cycle distribution presented on Figure 4B.

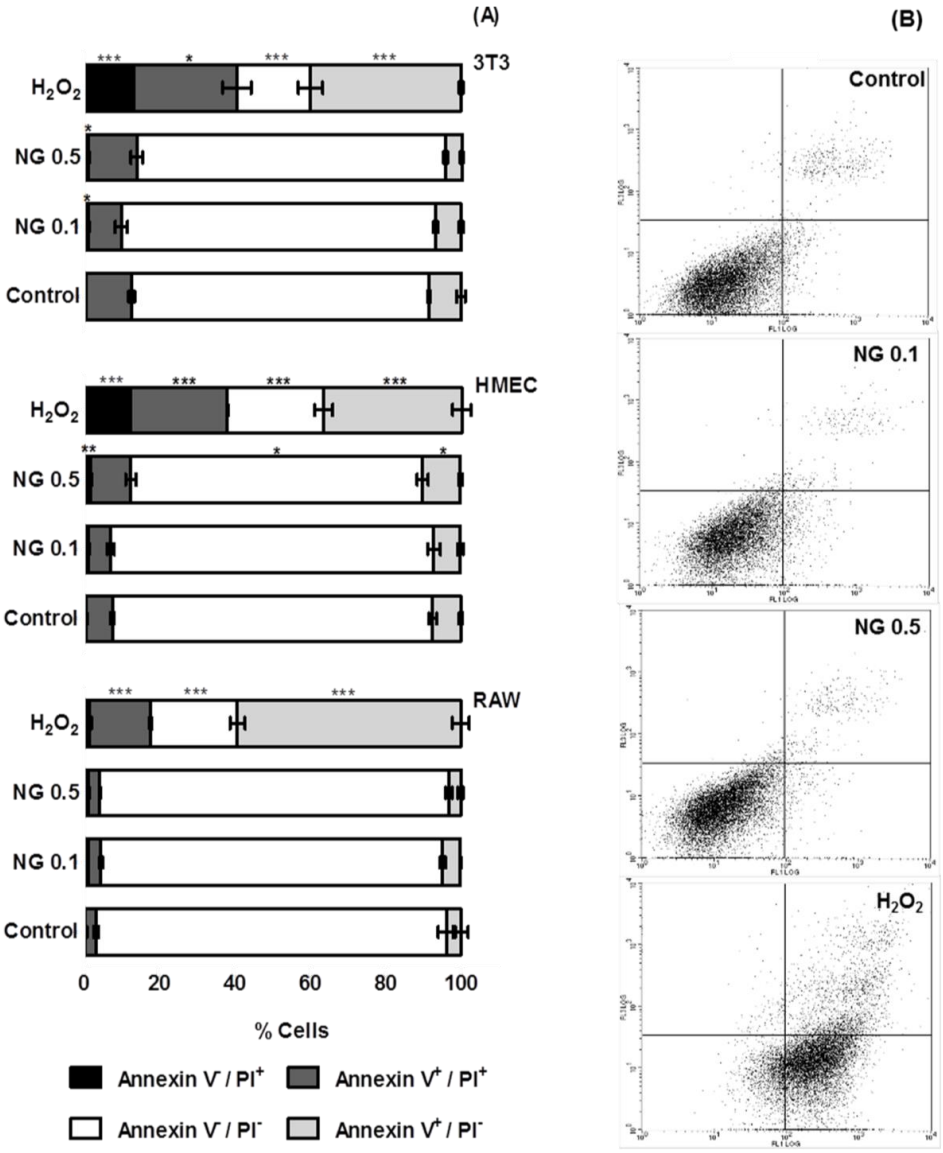

Figure 3. Flow cytometry analysis of Annexin V-FITC/PI double staining of (A) 3T3, HMEC and RAW cell lines, after incubation for 24 h with the nanogel or with H_2O_2 as positive control, at different concentrations and periods of incubation for each cell line (0.5 mM for 6 h - RAW; 0.3 mM for 24 h – HMEC and 5 mM for 3 h - 3T3). The statistical differences between negative control (25% of water content in cell culture medium) and remaining samples were obtained by a t-test and represented as (*). (B) Dot plots correspond to the analysis of RAW cells and are shown as an illustrative example. Top left quadrant, dead cells (Annexin V^- / PI $^+$); top right quadrant cells in a late stage of apoptosis (Annexin V^+ / PI $^+$); bottom right quadrant, apoptotic cells (Annexin V^+ / PI $^-$) and bottom left quadrant, viable cells (Annexin V^- / PI $^-$).

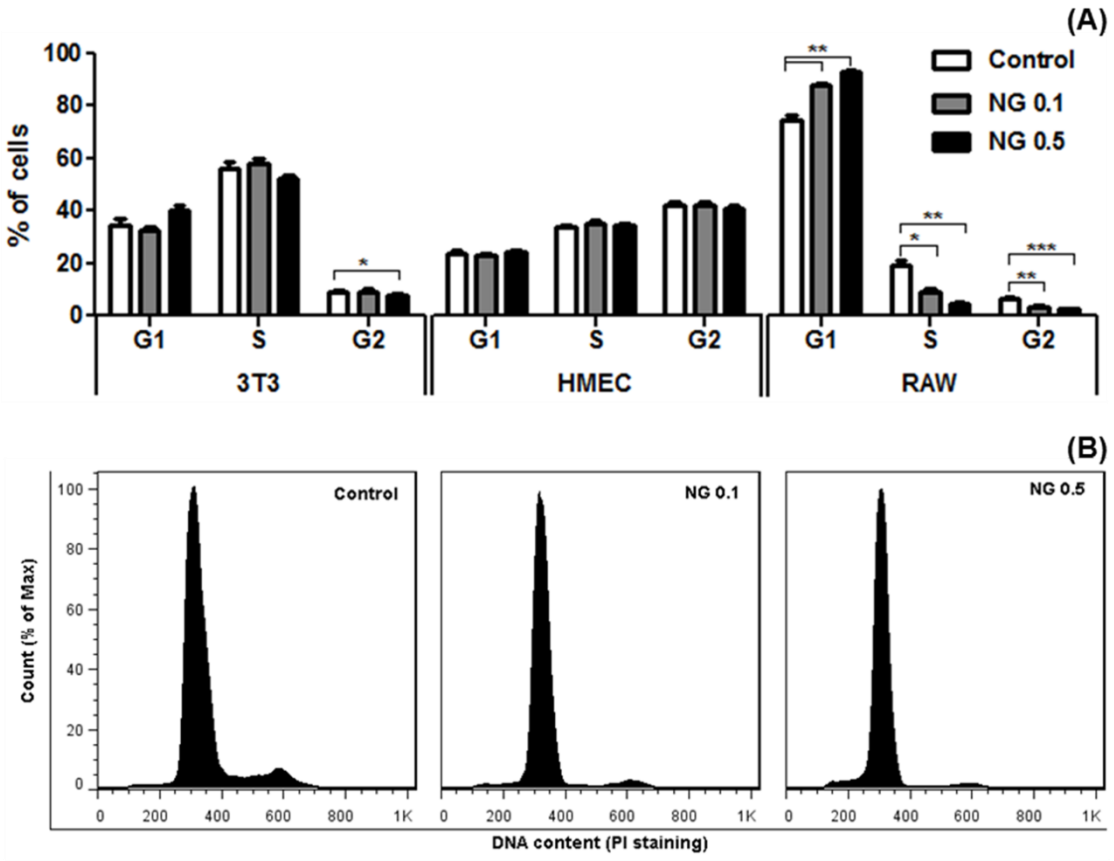

Figure 4. Cell cycle analysis data (A) of the 3T3, HMEC and RAW cells after 24 h of nanogel treatment at 0.1 and 0.5 mg/mL (NG0.1 and NG0.5, respectively); (B) Effect of the nanogel on RAW cells cycle progression as representative example. Statistical differences between negative control group (25% of water content in cell culture medium) and both nanogel concentrations were found by a t-test and represented as (*).

3.3.5. Evaluation of complement activation

In this assay the cleavage product of the C3 component was used as a marker for complement activation by any pathway. Therefore, by studying the degradation of the C3 factor we can determine whether the nanogels have a potential effect on the complement activation cascade. The western blot assay for the C3 fragment detection was performed after incubation of the GC nanogel (1 mg/mL) with human plasma. The results are shown in Figure 5A. The upper band of 115 kDa corresponds to the intact C3 factor and the one with 43 kDa to the main degradation product. The protein degradation was quantified considering the intensity of the band at 43 kDa normalized to the value obtained with the positive control (cobra venom factor). As could be observed in Figure 5B the percentage of C3 cleavage product(s) was similar to those found in the negative control, so it may be concluded that the GC nanogel does not activate the complement system.

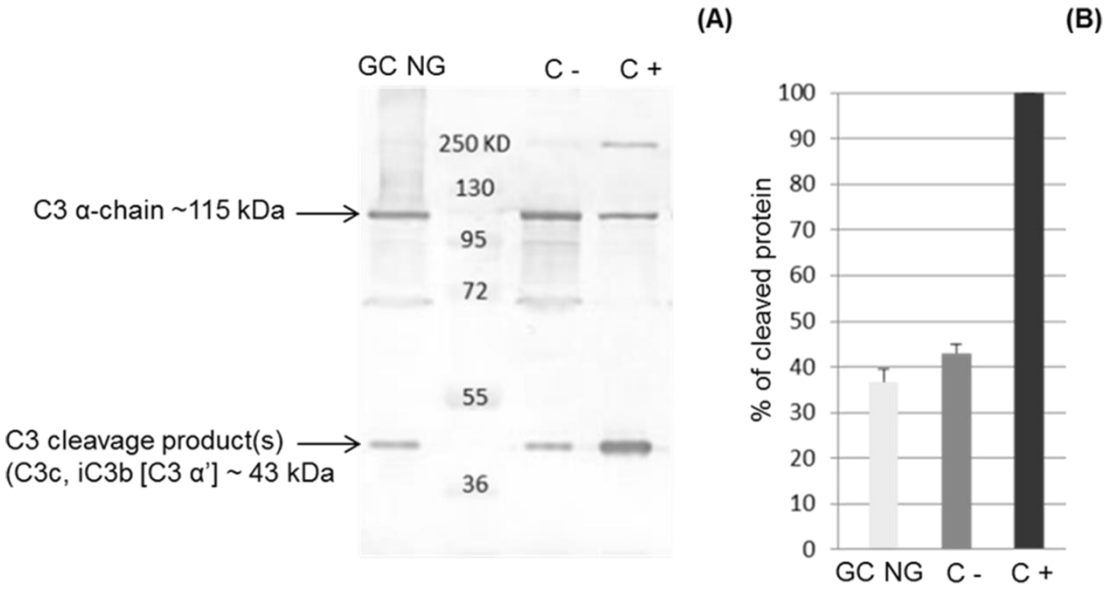

Figure 5. Evaluation of GC nanogel (GC NG) complement activation through C3 protein cleavage. (A) Western blot membrane incubated with a mouse monoclonal antibody against human C3 and a secondary polyclonal goat anti-mouse IgG antibodies conjugated with alkaline phosphatase. (B) Graphical representation of the % of cleavage of C3 protein induced by GC nanogel (GC NG) as compared to negative (C-) and positive (C+) controls (PBS and Cobra venom factor, respectively).

3.3.6. Murine macrophages cellular uptake

In order to investigate whether the nanogels are phagocytosed by macrophages, fluorescent nanogels were incubated with murine macrophages. Figure 6A and B illustrate the cellular uptake of FITC labelled dextrin nanogel (used as a positive control of macrophages uptake, as shown by Gonçalves et al. [17] and NHS-Fluorescein labelled GC nanogels, respectively. Interestingly, the GC nanogel was poorly internalized by murine macrophages as compared with dextrin nanogel.

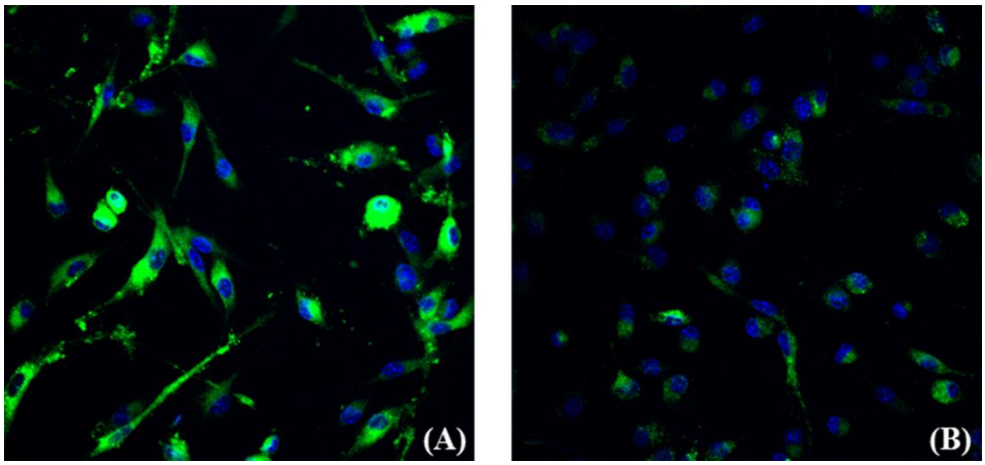

Figure 6. Confocal microscopy images of murine bone marrow derived macrophages treated with fluorescent labelled (A) dextrin and (B) GC nanogels for 6 h.

3.3.7. Haemocompatibility studies

3.3.7.1. Haemolysis index

According to the *Standard Pratice for Assessement of Haemolytic Properties of Materials from the American Society for Testing Materials (ASTM F756-00, 2000)* the nanogel was non-haemolytic at the concentrations tested, since the haemolytic index is inferior to 5% (Table 1), although a slight effect is observed for the higher concentration.

Table 1. Blood haemolysis index after treatment with nanogel samples for 3 h at 37 ºC.

Sample	Haemolysis Index
GC nanogel 0.5 mg/mL	3.183 ± 0.137
GC nanogel 0.1 mg/mL	1.423 ± 0.366
C+ (ultrapure water)	98.773 ± 0.816

3.3.7.2. Whole Blood Clotting time

In this assay, human whole blood was allowed to clot in contact with the GC nanogel to assess the nanomaterial likelihood to be thrombogenic in vivo. As clotting occurs, more RBCs are retained in the clot, and therefore less haemoglobin is released by lysis upon addition of distilled water. The results (figure 7) showed that the nanogel samples exhibited a similar behaviour to the negative control (PBS), thus being classified as non-thrombogenic; conversely, as expected, the glass microspheres showed the quickest clotting time.

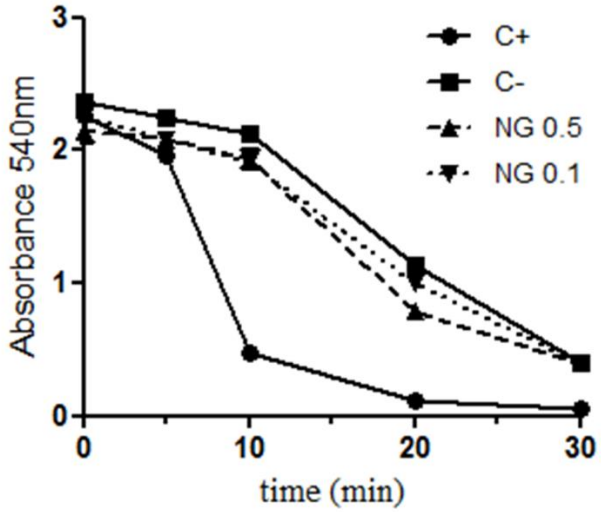

Figure 7. Whole blood clotting time for nanogel samples at 0.1 and 0.5 mg/mL. The positive control (C+) used were glass microspheres and the negative (C-) PBS. No statistical differences were observed between negative control and nanogel samples.

3.4. Discussion

Although GC is recognized as a highly biocompatible chitosan derivative [18], a definitive statement on this matter requires further experimental evidences. Thus, the purpose of the present work was to perform a comprehensive study of the GC based-nanogel biocompatibility. The GC used for nanogel synthesis, purchase from Sigma-Aldrich, were thoroughly characterized in our previous work, due to the lack of consistent data in literature. The amphiphilic polymer resultant from covalent attachment of hydrophobic chains on the hydrophilic GC backbone (100 kDa) self-assembles in water medium originating nanogels with an average size of the 250nm and positive surface charge (+ 30 mV). [7]

The metabolic activity studies show that the GC nanogel does note reduce the mitochondrial activity overtime; however, cell growth inhibition was observed in all cell lines. The HMEC cell proliferation reduction (at 48 and 72 h incubation time) was found to be dose dependent, while no such correlation was observed for 3T3 an RAW cells. Anitha *et al.* [19] reported a similar dose independent effect observed in two cell lines of fibrosblasts (L929, NIH3T3) after 48 h exposure to thiolated chitosan NPs. Absence of cytotoxicity and cell growth inhibition effect in L929 fibroblasts treated with chitosan-g-poly(N-vinylcaprolactam) NPs was reported by Rejinold *et al.* [20] after 24h of incubation. The same was observed in this work for the 3T3 cell line, after short incubation period (24 h). The HMEC and RAW cell lines were clearly more susceptible to nanogel treatment, mainly for later incubation periods. Equivalent RAW cell growth inhibition rate was obtained by Kim *et al.* [21] for NCTC 3749 macrophage cells (20-30%) treated with 0.1 mg/mL of mannosylated NPs for 24 h. It is noteworthy that fairly high concentrations of the nanogel were used in the current study, purposely to detect toxic effects. Applications of the biomaterial are not likely to reach such concentrations in vivo, nor the contact time with cells will be as long as the tested ones; hence the results achieved can be considered indicative of the safety of the material. The absence of the GC nanogel cytotoxicity was also confirmed by measuring the cell membrane integrity through LDH leakage quantification. According to Fotakis and Timbrell [22], the LDH leakage assay is not as sensitive as the MTT assay for cytotoxicity detection, since it requires higher concentration of the sample or longer incubation time. Although being a cell-type dependent method, we did not observe significant differences by increasing the incubation time or varying the sample concentration. The apoptosis assay

corroborate that GC nanogel didn´t induce cell death by necrosis and/or apoptosis, in agreement with LDH release results, since necrosis would result in the loss of cell membrane integrity [16]. Moreover, the cell cycle analysis demonstrated that any effect on HMEC and 3T3 cell cycle progression was verified. However, in RAW cells a highly significant dose dependent cell cycle arresting was found on G1 phase, which may be due to phagocytic activity, and therefore higher concentration of the nanogel inside the cells. Nevertheless, as shown above bone marrow derived macrophages internalize GC nanogel to little extent. Similar studies on the effect of drug loaded GC NPs on the cell cycle arresting have been reported. Surprisingly, these studies usually just show the effect of the drug, and no data regarding to the effect of the nanocarrier alone could be found [23].

Depending on the nanoparticles administration pathways and their physicochemical properties, they could induce different immune reactions that are initiated with adsorption of opsonins to the nanoparticles surface, triggering the complement system. By itself, opsonization is not able to destroy the invaders but it acts as a border guard primimg the surface of nanoparticles for rapid recognition and clearance by complement receptor bearing cells such as blood monocytes and macrophages of the MPS [24, 25]. Regardless the initial events that determine which pathway leads to complement activation, all converge to the cleavage of the central component C3 [26]. So, as human serum in the presence of the GC nanogel revealed similar percentages of C3 cleavage product(s) to those found in the negative control, could be concluded that the GC nanogel does not activate the complement system. Indeed, Bertholon *et al.* [27] refers chitosan as a weaker activator of the complement cascade. They showed that increasing the molecular weight of chitosan led to decreased complement activation, reaching negligible levels. Marchand *et al.* [28] also concluded that chitosan is a non-activating biomaterial; in spite of binding anionic plasma and serum proteins like C3, it does not led to complement activation. As the long systemic circulation half-life of the NPs is dependent on their ability to avoid the capture by macrophages of the MPS, the development of ‘stealth’ NPs is highly desirable [29]. Interestingly, we found that GC nanogel was poorly internalized by bone marrow derived macrophages as compared with dextrin NPs [17]. Sarmento *et al.* [30] also reported that chitosan coated solid lipid NPs were neglectfully internalized within RAW 264.7 cells, as compared with uncoated solid lipid NPs. Indubitably this is a promising result since GC nanogel may thus evade blood clearance and keep on circulation enough time to find the target site.

Charged particles readily interact with negatively charged cell surface; probably, they can do so with negatively charged RBCs [31]. Therefore, we investigated the release of haemoglobin from RBCs. The GC nanogel was found to be non-haemolytic, even though both haemolytic and non-haemolytic effects have been previously assigned to chitosan based NPs [32, 33]. The GC nanogel was found to be non-haemolytic, and may also be considered non-thrombogenic, in agreement with He *et al*. [34], who have found that the positive charge of chitosan retarded thrombin generation and blood coagulation.

3.5. Conclusion

The biocompatibility of GC nanogels was comprehensively characterized. Although slightly reducing the growth rate of RAW and HMEC cell lines such an effect could not be explained by cell membrane compromising nor apoptosis/necrosis induction. A more severe effect observed in the case of RAW cells could be at least partially explained by the observed effect of cell cycle arrest; however for the HMEC this was not the case, an issue that remains to be clarified. It must be remarked that fairly high concentrations of the nanogel were used in these assays. Under physiological conditions associated to a possible application of this material, lower concentrations and contact times should arise, such that we may classify the GC nanogel as safe. In conclusion, the present study demonstrate that the GC nanogel is able to be systemically administered, since it didn´t activate the complement system, evade the MPS, didn´t interact with RBCs and was found to be non-thrombogenic. These findings indicate that GC nanogel is a promising biocompatible vehicle for drug delivery.

Acknowledgments

Paula Pereira thanks FCT, the Ph.D. grant ref SFRH/BD/64977/2009. This work was also supported by a grant from the Spanish Ministry of Economy and Competitivity (SAF2011-30337-C02-02). We also acknowledge the European Union Seventh Framework Programme [FP7/REGPOT-2012-2013.1] under grant agreement BIOCAPS-316265. MP acknowledges fellowship from Spanish Ministry of Education (FPU predoctoral grant program).

3.6. References

1. Naahidi, S.; Jafari, M.; Edalat, F.; Raymond, K.; Khademhosseini, A.; Chen, P., Biocompatibility of engineered nanoparticles for drug delivery. Journal of controlled release : official journal of the Controlled Release Society 2013, 166, (2), 182-94.
2. Rodrigues, S.; Dionísio, M.; López, C. R.; Grenha, A., Biocompatibility of Chitosan Carriers with Application in Drug Delivery. Journal of Functional Biomaterials 2012, 3, (3), 615-641.
3. Gaspar, R.; Duncan, R., Polymeric carriers: Preclinical safety and the regulatory implications for design and development of polymer therapeutics. Advanced Drug Delivery Reviews 2009, 61, (13), 1220-1231.
4. Liu, Y.; Kong, M.; Feng, C.; Yang, K. K.; Li, Y.; Su, J.; Cheng, X. J.; Park, H. J.; Chen, X. G., Biocompatibility, cellular uptake and biodistribution of the polymeric amphiphilic nanoparticles as oral drug carriers. Colloids and surfaces. B, Biointerfaces 2013, 103, 345-53.
5. Bernkop-Schnurch, A.; Dunnhaupt, S., Chitosan-based drug delivery systems. Eur J Pharm Biopharm 2012, 81, (3), 463-9.
6. Croisier, F.; Jérôme, C., Chitosan-based biomaterials for tissue engineering. European Polymer Journal 2013, 49, (4), 780-792.
7. Pereira, P.; Morgado, D.; Crepet, A.; David, L.; Gama, F. M., Glycol chitosan-based nanogel as a potential targetable carrier for siRNA. Macromolecular bioscience 2013, 13, (10), 1369-78.
8. Carvalho, V.; Castanheira, P.; Madureira, P.; Ferreira, S. A.; Costa, C.; Teixeira, J. P.; Faro, C.; Vilanova, M.; Gama, M., Self-assembled dextrin nanogel as protein carrier: controlled release and biological activity of IL-10. Biotechnology and bioengineering 2011, 108, (8), 1977-86.
9. Cerca, F.; Andrade, F.; Franca, A.; Andrade, E. B.; Ribeiro, A.; Almeida, A. A.; Cerca, N.; Pier, G.; Azeredo, J.; Vilanova, M., Staphylococcus epidermidis biofilms with higher proportions of dormant bacteria induce a lower activation of murine macrophages. Journal of medical microbiology 2011, 60, (Pt 12), 1717-24.
10. Mosmann, T., Rapid colorimetric assay for cellular growth and survival: Application to proliferation and cytotoxicity assays. Journal of Immunological Methods 1983, 65, (1–2), 55-63.
11. Piao, S.; Cha, Y. N.; Kim, C., Taurine chloramine protects RAW 264.7 macrophages against hydrogen peroxide-induced apoptosis by increasing antioxidants. Journal of clinical biochemistry and nutrition 2011, 49, (1), 50-6.
12. Wang, J.; Shen, W. H.; Jin, Y. J.; Brandt-Rauf, P. W.; Yin, Y., A molecular link between E2F-1 and the MAPK cascade. The Journal of biological chemistry 2007, 282, (25), 18521-31.
13. Lozano, T.; Rey, M.; Rojas, E.; Moya, S.; Fleddermann, J.; Estrela-Lopis, I.; Donath, E.; Wang, B.; Mao, Z.; Gao, C.; González-Fernández, Á., Cytotoxicity

effects of metal oxide nanoparticles in human tumor cell lines. Journal of Physics: Conference Series 2011, 304, (1), 012046.

14. Leitao, A. F.; Gupta, S.; Silva, J. P.; Reviakine, I.; Gama, M., Hemocompatibility study of a bacterial cellulose/polyvinyl alcohol nanocomposite. Colloids and surfaces. B, Biointerfaces 2013, 111C, 493-502.
15. Koopman, G.; Reutelingsperger, C. P.; Kuijten, G. A.; Keehnen, R. M.; Pals, S. T.; van Oers, M. H., Annexin V for flow cytometric detection of phosphatidylserine expression on B cells undergoing apoptosis. Blood 1994, 84, (5), 1415-20.
16. Vermes, I.; Haanen, C.; Steffens-Nakken, H.; Reutelingsperger, C., A novel assay for apoptosis. Flow cytometric detection of phosphatidylserine expression on early apoptotic cells using fluorescein labelled Annexin V. J Immunol Methods 1995, 184, (1), 39-51.
17. Goncalves, C.; Torrado, E.; Martins, T.; Pereira, P.; Pedrosa, J.; Gama, M., Dextrin nanoparticles: studies on the interaction with murine macrophages and blood clearance. Colloids and surfaces. B, Biointerfaces 2010, 75, (2), 483-9.
18. Carreño-Gómez, B.; Duncan, R., Evaluation of the biological properties of soluble chitosan and chitosan microspheres. International Journal of Pharmaceutics 1997, 148, (2), 231-240.
19. Anitha, A.; Deepa, N.; Chennazhi, K. P.; Nair, S. V.; Tamura, H.; Jayakumar, R., Development of mucoadhesive thiolated chitosan nanoparticles for biomedical applications. Carbohydrate Polymers 2011, 83, (1), 66-73.
20. Rejinold, N. S.; Chennazhi, K. P.; Nair, S. V.; Tamura, H.; Jayakumar, R., Biodegradable and thermo-sensitive chitosan-g-poly(N-vinylcaprolactam) nanoparticles as a 5-fluorouracil carrier. Carbohydrate Polymers 2011, 83, (2), 776-786.
21. Kim, T. H.; Jin, H.; Kim, H. W.; Cho, M. H.; Cho, C. S., Mannosylated chitosan nanoparticle-based cytokine gene therapy suppressed cancer growth in BALB/c mice bearing CT-26 carcinoma cells. Mol Cancer Ther 2006, 5, (7), 1723-32.
22. Fotakis, G.; Timbrell, J. A., *In vitro* cytotoxicity assays: comparison of LDH, neutral red, MTT and protein assay in hepatoma cell lines following exposure to cadmium chloride. Toxicology letters 2006, 160, (2), 171-7.
23. Park, J. S.; Han, T. H.; Lee, K. Y.; Han, S. S.; Hwang, J. J.; Moon, D. H.; Kim, S. Y.; Cho, Y. W., N-acetyl histidine-conjugated glycol chitosan self-assembled nanoparticles for intracytoplasmic delivery of drugs: endocytosis, exocytosis and drug release. J Control Release 2006, 115, (1), 37-45.
24. Peter, P. W.; Moghimi, S. M., Complement Sensing of Nanoparticles and Nanomedicines. In Functional Nanoparticles for Bioanalysis, Nanomedicine, and Bioelectronic Devices Volume 2, American Chemical Society: 2012; Vol. 1113, pp 365-382.
25. Denis, L., The Interactions between Blood and Polymeric Nanoparticles Depend on the Nature and Structure of the Hydrogel Covering the Surface. Polymers 2012, 4, (2).
26. Carroll, M. C., The complement system in regulation of adaptive immunity. Nat Immunol 2004, 5, (10), 981-986.

27. Bertholon, I.; Vauthier, C.; Labarre, D., Complement activation by core-shell poly(isobutylcyanoacrylate)-polysaccharide nanoparticles: influences of surface morphology, length, and type of polysaccharide. Pharmaceutical research 2006, 23, (6), 1313-23.

28. Marchand, C.; Bachand, J.; Perinet, J.; Baraghis, E.; Lamarre, M.; Rivard, G. E.; De Crescenzo, G.; Hoemann, C. D., C3, C5, and factor B bind to chitosan without complement activation. Journal of biomedical materials research. Part A 2010, 93, (4), 1429-41.

29. Fang, R. H.; Hu, C. M.; Zhang, L., Nanoparticles disguised as red blood cells to evade the immune system. Expert opinion on biological therapy 2012, 12, (4), 385-9.

30. Sarmento, B.; Mazzaglia, D.; Bonferoni, M. C.; Neto, A. P.; do Céu Monteiro, M.; Seabra, V., Effect of chitosan coating in overcoming the phagocytosis of insulin loaded solid lipid nanoparticles by mononuclear phagocyte system. Carbohydrate Polymers 2011, 84, (3), 919-925.

31. Sarkar, K.; Chatterjee, A.; Chakraborti, G.; Kundu, P. P., Blood compatible N-maleyl chitosan-graft-PAMAM copolymer for enhanced gene transfection. Carbohydrate Polymers 2013, 98, (1), 596-606.

32. Nogueira, D. R.; Tavano, L.; Mitjans, M.; Perez, L.; Infante, M. R.; Vinardell, M. P., *In vitro* antitumor activity of methotrexate via pH-sensitive chitosan nanoparticles. Biomaterials 2013, 34, (11), 2758-72.

33. Layek, B.; Singh, J., Amino acid grafted chitosan for high performance gene delivery: comparison of amino acid hydrophobicity on vector and polyplex characteristics. Biomacromolecules 2013, 14, (2), 485-94.

34. He, Q.; Gong, K.; Ao, Q.; Ma, T.; Yan, Y.; Gong, Y.; Zhang, X., Positive charge of chitosan retards blood coagulation on chitosan films. Journal of biomaterials applications 2013, 27, (8), 1032-45.

4. siRNA inhibition of endocytic pathways to characterize the cellular uptake mechanisms of folate functionalized glycol chitosan nanogels

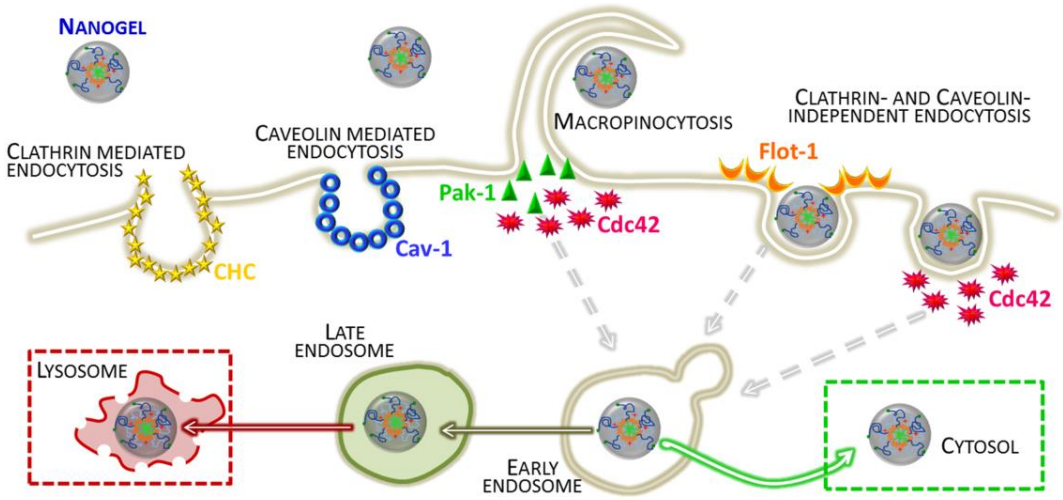

GC nanogels have been widely used in gene, drug and contrast agent delivery in an effort to improve disease diagnosis and treatment. Herein, we evaluate the internalization mechanisms and intracellular fate of previously described GC nanogels decorated with folate to target the folate receptor. Nanogel internalization in HeLa cells was folate dependent and occurred mainly through flotillin-1 and Cdc42-dependent endocytosis. This was determined by inhibition of uptake reduction observed upon siRNA depletion of these two proteins and the pathways that they regulate. The data also suggest the involvement of the actin cytoskeleton in nanogel uptake via macropinocytosis. After 7 h of incubation with HeLa cells, approximately half of the nanogel population was localised in endolysosomal compartments, while the remaining 50% of the material was in undefined regions of the cytoplasm. Glycol chitosan nanogels may thus have potential as drug delivery vectors for targeting different intracellular compartments.

4.1. Introduction

Macromolecular micelles, also designed nanogels, have been synthesized, characterized and studied for numerous biomedical applications including delivery of therapeutic entities. Active targeting strategies have been conceived to enhance the NPs site-specific delivery by, for example, decorating the surface with ligands of plasma membrane receptors that are over-expressed on target cells [1].

A major advantage in the use of NPs as drug delivery systems lies in their amenability to modifications that allow them to cross biological barriers. The cell membrane is naturally impermeable to complexes larger than 1 kDa, however, NPs uptake may occur through a variety of active endocytic mechanisms, which depend on the physicochemical features of the NPs and the nature of the target cells. For the successful development of nanocarriers it is crucial to understand the molecular mechanisms involved in their interactions with the cell membrane, in addition to their entry via endocytic pathways and subsequent intracellular fate [2-4].

Generally, endocytosis can be divided into two broad categories: phagocytosis (uptake of large particles) and pinocytosis (uptake of fluids, solutes and also ligands via plasma membrane receptors). Phagocytosis is characteristic of specialized professional phagocytes, while pinocytosis is present in virtually all cells and has multiple forms depending on the cell origin and function.[5] Several different classifications for pinocytosis have been proposed, and a common approach is to order according to the key proteins involved: clathrin-mediated endocytosis (CME), caveolae-mediated endocytosis (CvME), clathrin- and caveolae-independent endocytosis and macropinocytosis. Clathrin- and caveolae-independent pathways can be further sub-classified as Arf6-dependent, flotillin-1-dependent, Cdc42-dependent and RhoA-dependent endocytosis [5-9].

The uptake mechanism of a drug delivery system is likely to influence its intracellular fate and capacity to mediate a biological response. The aim of the present study was to identify the endocytic mechanisms responsible for the internalization of glycol chitosan nanogels functionalized with folate in HeLa (cervical adenocarcinoma) cells that overexpress folate receptors [10]. Conventionally, chemical endocytosis inhibitors have been used to analyse cellular uptake of drug delivery vectors including chitosan NPs, but these inhibitors are associated with problems related to low specificity and toxicity [11-13]. Selective inhibition of different endocytic pathways can also be

attempted by siRNA-targeting and subsequent depletion of key proteins that orchestrate individual pathways [14, 15].

In this work, single siRNA sequences were used to attenuate pathways regulated by clathrin heavy chain (si-CHC), caveolin-1 (si-Cav-1), p21-activated kinase 1 (si-Pak-1), Flotillin-1 (si-Flot-1)[14] and Cdc42 (si-Cdc42). These cells were then used to determine the mechanism of uptake and intracellular fate of the nanogels to provide valuable information regarding their capacity to deliver different types of cargos.

4.2. Experimental

4.2.1. Reagents

GC (G7753), mercapto hexadecanoic acid (MHDA), N-hydroxysulfosuccinimide (NHS), 1-Ethyl-3-[3-dimethylaminopropyl]carbodiimide hydrochloride (EDC), O-methyl-O'-succinylpolyethyene glycol 2000 (PEG2000), O-(2-Aminoethyl)-O'-(2-carboxyethyl)polyethylene glycol 3000 hydrochloride (PEG3000), folate, 3-(4,5-dimethylthiazol-2-yl)-2,5-diphenyl tetrazolium bromide (MTT) and sulforhodamine B (SRB) were purchased from Sigma (St. Louis, MO, US). Folate-free RPMI 1640 medium, Opti-MEM, oligofectamine, Alexa Fluor® 647 Dextran 10.000 Mw (Alexa647-Dextran), Alexa Fluor® 647 transferrin (Alexa647-transferrin), Alexa Fluor® 488 carboxylic acid (succinimidyl ester) were bought from Invitrogen (Carlsbad, CA, USA). Complete mini protease inhibitor cocktail tablets were from Roche Diagnostics (Mannheim, Germany). Single siRNA sequences of 21-23 residues were acquired from Europhins MWG Operon (Ebesburg, Germany) as previously described. [14]

4.2.2. Antibodies

Antibodies recognizing Clathrin Heavy Chain was from NeoMarker (California, US); Anti-Cav-1 was from Cell signalling Technology (Hertfordishire, UK); Anti-Pak-1 was from Cell Signaling (Danvers, Massachusetts, US) and antibody to Flot-1 was from BD Bioscience (Oxford, UK); Anti-γ-tubulin was from Sigma (Dorset, UK). Secondary goat anti-mouse- and goat anti-rabbit- horseradish peroxidase were from Pierce (Loughborough, UK).

4.2.3. Cell culture

HeLa cancer cells were cultured in DMEM supplemented with 10 % foetal bovine serum (FBS), 100 IU/mL penicillin and 0.1 mg/mL streptomycin. The cells were maintained as a subconfluent monolayer in a humidified atmosphere containing 5 % CO_2 at 37 ºC.

4.2.4. Self-assembly of nanogels

Details of Glycol Chitosan nanogel synthesis and characterisation as folic acid functionalized nanogels were described in a previous report.[16] Briefly: nanogel synthesis was performed in two independent steps. Initially, folate is conjugated to PEG3000 (FA-PEG3000). In the second reaction, FA-PEG3000, PEG2000 and MHDA were grafted onto the GC polymer. The nanogel dispersions used in the different experiments were obtained after dispersing the lyophilized reaction product in distilled water, under magnetic stirring at 50 ºC for 48 h, and passing through a pore size 0.45 µm cellulose acetate syringe filter.

4.2.5. Preparation of the Alexa Fluor® 488 labelled nanogel

The nanogels were labelled with Alexa Fluor® 488 carboxylic acid (succinimidyl ester) through an amide linkage. The Alexa488 was dissolved in DMSO. The molar ratio of Alexa488 carboxylic groups to the nanogel free amine groups was 0.11. The dye was added to nanogel dispersions at 1 mg/mL in PBS and incubated in the dark at room temperature for 24 h. Thereafter, the reaction mixture was extensively dialysed (Mw cutoff 10-12 kDa) against distilled water to remove free Alexa488. To verify the absence of free dye, the conjugated Alexa488-nanogel was purified by centrifugation at 3,000 x g through a 10 kDa Mw cut-off filter.

4.2.6. Cellular uptake of nanogels by flow cytometry

HeLa cells were seeded onto 24-well plates at $2.0x10^5$ cells per well and left to adhere overnight. The cells were treated with nanogels at 0.2 and 0.4 mg/mL for 0, 0.5, 1, 2, 3, 5, 7 and 24 h. After each time point the mixture, the culture medium and nanogels suspensions were removed and the cells were washed with PBS and collected using 150 µL of trypsin/EDTA (0.25%/0.02%) in PBS 2 min at 37 ºC; after addition of FBS supplemented medium the cell suspension was centrifuged at 300 x g for 10 min

and rinsed with PBS. The cell associated fluorescence was measured by flow cytometry using a Coulter Epics XL Flow Cytometer (Beckman Coulter Inc., Miami, FL, USA).

4.2.7. siRNA transfection

The transfections were performed as described by Soraj *et al*. [14] Briefly: cells were seeded in antibiotic-free medium at a density of $1.6x10^5$ cells in a 35 mm glass bottomed imaging dish (MatTek, Ashland, USA) and per well in a 6-well plate. For 12-well plates the density was reduced to $6.7x10^4$ cells per well. The cells were cultured overnight to obtain the desirable confluency at the beginning of the transfection (~60%). The siRNA transfection procedure was adjusted according to well diameter. Volumes used for a 12-well plate were: 0.5 µL of 50 µM of stock siRNA diluted in 89.5 µL of Opti-MEM and 2.0 µL of oligofectamine in 8.0 µL of Opti-MEM. The diluted solutions were then gently mixed and stored at room temperature for 30 min. For each well, the media was removed and replaced with 400 µL of Opti-MEM. The complex siRNA-oligofectamine was added dropwise to the wells and incubated at 37 ºC and 5 % CO_2 for 4 h. Thereafter 250 µL of Opti-MEM containing 30 % (v/v) of FBS was added to the transfection mixture and the cells were incubated under tissue culture conditions for 48 h.

4.2.8. *In vitro* viability of the transfected cells

4.2.8.1. MTT assay

The effect of siRNA transfection on cell metabolic activity was evaluated using the quantitative colorimetric MTT assay. The cells were seeded onto 24-well cell culture plates at a density of $3.4x10^4$ cells per well and transfected with the different siRNAs as described above. After the transfection period (48 h) cell metabolic activity was measured by adding MTT (3-(4,5-dimethylthiazol-2-yl)-2,5-diphenyl tetrazolium bromide).[17] The MTT solution (0.5 mg/mL in PBS) was carefully removed from each well and the resulting dark blue formazan crystals were solubilized in dimethyl sulfoxide and quantified spectrophotometrically at 570 nm. A reference absorbance at 690 nm was measured for the purposes of background subtraction.

4.2.8.2. Sulforhodamine B assay

Cell proliferation of the siRNA transfected cells was assessed using the Sulforhodamine B (SRB) assay, which provides an estimate of total protein which in turn is related to cell number. [18, 19] After transfecting cells with siRNAs for 48 h, 24-well plates were rinsed with PBS and left to dry at 37 ºC, 5 % CO_2. Ice cold 1% acetic acid: 100% methanol solution was then used to fix the cells at -20 ºC for 30 min. After discarding the fixative solution the plates were left dry at 37 ºC before adding 250 µL of 0.5 % of SRB in 1 % acetic acid to each well. Ninety minutes later the cells were 4x washed with 1 % of acetic acid to remove the excess Sulforhodamine B and then left dry. 1.0 mL of 10 mM Tris solution was used to dissolve the Sulforhodamine. The supernatant was used for quantification of SRB protein staining that was quantified by a spectrophotometer at 540 nm.

4.2.9. Nanogel internalization in endocytosis compromised cells

4.2.9.1. Fluorescence microscopy

4.2.9.1.1. Live cell imaging via confocal microscopy

siRNA-transfected cells, 48 h post transfection (Section 2.7) in glass-bottomed 35 mm culture dishes were incubated with nanogels at 0.2 mg/mL for 7 h. The cells were then rinsed extensively with PBS and immediately imaged as live cells in phenol red free-DMEM by confocal microscopy at 37 ºC on a Leica SP5 system, as previously described.[14] Control and CHC depleted cells, were also incubated for 16 min with the CME probe Alexa647-transferrin (50 nM) to evaluate the efficiency of transfection.

4.2.9.1.2. Immnunolabelling

Cav-1 depletion was confirmed by immunolabelling and confocal microscopy. At the end of the transfection the cells on glass coverslips were rinsed with PBS and fixed with 3 % PFA for 15 min at room temperature. Then the samples were treated with 50 mM of PBS/NH_4 for 10 min to quench reactive species resulting from fixation. After 3x PBS washing the cells were permeabilized with PBS/0.2 % Triton X-100, washed and immersed in blocking buffer, 2 % (v/v) foetal calf serum and 2 % (w/v) BSA in PBS, for 30 min. Cells were then incubated with the primary antibody recognizing Cav-1 and subsequently with secondary Alexa546 labelled antibody. The cells were finally incubated in Hoechst 33342 for 10 min at room temperature to label the nucleus. Finally, the coverslips were mounted on glass sides and the cells were visualized by

confocal microscopy. Cells were imaged through the z-axis to generate z-projection images.

4.2.9.2. Flow cytometry

Quantification of cell associated fluorescence in siRNA transfected cells following incubation with nanogel was performed by flow cytometry. For this, siRNA transfected cells in a 12-well plate were incubated with Alexa488-nanogel (0.2 mg/mL) for 7 h under tissue culture conditions. The cells were then thoroughly washed with PBS, trypsinized with trypsin/EDTA 0.25%/0.02% in PBS for 2 min at 37 ºC; after addition of FBS supplemented medium the cell suspension was centrifuged at 300 x g for 10 min. The cell suspension was washed with PBS. Cell-associated fluorescence of the cell suspension was measured using a Coulter Epics XL Flow Cytometer (Beckman Coulter Inc., Miami, FL, USA).

4.2.9.3. SDS-PAGE and Western blotting

Following 48 h of siRNA transfection, the cells from 6 well plates were washed in ice-cold PBS and collected on ice by scraping in 100 µL of lysis buffer (50 mM Tris-HCl, 150 mM NaCl, pH 8.0, 1 % Triton X-100), containing protease inhibitor cocktail. Lysates were then centrifuged at 13,000 x g (4 ºC) for 10 min before adding three parts supernatant to one part 4x Laemmli buffer. The samples were heated at 95 ºC for 5 min and centrifuged at 13,000 x g (4 ºC) for 1 min prior to loading (18 µg of protein per well) onto 10 % acrylamide gels for separation by SDS-PAGE. Following electrophoresis the separated proteins were transferred to PVDF membranes that were rinsed with PBS and blocked in 5 % milk in PBS Tween 20 (0.025%; PBST) for 1 hr. The membranes were then probed with antibodies recognising CHC, Cav-1, Pak-1, Flot-1, γ-tubulin and β-actin diluted in 2 % milk in PBST. Following washing in PBST, species specific secondary antibodies conjugated to horseradish peroxidase and diluted in 2 % milk in PBST were applied to the membrane. Protein bands were detected by Enhanced Chemiluminescence.

4.2.10. Nanogel intracellular localisation

HeLa cells were seeded at $3x10^5$ cells in glass bottom dishes and left to adhere overnight. 0.2 mg/mL of the Alexa488-nanogel and 0.025 mg/mL of Alexa647-Dextran were then co-incubated with cells for 7 h in folic acid free medium. In the case of

Alexa488-nanogels co-incubation with Alexa647- transferrin (50 nM) was performed by adding transferrin 16 min before the end of the nanogel incubation period (7 h). The cells were extensively rinsed with PBS and immediately imaged as live cells in phenol red free-DMEM by confocal microscope at 37 ºC.

4.2.11. Statistical analysis

Results are expressed as mean ± S.D. of three independent experiments, each one with n=3. Statistical significances were determined by applying a one-way ANOVA with a Dunnett's Multiple comparison test through Prism software (GraphPad software version 5.00, USA). Significance of the results is indicated according to p values * $p<0.05$, ** $p<0.005$ and *** $p<0.0001$.

4.3. Results and Discussion

4.3.1. Cellular uptake of nanogels as a function of time, concentration and presence of folate

We examined the effects of nanogel concentration and the presence of folate in the culture medium on the internalization of Alexa488-nanogel at different time points. HeLa cells were incubated for different time periods with the fluorescent nanogels at concentrations of 0.2 and 0.4 mg/ml, in media either depleted of, or containing folate. Cells were collected and the mean fluorescence intensity (a proxy for nanogel uptake) was measured by flow cytometry.

Figure 1 (A) shows that nanogel uptake increases with time over a 24 hour period in cells incubated with 0.4 mg/ml nanogel. However, in cells incubated with 0.2 mg/ml nanogel, uptake increases over the first 7 h but then at some time during the 7-24 h incubation period the mean fluorescence intensity decreases. The data indicate not only reduced uptake at this lower concentration but also a loss of the nanogel from the cells. This suggests that during longer incubation periods (7 h+) at this concentration the fluorescently labelled nanogel may either be recycled out of the cell or degraded. Degradation would seem more likely as recycling would potentially lead to reuptake of the nanogel and as such we would expect to see stabilization in the level of internalised nanogel rather than loss.

Figure 1B demonstrates that internalization of the Alexa488-nanogel is significantly increased in folate-depleted culture conditions compared with culture in normal media.

The presence of free folate in the culture medium has previously been shown to lead to a decrease in uptake of folate-conjugated NPs by cells overexpressing folate receptors.[7, 20] Viewed in this context we suggest that the folate receptors may be involved in the internalization of the Alexa488-nanogel, although other non-specific mechanisms may also contribute to the uptake. To eliminate the inhibitory and potentially confounding effects of folate in the media, folate was eliminated from subsequent uptake experiments.

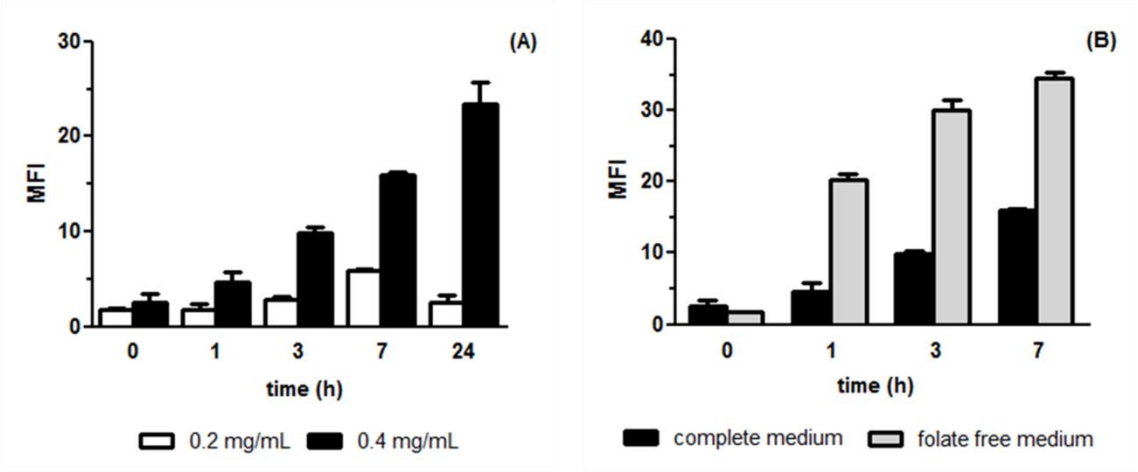

Figure 1. Effects of nanogel concentration (A) and the presence of folate in the culture medium (B) on the internalization of Alexa488-nanogel at different time points in HeLa cells. Mean fluorescence intensity (MFI) was used as a proxy for fluorescent nanogel uptake and was measured by flow cytometry at various time points up to 24 h (A) and 7 h (B).

4.3.2. Inhibition of endocytic pathways through si-RNA depletion of endocytic proteins

4.3.2.1. Viability of siRNA-transfected cells

The mechanism of nanogel internalization was studied using siRNA transfection as a tool to silence endocytic proteins and inhibit distinct endocytic pathways. It is known that the level of cellular toxicity caused by transfection is dependent on the reagent used and on the nature of the cells. Cell proliferation and metabolic activity of HeLa cells transfected using oligofectamine were studied to ensure that the viability was not compromised by the procedure. The metabolic activity of HeLa cells was not significantly affected by transfection (Figure 2, A). Although statistically significant differences were detected in total protein levels, these are relatively small and unlikely to be of biological significance (Figure 2, B).

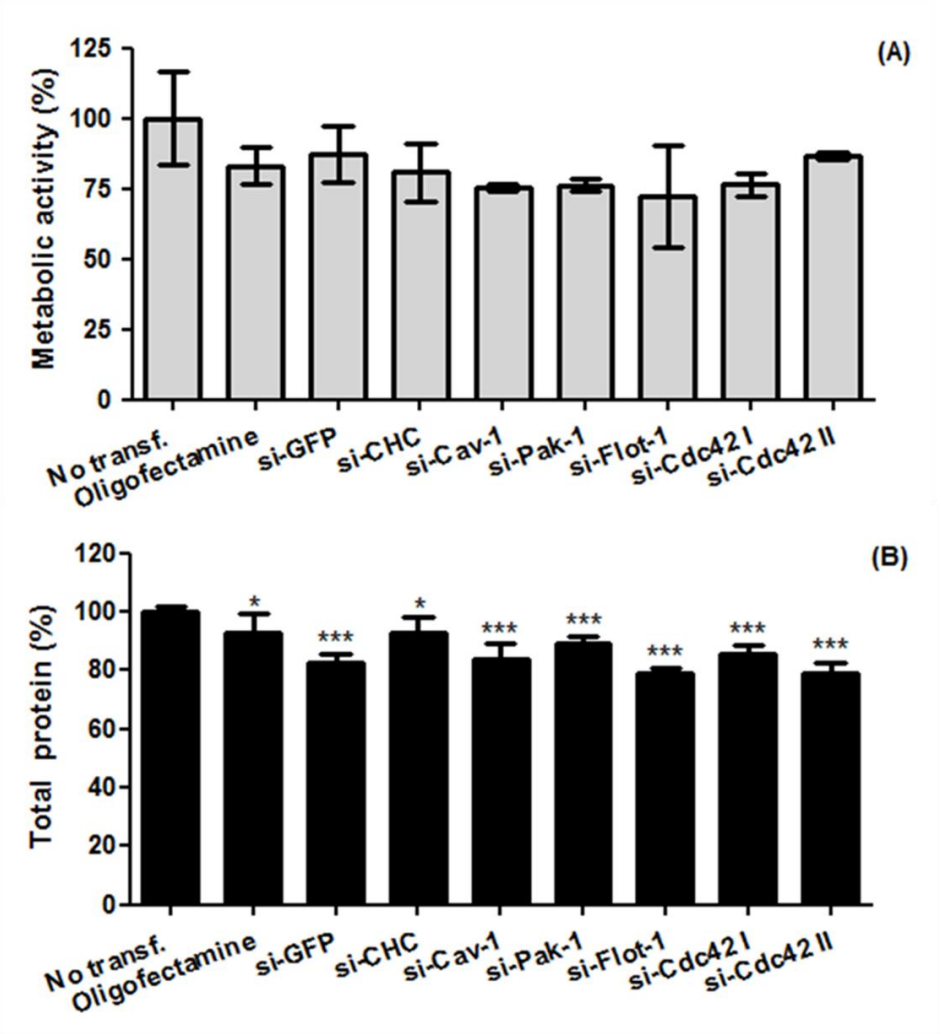

Figure 2. Effect of the si-RNA transfection on metabolic activity and total protein mass of HeLa cells assed by the MTT (A) and SRB (B) assays. * $p<0.05$ or *** $p<0.001$ represent the statistical significance of differences in viability between non-transfected cells and the siRNA depleted samples. The results were expressed as mean ± SD.

4.3.2.2. Cellular uptake mechanism(s) of the nanogels by endocytosis compromised cells

4.3.2.2.1. Inhibition of clathrin mediated endocytosis (CME)

CME is the best-characterized mechanism of endocytosis and requires the Adaptor-2 complex in association with clathrin heavy and light chain.[7, 8] Cargos taken up by clathrin-coated vesicles follow the classical endocytic pathway to early endosomes where sorting occurs for delivery to other organelles such as the lysosomes or back to the cell surface through recycling endosomes.[13] The uptake and recycling of transferrin occurs through this endocytic pathway, hence this protein is traditionally used as a marker to detect interference with CME.[14, 21] CHC is the major coat protein associated to this internalisation pathway;[7] thus in the present study si-CHC transfected HeLa cells

were incubated with Alexa647-transferrin to evaluate the efficiency of CME inhibition. Transferrin uptake in clathrin depleted cells was visibly lower compared with non-transfected and si-GFP transfected cells (Figure 3, A), reflecting successful and population-wide transfection. CHC knockdown was directly confirmed through CHC expression analyses in cell lysates (Figure 3, B). In order to ascertain if the nanogel utilises this internalisation pathway, si-CHC transfected HeLa cells and the respective controls were incubated with nanogels and then analysed via confocal microscopy (Supplementary Figure 1) and flow cytometry (Figure 3, C) revealed no differences in nanogel uptake between control cells and those deficient in CME suggesting that this pathway is not involved in nanogel uptake.

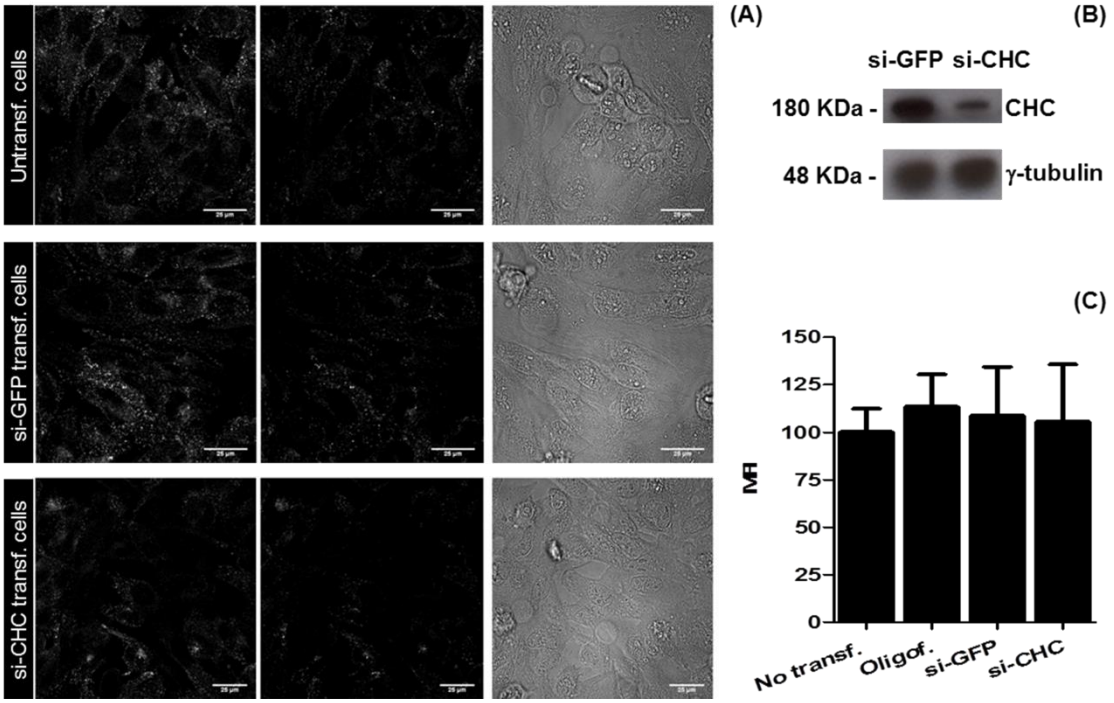

Figure 3. CME inhibition. (A) Confocal visualisation of HeLa cells transfected with si-CHC or si-GFP control for 48 hr prior to incubation with Alexa647-transferrin for 16 min. For each condition (rows) the images correspond to (left to right) maximum projection, middle z section through the cells and DIC images. The scale bars represent 25 µm. (B) CHC expression after transfecting HeLa cells with si-CHC for 48 hr. (C) Effect of the CME silencing on nanogel cellular uptake expressed as MFI. Error bars represent S.D.

4.3.2.2.2. Inhibition of caveolae-mediated endocytosis (CvME)

CvME starts with the formation of caveolae on the plasma membrane of cells, often in lipid rafts. Caveolae are noted as being enriched in the protein Cav-1 and have a diameter between 50-100 nm. A dynamin dependent scission of the caveolae from the membrane then results in the formation of the endosome-like caveosome. Initially the caveosome interior was thought not to acidify to any great extent with delivery of cargo

to the Golgi and/or endoplasmic reticulum, thus avoiding the lysosomal degradation [8]. However, Chiu *et al*. [22] revealed that N-palmitoyl chitosan NPs enter cells via caveolae and were transiently localized in caveosomes before trafficking to the canonical endosomal pathway en route to lysosomes. Agents, such as viruses, that are taken up by caveolae are also thought to end up in endosomes that can be directed to lysosomes. Evidence from electron microscopy studies suggest that caveosomes represent a special type of caveolar endosome that always associates with the plasma membrane. The theory behind the existence of caveosomes mostly results from studies which involve caveolin overexpression or caveolin mutants and as such may or may not be a naturally occurring phenomenon [23].

CvME inhibition was achieved through depletion of Cav-1 using transfection with si-Cav-1. Since Cav-1 is a critical component of caveolae formation at the plasma membrane, its depletion results in the impairment of CvME.[8] The efficiency of siRNA transfection was visualized by immunofluorescence microscopy of Cav-1, since a reliable endocytic marker equivalent to transferrin for CME, for assessing uptake via caveolae has not yet been identified. As shown in Figure 4 (A) a decrease in caveolin vesicle labelling was clearly observed in si-Cav-1 transfected cells. Significant Cav-1 depletion was also confirmed through Western blot analysis of cell lysates (Figure 4, B).

There is data to suggest that folate internalisation through the folate receptor occurs via CvME [3]. For example, folate-targeted PEG-coated NPs were thought to internalize via caveolae-assisted endocytosis and the NPs were subsequently visualized in punctate structures [24]. Conversely, internalisation and trafficking of folate receptors was found not to be exclusively caveolae dependent: specifically, folate-protein conjugates after binding to folate receptors on the surface of cancer cells, irrespective of size, were internalized via uncoated pits or caveolae, however at later times (6 h), some conjugates were found in lysosomes; so caveolae-mediated endocytic pathway converged with a pathway utilized by clathrin-coated pits [25]. In agreement with this, as shown by confocal microscopy in supplementary Figure 2 and quantified by flow cytometry in Figure 4 (C), nanogel uptake was reduced, but not significantly ($p \geq 0.05$), in Cav-1 depleted cells. However, it should be noted that when a particular route is inhibited others may become activated as a compensatory mechanism [22]. For example, Cav-1 depletion resulted in increased levels of activated Cdc42 at the plasma membrane [5]; this protein is thought to regulate the actin cytoskeleton and folate internalisation through the glycosylphosphatidylinositol (GPI)-anchored folate receptor [26].

The hydrophobicity of the cargo may be a determining factor for its internalisation via CvME. The uptake of N-palmitoyl CS NPs was associated with lipid raft-mediated endocytic routes, and substitution of chitosan with a higher level palmitoyl groups (>10 %) increased the fraction of nanogel uptake via CvME [22].

Also noteworthy is the impact of nanogel size distribution on CvME and indeed on other pathways. The nanogels in this study have mean diameters of around 200 nm and size may play a critical role in their mechanism of uptake. To our knowledge no studies have unambiguously demonstrated that caveolae can accommodate particles larger than 100 nm and this has previously been noted [27]. However, CvME was thought to play a major role in the cellular uptake of CS/DNA/γ-PGA complexes with an average size of approximately 150 nm [28]. It should be noted that most studies suggesting that caveolae are involved in the uptake of drug delivery vectors rely on the use of chemical endocytosis inhibitors, which often influence more than one pathway [12].

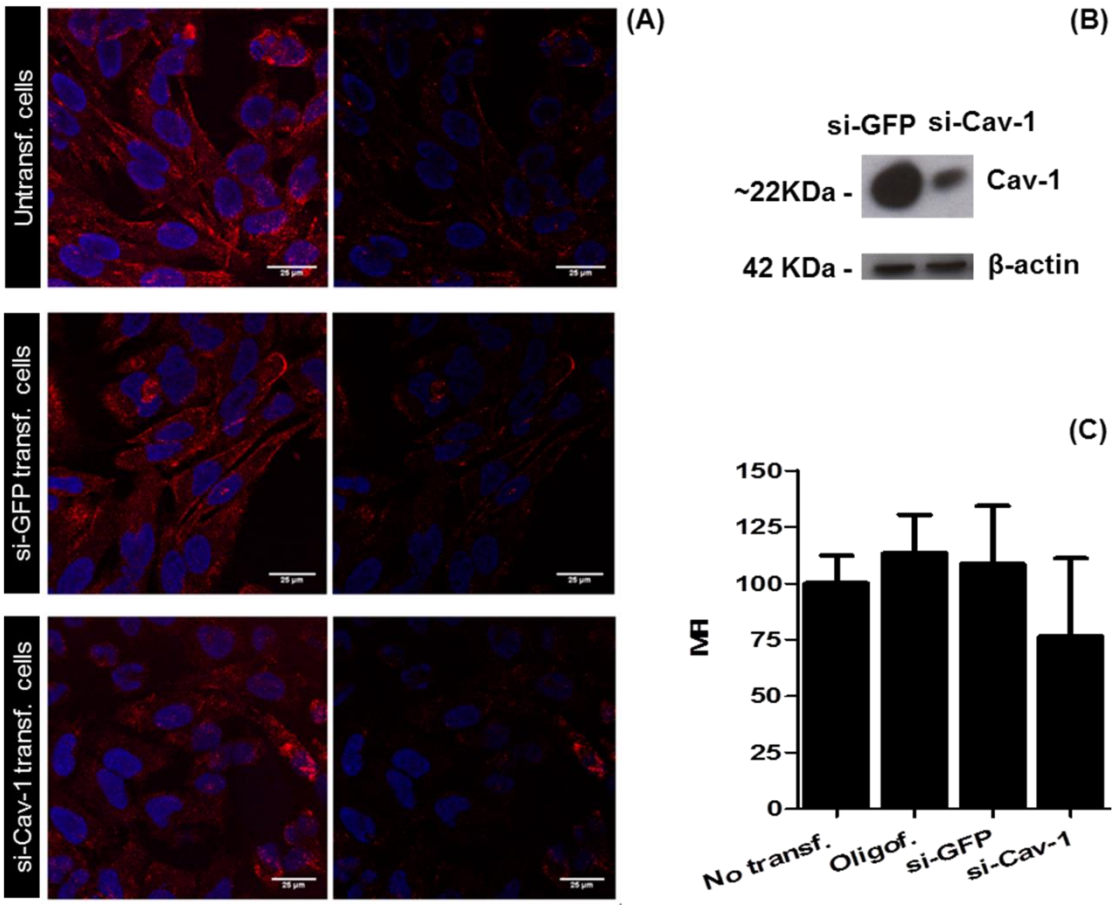

Figure 4. CvME inhibition in HeLa cells. (A) Control and si-Cav-1 or GFP treated cells, were fixed after 48 h, labelled with antibodies against Cav-1 and Alexa546 conjugated secondary antibody and then analysed by confocal fluorescence microscopy. Maximum projection (left) and a single z section (right) is shown to each condition; nuclei are labelled with Hoechst 33342. Scale bars represent 25 µm. (B) Cav-1 expression after transfecting HeLa cells with si-Cav-1 for 48 h. (C) Effect of the CvME inhibition on cellular uptake of nanogels expressed as MFI. Error bars represent S.D.

4.3.2.2.3. Inhibition of macropinocytosis

Macropinocytosis is a poorly characterised pathway that internalises extracellular material in the fluid-phase. This process involves, especially after growth factor activation, membrane ruffling and formation of relatively large vesicles, named macropinosomes. These are heterogeneous in size, generally considered larger than 0.2 μm and have no clearly identified and unique coat structures [29, 30]. It is known that p21-activated kinase (Pak-1) is associated with growth factor induced macropinosomes and can be activated by the small GTPases Cdc42 and Rac1[14, 31]. Whether the fate of macropinosomes inside the cells involves fusion with lysosomes or recycling to the plasma membrane, or a mixture of both, is unclear, and likely to dependent on cell type [8]. The addition of cationic molecules and particles to cells will inevitably result in interaction with the negative surface mediated by surface sugars [2, 3]. This may or may not lead to internalisation via membrane turnover or activation of macropinocytosis through ruffling. Membrane ruffling has been extensively studied in the field of cationic cell penetrating peptides.[14, 30] In the present study we found that the cellular uptake of the positively charged nanogel (+ 25 mV),[16] was significantly affected in Pak-1 depleted cells (Figure 5, A and B).

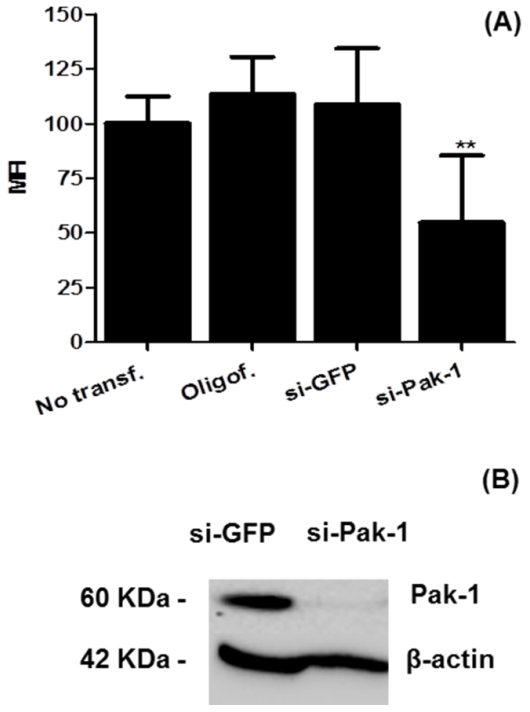

Figure 5. Pak-1 depletion of HeLa cells (A) inhibition of nanogel cellular uptake, expressed as MFI. ** represents statistical significance of $p < 0.01$ for differences in nanogel uptake between untransfected cells and si-Pak-1 transfected cells, error bars represent S.D.; (B) Pak-1 expression after transfecting HeLa cells for 48 h with control or si-Pak-1.

Studies using chemical inhibitors in HeLa cells have suggested that macropinocytosis plays a crucial role in the internalisation of hydrophobically modified glycol chitosan NPs (mean size 350 nm and positive surface charge, + 22 mV) [4]. However, other uptake pathways were also thought to be involved in uptake of these NPs.

4.3.2.2.4. Inhibition of clathrin- and caveolin-independent endocytosis: Cdc42 and flotillin dependent endocytosis

NPs and polymers modified with folate have been shown to bind to folate receptors that are often over-expressed in tumour cells [6, 32]. These multiple glycophosphatidylinositol-anchored proteins (GPI-Aps) are slowly internalised by cells and can be detected in a population of early endosomal organelles referred to as GPI-enriched early endosomal compartments, or GEECs. The uptake process is not blocked by perturbations of CME [26, 31]. Cdc42-dependent endocytosis has been reported to be involved in the uptake of GPI-anchored proteins, [23] and due to the actin mediated effects of Cdc42 it is also a well characterised regulator of micropinocytosis [29]. Raft-associated proteins flotillin -1 and flotillin-2 are also thought to play a role in cellular uptake and trafficking mechanisms of NPs. Flotillin-1 has been described as regulator of specific clathrin and caveolae-independent uptake mechanisms [15, 23]. Furthermore, flotillins appear to play a general function in late- or lysosomal degradation or storage processes.[33]

In order to investigate whether the nanogel internalisation is affected by flotillin-1 and/or Cdc42-dependent pathways, expression of these proteins in HeLa cells was siRNA-depleted prior to performing uptake assays. The results shown in Figure 6 (A) demonstrate that cellular uptake is significantly affected in these endocytosis compromised cells: nanogel uptake was inhibited by approximately 70% and 65% in cells depleted of flottilin-1 (Figure 6, B) or Cdc42, respectively. We are currently unable to label Cdc42 on membranes to investigate the extent of protein depletion but importantly, two different sequences targeting Cdc42 were shown to have almost identical effects on nanogel uptake.

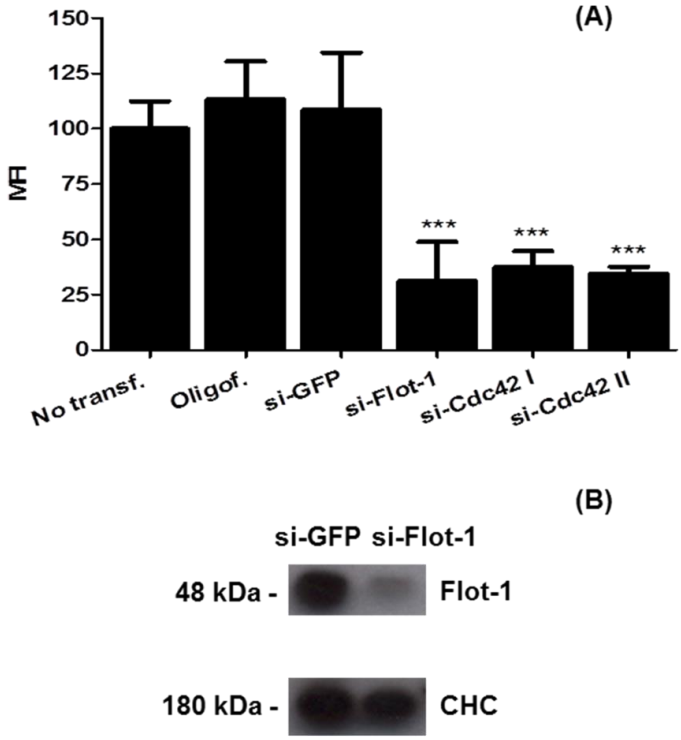

Figure 6. (A) Flow cytometry analysis of the Hela cells depleted of flot-1 or Cdc42 and incubated with Alexa488-nanogel by 7 h. Error bars represent S.D. *** indicates a statistical significance of $p<0.001$ for the differences in nanogel uptake between untransfected cells and the siRNA transfected cells. Error bars represent S.D.; (B) Flotillin-1 expression after transfecting HeLa cells for 48 h with siRNA targeting Flot-1. CHC expression was measured as a loading control.

The complete siRNA data presented in this study are summarized in Figure 7, highlighting that the nanogel internalisation appears to be dependent on multiple endocytic pathways. This has been previously reported for chitosan and chitosan derived NPs using chemical inhibitors of endocytosis [13, 34], It remains to be determined whether the nanogel is actually entering via a flotillin or Cdc42 mediated pathway or even macropinocytosis, but it raises interesting questions regarding the effect of depletion of these proteins on the overall organisation of the plasma membrane. The effects of depletion of Cdc42 and Pak-1 also highlight the importance of the actin cytoskeleton and most probably macropinocytosis in the uptake of the nanogels. We suggest that nanogels enter the cell through their activation of the cell membrane, promoting their own uptake via actin reorganisation and membrane ruffling. Further experiments are required to test this hypothesis more thoroughly.

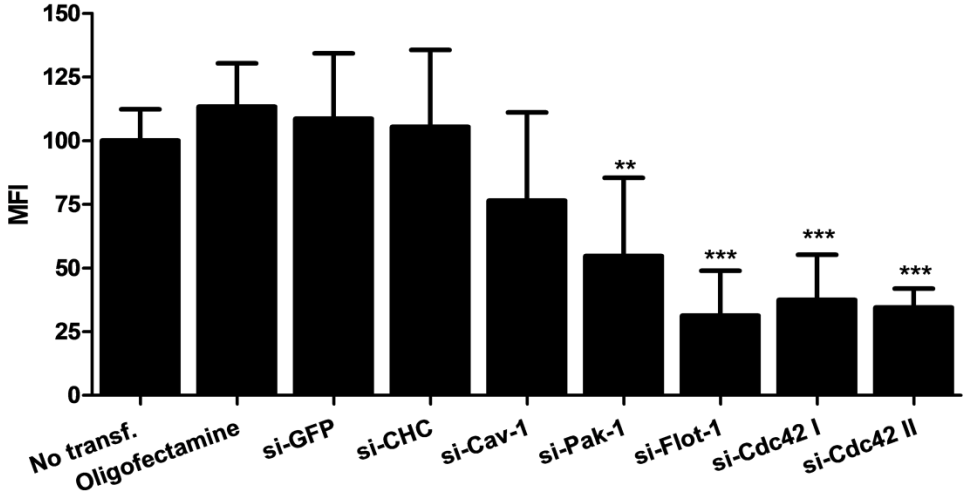

Figure 7. MFI of the nanogel internalized by HeLa cells transfected with si-CHC, si-Cav-1, si-Pak-1, si-Flot-1 and si-Cdc42, measured by flow cytometry. Untreated cells, cells incubated with oligofectamine alone or transfected with oligofectamine/si-GFP were tested as negative controls. 48 h post transfection the cells were incubated with nanogels, trypsinised and analysed by flow cytometry. ** $p<0.01$ or *** $p<0.001$ represent the statistical significance of differences in nanogel between untransfected cells and the remaining samples. Error bars represent S.D.

4.3.3. Nanogel intracellular localisation

Once the key mechanisms of nanogel internalisation had been identified, we aimed to investigate their intracellular fate by confocal laser scanning microscopy. Determining the subcellular localisation of these vectors at different time points can give important information regarding their suitability for delivering therapeutic cargo into cells and specific subcellular compartments. For this, we made use of well-characterised endocytic probes whose mechanism of uptake is understood, as is their eventual cellular fate. The intracellular localisation of the Alexa488-nanogel was compared with transferrin and dextran, both labelled with Alexa647. By using specific experimental conditions, these probes can be used to identify early, recycling and late endosomes as well as terminal lysosomes [21, 35].

When internalised, iron loaded holo-transferrin is trafficked via clathrin coated vesicles to early endosomes and then further directed to recycling endosomes. Finally, it is returned to the cell surface as apo-transferrin for another constitutive cycle of iron loading [21]. To determine if the nanogels enter the same early/recycling endosomal compartment as transferrin we co-incubated the two compounds for the final 16 min of the 7 h nanogel uptake period prior to performing live cell confocal microscopy. This short period allows the transferrin to label early endosomes and recycling endosomes. The images and colocalisation data shown in Figure 8 (A-C) demonstrate that there is

very little colocalisation between transferrin and the nanogel after they have entered the cell. This is expected based on data in Figure 3 and also the possibility that most of the nanogels have trafficked to other endocytic compartments that would be devoid of transferrin labelling, i.e. late endosomes and lysosomes.

To test whether the nanogel was in fact being trafficked via endolysosomal structures, nanogel/dextran co-incubation experiments were performed. These experiments revealed considerable colocalisation (~50%) between nanogel and dextran, as illustrated by co-localisation of the two probes in distinct intracellular yellow dots Figure 8 (D-F).

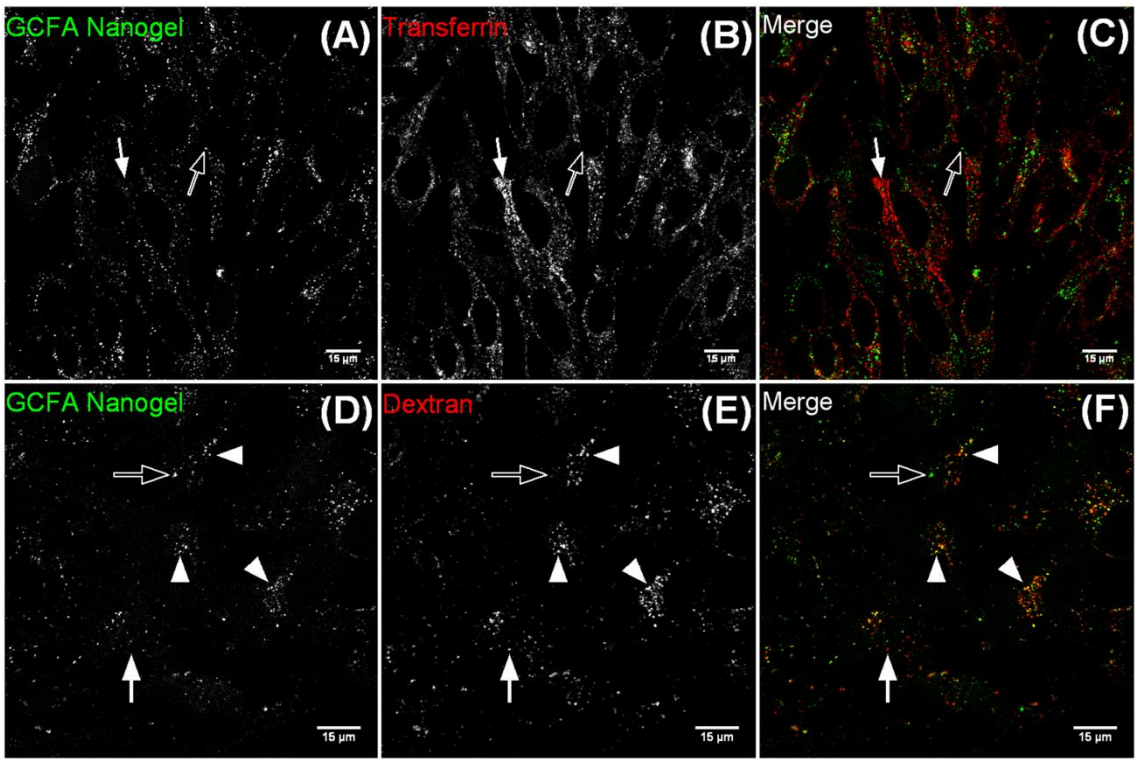

Figure 8. Nanogel subcellular distribution in HeLa cells after 7h of incubation with (A-C) Alexa647-transferrin (16 min prior to analysis) or (D-F) Alexa647-Dextran (7 h co-incubation). The images correspond to single channel capture of nanogels (A,D) transferrin (B) and Dextran (E) and respective merged images (C, F) Unfilled arrows show single nanogel structures, filled arrows show single transferrin or dextran images and arrowheads show colocalisation between nanogel and probe. Scale bars represent 15 µm.

Cdc42 has also been shown to regulate fluid phase endocytosis and dextran enters cells via this mechanism [36]. Thus the inference from the data in Figure 8 F, would be that the nanogel colocalised with the dextran represents the fraction of nanogel that enter the cell in a Cdc42 dependent manner. This conclusion is strengthened by our findings in Figure 6 that Cdc42 is required for ~70% of nanogel uptake. The absence of

complete colocalisation may be attributed to the fraction that enters the cell via lipid rafts and regulated by expression of flot-1. Similarly, a high extent of colocalisation with acidic organelles was observed when hydrophobically modified GC NPs were studied in HeLa H2B-GFP cells labelled with LysoTracker© Red probe.[4] Other studies, using human renal proximal tubular KHC cells revealed that 50 % of positively charged chitosan based NPs could escape from lysosomes and reach the cytosol, after 6 h of incubation [37]. Lower levels of colocalisation (~20%) of hydrophobically modified glycol chitosan NPs/lysosomal vesicles labelled with LysoTracker© in HeLa cells has also been noted [34].

The data from this study suggest that a fraction of nanogel may ultimately be delivered to lysosomes. This is not unexpected as pathways such as CME, caveolae and macropinocytosis have been shown to deliver some ligands and their receptors to lysosomes. However, because molecules such as transferrin can enter cells via CME but are recycled rather than degraded it remains to be determined what, if any, fraction of the nanogels recycles. The possibility exists that recycling could be mediated from late endocytic structures via a pathway that may be distinct from that used by transferrin [38].

Although undesirable in many cases for therapeutic cargo that would be inactivated in lysosomes e.g. siRNA or DNA, specific lysosome targeting may be beneficial for drug delivery strategies to replace deficient enzymes to treat conditions such as lysosomal storage diseases [39]. Beyond this, nanomedicines targeting the endolysosomal pathway also have potential for improving drug delivery to address other major disease burdens including Alzheimer Disease and cancer [3, 37].

4.4. Conclusions

Inhibition of endocytic pathways via siRNA depletion of specific endocytic proteins has provided new insights into the way that nanogel enters cells with respect to the requirements for specific proteins and the types of pathways that they orchestrate.

The involvement of Cdc42 and Pak-1 strongly suggest that actin reorganisation is also required for uptake but whether this is constitutive or active macropinocytosis remains to be determined. Colocalisation studies with endocytic probes showed that some of nanogel is delivered to endolysosomal compartments but a significant fraction was also in uncharacterised organelles that await further characterisation.

4.5. Supporting Information material

Live cell confocal microscopy observation of Alexa488-nanogels incubated with si-CHC and si-Cav-1 transfected cells. This material is available from the Wiley Online Library or from the author.

Supplementary Figures

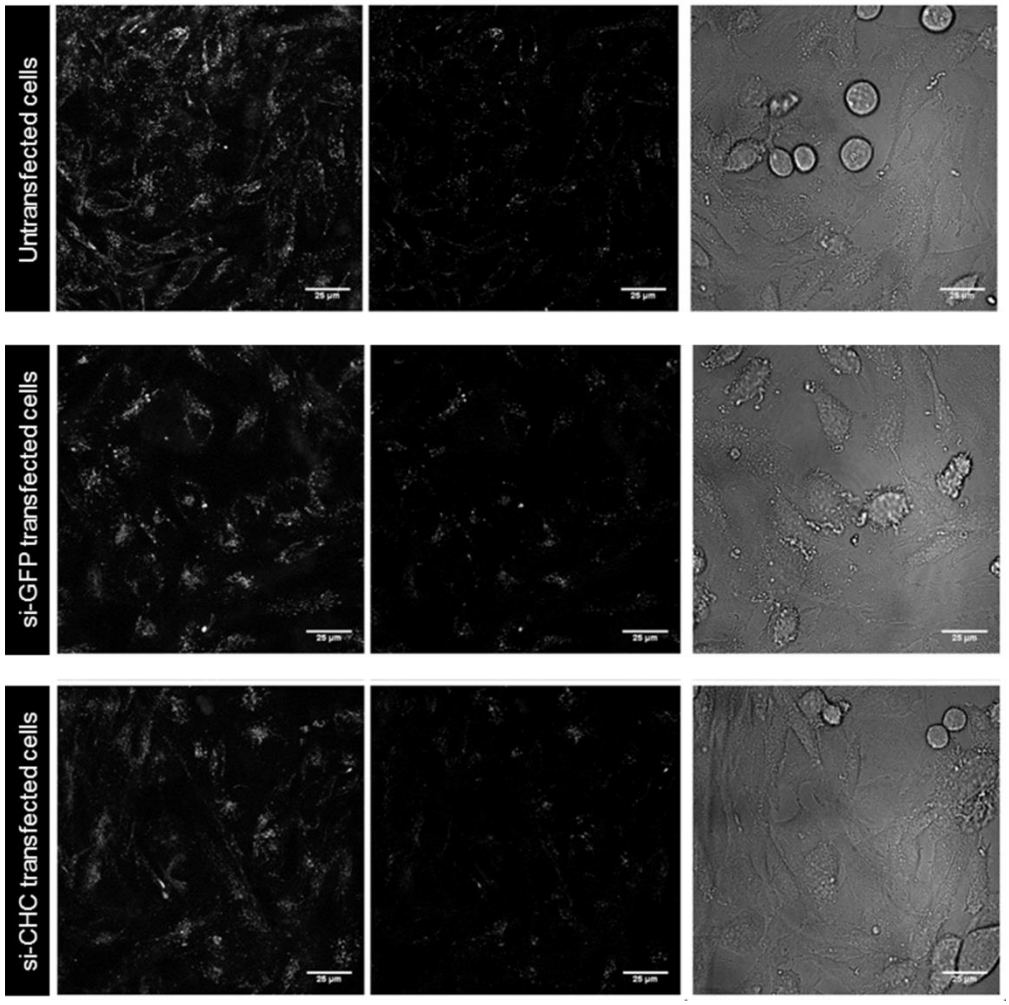

Supplementary Figure 1. Effect of CME inhibition on cellular uptake of the nanogel. Live cell confocal fluorescence microscopy images of the Hela cells transfected with si-CHC treated with nanogels for 7 h. Each row, from left to the right, represent maximum projection, Z section and DIC images.

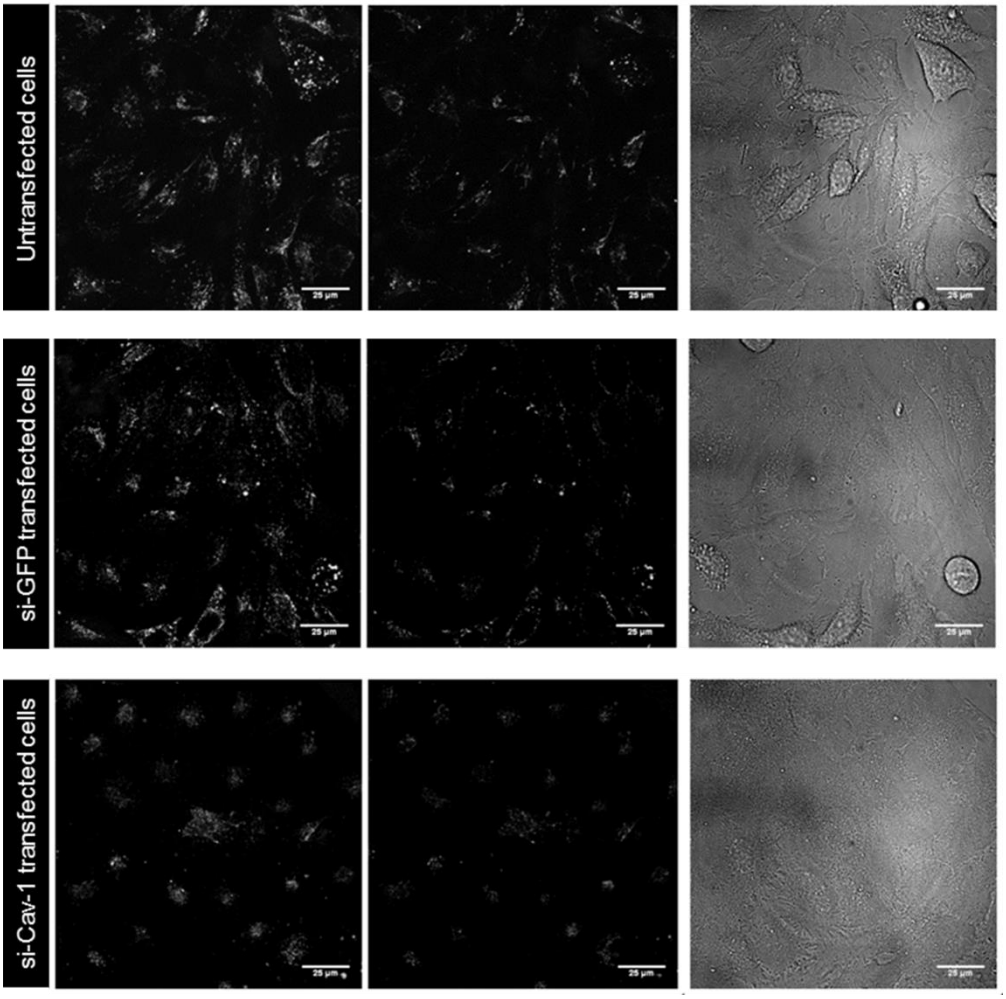

Supplementary Figure 2. Effect of si-Cav-1depletion on cellular uptake of the nanogel. Live cell confocal microscopy observation of the Alexa488-nanogels incubated with si-Cav-1 transfected cells for 7 h. Each row, from left to the right, represent maximum projection, Z section and DIC images.

4.6. References

1. Gao, H.; Yang, Z.; Zhang, S.; Cao, S.; Shen, S.; Pang, Z.; Jiang, X., Ligand modified nanoparticles increases cell uptake, alters endocytosis and elevates glioma distribution and internalization. Sci. Rep. 2013, 3.
2. Harush-Frenkel, O.; Debotton, N.; Benita, S.; Altschuler, Y., Targeting of nanoparticles to the clathrin-mediated endocytic pathway. Biochemical and biophysical research communications 2007, 353, (1), 26-32.
3. Bareford, L. M.; Swaan, P. W., Endocytic mechanisms for targeted drug delivery. Advanced drug delivery reviews 2007, 59, (8), 748-58.
4. Park, S.; Lee, S. J.; Chung, H.; Her, S.; Choi, Y.; Kim, K.; Choi, K.; Kwon, I. C., Cellular uptake pathway and drug release characteristics of drug-encapsulated glycol chitosan nanoparticles in live cells. Microscopy research and technique 2010, 73, (9), 857-65.
5. Doherty, G. J.; McMahon, H. T., Mechanisms of endocytosis. Annual review of biochemistry 2009, 78, 857-902.
6. Sahay, G.; Alakhova, D. Y.; Kabanov, A. V., Endocytosis of nanomedicines. Journal of controlled release : official journal of the Controlled Release Society 2010, 145, (3), 182-95.
7. Xu, S.; Olenyuk, B. Z.; Okamoto, C. T.; Hamm-Alvarez, S. F., Targeting receptor-mediated endocytotic pathways with nanoparticles: rationale and advances. Advanced drug delivery reviews 2013, 65, (1), 121-38.
8. Xiang, S.; Tong, H.; Shi, Q.; Fernandes, J. C.; Jin, T.; Dai, K.; Zhang, X., Uptake mechanisms of non-viral gene delivery. Journal of controlled release : official journal of the Controlled Release Society 2012, 158, (3), 371-8.
9. Ilina, P.; Hyvonen, Z.; Saura, M.; Sandvig, K.; Yliperttula, M.; Ruponen, M., Genetic blockage of endocytic pathways reveals differences in the intracellular processing of non-viral gene delivery systems. Journal of controlled release : official journal of the Controlled Release Society 2012, 163, (3), 385-95.
10. Wang, X.; Yao, S.; Ahn, H.-Y.; Zhang, Y.; Bondar, M. V.; Torres, J. A.; Belfield, K. D., Folate receptor targeting silica nanoparticle probe for two-photon fluorescence bioimaging. 2010; Vol. 1, p 453-462.
11. Vercauteren, D.; Vandenbroucke, R. E.; Jones, A. T.; Rejman, J.; Demeester, J.; De Smedt, S. C.; Sanders, N. N.; Braeckmans, K., The use of inhibitors to study endocytic pathways of gene carriers: optimization and pitfalls. Molecular therapy : the journal of the American Society of Gene Therapy 2010, 18, (3), 561-9.
12. Ivanov, A. I., Pharmacological inhibition of endocytic pathways: is it specific enough to be useful? Methods in molecular biology (Clifton, N.J.) 2008, 440, 15-33.
13. Garaiova, Z.; Strand, S. P.; Reitan, N. K.; Lelu, S.; Storset, S. O.; Berg, K.; Malmo, J.; Folasire, O.; Bjorkoy, A.; Davies Cde, L., Cellular uptake of DNA-chitosan nanoparticles: the role of clathrin- and caveolae-mediated pathways. International journal of biological macromolecules 2012, 51, (5), 1043-51.

14. Al Soraj, M.; He, L.; Peynshaert, K.; Cousaert, J.; Vercauteren, D.; Braeckmans, K.; De Smedt, S. C.; Jones, A. T., siRNA and pharmacological inhibition of endocytic pathways to characterize the differential role of macropinocytosis and the actin cytoskeleton on cellular uptake of dextran and cationic cell penetrating peptides octaarginine (R8) and HIV-Tat. Journal of controlled release : official journal of the Controlled Release Society 2012, 161, (1), 132-41.

15. Vercauteren, D.; Piest, M.; van der Aa, L. J.; Al Soraj, M.; Jones, A. T.; Engbersen, J. F.; De Smedt, S. C.; Braeckmans, K., Flotillin-dependent endocytosis and a phagocytosis-like mechanism for cellular internalization of disulfide-based poly(amido amine)/DNA polyplexes. Biomaterials 2011, 32, (11), 3072-84.

16. Pereira, P.; Morgado, D.; Crepet, A.; David, L.; Gama, F. M., Glycol chitosan-based nanogel as a potential targetable carrier for siRNA. Macromolecular bioscience 2013, 13, (10), 1369-78.

17. Mosmann, T., Rapid colorimetric assay for cellular growth and survival: Application to proliferation and cytotoxicity assays. Journal of Immunological Methods 1983, 65, (1–2), 55-63.

18. Papazisis, K. T.; Geromichalos, G. D.; Dimitriadis, K. A.; Kortsaris, A. H., Optimization of the sulforhodamine B colorimetric assay. Journal of immunological methods 1997, 208, (2), 151-8.

19. Skehan, P.; Storeng, R.; Scudiero, D.; Monks, A.; McMahon, J.; Vistica, D.; Warren, J. T.; Bokesch, H.; Kenney, S.; Boyd, M. R., New colorimetric cytotoxicity assay for anticancer-drug screening. Journal of the National Cancer Institute 1990, 82, (13), 1107-12.

20. Liu, L.; Zheng, M.; Renette, T.; Kissel, T., Modular Synthesis of Folate Conjugated Ternary Copolymers: Polyethylenimine-graft-Polycaprolactone-block-Poly(ethylene glycol)-Folate for Targeted Gene Delivery. Bioconjugate Chemistry 2012, 23, (6), 1211-1220.

21. Mayle, K. M.; Le, A. M.; Kamei, D. T., The intracellular trafficking pathway of transferrin. Biochimica et biophysica acta 2012, 1820, (3), 264-81.

22. Chiu, Y. L.; Ho, Y. C.; Chen, Y. M.; Peng, S. F.; Ke, C. J.; Chen, K. J.; Mi, F. L.; Sung, H. W., The characteristics, cellular uptake and intracellular trafficking of nanoparticles made of hydrophobically-modified chitosan. Journal of controlled release : official journal of the Controlled Release Society 2010, 146, (1), 152-9.

23. Sandvig, K.; Pust, S.; Skotland, T.; van Deurs, B., Clathrin-independent endocytosis: mechanisms and function. Current Opinion in Cell Biology 2011, 23, (4), 413-420.

24. Dauty, E.; Remy, J. S.; Zuber, G.; Behr, J. P., Intracellular delivery of nanometric DNA particles via the folate receptor. Bioconjug Chem 2002, 13, (4), 831-9.

25. Turek, J. J.; Leamon, C. P.; Low, P. S., Endocytosis of folate-protein conjugates: ultrastructural localization in KB cells. Journal of cell science 1993, 106 (Pt 1), 423-30.

26. Sabharanjak, S.; Sharma, P.; Parton, R. G.; Mayor, S., GPI-anchored proteins are delivered to recycling endosomes via a distinct cdc42-regulated, clathrin-independent pinocytic pathway. Developmental cell 2002, 2, (4), 411-23.

27. Iversen, T.-G.; Skotland, T.; Sandvig, K., Endocytosis and intracellular transport of nanoparticles: Present knowledge and need for future studies. Nano Today 2011, 6, (2), 176-185.

28. Peng, S. F.; Tseng, M. T.; Ho, Y. C.; Wei, M. C.; Liao, Z. X.; Sung, H. W., Mechanisms of cellular uptake and intracellular trafficking with chitosan/DNA/poly(gamma-glutamic acid) complexes as a gene delivery vector. Biomaterials 2011, 32, (1), 239-48.

29. Kerr, M. C.; Teasdale, R. D., Defining macropinocytosis. Traffic (Copenhagen, Denmark) 2009, 10, (4), 364-71.

30. Jones, A. T., Macropinocytosis: searching for an endocytic identity and role in the uptake of cell penetrating peptides. Journal of cellular and molecular medicine 2007, 11, (4), 670-84.

31. Hansen, C. G.; Nichols, B. J., Molecular mechanisms of clathrin-independent endocytosis. Journal of cell science 2009, 122, (Pt 11), 1713-21.

32. Lu, Y.; Low, P. S., Folate-mediated delivery of macromolecular anticancer therapeutic agents. Advanced drug delivery reviews 2002, 54, (5), 675-93.

33. Kasper, J.; Hermanns, M. I.; Bantz, C.; Utech, S.; Koshkina, O.; Maskos, M.; Brochhausen, C.; Pohl, C.; Fuchs, S.; Unger, R. E.; Kirkpatrick, C. J., Flotillin-involved uptake of silica nanoparticles and responses of an alveolar-capillary barrier In vitro. European journal of pharmaceutics and biopharmaceutics : official journal of Arbeitsgemeinschaft fur Pharmazeutische Verfahrenstechnik e.V 2013, 84, (2), 275-87.

34. Nam, H. Y.; Kwon, S. M.; Chung, H.; Lee, S. Y.; Kwon, S. H.; Jeon, H.; Kim, Y.; Park, J. H.; Kim, J.; Her, S.; Oh, Y. K.; Kwon, I. C.; Kim, K.; Jeong, S. Y., Cellular uptake mechanism and intracellular fate of hydrophobically modified glycol chitosan nanoparticles. Journal of controlled release : official journal of the Controlled Release Society 2009, 135, (3), 259-67.

35. Pangarkar, C.; Dinh, A. T.; Mitragotri, S., Endocytic pathway rapidly delivers internalized molecules to lysosomes: an analysis of vesicle trafficking, clustering and mass transfer. Journal of controlled release : official journal of the Controlled Release Society 2012, 162, (1), 76-83.

36. Cheng, Z. J.; Singh, R. D.; Holicky, E. L.; Wheatley, C. L.; Marks, D. L.; Pagano, R. E., Co-regulation of caveolar and Cdc42-dependent fluid phase endocytosis by phosphocaveolin-1. The Journal of biological chemistry 2010, 285, (20), 15119-25.

37. Yue, Z.-G.; Wei, W.; Lv, P.-P.; Yue, H.; Wang, L.-Y.; Su, Z.-G.; Ma, G.-H., Surface Charge Affects Cellular Uptake and Intracellular Trafficking of Chitosan-Based Nanoparticles. Biomacromolecules 2011, 12, (7), 2440-2446.

38. Grant, B. D.; Donaldson, J. G., Pathways and mechanisms of endocytic recycling. Nat Rev Mol Cell Biol 2009, 10, (9), 597-608.

39. Desnick, R. J.; Schuchman, E. H., Enzyme replacement therapy for lysosomal diseases: lessons from 20 years of experience and remaining challenges. Annual review of genomics and human genetics 2012, 13, 307-35.

5. *In vivo* imaging of glycol chitosan-based nanogel biodistribution

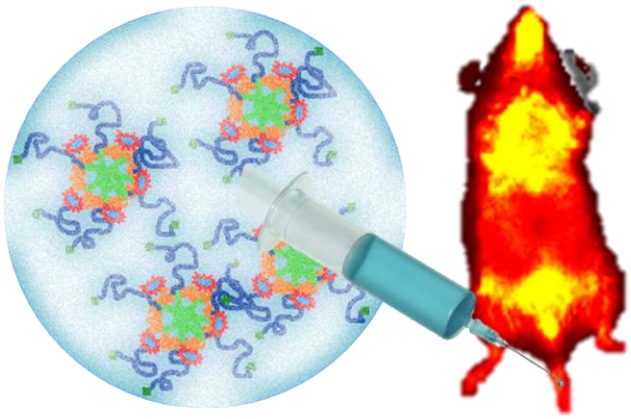

The preclinical development of nanomedicines raises several challenges. Among them is the biodistribution evaluation after systemic administration. In the present study, having in previous work validated the biocompatibility and targeting ability of a GC based nanogel, we intend to assess its biodistribution profile using *in vivo* near infrared (NIR) fluorescence imaging as tool to track the nanogel in mice model over time, after intra venous administration. Rapid whole body biodistribution of Cy5.5 labelled nanogel and GC polymer was found at early times. It remained widespreadly distributed in the body for at least until 6 h post-injection, then decreasing drastically after 24 h. Nanogel blood circulation half-life lies around 2 h, the free linear GC polymer presenting lower blood clearance rate. After 24 h, the blood NIR fluorescence intensity associated to both samples decrease to insignificant values. NIR imaging of the organs show that the nanogel had a body clearance time of approximately 48 h, because at this time point only a weak signal of NIR fluorescence was observed in the kidneys. Hereupon it could be concluded that engineered GC nanogel has fairly long blood circulation time, suitable for biomedical applications namely drug delivery, associated to efficient body clearance.

5.1. Introduction

The use of engineered NPs in Nanomedicine is revolutionizing the clinical practice, regarding both diagnosis and therapy [1]. Due to their multifunctional nature, large surface area, structural diversity, and long circulation time in blood (as compared to small molecules), NPs have emerged as attractive vehicle for improved therapy. In addition to NPs being used as tools for molecular imaging they also could deliver therapeutic agents to the disease site, thus allowing simultaneously imaging and therapy, called theragnosis [2, 3]. Such nanoparticulate systems should enable appropriate residence time in blood stream, long enough as to ensure particle localization and delivery of the drug and/or diagnostic at target site, at the same time allowing its complete elimination within an acceptable time, in order to avoid toxicity or chronic effects [4, 5]. Unfortunately, many types of systemically injected NPs have a rapid blood clearance, essentially due to the action of the mononuclear phagocytic system mainly through the liver, spleen, lung and bone marrow. So, NPs formulation that avoids rapid clearance is a requirement for suitable delivery to the desired target [5].

In a previous study we reported the synthesis of a GC nanogel functionalized with folate with an average size of 200 nm and positive surface charge (+ 25 mV) [6]. *In vitro* assays confirmed its targeting ability to folate receptors and also the efficient encapsulation of siRNA. Thus in the current work we intend to show a preliminary assessment of the GC nanogel biodistribution in a mice model, using optical fluorescence imaging technology. The NIR probe Cy5.5 was chosen to label the nanogel as well as the free polymer. Fluorophores with a red or near infrared emission range (600-1000 nm) bear a high photon penetration into living tissues, and low photon absorption and tissue autofluorescence, thus allowing effective imaging of deep tissues [7, 8].

5.2. Material and methods

5.2.1. Materials

GC (G7753, Mw=100kDa), mercapto hexadecanoic acid (MHDA), N-hydroxysulfosuccinimide (NHS), 1-Ethyl-3-[3-dimethylaminopropyl]carbodiimide hydrochloride (EDC), folate, O-methyl-O'-succinylpolyethyene glycol 2000 (PEG2000), O-(2-Aminoethyl)-O'-(2-carboxyethyl)polyethylene glycol 3000 hydrochloride (PEG3000) were acquired from Sigma-Aldrich (St. Louis, MO, US).

Cy5.5 mono-reactive NHS ester was purchased from GE Healthcare (Little Chalfont, UK).

5.2.2. Synthesis and self-assembly of GC nanogels

Details on the synthesis of the GC nanogel synthesis and its decoration with folic acid were described in a previous report [6]. Briefly: nanogel synthesis was performed in two independent steps. Initially, folate is conjugated to PEG3000 (FA-PEG3000). In the second reaction, FA-PEG3000, PEG2000 and MHDA were grafted onto the GC polymer. The nanogel colloidal suspensions were obtained after dispersing the lyophilized reaction product in saline buffer (PBS), under magnetic stirring at 50 ºC for 48 h, and filtration through a pore size 0.45 µm cellulose acetate syringe filter.

5.2.3. Preparation of GC and nanogel Cy5.5 conjugation

Free polymer and nanogels were labelled with a near infrared (NIR) fluorescent probe, Cy5.5 mono-reactive NHS ester. The dye solution (10 mg/mL, in DMSO) was added to GC or nanogel dispersion (1 mg/mL, in PBS) at 0.04 and 0.06 molar ratios of Cy5.5 reactive carboxylic groups to GC or nanogel free amine groups, respectively. The reaction was allowed to occur for 24h in the dark at room temperature. Thereafter, the reaction mixture was extensively dialysed (MW cutoff 10-12 kDa) against distilled water to remove unreacted Cy5.5 molecules. To confirm the absence of free dye, Cy5.5-GC or Cy5.5-Nanogel was purified by centrifugation at 3,000 x g through a 10 kDa MW cut-off filter. Then, Cy5.5 was quantified spectrophotometrically in the resultant fractions (filtrate and concentrate).

5.2.4. *In vivo* biodistribution of GC and GC nanogels

The animal experiments were performed in agreement with and approved by IMM (Institute of medicine and Molecular, Lisbon, Portugal) Animal Ethics Committee and DGAV (entity responsible for animal welfare). Male BALB/c mices, 8-weeks-old, (Charles River, L'Arbresle, France) were used for animal experiments. 5 mg/Kg of Cy5.5-GC or Cy5.5-Nanogel were intravenously injected via the tail vein. After injection, the time-dependant *in vivo* samples biodistribution were non-invasively imaged using the IVIS Lumina fluorescence imaging system. For the imaging study, exposure time (3 s), pixel binning (CCD resolution, medium), and lens aperture (amount

of light collected and depth-of-field, f/stop 16) were optimized. The NIR fluorescence signal intensity of each Cy5.5 labelled samples on respective injected animals were imaged using a CCD camera equipped with a Cy5.5 emission filter sets. The obtained results were resultant from two independent experiments with a single animal for each condition. Consistent results were obtained in the independent assays. Since only a qualitative analysis of the results is performed, it has been decided not to perform additional replicates.

5.2.5. Fluorescence intensity measurement in the blood and different organs

At the end of each time point whole blood (about 0.8 mL) was collected from anesthetised animals using cardiac puncture. Immediately after, they were sacrificed through cervical dislocation to collect the organs of interest: spleen, heart, liver, kidneys, brain, lungs, muscle, and skin. Blood and organs were placed in a 6- well plate for IVIS Lumina fluorescence imaging system visualization. The semi-quantification of NIR fluorescence signal in different organs and blood acquired images was performed using a Living image software and measured as total photons per centimeter squared per steradian (p/sec/cm2/sr).

5.3. Results and discussion

5.3.1. GC and Nanogel labelling

CyDyes are commonly used in a wide range of biological assays. Cy5.5 has been used historically for imaging, even though its excitation/emission maxima wavelengths (675/694 nm) are very close to the wavelength range (400-650 nm, visible spectrum) which is affected by tissue autofluorescence [9, 10]. In order to comparatively study the *in vivo* biodistribution of the unmodified GC and its derived nanogel, Cy5.5 mono-reactive ester was chosen to label both samples. The comparison is only possible if samples were similarly labelled. Therefore, a theoretical molar ratio of 4% and 6% of Cy5.5 reactive carboxylic groups in regard to the free amine groups, respectively of the GC polymer and its nanogel, were experimentally observed to be effective as to provide a similar Cy5.5 labelling, as shown in Figure 1. Indeed, the resulting fluorescence signal obtained in the different samples is comparable.

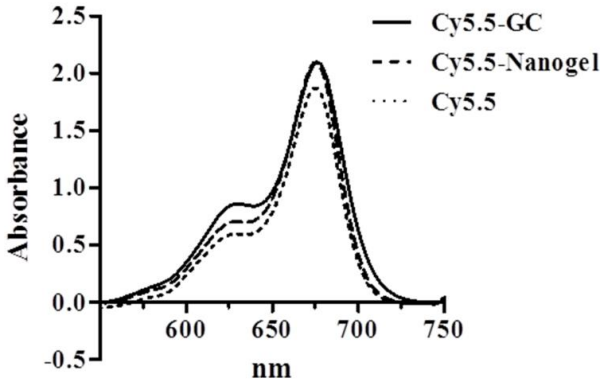

Figure 1. Absorbance spectral scans of free Cy5.5 and of Cy5.5 conjugated with GC or GC nanogel.

The lack of unconjugated Cy5.5 in the labelled GC and nanogel was also assessed spectrophotometrically. Basal absorbance was measured on the filtered fraction obtained following ultrafiltration, thus demonstrating that all of the conjugate is properly grafted on the polymer (data not shown).

5.3.2. Unconjugated Cy5.5 biodistribution

The biodistribution/body clearance profile of free Cy5.5 was assessed 6 h post administration. Whole body imaging showed that free Cy5.5 was distributed to little extension, as compared to conjugated dye (Figure 2 A), indicating faster body clearance. Negligible NIR fluorescence was detected in blood, spleen, heart, kidneys and brain (Figure 2 B and C) using the free dye, a weak signal being found in lungs, muscle and liver. Remarkably, 6 h after injection an intense NIR fluorescence signal was observed in the skin, as also observed in animals treated with Cy5-5-GC or nanogel. Hue *et al.* [11] found that Cy5.5 fluorescence in several organs was rapidly eliminated from 30min to 24h post-injection, fairly high fluorescence signal being reached in liver, lung, kidney and stomach within 1 day post-treatment.

5.3.3. Whole body *in vivo* biodistribution

It is known that autofluorescence naturally occur in animal tissues through the visible spectral range up to 700 nm, which may mask the probe signal [9]. Hence, this feature was taken into consideration and system image acquisition parameters were optimized using a non-injected mouse (Cont-). As could be observed in Figure 3, no interference of tissues autofluorescence was visualized under the used conditions. So, the NIR fluorescence signal detected by CCD camera is exclusively associated to Cy5.5.

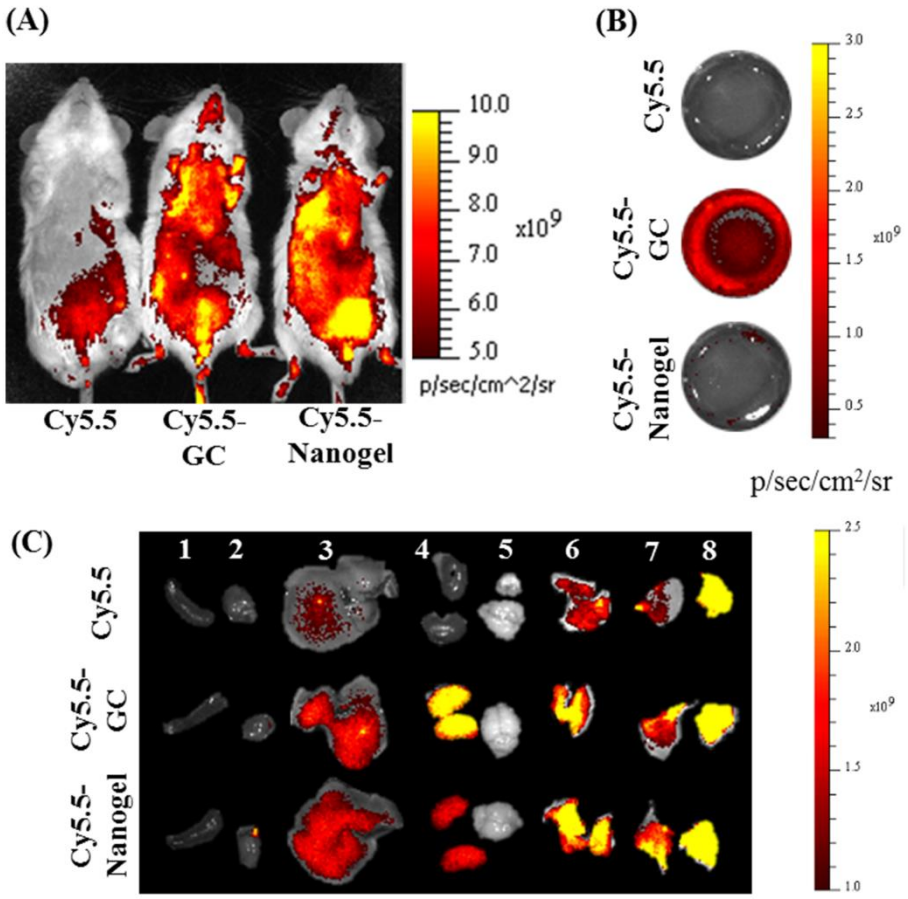

Figure 2. Biodistribution of unconjugated Cy5.5 as compared with Cy5.5 conjugated with GC or nanogel, in BALB/c mice 6 h post-intravenous injection. (A) NIR imaging of whole body, (B) total blood and *ex vivo* organs (1-spleen; 2- heart; 3-liver; 4-kidneys; 5-brain; 6-lungs, 7- muscle; and 8-skin).

In order to observe *in vivo* biodistribution of Cy5.5-GC and Cy5.5-Nanogel, a 5 mg/Kg dosage of the samples homogenously dispersed in 100 µL of PBS were intravenously administered into the tail vein of BALB/c mice. A time dependent distribution was observed using a non-invasive NIR fluorescence imaging technique in live animals, as shown in Figure 3. An intense NIR fluorescence signal was observed in the whole body 15 min only after injection (reflecting the rapid sample biodistribution), the signal remaining intense for at least 6 h. The fluorescence signal fades drastically after 24 h post-injection. It is noteworthy that a strongest fluorescent signal was observed on the mice treated with Cy5.5-Nanogel and the distribution pattern clearly progresses from a widespread distribution at early time points, to a more posterior concentrated distribution (kidneys and bladder) in a later stage, showing the predictable fate of the sample, its elimination by filtration. Likewise, in a similar study, the biodistribution profile of nanoparticles of a N,N-diethylnicotinamide-based oligomer

conjugated with GC showed high NIR fluorescent signal 1h after injection, which was preserved for up to 1 day, followed by a reduction [12].

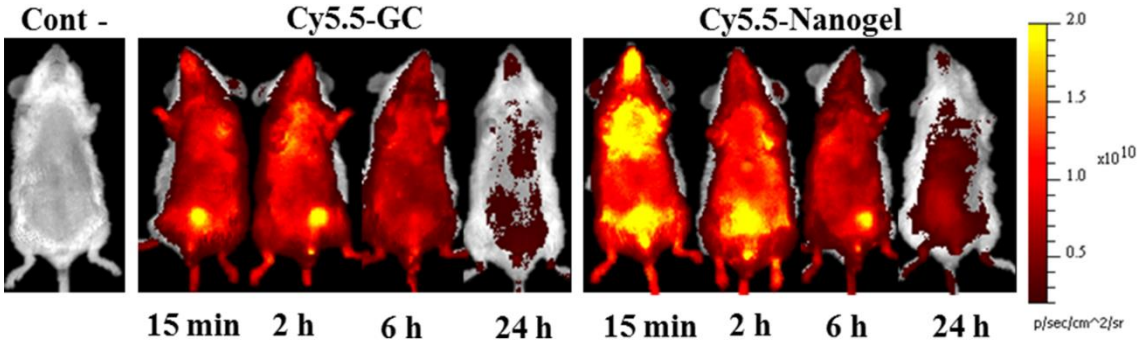

Figure 3. Representative experiment of whole body NIR fluorescence images of Balb/C mice intravenously injected with Cy5.5-GC and Cy5.5-Nanogel (xmg/Kg), observed over time.

5.3.4. Blood clearance

One of the major design considerations for nanoparticulate drug delivery systems is the circulation half-life, since the longer this is the more effectively the NPs may accumulate at the target site, either by passive or active mechanisms [13]. Thus, in order to study the blood half-life, whole blood was collected from mice injected with the samples at different time points and scanned using the IVIS Lumina system (Figure 4). NIR fluorescence intensity of whole blood in each condition was semi-quantified using Living image software and expressed as average radiance. Liu *et al.* [7] classifies the fluorescence imaging as a semi-quantitative technique, as they proved that the quantitative data from whole organs is strongly affected by the scattering and the absorption properties of the organ. Therefore the fluorescence intensity detected may not necessarily be proportional to the number of molecules present, and thus the results are here discussed qualitatively.

The Cy5.5-Nanogel exhibited a fairly long blood circulation half-life, about 2h, which is compatible with the general aim of addressing NPs to a particular tissue in the body. Nevertheless, the NIR fluorescence intensity signal decays faster at the initial stage after administration, probably due to kidneys filtration and retention in the organs. Surprisingly, GC polymer presented a higher blood circulation half-life, being detected in significantly higher intensity than the nanogel 6h post-injection. In both cases, however, 24 h after administration only a residual amount is detectable. Apparently, the free polymer is thus more effective in evading the mononuclear phagocytic system.

Foreign entities in bloodstream circulation are generally marked for uptake by mononuclear phagocytic system, through a process known as opsonisation. Particles functionalized with PEG, or other hydrophilic polymers, have increased circulation half-life because they are shielded with water molecules remaining invisible to opsonins and macrophages[5, 13]. Hence, lower circulation half-life of the GC nanogel comparatively to free polymer was unexpected, because on nanogel formulation were included PEG chains of 2000 and 3400 Da, whose ability for prolonging circulation time in blood is well reported [14, 15]. On the other hand, the size of the nanogel is much higher than that of the GC polymer (with a Mw of 100kDa an hydrodynamic size of a few nanometers is expected, while the nanogel has about 200nm), hence a faster kidney filtration would be expectable for the polymer. The larger size could justify a more effective recognition of the nanogel by macrophages and the results that consistently suggest the GC polymer has a longer blood circulation time. However, the accumulation of the nanogel in the liver, although occurring to larger extent than the free polymer, is only transient, as discussed below.

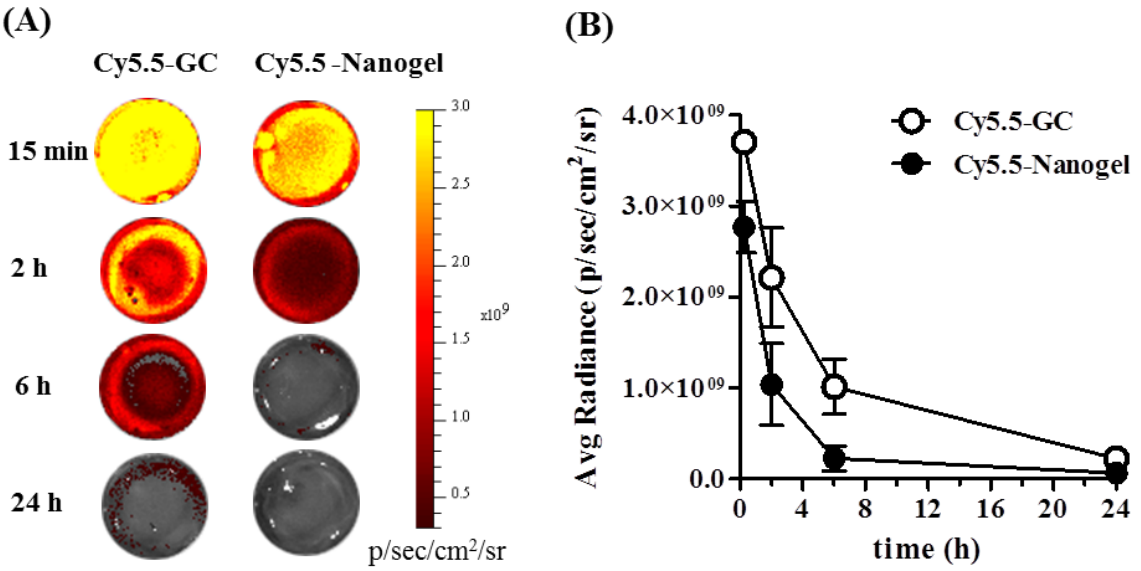

Figure 4. Blood circulation half-life of GC and nanogel. (A) Representative NIR fluorescent images of whole blood collected over time after intravenous injection of Cy5.5-GC and Cy5.5-Nanogel samples in BALB/c mice. (B) NIR fluorescence intensity signal quantification of Cy5.5 labelled samples.

Also N-succinyl-CS was reported as a systemically long circulating polymer. The retention of Succinyl-CS in blood was much higher than that in other tissues even at 72 h after injection. The half-life was calculated to be around 100 h by log-linear elimination analysis. Kato and colleagues argued that this longer retention was probably

due to high molecular weight (>100 kDa), difficult biodegradation and poor interaction with tissues due to its high negative charge, differently from the here analysed nanogel [16].

Controversially, Richardson and colleagues reported rapid blood clearance for three tested samples of CS with different Mw (< 5 kDa, 5-10 kDa and > 10 kDa). In this study, 1 h after injection only 2.6 % of the radiolabeled CS (^{125}I) with > 10 kDa remain in the blood [17]. Na *et al.* [18] verified that GC NPs synthesized with increasing degrees of substitution of 5β-cholonic acid had higher blood circulation time compared to the GC linear polymer, whose fluorescence intensity decrease 1 day post injection. Also Kim *et al.* [19] found that Cy5.5 and Cy5.5 labelled GC were excreted from body within 1 day, while hydrophobically modified GC takes 3 days.

5.3.5. Organs biodistribution

In order to evaluate the nanogel and linear GC organ distribuition at defined time points, the organs were excised and imaged in the IVIS Lumina system. NIR fluorescence intensity of each organ was semi-quantified using Living image software and expressed as average radiance. Overall, GC nanogel show high tissue accumulation at earlier biodistribution times (t 15 min and t 2 h), mainly in lungs and skin (highly vascularized organs) as compared to free polymer, as could be observed in Figure 5 (A and B). Probably organs distribution profile is associated to the shorter circulation half-life of the nanogel and consequently faster organs accumulation. This is somewhat surprising, since the positive charges of the free polymer would be expected to interact with cells more readily than the nanogel, which is decorated with PEG. Maybe the folate receptor plays therefore a relevant role and it may be responsible for the quicker retention of the nanogel in the tissues. After 24h post-injection, where no GC or nanogel were observed in blood, similar organs distribution pattern were observed for both samples; exception made to higher accumulation of the free polymer in lungs and kidneys, as observed in NIR images (Figure 5 C). For later post-injection periods (48 h) higher NIR fluorescence signal was found in the organs of mice injected with linear GC compared to nanogel, where barely detectable signal was found, with exception to kidneys. The non-specific interaction of the free GC with cells seems to proceed at lower pace than those promoted by specific interactions mediated by the folate receptor. Localization of the nanogel and GC polymer in the kidneys is expected, and common to other CS NPs because they play an important role in the clearance of biodegradable

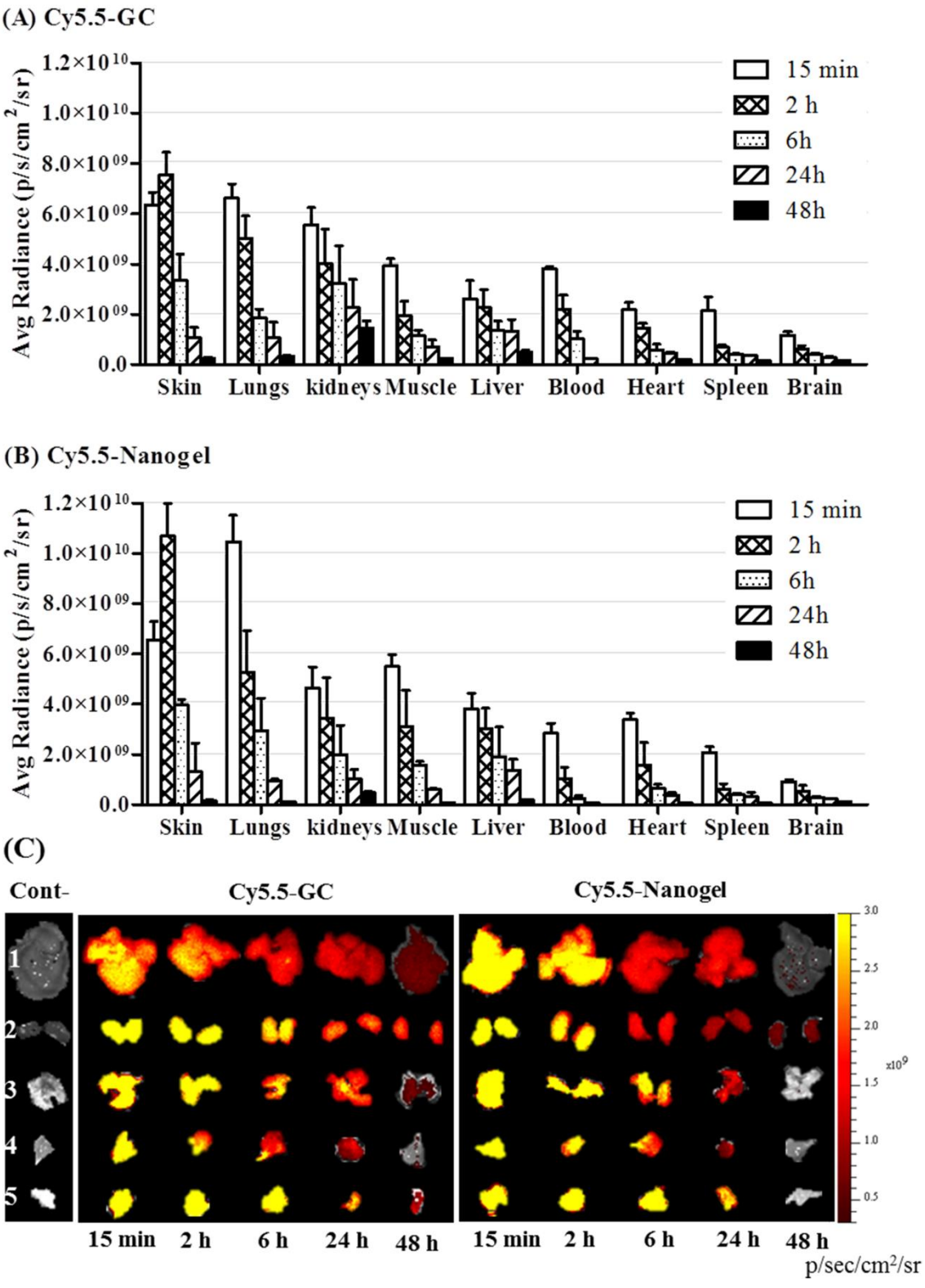

Figure 5. *Ex vivo* NIR fluorescence imaging of Cy5.5-GC and –Nanogel organ biodistribution. (A, B) Quantification of NIR fluorescence signal of Cy5.5-GC or Nanogel (respectively) organs accumulation at different time points, recorded as total photon counts per centimeter squared per steradian (p/sec/cm^2/sr) per excised organ as function of time. (C) Representative *ex vivo* images of normal organs (1- Liver, 2- Kidneys, 3-Lungs, 4- Muscle, and 5-Skin) acquired over time after Cy5.5-GC or Nanogel intravenous injection. Organs of non-injected mice were used as negative control of NIR fluorescence.

macromolecules circulating in the bloodstream [19-21]. So, 48h post injection almost all of the injected nanogel was almost fully eliminated from mice body, which represent a great advantage concerning toxicity issues. This result suggests that the nanogel disassembles *in vivo*, being excreted in about 2-3 days. Nanomaterials body clearance is particularly important due to concerns over long-term exposure and interference with other diagnostics and therapies [4].It should be noted that NIR signal disappearance corresponds to conjugated dye, and is not associated to dye instability, or loss of signal over time. Similar studies, such as biodistribution of Cy5.5 labelled CS coated iron oxide NPs showed high signal intensity for at least 72 h in kidneys, spleen, liver and bone marrow [5].

Based on this observation, an interesting approach for kidneys targeted drug delivery was developed by Gao *et al.*[22]. They reported for the first time the use of CS/siRNA NPs for extended siRNA accumulation in the kidneys, which may have potential for treatment of renal diseases using RNAi therapeutics.

Curiously, in spite of liver, spleen and lung being important components of the mononuclear phagocytic system and consequently involved in macromolecules clearance, in the current study nanogel and even free GC were poorly taken up by liver and spleen, unlike described by other authors [5]. Nevertheless also He *et al.* [23] verified that rhodamine B labelled CS hydrochloride distribution in spleen decreased with the increase of the particle size from 150 nm to 300 nm, which was probably due to the splenic physical filtration effect that excluded NPs with particle size ranging in 200–500 nm. Indeed, the size distribution of the GC nanogel studied in the present work lies within this range, so is somewhat expected that this nanogel with an average size of 200 nm would show minor accumulation in spleen rather than other organs.

Lungs, together with skin, is one of the organs where higher nanogel accumulation was found 24h post-administration, as also the free polymer - although to less extent in this case. He *et al.* [23] assigned the higher concentration of rhodamine B labeled CS hydrochloride in the lungs to the high positive charge, which would lead to the NPs forming aggregates with blood cells by electrostatic interaction, consequently being entrapped in lungs. Sykes *et al.* [24] also showed that skin is an important site of NP accumulation following systemic administration. Their results suggest that dermal accumulation should be exploited to trigger the release of ultraviolet and visible light-sensitive therapeutics which are currently impractical *in vivo*. Nevertheless, further tests should be performed in order to clarify whether the GC and nanogel skin accumulation

24 h post-injection are independent of the dye, because as shown ahead in Figure 2 fairly high NIR fluorescence intensity was observed is this tissue 6 h after free dye administration.

5.4. Conclusion

The rapid biodistribution of GC nanogel and linear GC labelled with Cy5.5 was readily observed through *in vivo* NIR imaging system. Whole body images acquisition provides an overview on the extension of sample biodistribution, however it is the whole blood and organs analysis that renders more accurate information on nanogel blood clearance, organs accumulation and consequently sample body clearance. In summary, it could be concluded that the nanogel has a blood clearance rate higher than that of the free polymer. Even so, the nanogel exhibit a satisfactory blood circulation half-life of about 2 h and its body clearance occur approximately 48 h after administration; key findings in the use of GC nanogel as drug/imaging agent delivery system.

5.5. References

1. Petros, R. A.; DeSimone, J. M., Strategies in the design of nanoparticles for therapeutic applications. *Nat Rev Drug Discov* **2010,** 9, (8), 615-627.
2. Lee, D.-E.; Koo, H.; Sun, I.-C.; Ryu, J. H.; Kim, K.; Kwon, I. C., Multifunctional nanoparticles for multimodal imaging and theragnosis. *Chemical Society Reviews* **2012,** 41, (7), 2656-2672.
3. Nam, T.; Park, S.; Lee, S.-Y.; Park, K.; Choi, K.; Song, I. C.; Han, M. H.; Leary, J. J.; Yuk, S. A.; Kwon, I. C.; Kim, K.; Jeong, S. Y., Tumor Targeting Chitosan Nanoparticles for Dual-Modality Optical/MR Cancer Imaging. *Bioconjugate Chemistry* **2010,** 21, (4), 578-582.
4. Phillips, M. A.; Gran, M. L.; Peppas, N. A., Targeted nanodelivery of drugs and diagnostics. *Nano Today* **2010,** 5, (2), 143-159.
5. Lee, M. J.; Veiseh, O.; Bhattarai, N.; Sun, C.; Hansen, S. J.; Ditzler, S.; Knoblaugh, S.; Lee, D.; Ellenbogen, R.; Zhang, M.; Olson, J. M., Rapid pharmacokinetic and biodistribution studies using cholorotoxin-conjugated iron oxide nanoparticles: a novel non-radioactive method. *PloS one* **2010,** 5, (3), e9536.
6. Pereira, P.; Morgado, D.; Crepet, A.; David, L.; Gama, F. M., Glycol chitosan-based nanogel as a potential targetable carrier for siRNA. *Macromolecular bioscience* **2013,** 13, (10), 1369-78.
7. Liu, Y.; Tseng, Y. C.; Huang, L., Biodistribution studies of nanoparticles using fluorescence imaging: a qualitative or quantitative method? *Pharmaceutical research* **2012,** 29, (12), 3273-7.
8. Choi, H. S.; Ipe, B. I.; Misra, P.; Lee, J. H.; Bawendi, M. G.; Frangioni, J. V., Tissue- and organ-selective biodistribution of NIR fluorescent quantum dots. *Nano letters* **2009,** 9, (6), 2354-9.
9. Adams, K. E.; Ke, S.; Kwon, S.; Liang, F.; Fan, Z.; Lu, Y.; Hirschi, K.; Mawad, M. E.; Barry, M. A.; Sevick-Muraca, E. M., Comparison of visible and near-infrared wavelength-excitable fluorescent dyes for molecular imaging of cancer. *BIOMEDO* **2007,** 12, (2), 024017-024017-9.
10. Hwang, H. Y.; Kim, I. S.; Kwon, I. C.; Kim, Y. H., Tumor targetability and antitumor effect of docetaxel-loaded hydrophobically modified glycol chitosan nanoparticles. *Journal of controlled release : official journal of the Controlled Release Society* **2008,** 128, (1), 23-31.
11. Hue, J. J.; Lee, H. J.; Jon, S.; Nam, S. Y.; Yun, Y. W.; Kim, J. S.; Lee, B. J., Distribution and accumulation of Cy5.5-labeled thermally cross-linked superparamagnetic iron oxide nanoparticles in the tissues of ICR mice. *Journal of veterinary science* **2013,** 14, (4), 473-9.
12. Saravanakumar, G.; Min, K. H.; Min, D. S.; Kim, A. Y.; Lee, C. M.; Cho, Y. W.; Lee, S. C.; Kim, K.; Jeong, S. Y.; Park, K.; Park, J. H.; Kwon, I. C., Hydrotropic oligomer-conjugated glycol chitosan as a carrier of paclitaxel: synthesis, characterization, and in vivo biodistribution. *Journal of controlled release : official journal of the Controlled Release Society* **2009,** 140, (3), 210-7.

13. Fang, R. H.; Hu, C. M.; Zhang, L., Nanoparticles disguised as red blood cells to evade the immune system. *Expert opinion on biological therapy* **2012,** 12, (4), 385-9.

14. Sheng, Y.; Liu, C.; Yuan, Y.; Tao, X.; Yang, F.; Shan, X.; Zhou, H.; Xu, F., Long-circulating polymeric nanoparticles bearing a combinatorial coating of PEG and water-soluble chitosan. *Biomaterials* **2009,** 30, (12), 2340-2348.

15. Hou, Z.; Zhan, C.; Jiang, Q.; Hu, Q.; Li, L.; Chang, D.; Yang, X.; Wang, Y.; Li, Y.; Ye, S.; Xie, L.; Yi, Y.; Zhang, Q., Both FA- and mPEG-conjugated chitosan nanoparticles for targeted cellular uptake and enhanced tumor tissue distribution. *Nanoscale research letters* **2011,** 6, (1), 563.

16. Kato, Y.; Onishi, H.; Machida, Y., Evaluation of N-succinyl-chitosan as a systemic long-circulating polymer. *Biomaterials* **2000,** 21, (15), 1579-85.

17. Richardson, S. C.; Kolbe, H. V.; Duncan, R., Potential of low molecular mass chitosan as a DNA delivery system: biocompatibility, body distribution and ability to complex and protect DNA. *International journal of pharmaceutics* **1999,** 178, (2), 231-43.

18. Na, J. H.; Lee, S. Y.; Lee, S.; Koo, H.; Min, K. H.; Jeong, S. Y.; Yuk, S. H.; Kim, K.; Kwon, I. C., Effect of the stability and deformability of self-assembled glycol chitosan nanoparticles on tumor-targeting efficiency. *Journal of controlled release : official journal of the Controlled Release Society* **2012,** 163, (1), 2-9.

19. Kim, J.-H.; Kim, Y.-S.; Park, K.; Lee, S.; Nam, H. Y.; Min, K. H.; Jo, H. G.; Park, J. H.; Choi, K.; Jeong, S. Y.; Park, R.-W.; Kim, I.-S.; Kim, K.; Kwon, I. C., Antitumor efficacy of cisplatin-loaded glycol chitosan nanoparticles in tumor-bearing mice. *Journal of Controlled Release* **2008,** 127, (1), 41-49.

20. Pereira, V. H.; Salgado, A. J.; Oliveira, J. M.; Cerqueira, S. R.; Frias, A. M.; Fraga, J. S.; Roque, S.; Falcão, A. M.; Marques, F.; Neves, N. M.; Mano, J. F.; Reis, R. L.; Sousa, N., In vivo biodistribution of carboxymethylchitosan/poly(amidoamine) dendrimer nanoparticles in rats. *Journal of Bioactive and Compatible Polymers* **2011,** 26, (6), 619-627.

21. Lee, S. J.; Huh, M. S.; Lee, S. Y.; Min, S.; Lee, S.; Koo, H.; Chu, J. U.; Lee, K. E.; Jeon, H.; Choi, Y.; Choi, K.; Byun, Y.; Jeong, S. Y.; Park, K.; Kim, K.; Kwon, I. C., Tumor-homing poly-siRNA/glycol chitosan self-cross-linked nanoparticles for systemic siRNA delivery in cancer treatment. *Angewandte Chemie (International ed. in English)* **2012,** 51, (29), 7203-7.

22. Gao, S.; Dagnaes-Hansen, F.; Nielsen, E. J.; Wengel, J.; Besenbacher, F.; Howard, K. A.; Kjems, J., The effect of chemical modification and nanoparticle formulation on stability and biodistribution of siRNA in mice. *Molecular therapy : the journal of the American Society of Gene Therapy* **2009,** 17, (7), 1225-33.

23. He, C.; Hu, Y.; Yin, L.; Tang, C.; Yin, C., Effects of particle size and surface charge on cellular uptake and biodistribution of polymeric nanoparticles. *Biomaterials* **2010,** 31, (13), 3657-3666.

24. Sykes, E. A.; Dai, Q.; Tsoi, K. M.; Hwang, D. M.; Chan, W. C. W., Nanoparticle exposure in animals can be visualized in the skin and analysed via skin biopsy. *Nat Commun* **2014,** 5.

6. Concluding remarks and future perspectives

Self-assembled glycol chitosan nanogel was successfully prepared through a simple, rapid and reproducible method. Attractive nanogel physicochemical properties were achieved, namely with regards to the satisfactory solubility at physiological pH, narrow size distribution profile, colloidal stability in aqueous medium , enough positive surface charge able to provide nucleic acid complexation through electrostatic interactions. *In vitro* active targeting was found using nanogel decorated with folate moieties, which promoted improved interaction with folate-receptor expressing cells and consequent internalization through receptor mediated endocytosis. Several assays performed to assess cell metabolic activity, membrane integrity, cell death by apoptosis or necrosis, cell cycling arresting, complement activation, macrophages cellular uptake and blood compatibility support the conclusion that the nanogel has a satisfactory biocompatibility. New insights into the way that nanogel enters cells has been reached through a novel and effective inhibition of endocytic pathways via siRNA depletion of specific endocytic proteins that orchestrate the different pathways. Colocalisation studies with endocytic probes showed that some of nanogel is delivered to endolysosomal compartments but a significant fraction was also in undefined organelles that await further characterisation. Intravenously injected nanogel decorated with folate and linear glycol chitosan exhibited a rapid whole body distribution in a model mice. Nanogel showed a blood clearance rate higher than free polymer. However the nanogel exhibited a satisfactory blood circulation half-life, of about 2 h, which may allow accumulation in a supposed target site, and a suitable body clearance period that occurs approximately 48 h after administration.

Glycol chitosan nanogels, easily decorated with specific ligands due to the presence of functional groups, showed to be a promising drug delivery vehicle, namely to gene delivery, with proved *in vitro* targeting ability. Even though some nanogels once internalized were delivered in endolysosomal compartments, a significant fraction of

nanogels were distributed in cytoplasm and cytoplasmic organelles. The *in vivo* nanogel biodistribution profile also support their possible applicability as drug delivery system.

Following the fundamental work presented in this thesis, more applied tasks are suggested:

- Transfection studies need to be performed to quantify the transfection efficiency of the developed nanoparticulate system. If necessary, optimization of the transfection efficiency by tuning the DS of hydrophobic chains.
- Studies on the encapsulation and controlled release of poorly water soluble low molecular weight pharmaceuticals;
- *In vivo* biodistribution study of a model of low molecular weight drugs loaded GC nanogel, both labelled with different NIR dyes in order to assess in a non-invasive imaging system the potential of the carrier to deliver this kind of pharmaceutical *in vivo*. More specifically ascertain if the drug loaded nanogel remains stable in bloodstream as also evaluate whether the vehicle (nanogel) is able to transport the drug until the target site.
- Improve the stability of the nanogel, upon dilution, through covalent crosslinking. Preliminary tests confirm the success of the nanogel reticulation by dissulfide bound of thiolated hydrophobic molecule grafted onto GC backbone with a homofunctional crosslinker - 1,4-Bis(3-[2-pyridyldithio]propionamido)butane (DPDPB).
- *In vivo* trials on a tumor bearing mice, using of HeLa cells, in order to visualize the tumor targeting ability and treatment;